JAERI-Conf--97-001

JAERI-Conf
97-001

SELECTED PAPERS OF ISTC WORKSHOP ON NUCLEAR DATA OF MINOR ACTINIDES

May 27~31, 1996, JAERI, Tokai, Japan

March 1997

(Ed.) Jun-ichi KATAKURA

日本原子力研究所
Japan Atomic Energy Research Institute

本レポートは，日本原子力研究所が不定期に公刊している研究報告書です。
入手の問合わせは，日本原子力研究所研究情報部研究情報課（〒319-11 茨城県那珂郡東海村）あて，お申し越しください。なお，このほかに財団法人原子力弘済会資料センター（〒319-11 茨城県那珂郡東海村日本原子力研究所内）で複写による実費頒布をおこなっております。

This report is issued irregularly.
Inquiries about availability of the reports should be addressed to Research Information Division, Department of Intellectual Resources, Japan Atomic Energy Research Institute, Tokai-mura, Naka-gun, Ibaraki-ken 319-11, Japan.

編集兼発行　日本原子力研究所
印　　刷　㈱原子力資料サービス

JAERI－Conf 97－001

Selected Papers of ISTC Workshop on Nuclear Data of Minor Actinides May 27～31, 1996, JAERI, Tokai, Japan

(Ed.) Jun-ichi KATAKURA

Department of Reactor Engineering
Tokai Research Establishment
Japan Atomic Energy Research Institute
Tokai-mura, Naka-gun, Ibaraki-ken

(Received January 6, 1997)

Workshop on the ISTC (International Science and Technology Center) projects, the monitor and/or collaborator of which is Nuclear Data Center, JAERI, was held to discuss the status and the results of the projects. The ISTC was established as an intergovemmental organization which finances and monitors science and technology projects to ensure that CIS scientists, especially those with expertise in developing weapons of mass destruction, are offered the opportunity to use their skills in civilian scientific and technical fields. There are three projects Nuclear Data Center supports. They are following:

1) Evalustion of Actinide Nuclear Data
2) Measurements of Fission Neutron Spectra of the Minor Actinides Spontaneous Fission of Curium Isotopes
3) Measurements and Analysis of the Basic Nuclear Data for Minor Actinides

The workshop was held with 11 participants from the CIS and 16 domestic participants who have interest on the minor actinide nuclear data. This report includes the papers on the projects presented at the workshop.

Keywords: Minor Actinides, Nuclear Data, ISTC Project

マイナーアクチニドの核データに関するISTC日露ワークショップ報文集
1996年5月27日～31日，東海研究所，東海村

日本原子力研究所東海研究所原子炉工学部
（編）片倉　純一

（1996年1月6日受理）

核データセンターでモニターあるいは協力者となっている3件のISTC（International Science and Technology Center）プロジェクトに関し，その進捗状況，成果を検討するために，ワークショップを開催した。ISTCは，旧ソ連の兵器関係研究者の第三国への拡散を防止し，平和産業への転換を支援するために，日米殴の資金でモスクワに設立されたものである。核データセンターが支援している3件のプロジェクトは，以下の通りです。

1) Evalustion of Actinide Nuclear Data
2) Measurements of the Fission Neutron Spectra of the Minor Actinides Spontaneous Fission of Curium Isotopes
3) Measurements and Analysis of the Basic Nuclear Data for Minor Actinides

ワークショップは，旧ソ連から11名，日本から核データセンター及びマイナーアクチニドに関連のある国内研究者16名の参加によって行われた。本報文集は，ワークショップで発表された各プロジェクトに関する報告をまとめたものである。

東海研究所：〒319-11　茨城県那珂郡東海村白方白根2－4

Contents

目　　次

1. Evaluation of Actinide Nuclear Data

(Radiation Physics and Chemistry Problems Institute)

1. 1 Annual Report of the Project CIS-03-95 "Evaluation of Actinide Nuclear Data"

V.M. Maslov
Radiation Physics and Chemistry Problems Institute, 220109,
Minsk-Sosny, Belarus

Abstract

The evaluation of neutron data for ^{243}Cm, ^{245}Cm and ^{246}Cm is made in the energy region from 10-5 eV up to 20 MeV. The results of the evaluation are compiled in the ENDF/B-VI format.
This work is performed under the Project Agreement CIS-03-95 with the International Science and Technology Center (Moscow). This is the annual report of the project CIS-03-95. (Editor)

ANNUAL REPORT OF THE PROJECT CIS-03-95 "EVALUATION OF ACTINIDE NUCLEAR DATA"

March 4, 1996

1 Contracting Institute

Radiation Physics and Chemistry Problems Institute, 220109, Minsk-Sosny, Belarus

2 Participating Institutes

The Project is accomplished in collaboration with the Japan Atomic Energy Research Institute

3 Project Manager

Dr. Vladimir Maslov
Tel/fax: (0172) 46 73 41
E-mail: maslov@ndel.basnet.minsk.by

4 Contract Duration

36 months from March 1, 1995

5 Brief description of the plan

5.1 The scope of work

5.1.1 Objective of the project

The advanced nuclear fuel cycle studies request the nuclear data of transplutonium isotopes. During the Project the neutron data for the ^{243}Cm, ^{245}Cm, ^{246}Cm, ^{241}Am, ^{242m}Am, ^{242}Am, ^{243}Am and ^{238}Np should be evaluated. The previously evaluated by the members of the Project team neutron data files of ^{242}Cm, ^{244}Cm and ^{238}Pu would be revised. The curium and americium isotopes data to be evaluated were requested by the General Manager of Japan Nuclear Data Center Dr. Y. Kikuchi.

The numerical data files would be compiled in computer-readable format of Evaluated Nuclear Data File, B Library, Version VI.

5.1.2 Expected results

During first year of the Project the neutron data for the ^{243}Cm, ^{245}Cm and ^{246}Cm were evaluated. The quantities evaluated are resolved and unresolved resonance parameters, total, elastic and inelastic scattering, fission, capture, (n,2n) and (n,3n) reaction cross sections, angular and energy distributions of secondary neutrons, including partial (n,xn) and (n,xnf) reaction spectra, fission spectra and number of neutrons per fission. The incident neutron energy range covered is from 10^{-5} eV up to 20 MeV. The evaluated quantities are compared mainly with JENDL-3 evaluation, since the detailed documentation on other libraries (ENDF/B-VI, JEF) is unavailable.

The main goal of the neutron data evaluation is to provide a consistent set of resonance parameters and cross section values describing the available measured data. When there is no data available, the proven theoretical approaches alongside with parameter systematics are used. These approaches are tested in case of major actinides, i.e. ^{235}U, ^{238}U, ^{239}Pu.

5.1.3 The technical approach

5.1.3.1 Neutron resonance parameters The neutron resonance parameters are obtained by simultaneous fit of available measured data on total, fission and capture cross sections within a multilevel Breit-Wigner approach. Then neutron resonance parameters of first resonances are made consistent with available data on thermal fission and capture cross sections.

5.1.3.2 Average resonance parameters The preliminary estimates of average resonance parameters are obtained by averaging the evaluated resolved resonance ($E_r > 0$) parameters. They are: reduced neutron width

$< g\Gamma_n^o >$, fission width $< \Gamma_f >$, radiative width $< \Gamma_\gamma >$ and observed neutron resonance spacing $< D_{obs} >$.

Due to missing of weak resonances these values overestimate actual reduced neutron width $< g\Gamma_n^o >$ and neutron resonance spacing $< D_{obs} >$. To get a physically justified values for $< g\Gamma_n^o >$ and $< D_{obs} >$ we employ a theoretical method. With this method we take into account the correlation of weak resonance missing and resonance missing due to poor experimental resolution. Both reduced neutron width and neutron resonance spacing distributions are obtained in a unified approach. The resolution function parameters as well as $< g\Gamma_n^o >$ and $< D_{obs} >$ are obtained by maximum likelihood method when comparing experimental distributions of reduced neutron width and resonance spacing with Porter-Thomas and Wigner distributions, modified for the resonance missing. Average fission and radiation widths are virtually insensitive to resonance missing, so we use values obtained by averaging of resolved resonance parameters.

The average resonance parameters are used to fix the statistical model parameters at the end-point of the resolved resonance energy region. So, in the whole energy region the resonance parameters, average resonance parameters and statistical model parameters are consistent with each other.

5.1.3.3 Deformed optical potential The deformed optical potential is obtained for neutron-nucleus interaction description. The starting values for the potential parameters were those for n+^{238}U interaction by Haouat et al.(1982). The isotopic dependences of real and imaginary parts of the potential were calculated using the optical potential parameter systematics. Five levels (or more) of the ground state band are coupled. The deformation parameters β_2 and β_4 are obtained by fitting $s-$wave strength function S_0 value. We modified the original potential geometry parameters to fit total cross section and differential scattering data for N-odd and N-even targets above 10 MeV. This procedure of parameter fitting is well tested in case of and ^{233}U, ^{239}Pu, ^{235}U, ^{232}Th and ^{238}U targets.

5.1.3.4 Fission cross section For Cm nuclei the measured neutron data in fast energy region, i.e. above unresolved resonance energy region, are available only for fission cross section. So, the available fission data fit have been used as a constraint for (n, n') and (n, γ) reaction cross sections calculation. Neutron-induced fission cross section is described within the statistical theory approach. Up to the second chance fission threshold the fission cross section description is accomplished through the modelling of level densities of fissioning and residual nuclei. We reproduce also the average resonance fission width value. Fission widths are calculated within a double-humped fission barrier. Energy and angular momentum depen-

dence of fission width is defined by the transition state spectra at inner and outer barrier humps. We constructed both spectra by supposing the triaxiality of inner saddle and mass asymmetry at outer saddle. The calculated widths $< \Gamma_f^{J^\pi+1/2} >$ and $< \Gamma_f^{J^\pi-1/2} >$ are normalized to the adopted average fission width $< \Gamma_f >$. The different behavior of level densities of even-even and even-odd nuclei at low excitation energies is taken into account. In case of both N-odd fissile target nuclei (^{243}Cm and ^{245}Cm) and N-even non-fissile target nucleus (^{246}Cm) the discrete character of few-quasiparticle excitations was approximated within a generalized pairing model. In case of N-odd fissile nuclei (^{243}Cm and ^{245}Cm) the collective levels of the fissioning nuclei (^{244}Cm, ^{246}Cm) lying within a pairing gap were modelled. To fix fission channel parameters the systematic trends are used. Above the second chance fission threshold the behavior of the first chance fission cross section is defined using the statistical model parameter systematics.

5.1.3.5 Inelastic scattering cross section The discrete level excitation (compound and direct), continuum excitation and pre-equilibrium emission contribute to the inelastic scattering cross section. Above 5 MeV incident neutron energy pre-equilibrium emission and direct inelastic scattering are the two reaction mechanisms which define inelastic scattering cross section. The pre-equilibrium model parameters were tested by the statistical model description of ^{238}U+n interaction secondary neutron spectra and consistent description of fission and (n,xn) reaction data for major actinides.

The direct inelastic scattering defines the shape of ground state band levels excitation cross sections above 1 MeV incident neutron energy. This mechanism defines partly the hard-energy tail in total inelastic scattering cross section.

5.1.3.6 Cross sections of (n,2n) and (n,3n) reactions The magnitude of (n,2n) cross section below the (n,2nf) reaction threshold is defined by (n,nf) and (n,2n) reaction competition. To calculate the (n,2n) reaction cross section we use an approach, developed for description of the ^{238}U(n,2n) reaction cross section. There is a hard-energy tail in (n,2n) reaction cross sections predicted. To calculate the (n,2n) reaction cross section of N-odd target nuclei in a threshold region we use an approach, developed for description of the ^{239}Pu(n,2n) reaction cross section. Above the pairing gap for the even-even residual nuclei the two-quasiparticle states level density is used.

5.1.3.7 Radiative capture cross section Energy and angular momentum dependence of radiative capture width are calculated within a two-cascade γ-emission model with allowance for the (n,γf) and (n,γn') reaction

competition to the (n,$\gamma\gamma$) reaction. The (n,$\gamma\gamma$) reaction is supposed to be a radiative capture reaction. The radiative capture width is normalized to the radiative capture width $< \Gamma_\gamma >$. For fissile nuclei the competition of (n,γf) reaction is especially important.

5.1.3.8 Secondary neutron spectra There is no measured data on secondary neutron spectra. To calculate partial neutron energy distributions of (n,xnγ) and (n,xnf), x=1, 2, 3 reactions we use a simple Weisscopf-Ewing evaporation model taking into account fission and gamma competition to neutron emission. The pre-equilibrium emission of first neutron is included.

6 Technical progress

6.1 New findings and achievements

We have evaluated neutron data for ^{243}Cm, ^{245}Cm and ^{246}Cm. The data are compiled in ENDF/B-VI format and are available in computer-readable form.

Comprehensive analysis of available measured data within our approach have lead to the following main conclusions. For detailed explanations see references, given at the end of this Report.

6.1.1 ^{243}Cm

The resolved resonance region is extended up to 100 eV, the total and fission data are fitted simultaneously. The $< \Gamma_n^o >$ value is ~1.5 lower, than that of JENDL-3 evaluation, since in present evaluation the cluster of 6 resonances is resolved around 66 eV (see Fig.1).

The difference in thermal scattering cross section σ_n is due to scattering radius value of 9.4757 fm, which is taken from the coupled channel calculations (10 fm was assumed in JENDL-3). Up to 63 eV incident neutron energy the total and fission cross sections, calculated with current and JENDL-3 parameters are rather compatible. The differences around 66 eV are due to resolving of multiplet around 66 eV using fission data by Silbert (1976). This 66.03 eV resonance cluster, if not resolved, would appreciably change the average values of $< \Gamma_n^o >$ and $< \Gamma_f >$.

To parameterize the fission data in energy region of 63-100 eV 53 resonances are involved. The values of $< \Gamma_n^o >$ = 0.17 meV and $< D_{obs} >$ = 0.71 eV are compatible with appropriate values for the energy region of 0-70 eV, derived with missing of levels taken into account (see below).

The bomb-shot fission data of Silbert (1976) available in the unresolved resonance region were fitted at chosen energy intervals by varying the neutron strength function S_0 value. The possibility of varying $< \Gamma_f^{2+} >$ or(and)

$< \Gamma_f^{3+} >$ was rejected, since inherently the fission width should fluctuate less vigorously, than neutron width because of greater degrees of freedom number. That decision was justified by the experience obtained in case of ^{235}U and ^{239}Pu neutron data evaluation. For these nuclei there are measured data on total and fission cross sections. Varying $s-$wave strength function S_0 values to fit total cross section data in chosen intervals we can reproduce simultaneously most of the fission cross section fluctuations.

The discrepancies are noticed when comparing the evaluated (n,γ) reaction cross sections. Current evaluated cross section is almost 1.5 times as large as JENDL-3 evaluated capture cross section. This discrepancy is due to strong $(l,J)-$ channel dependence of fission width in our approach. This dependence is due to adopted transition states spectra structures. Specifically the ratio of calculated widths $< \Gamma_f^{2+} > / < \Gamma_f^{3+} > \simeq 2.5$ is almost independent on incident neutron energy. That will lead to the increased capture cross section for the $(l = 0, J = 3)$ channel as compared with JENDL-3 approach. In JENDL-3 approach the fission width value is channel, i.e. spin and parity independent, while its value of $< \Gamma_f >$ =1.481 eV is anomalously high. With this high value of fission width Silbert (1976) data can not be reproduced in our approach.

The levels, which were added for the K^π =1/2$^+$ band of ^{243}Cm are: J = 5/2 ,7/2, 11/2,13/2 (J = 1/2, 3/2 and 9/2 levels are present). The resulted strong inelastic scattering due to the K^π =1/2$^+$ band levels (see Fig.2) produces a strong 'dip' in calculated fission cross section around 0.4 MeV.

The fission cross section is calculated with the statistical model, the fission widths for $s-$wave neutrons Γ_f^{2+} and Γ_f^{3+} are fitted at 0.1 keV by varying transition spectra band-heads to get average fission width of 0.355 eV. The fission cross section above 1 MeV incident neutron energy was adopted to be consistent with data of Fomushkin et al. (1987,1990). The slope of the cross section with energy in the first plateau region is consistent with the systematic trends. It is less steep than that of Fursov et al. (1994) data for ^{245}Cm(n,f) and ^{247}Cm(n,f). The comparison of calculated cross section with JENDL-3 evaluation and measured data of Fomushkin et al. is shown in Fig. 3.

The role of (n,γf) reaction competition in radiative capture cross section calculation, due to high fissility of ^{244}Cm compound nuclide is emphasized.

The number of prompt fission neutrons ν_p is calculated with Madland-Nix model, pre-equilibrium emission of first neutron being included. Our prediction is rather different from Howerton (1977) systematics.

6.1.2 ^{245}Cm

The purpose of present resonance parameter evaluation is to extend the resolved resonance region up to 100 eV. We have got 91 resonance parameters up to 100 eV, including three negative resonance parameters at $E_r = -5.0$ eV, $E_r = -2.0$ eV, $E_r = -0.1$ eV. The assigning of resonance spins was done as follows. Two assumptions were adopted: the number of resonances with spin J is proportional to $(2J+1)$, reduced neutron width distribution should obey that of Porter-Thomas, neutron resonance spacing distribution should obey that of Wigner. Obtained neutron resonance spacings obey Wigner distribution. In case of reduced neutron widths the number of small Γ_n^o values is too low, which is due to missing of resonances.

Evaluated fission cross sections of this work is ~20% higher than that of JENDL-3 at lower edge of unresolved resonance region. Larger discrepancies are noticed when comparing the (n,γ) reaction cross sections. Current evaluated cross section is more than 1.5 times as large as JENDL-3 evaluated capture cross section. This discrepancy is due to much lower values of $< D >$, $< \Gamma_f >$ and partly to $(l,J)-$ channel dependence of fission width in our approach. This dependence is due to adopted transition states spectra structures. Specifically the ratio of $< \Gamma_f^{4+} > / < \Gamma_f^{3+} > \simeq 1.3$ is almost independent on incident neutron energy, that will lead to the increased capture reaction cross section for the $(l=0, J=4)$ channel as compared with JENDL-3 approach. In an approach, adopted in JENDL-3 the fission width value is independent on spin and parity. Furthermore, the adopted in JENDL-3 average fission width value of ~1.8 eV is anomalously high. With this value of fission width measured fission data can not be reproduced in our approach.

We consider the fission data base to be fairly consistent in the first plateau region, i.e. above ~1.5 MeV. At lower energies we will follow the trend of data by Fomushkin et al. (1990). The fission cross section is calculated within the statistical model. The fission widths for $s-$wave neutrons Γ_f^{3+} and Γ_f^{4+} are fitted at 0.1 keV by varying the positions of transition spectra band-heads to reproduce the average fission width $< \Gamma_f >= 0.345$ eV. To calculate fission cross section below 0.3 MeV we fit the fission cross section value at 54 keV, evaluated with the average resonance parameters. The fission cross section above 0.3 MeV incident neutron energy is consistent with data of Fomushkin et al.(1990). The slope of the calculated fission cross section with energy in the first plateau region is consistent with the measured data base.

The comparison of calculated fission cross section with JENDL-3 evaluation and measured data is shown in Fig. 4. The statistical theory calculation of fission cross section was accomplished within the double-humped barrier model. The procedure of calculating fission transmission coefficients

is briefly described below.

The collective levels of ^{246}Cm fissioning nuclide, lying within pairing gap define the ^{245}Cm(n,f) fission cross section below incident neutron energy of ~0.5 MeV. These levels comprise the discrete transition spectra at both saddles. The discrete transition spectra contribution to the fission transmission coefficient is dependent upon the order of symmetry for ^{246}Cm fissioning nucleus at inner and outer saddles. Due to the axial asymmetry at the inner saddle the respective 2^+-band-heads are lowered as compared with the respective positions of 2^+ -band-heads at ground state deformation. The positions of negative parity bands $K^\pi = 0^-, 1^-, 2^-$ at outer saddle are lowered due to mass asymmetry. With transition state spectra thus defined the fission barrier parameters are obtained. The calculated fission widths at incident neutron energy of 0.1 keV are $\Gamma_f^{3+} = 0.291$ eV and $\Gamma_f^{4+} = 0.391$ eV reproduce the average fission width $< \Gamma_f > = 0.345$ eV.

At excitation energies above the pairing gap, which is assumed to be 1.0 MeV, level density of axially symmetric fissioning nucleus is calculated in constant temperature approximation, i.e. $\rho(U) = T_f^{-1} \exp((U - U_o)/T_f)$. The respective parameters, nuclear temperature T_f and excitation energy shift U_o are defined at the matching energy U_c =3.6 MeV. At excitation energies above U_c the continuum part of the transition state spectrum is represented with the phenomenological model, which takes into account pairing, shell and collective effects at saddle deformations. After that the effects of non-axiality and mass asymmetry are included.

The generalized pairing model provides the means of taking into account the discrete character of few quasi-particle excitations just above the pairing gap. It was shown to be important in case of even-even fissioning nucleus ^{236}U in the ^{235}U(n,f) reaction. We modelled the nuclear level density $\rho(U)$ above the pairing gap up to the four-quasi-particle excitation threshold as $\rho(U) = \rho(\hat{U})/(1 + \exp(U_2 - U + \delta_1)/\delta_2)$. The two-quasi-particle states level density of even-even fissioning nucleus ^{246}Cm defines the fission cross section shape at incident neutron energies ~ 0.5÷2MeV (see Fig. 4), the parameters $\hat{U}$ = 1.7 MeV, $\delta_1 = \delta_2 = 0.2$ MeV values were extracted. Above ~2 MeV incident neutron energy fission cross section data were fitted (see Fig. 4) by slight increase of pairing correlation function.

Radiative strength function value obtained in current analysis is rather low, as compared with BNL-325 recommendations. The (l, J)−channel dependence of fission width influences strongly the capture cross section in unresolved resonance region. The radiative capture cross section is calculated within a statistical approach up to 5 MeV. Radiative capture strength function $S_{\gamma 0} = 541.55$. At higher incident neutron energies we assume radiative capture cross section to be 0.1 mbarn. The radiative capture width was calculated with (n,γf) and (n,γn') reactions competition against "true"

capture reaction (n,$\gamma\gamma$). The role of (n,γf) and (n,γn') reactions is illustrated on Fig. 5 by sharp decrease of capture cross section above 0.5 MeV incident neutron energy, as compared with JENDL-3 evaluation.

The present evaluation of $\nu_p(E)$ is based on calculation within Madland-Nix model, fitted to the data of Khokhlov et al.(1994) in the energy range 0.5÷4 MeV. The calculated $d\nu_p/dE = 0.133$ is considerably higher than that predicted by Howe et al.(1983). Calculated $\nu_p(E)$ is roughly consistent with data by Khokhlov et al.(1994) above 4 MeV. The Madland-Nix model calculations predict non-linear increase of $\nu_p(E)$ above emissive threshold. The influence of pre-equilibrium pre-fission neutrons manifests in additional appreciable decrease of $d\nu_p/dE$ above 12 MeV (see Fig. 6).

6.1.3 ^{246}Cm

With current resonance parameter evaluation we extended the resolved resonance region up to 400 eV and to reconciled the available fission data by Maguire et al. (1985), revised by Danon et al.(1991) with resonance parameters by Moore et al. (1971). We have got 17 neutron resonance parameters up to 400 eV.

The fission data of Moore et al. (1971) and data of Maguire et al. (1985), revised by Danon et al. (1991) covering the unresolved resonance energy region, their shapes are rather different (see Fig.7). The shape of data by Maguire et al. (1985), revised by Danon et al. (1991) is reproduced with average resonance parameters. Fission cross section calculations with the average resonance parameters are compatible with measured data within errors, except 0.4-1.0 keV and 2.6 -5.0 keV energy intervals. We fitted the measured data in these intervals adjusting $\langle\Gamma_f^{1/2+}\rangle$ fission width. The calculated fission cross section is compared with measured data on Fig. 7.

We fitted the fission data by Maguire et al. (1985), revised by Danon et al. (1991) below 80 keV. At higher neutron energies we follow the trend of data by Fomushkin et al. (1980). The most peculiar feature of data by Fomushkin et al. (1980) is the broad quasi-resonance structure above the fission threshold and steep decreasing trend of data above ~3 MeV incident neutron energies. Both features are reproduced within the statistical model calculations. To describe the broad quasi-resonance structure above 1 MeV, we assume it to be due to interplay of level densities of even-odd ^{247}Cm fissioning nuclide and even-even ^{246}Cm residual nuclide. We modelled the few-quasiparticle excitations in fissioning and residual nuclei.

The comparison of calculated fission cross section with measured data is shown in Fig. 8. The statistical theory calculation of fission cross section was accomplished within the double-humped fission barrier model.

The low-lying levels of ^{246}Cm were treated within a model of deformable non-axial rotator, ~10 positive and negative parity levels were added up to

~1.5 MeV.

The radiative capture cross section is calculated within a statistical approach up to 5 MeV. Radiative capture strength function equals $S_{\gamma 0}$ = 19.828. At higher incident neutron energies we assume radiative capture cross section to be 1 mbarn. The radiative capture width was calculated with (n,γf) and (n,γn') reactions competition against "true" capture reaction (n,$\gamma\gamma$). Due to high fission threshold for ^{247}Cm compound nuclide the competition of (n,γn') reaction is stronger than that of (n,γf) reaction. The influence of (n,γn') and (n,γf) reaction competition on radiative capture cross section is illustrated on Fig. 9 by sharp decrease of capture cross section above 1 MeV incident neutron energy, as compared with (n,γx) reaction cross section. The capture cross section of JENDL-3 is systematically lower than present evaluation due to lower value of $S_{\gamma 0}$ = 9.779.

The inclusion of pre-equilibrium emission changes significantly the average energies of secondary neutron spectra. The most significant is the change of neutron spectra of (n,nγ) reaction (see Fig. 10).

The comparison of calculated $\nu_p(E)$ with JENDL-3 evaluation shows that the calculated slope of $d\nu_p/dE$ = 0.135 is considerably lower than that of Howerton systematics[47] prediction, adopted in JENDL-3. However, it is consistent with $d\nu_p/dE$ for neighboring nuclei. The Madland-Nix model calculations predict non-linear shape of $\nu_p(E)$ above emissive fission threshold. The influence of pre-equilibrium pre-fission neutrons manifests in additional appreciable decrease of $d\nu_p/dE$ above 12 MeV.

7 Current technical status

We are moving in strict agreement with technical schedule, no changes are foreseen in initial technical schedule. Within the second year of the Project the neutron data for the ^{241}Am, ^{242m}Am, ^{242}Am, ^{243}Am will be evaluated.

8 Cooperation with foreign collaborators

Dr. Y. Kikuchi, General Manager of Nuclear Data Center, JAERI, visited the Project site on 21-25, May, 1995. The evaluation of ^{243}Cm nuclear data was discussed.

Dr. Y. Kikuchi, General Manager of Nuclear Data Center, JAERI, visited the Project site on 2-5, October, 1995. The evaluated data for ^{243}Cm were discussed. The comments by Y. Kikuchi, T. Nakagawa, K. Shibata and Y. Nakajima on the report "Evaluation of Neutron Data for Curium-243" are supplemented, as well as our reply to the Comments (see annex 2). The evaluation of ^{245}Cm nuclear data was also discussed.

Dr. Y. Kikuchi, General Manager of Nuclear Data Center, JAERI and Dr. K. Shibata, Senior Scientist of NDC(JAERI) visited the Project site on 11-15, February, 1996. The evaluated data files for ^{243}Cm, ^{245}Cm and ^{246}Cm were discussed.

Workshop on the Project will be held on 27-31, May 1996 in Japan Atomic Energy Research Institute, Tokai, Japan.

Working Party on International Evaluation Cooperation of Nuclear Energy Agency Nuclear Science Committee (NEANSC WPEC), NEA Headquarters, Paris, France 17-18 of May 1995 Been nominated by the International Atomic Energy Agency as observer, Project Manager V.Maslov participated in the Meetings listed above. Results achieved. During the meeting V. Maslov was included to the Subgroup 8 of WPEC " Minor Actinide Data". Within this subgroup activity we can be provided testing in integral data benchmarks of our evaluated data files for minor actinides. The next meeting of the WPEC will be held at Argonne National Laboratory,USA on 10-13 June, 1996. V. Maslov has got an invitation to attend the WPEC and WPMA meeting at ANL (USA), since our recent evaluation activities are of great interest to the Working Party.

Second Research Co-ordination Meeting of the IAEA Co-ordinated Research Program (CRP) on Development of Reference Input Parameter Library for Nuclear Model Calculations of Nuclear Data (RIPL) held at the Agency Headquarters in Vienna (Austria), from 30 October to 3 November 1995. Two members of the Project attended the Meeting: V. Maslov, and E. Sukhovitskij. V. Maslov presented a talk on fission barriers and level densities. E. Sukhovitskij presented a talk on deformed optical model. V. Maslov informed the RIPL participants about the Project results, relevant for the RIPL. ISTC may get requests on our actinide data files. We will participate in preparation of the final library of the CRP in case of fission barriers and level densities and the potential parameters. This activity will take place in current and next year. V. Maslov was granted an additional support through the individual Research Contract within the scope of CRP with IAEA for the 1996 year. The phase II of the RIPL is foreseen for the 1998-2000. It is likely that we will participate in it on a regular basis, i.e. with a IAEA support.

9 Delay, problems, suggestions

Drs. Y. Kikuchi and K. Shibata, during their last visit, suggested the inclusion of covariance and γ−production files for Cm and Am data files. However, if accepted, this may influence the initial Project working schedule.

10 Perspectives of the future applications and development

Present evaluated data files for minor actinides might be considered about the inclusion to the Actinoid File of JENDL. The theoretical evaluation methods could be used for updating other actinide nuclear data files.

11 Annex 1

11.1 Figure captions

Fig.1 Fission cross section of ^{243}Cm in the energy region 55-70 eV.
Fig. 2 Inelastic scattering cross section of ^{243}Cm.
Fig. 3 Fission cross section of ^{243}Cm in the energy region.
Fig. 4 Fission cross section of ^{245}Cm.
Fig. 5 Capture cross section of ^{245}Cm.
Fig. 6 Prompt fission neutron multiplicity for ^{245}Cm.
Fig. 7 Fission cross section of ^{246}Cm in unresolved resonance region.
Fig. 8 Fission cross section of ^{246}Cm.
Fig. 9 Radiative capture cross section of ^{246}Cm.
Fig. 10. Comparison of (n,n'γ) reaction neutron spectra of ^{246}Cm for incident neutron energy 14 MeV.

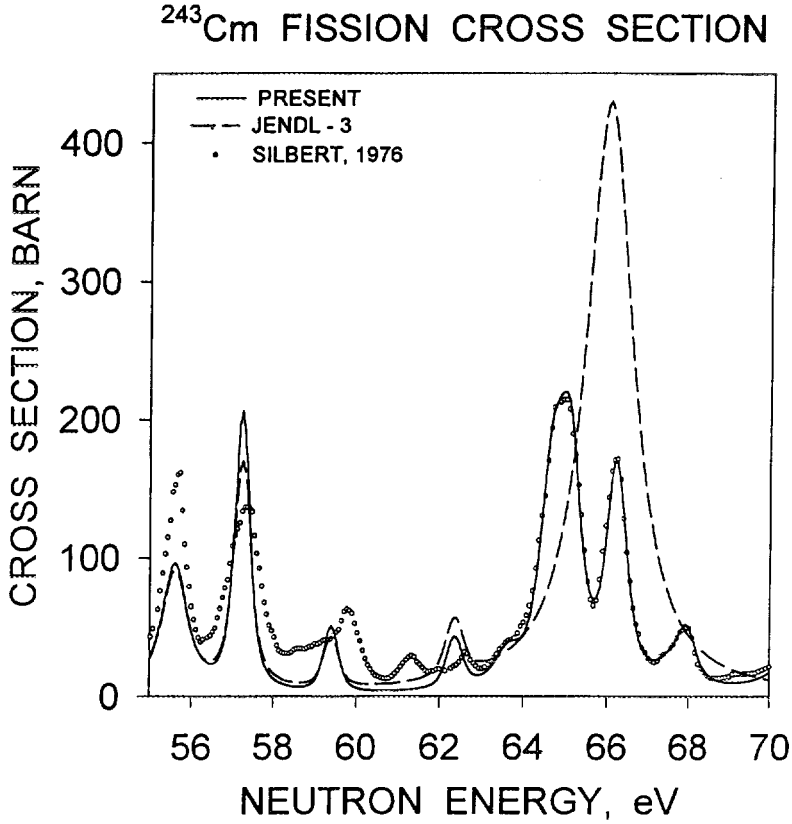
^{243}Cm FISSION CROSS SECTION
PRESENT
JENDL - 3
SILBERT, 1976
CROSS SECTION, BARN
0
100
200
300
400
56
58
60
62
64
66
68
70
NEUTRON ENERGY, eV

FIG. 1

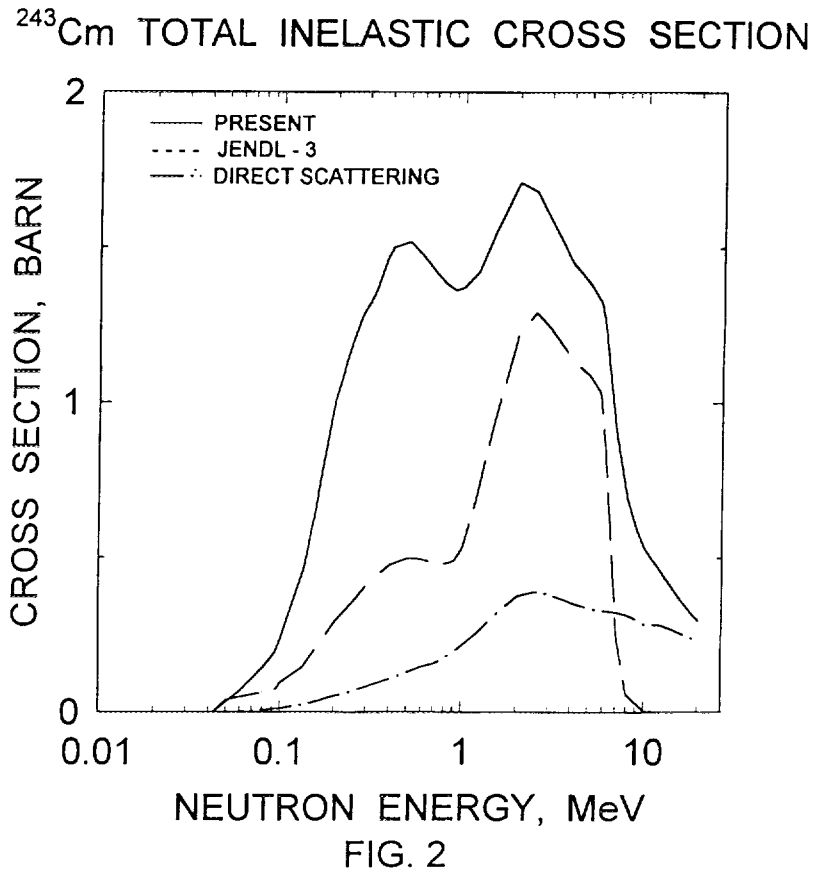
^{243}Cm TOTAL INELASTIC CROSS SECTION
PRESENT
JENDL - 3
DIRECT SCATTERING
CROSS SECTION, BARN
0
1
2
0.01
0.1
1
10
NEUTRON ENERGY, MeV

FIG. 2

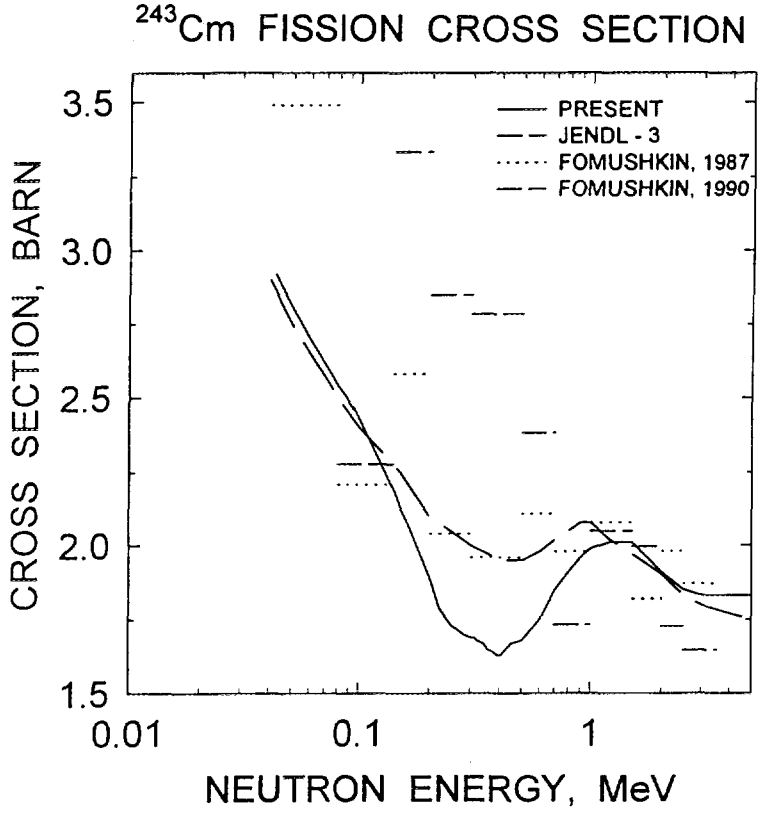
243Cm FISSION CROSS SECTION
PRESENT
JENDL - 3
FOMUSHKIN, 1987
FOMUSHKIN, 1990
CROSS SECTION, BARN
3.5
3.0
2.5
2.0
1.5
0.01
0.1
1
NEUTRON ENERGY, MeV

FIG. 3

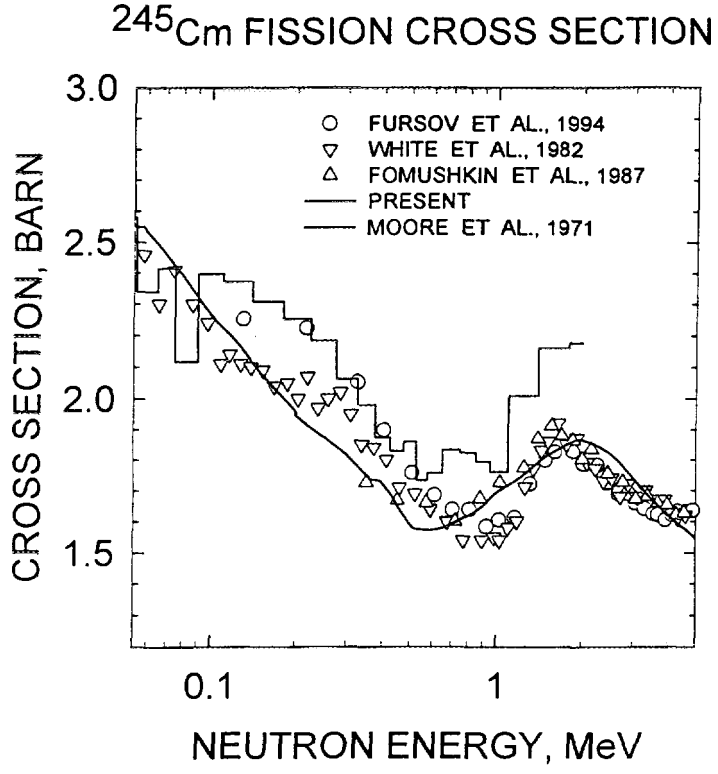
245Cm FISSION CROSS SECTION
FURSOV ET AL., 1994
WHITE ET AL., 1982
FOMUSHKIN ET AL., 1987
PRESENT
MOORE ET AL., 1971
CROSS SECTION, BARN
3.0
2.5
2.0
1.5
0.1
1
NEUTRON ENERGY, MeV

FIG 4

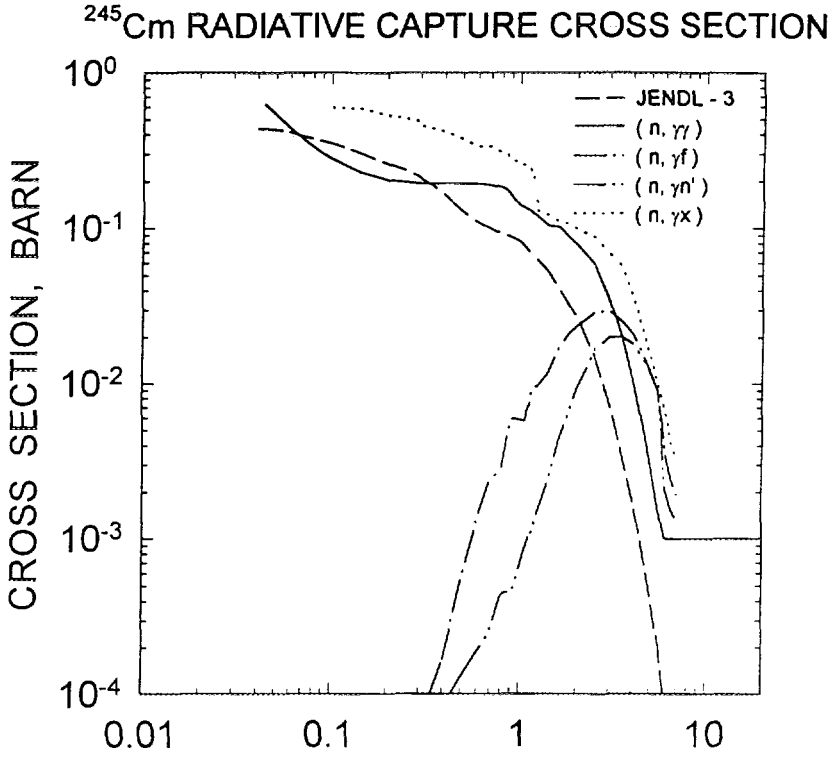
245Cm RADIATIVE CAPTURE CROSS SECTION
JENDL - 3
(n, γγ)
(n, γf)
(n, γn')
(n, γx)
CROSS SECTION, BARN
10^0
10^-1
10^-2
10^-3
10^-4
0.01
0.1
1
10
NEUTRON ENERGY, MeV

FIG. 5

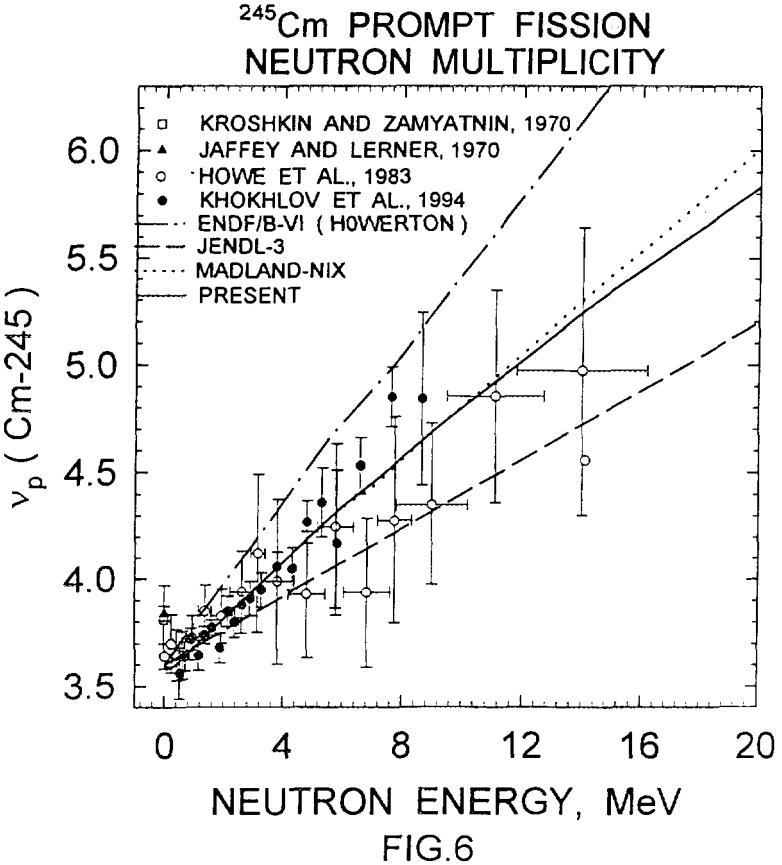
245Cm PROMPT FISSION
NEUTRON MULTIPLICITY
KROSHKIN AND ZAMYATNIN, 1970
JAFFEY AND LERNER, 1970
HOWE ET AL., 1983
KHOKHLOV ET AL., 1994
ENDF/B-VI (HOWERTON)
JENDL-3
MADLAND-NIX
PRESENT
ν_p (Cm-245)
6.0
5.5
5.0
4.5
4.0
3.5
0
4
8
12
16
20
NEUTRON ENERGY, MeV

FIG.6

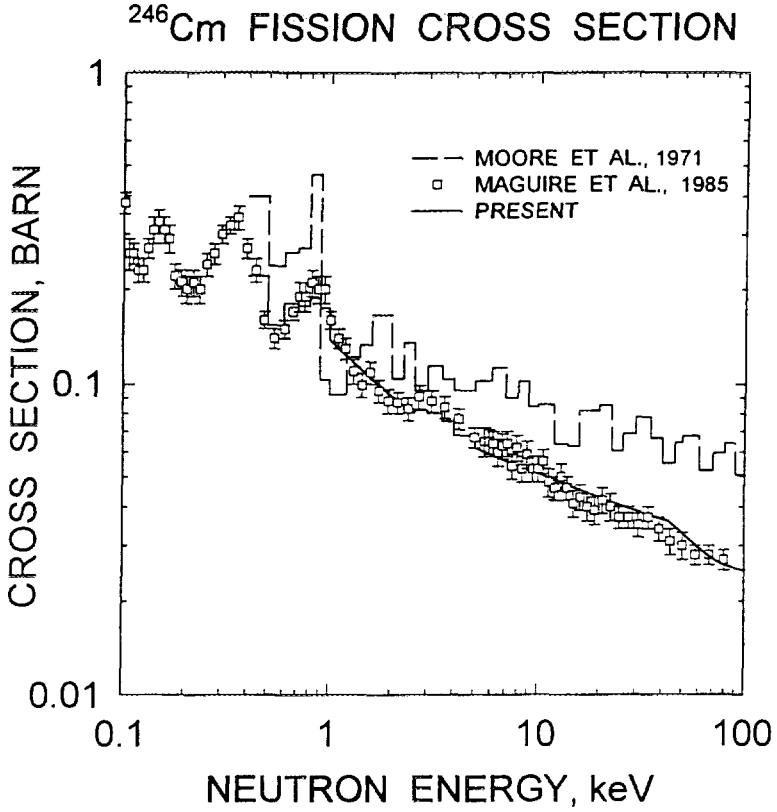
246Cm FISSION CROSS SECTION
MOORE ET AL., 1971
MAGUIRE ET AL., 1985
PRESENT
CROSS SECTION, BARN
1
0.1
0.01
0.1
1
10
100
NEUTRON ENERGY, keV

FIG.7

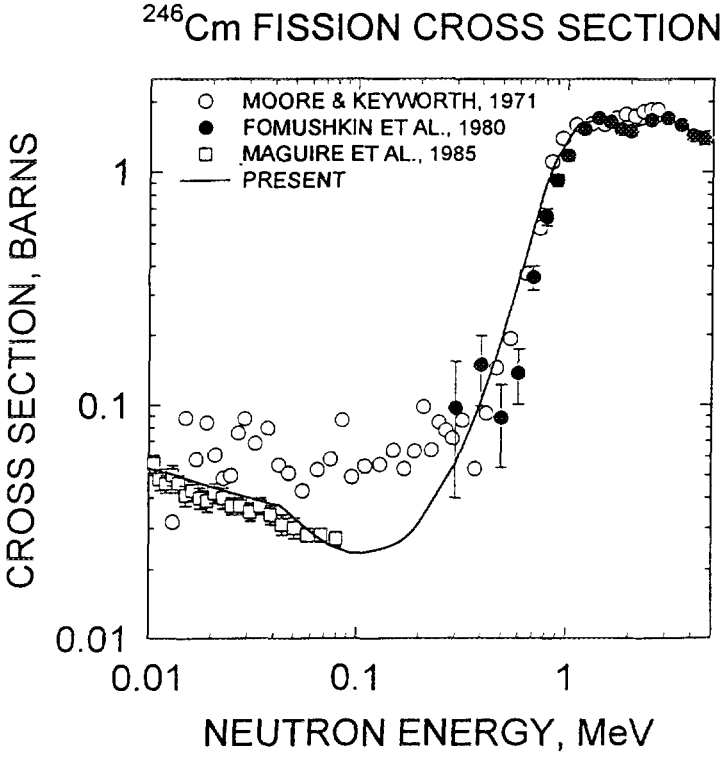
246Cm FISSION CROSS SECTION
MOORE & KEYWORTH, 1971
FOMUSHKIN ET AL., 1980
MAGUIRE ET AL., 1985
PRESENT
CROSS SECTION, BARNS
1
0.1
0.01
0.01
0.1
1
NEUTRON ENERGY, MeV

FIG. 8

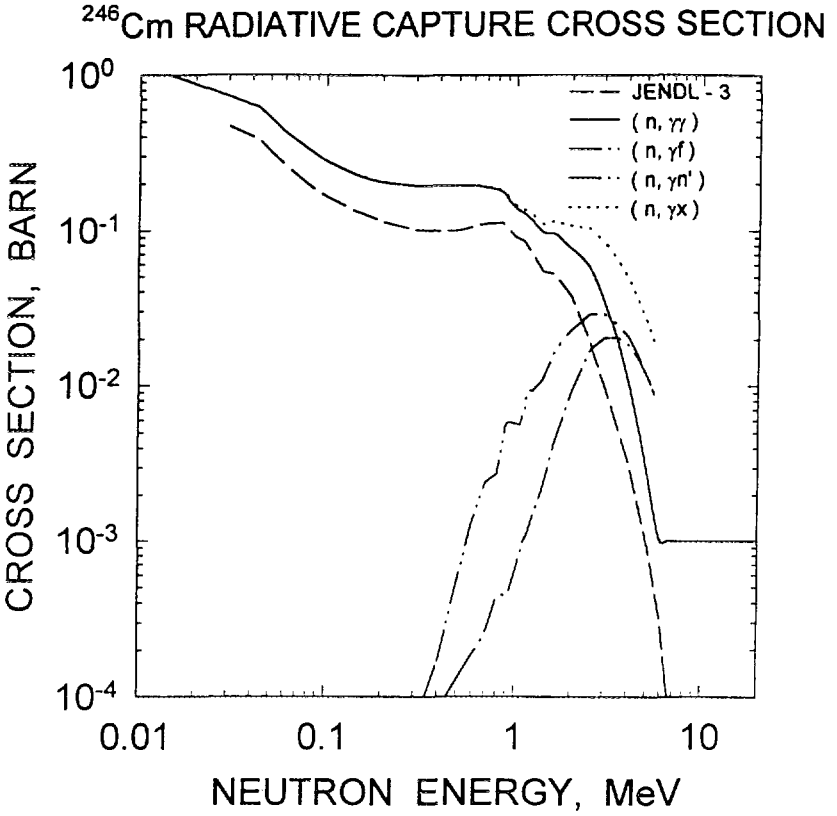
246Cm RADIATIVE CAPTURE CROSS SECTION
JENDL - 3
(n, γγ)
(n, γf)
(n, γn')
(n, γx)
CROSS SECTION, BARN
10^0
10^-1
10^-2
10^-3
10^-4
0.01
0.1
1
10
NEUTRON ENERGY, MeV

FIG. 9

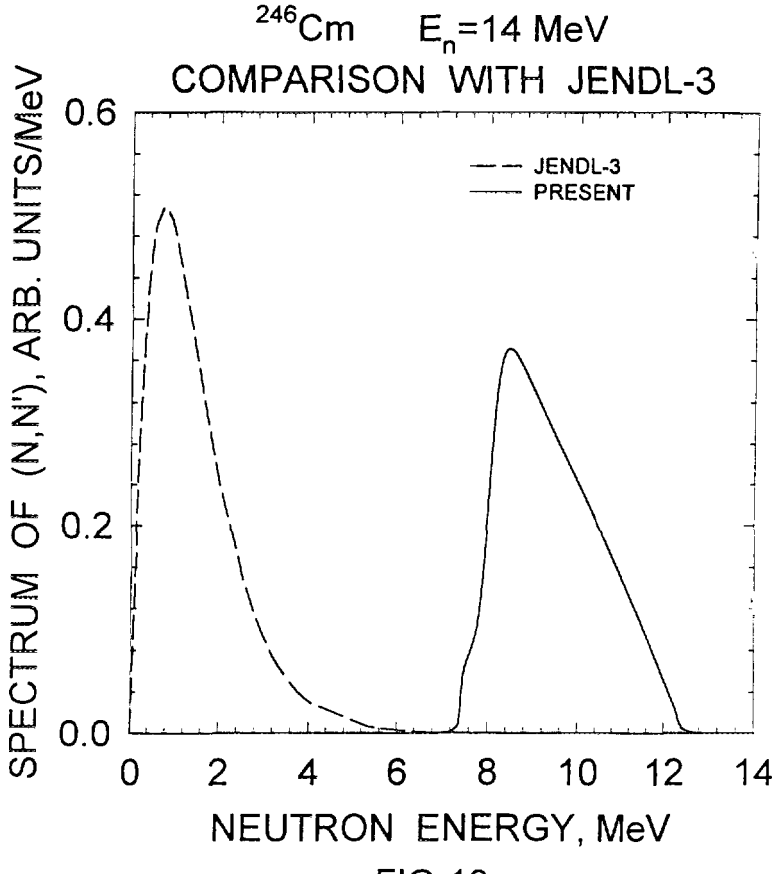
246Cm E_n=14 MeV
COMPARISON WITH JENDL-3
JENDL-3
PRESENT
SPECTRUM OF (N,N'), ARB. UNITS/MeV
0.6
0.4
0.2
0.0
0
2
4
6
8
10
12
14
NEUTRON ENERGY, MeV

FIG.10

12 Annex 2

Papers and reports, published in the reporting year

1. Maslov V.M., Porodzinskij Yu.V., Sukhovitskij E.Sh., Klepatskij A.B., Morogovskij G.B. "Evaluation of Neutron Data for Curium-243", INDC(BLR)-2, 1995.

2. Maslov V.M., Porodzinskij Yu.V., Sukhovitskij E.Sh., Klepatskij A.B., Morogovskij G.B. "Evaluation of Neutron Data for Curium-245", INDC(BLR)-3, 1996.

3. Maslov V.M., Porodzinskij Yu.V., Sukhovitskij E.Sh., Klepatskij A.B., Morogovskij G.B. "Evaluation of Neutron Data for Curium-246", INDC(BLR)-4, 1996.

EVALUATION OF NEUTRON DATA FOR CURIUM-243

Maslov V.M., Sukhovitskij E.Sh., Porodzinskij Yu.V.,
Klepatskij A.B., Morogovskij G.B.
Radiation Physics & Chemistry Problems Institute,
220109, Minsk-Sosny, Belarus

February 8, 1996

Abstract

The evaluation of neutron data for ^{243}Cm is made in the energy region from 10^{-5} eV up to 20 MeV. The results of the evaluation are compiled in the ENDF/B-VI format.

This work is performed under the Project agreement CIS-03-95 with the International Science and Technology Center (Moscow). The Financing Party for the Project is Japan. The evaluation was requested by Y. Kikuchi (JAERI).

EVALUATION OF NEUTRON DATA FOR CURIUM-246

Maslov V.M., Sukhovitskij E.Sh., Porodzinskij Yu.V.,
Klepatskij A.B., Morogovskij G.B.
Radiation Physics & Chemistry Problems Institute,
220109, Minsk-Sosny, Belarus

February 8, 1996

Abstract

The evaluation of neutron data for ^{246}Cm is made in the energy region from 10^{-5} eV up to 20 MeV. The results of the evaluation are compiled in the ENDF/B-VI format .

This work is performed under the Project Agreement CIS-03-95 with the International Science and Technology Center (Moscow). The Financing Party for the Project is Japan. The evaluation was requested by Y. Kikuchi (JAERI).

EVALUATION OF NEUTRON DATA FOR CURIUM-245

Maslov V.M., Sukhovitskij E.Sh., Porodzinskij Yu.V.,
Klepatskij A.B., Morogovskij G.B.
Radiation Physics & Chemistry Problems Institute,
220109, Minsk-Sosny, Belarus

November 23, 1995

Abstract

The evaluation of neutron data for ^{245}Cm is made in the energy region from 10^{-5} eV up to 20 MeV. The results of the evaluation are compiled in the ENDF/B-VI format .

This work is performed under the Project Agreement CIS-03-95 with the International Science and Technology Center (Moscow). The Financing Party for the Project is Japan. The evaluation was requested by Y. Kikuchi (JAERI).

1. 2 Evaluation of Secondary and Prompt Fission Neutron Spectra

Yu.V. Porodzinskij & E.Sh. Sukhovitskij
Radiation Physics & Chemistry Problems Institute
220109, Minsk-Sosny, Belarus

Abstract

A simple model allowing to split neutron emission spectra into reaction partials is suggested. Predicted spectra of $(n,n'\gamma),(n,n'f)$, etc appear to be much harder than usually evaluated.

Mechanism of neutron emission from excited nuclei being a matter of study by many authors is now well understood [1]. One does not find problems describing experimentally measured emitted neutrons energy distributions. Figures 1 and 2 show possible theoretical interpretation of experimental neutron emission spectra for neutrons with incident energies 6.1 and 14.05 MeV [2].

Theoretical spectra are the sum of neutron components in the decay chain $(A+1) \rightarrow A \rightarrow A-1 \rightarrow ...$ if possible. At each decay stage neutron emission competes with γ−emission and fission, that gives additional fission neutrons. First neutrons $N^1(E)$ are assumed to be emitted from pre-equilibrium and equilibrium nucleus. Second and third neutrons are considered to be emitted from equilibrated nuclei, added discrete lines of direct scattering (coupled channels calculations with coupling levels from four lower bands including $k = 2^+$ and $k = 0^-$) are broadened with the supposed experimental resolution.

Problems arise with the evaluation of the partial neutron emission spectra, according with the format requests. For high incident energy neutrons the spectrum of first emitted neutron must be divided among $(n,n'\gamma)$, $(n,n'f)$, and first neutron spectra of $(n,2n)$, $(n,3n)$, $(n,2n'f)$ ... reactions.

That means the correlation between the energy of the emitted neutrons and the later history of the nuclear decay must be controlled during such calculations.

This can be done easily if we do not take into account the angular momentum conservation. Here we suggest a very simplified method that was used in such calculations for the ISTC Project.

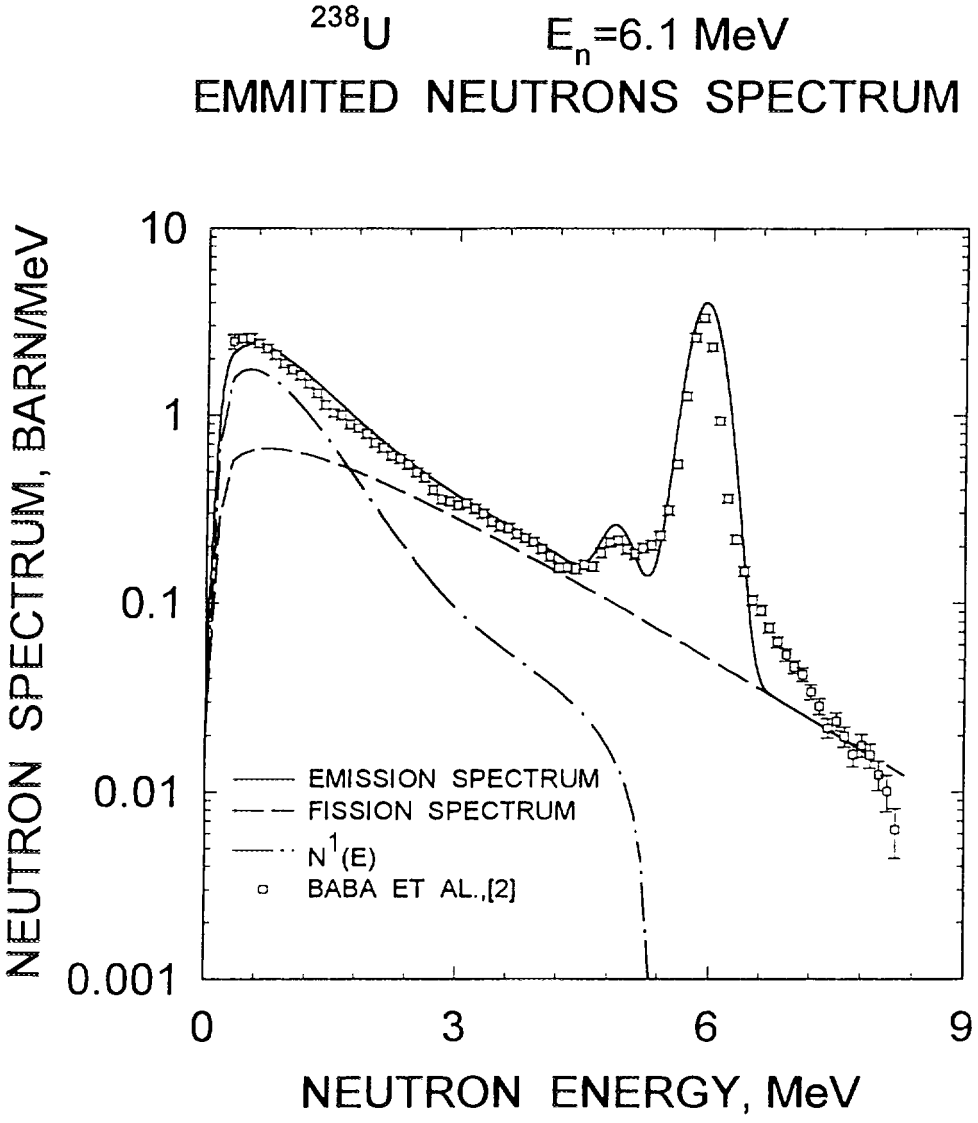
^{238}U E_n=6.1 MeV
EMMITED NEUTRONS SPECTRUM
NEUTRON SPECTRUM, BARN/MeV
10
1
0.1
0.01
0.001
0
3
6
9
NEUTRON ENERGY, MeV
EMISSION SPECTRUM
FISSION SPECTRUM
N^1(E)
BABA ET AL.,[2]

Figure 1:

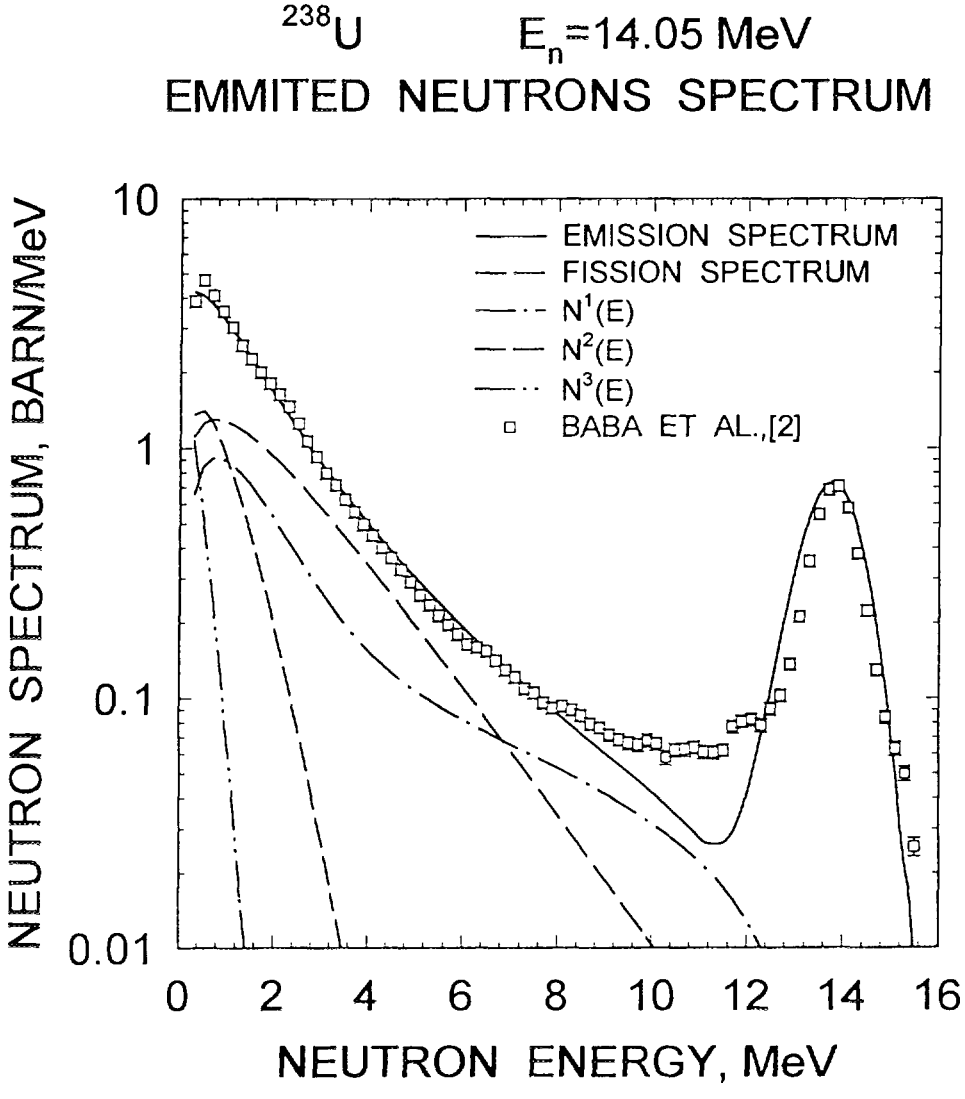
^{238}U E_n=14.05 MeV
EMMITED NEUTRONS SPECTRUM
EMISSION SPECTRUM
FISSION SPECTRUM
$N^1(E)$
$N^2(E)$
$N^3(E)$
BABA ET AL.,[2]
NEUTRON SPECTRUM, BARN/MeV
10
1
0.1
0.01
0
2
4
6
8
10
12
14
16
NEUTRON ENERGY, MeV

Figure 2:

Let us consider $N^1(E)$ to be the spectrum of the first emitted neutrons, then the spectrum of $(n, n'\gamma)$ process can be determined as:

$$N_{nn'\gamma}(E) = N^1(E)\frac{\Gamma^A_\gamma(E_n-E)}{\Gamma^A_{tot}(E_n-E)}, (1)$$

and the spectrum of the pre-fission neutrons of the $(n, n'f)$ reaction can be written as:

$$N_{nn'f}(E) = N^1(E)\frac{\Gamma^A_f(E_n-E)}{\Gamma^A_{tot}(E_n-E)}, (2)$$

while spectrum of the first neutrons of $(n, 2n)$ reaction:

$$N^1_{n,2n}(E) = N^1(E)P^1_{n,2n}(E_n, E), (3)$$

where

$$P^1_{n,2n}(E_n, E) = \begin{cases} 0, \ for\ E \geq E_n - B^A_n; \\ \int_0^{E_n-E-B^A_n} S^A(E_n-E,\varepsilon)\frac{\Gamma^{A-1}_\gamma(\varepsilon)}{\Gamma^{A-1}_{tot}(\varepsilon)}d\varepsilon, \ for\ E < E_n - B^A_n. \end{cases}$$

Spectrum of the first neutrons of $(n, 3n)$ reaction can be written as:

$$N^1_{n,3n}(E) = N^1(E)P^1_{n,3n}(E_n, E), (4)$$

where

$$P^1_{n,3n}(E_n, E) = \begin{cases} 0, \ for\ E \geq E_n - B^A_n - B^{A-1}_n; \\ \int_{B^{A-1}_n}^{E_n-E-B^A_n} S^A(E_n-E,\varepsilon_2)d\varepsilon_2 \int_0^{\varepsilon_2-B^{A-1}_n} S^{A-1}(\varepsilon_2,\varepsilon_3)\frac{\Gamma^{A-2}_\gamma(\varepsilon_3)}{\Gamma^{A-2}_{tot}(\varepsilon_3)}d\varepsilon_3, \\ for\ E < E_n - B^A_n - B^{A-1}_n. \end{cases}$$

Here E_n, E−incident and emitted neutron energies, B^A_n−neutron separation energy from A mass nucleus, $\Gamma^A_\gamma(E), \Gamma^A_f(E), \Gamma^A_{tot}(E)$−are radiation, fission and total widths accordingly, $S^A(E, E')$−probability for A mass nucleus with excitation E to emit a neutron with the energy $E - E' - B^A_n$ and become $A-1$ mass nucleus with excitation E'. In our assumption second and other neutrons are emitted from equilibrated nuclei, so its energy dependence follow the spectrum of neutrons emitted from equilibrated nucleus.

$$S^A(E,E') = f(E)\sigma^A_{comp}(E - B^A_n - E')(E - B^A_n - E')\rho(E'), (5)$$

where $\rho(E)$−level density of excited nucleus, $\sigma^A_{comp}(E)$−compound nucleus formation cross section, $f(E)$−function providing normalization of $S(E,E')$− probability, that appears to be

$$\int_0^{E-B^A_n} S^A(E,E')dE' = \frac{\Gamma^A_n(E)}{\Gamma^A_{tot}(E)} . (6)$$

Second neutron spectrum of $(n,2n)$ reaction can be written as:

$$N^2_{n2n}(E) = \int_{E+B^A_n}^{E_n} \chi^1(\varepsilon) S^A(\varepsilon, \varepsilon - B^A_n - E) \frac{\Gamma^{A-1}_\gamma(\varepsilon - B^A_n - E)}{\Gamma^{A-1}_{tot}(\varepsilon - B^A_n - E)} d\varepsilon, (7)$$

while second pre-fission neutron spectrum of $(n,2n'f)$ reaction

$$N^2_{n2n'f}(E) = \int_{E+B^A_n}^{E_n} \chi^1(\varepsilon) S^A(\varepsilon, \varepsilon - B^A_n - E) \frac{\Gamma^{A-1}_f(\varepsilon - B^A_n - E)}{\Gamma^{A-1}_{tot}(\varepsilon - B^A_n - E)} d\varepsilon, (8)$$

here $\chi^1(\varepsilon) = N^1(E_n - \varepsilon)$−spectrum of residual excitations in A mass nucleus after emitting the first neutron. All the other spectra may be presented in the analogous way.

It is quite understandable that the results of such calculations must be sensitive to the $N^1(E)$ spectrum form (ratio of pre-equilibrium and equilibrium components) and values of widths $\Gamma^A_i(\varepsilon)$, while any reasonable choice for the other parameters does not change the results notably. And results of our calculations corroborate this conclusion. That's why $N^1(E)$ and $\Gamma^A_i(E)$ incorporated in our model are taken from the calculations based on the most realistic physical assumptions about excited level densities with the parameters tested upon the available experimental data [3]. And what is more, predicted by both models cross sections $(n,n'\gamma)$, $(n,2n)$, $(n,n'f)$, $(n,3n)$, $(n,2n'f)$, etc. are controlled to coincide that guarantee the reliability of the predicted spectra.

Figures 3 and 4 demonstrate spectra of the first $N^1(E)$ and second $N^2(E)$ emitted neutrons for ^{238}U and partial spectra of the first and second neutrons accordingly. One can see that predicted $(n,n'\gamma)$ spectrum is very hard.

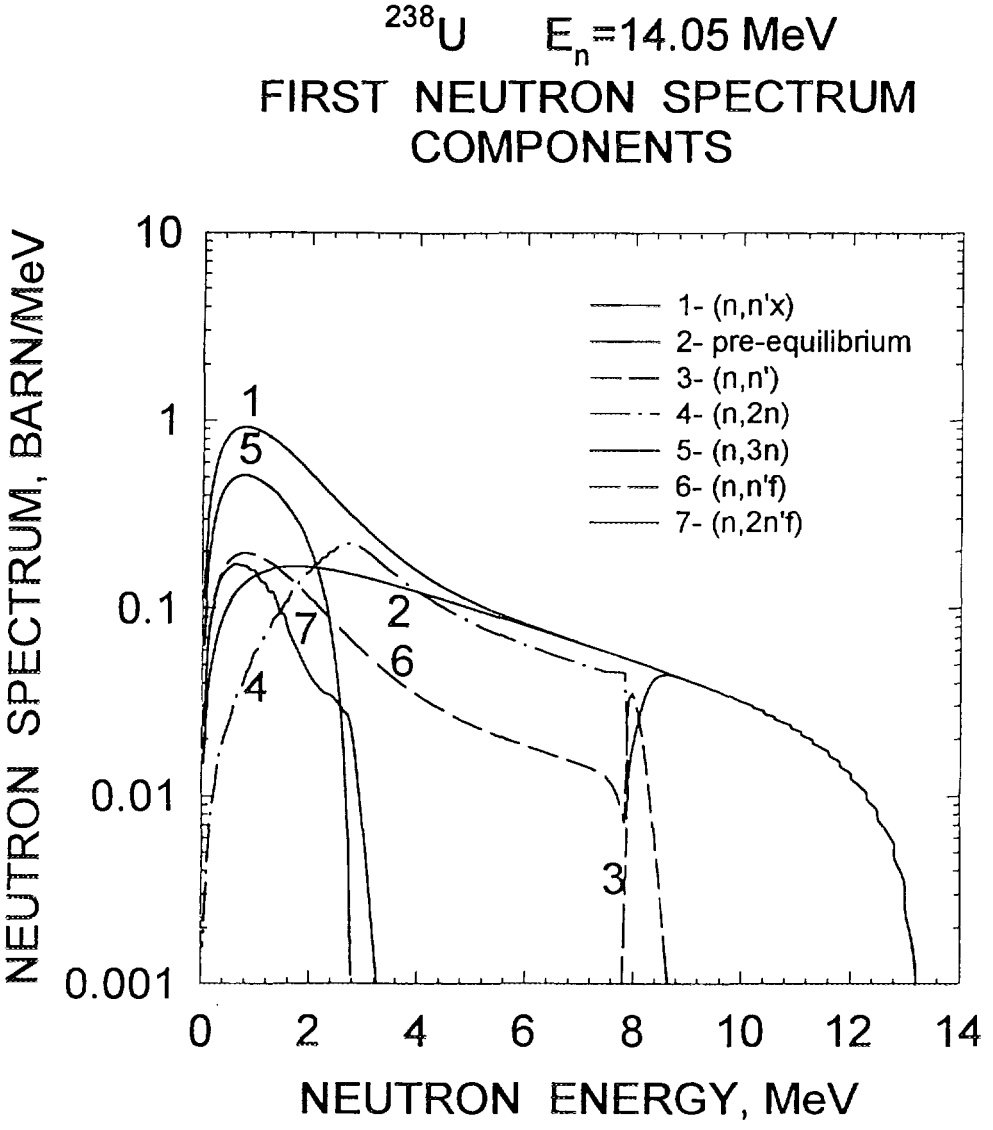
^{238}U E_n=14.05 MeV
FIRST NEUTRON SPECTRUM COMPONENTS
NEUTRON SPECTRUM, BARN/MeV
NEUTRON ENERGY, MeV
10
1
0.1
0.01
0.001
0
2
4
6
8
10
12
14
1- (n,n'x)
2- pre-equilibrium
3- (n,n')
4- (n,2n)
5- (n,3n)
6- (n,n'f)
7- (n,2n'f)
1
5
7
2
6
4
3

Figure 3:

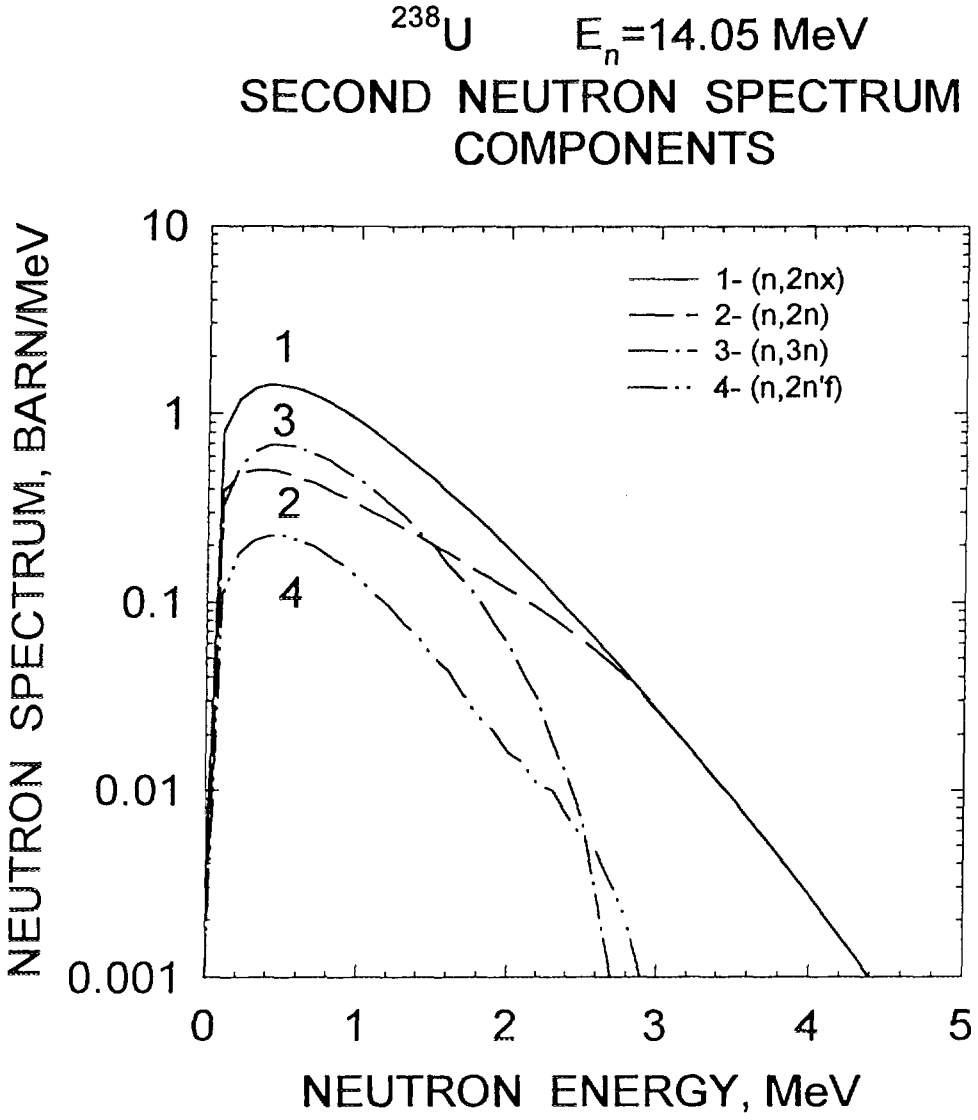
^{238}U E_n=14.05 MeV
SECOND NEUTRON SPECTRUM COMPONENTS
NEUTRON SPECTRUM, BARN/MeV
NEUTRON ENERGY, MeV
1- (n,2nx)
2- (n,2n)
3- (n,3n)
4- (n,2n'f)
10
1
0.1
0.01
0.001
0
1
2
3
4
5

Figure 4:

Table gives comparison of the predicted average partial spectra energies with the same values from ENDF/B-VI and JENDL-3 Libraries for ^{238}U. The differences are considerable.

Table. Comparison of the partial secondary neutron spectra average energies for ^{238}U

E_n, MeV	1st neutron average energy, MeV									
	n,n'			n,2n		n,n'f		n,3n		n,2n'f
	pres.	B-VI	J - 3	pres.	J - 3	pres.	B-VI	pres.	J - 3	pres.
3.0	0.60	0.29	0.59							
8.0	3.28	2.85	0.90	0.24	0.96	1.06	1.23			
14.0	9.73	9.24	1.25	3.57	1.38	2.28	1.98	1.07	1.31	1.08
20.0	15.7	15.2	1.51	10.3	1.66	3.71	2.64	2.65	1.66	2.59

E_n, MeV	2nd neutron average energy, MeV					3d neutron, MeV	
	n,2n		n,3n		n,2n'f		
	pres.	J - 3	pres.	J - 3	pres.	pres.	J - 3
8.0	0.34	0.66					
14.0	1.00	0.94	0.79	0.95	0.77	0.29	0.67
20.0	0.81	1.31	1.21	1.31	1.21	0.79	0.84

Reliable prediction of fission spectra and $\nu(E)$ requests the knowledge of pre-fission neutron spectra. In our calculations they are also much harder than these used in Madland-Nix calculations. Figure 5 shows evaluated fission spectra of ^{246}Cm, a bump at neutron emission energy about 13.5 MeV, can be understood as a result of pre-fission neutron spectra energy dependence. By now such bumps are measured for ^{235}U[4] and^{237}Np[5] and can be easily explained involving our pre-fission spectra.

References

[1]Gadioli E. and Hodgson P.E.,Pre-equilibrium Nuclear Reactions, Clarendon Press, Oxford,1992.

[2]Baba M. et al., J. Nucl. Sci. Techn.,27,601 (1989)

[3]Ignatjuk A.V., Maslov V.M., Proc. Int. Symp. Nuclear Data Evaluation Methodology, Brookhaven,USA,Oct.12-16,1992,p.440,Word Scientific,1993

[4]Bojkov G.S. et al., Atomnaja Energija, 69,23 (1990) (in Russian)

[5]Bojkov G.S. et al., Yadernaja Fizika,57,2126 (1994) (in Russian)

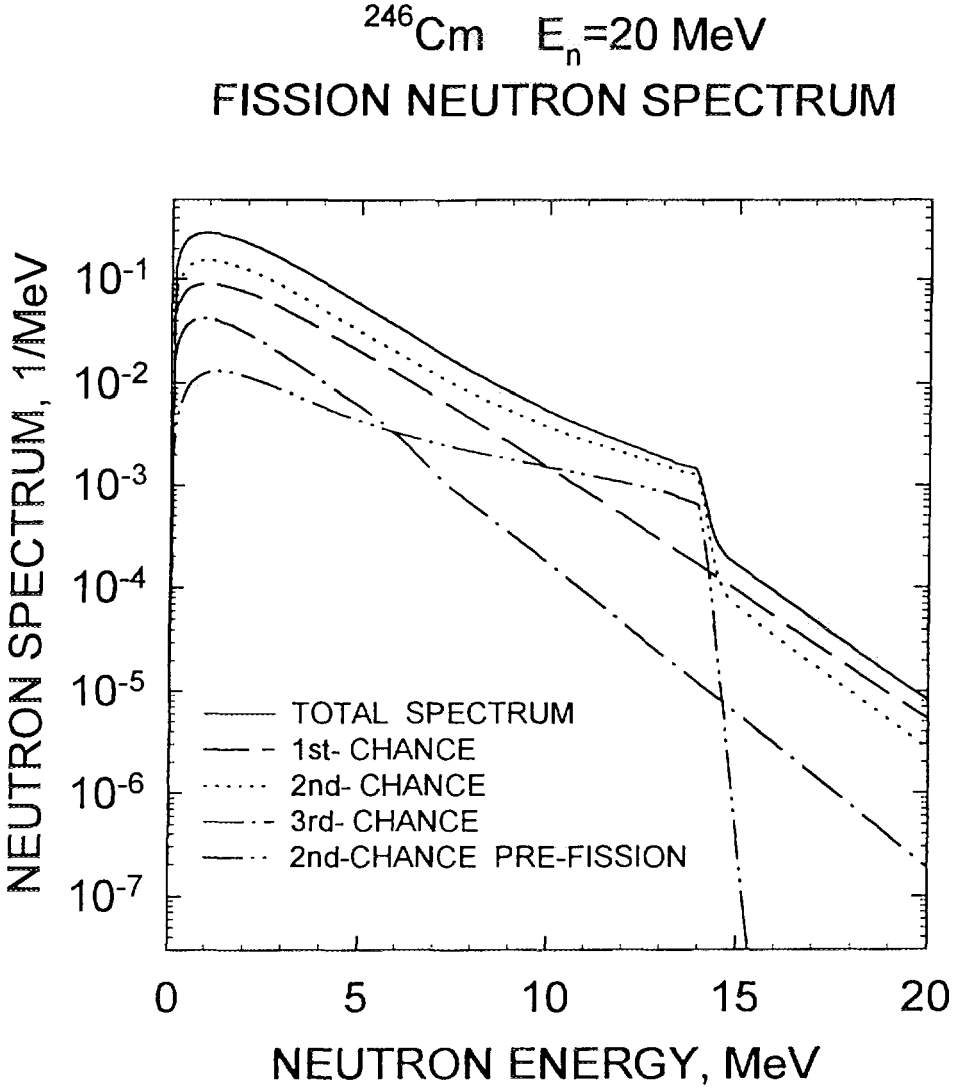
^{246}Cm E_n=20 MeV
FISSION NEUTRON SPECTRUM
NEUTRON SPECTRUM, 1/MeV
10^{-1}
10^{-2}
10^{-3}
10^{-4}
10^{-5}
10^{-6}
10^{-7}
TOTAL SPECTRUM
1st- CHANCE
2nd- CHANCE
3rd- CHANCE
2nd-CHANCE PRE-FISSION
0
5
10
15
20
NEUTRON ENERGY, MeV

Figure 5:

1. 3 Average Resonance Parameters Evaluation for Actinides

Yu.V. Porodzinskij & E.Sh. Sukhovitskij
Radiation Physics & Chemistry Problems Institute
220109, Minsk-Sosny, Belarus

Abstract

New evaluated $< \Gamma_n^0 >$ and $< D >$ values for ^{238}U,^{237}Np,^{243}Cm,^{245}Cm ,^{246}Cm and ^{241}Am nuclei in the resolved resonance region are presented. The applied method based on the idea that experimental resonance missing results in correlated changes of reduced neutron widths and level spacings distributions is discussed.

Evaluation of $< \Gamma_n^0 >$ and $< D >$ in the resolved resonance region used for adjusting input data of optical and statistical models and other applications is the starting point of such calculations making them more reliable. Simple averaging of existing resonance parameters does not seem to give reliable results even for thoroughly investigated nuclei, since due to poor experimental discrimination threshold and energy resolution some resonances are missed and thus $< D >$ and $< \Gamma_n^0 >$ are overestimated. Existing methods, taking missing into account [1-3], give the results different within quoted errors [4,5] using the same data bases. The drawback of these methods appears in separate consideration of the missing due to poor experimental energy resolution and discrimination threshold , although those two reasons of missing are correlated (two strong resonances are usually resolved even been situated close to each other, while weak resonance is shadowed by strong one and becomes unresolved).

Let us introduce the method that was developed for the determination of $< \Gamma_n^0 >$ and $< D >$. It is used in evaluations carried out for the ISTC Project.

Let us assume that reduced neutron widths and level spacings distributions are $f(x)$ and $\varphi(y)$ with $x = g\Gamma_n^0 / < g\Gamma_n^0 >$ and $y = D / < D >$ accordingly. We suppose reduced neutron widths and level spacings no correlating, hence $f(x)\varphi(y)$ is the distribution for resonances with the reduced

neutron width x to have neighbouring one at the distance y (this is the distance from one side of the resonance, for the sake of definition let it be from the left).

We also need to introduce an experimental probability $\Psi(x, y, E)$ to resolve the resonance with the reduced width x and the distance y to the neighbouring one in the vicinity of energy E. Now we can get the $f_1(x)$ distribution of the reduced neutron widths that were not missed during the experiment,

$$f_1(x) = \frac{f(x)}{E_2 - E_1} \int_{E_1}^{E_2} dE \int_0^\infty \varphi(y) \Psi(x, y, E) dy,$$

where E_1, E_2 are the lower and the upper boundaries of experimentally covered energy region. A - the portion of resonances resolved in the experiment can be found easily as $A = \int_0^\infty f_1(x)dx$. Of course $1 - A$ is the portion of the experimentally missed resonances. In analogous way we determine $\varphi_1(y)$:

$$\varphi_1(y) = \frac{\varphi(y)}{E_2 - E_1} \int_{E_1}^{E_2} dE \int_0^\infty f(x) \Psi(x, y, E) dx.$$

One can see that $\int_0^\infty \varphi_1(y)dy = A$, hence $f_1(x)$ and $\varphi_1(y)$ are normalized in the uniform correlated manner.

Let us now consider that missing of resonances results in resolving groups instead of isolated resonances. In our case we are taking into account grouping in doublets only hence $A > 0.5$. If energy resolution of the experiment is less than $< D >$ unresolved groups with three and more resonances have much lower probability. Missed level spacings distribution appears to be $\varphi(y) - \varphi_1(y)$. These level spacings are the distances between resonances in the unresolved doublets. In our assumptions these level spacings do not disappear, as they have common energy scale with the resolved , but are added to the neighbouring ones. As the result additional distribution $\varphi_2(y)$ is measured in experiment:

$$\varphi_2(y) = \frac{1}{A} \int_0^y [\varphi(z) - \varphi_1(z)] \varphi_1(y - z) dz.$$

Of course $\int_0^\infty \varphi_2(y)dy = 1 - A$. And at last we must take into account that distribution $\varphi_3(y)$ of the distances to which missed were added must be subtracted from experimentally measured distribution $\varphi_1(y)$. It is:

$$\varphi_3(y) = \varphi_1(y)\frac{1-A}{A}.$$

Now we can give the expected distribution of experimentally observed level spacings:

$$\varphi_{obs}(y) = [\varphi_1(y)(2 - 1/A) + \varphi_2(y)]/A.$$

Neutron reduced widths distribution transforms in the same correlated manner, since the area under the unresolved doublet is the sum of the areas under single resonances of the doublet. The areas are proportional to the reduced neutron widths, so:

$$f_2(x) = \frac{1}{A}\int_0^x [f(z) - f_1(z)]f_1(x-z)dz,$$

$$f_3(x) = f_1(x)\frac{1-A}{A}\ ,$$

$$f_{obs}(x) = [f_1(x)(2 - 1/A) + f_2(x)]/A.$$

Now we have to define $f(x)$, $\varphi(y)$ and $\Psi(x, y, E)$. For $f(x)$ we use:

$$f(x) = \frac{(1+\alpha)^{-3/2}}{\sqrt{2\pi x}}\{\frac{1}{\sqrt{g_1}}\exp[-\frac{x}{2g_1(1+\alpha)}] + \frac{\alpha^{3/2}}{\sqrt{g_2}}\exp[-\frac{x\alpha}{2g_2(1+\alpha)}]\}.$$

Please note that $x = \frac{g\Gamma_n^0}{<g\Gamma_n^0>}$, this is quite natural choice, since we usually get $g\Gamma_n^0$ from experiment. And for $\varphi(y)$ we use [6]:

$$\varphi(y) = \frac{\pi}{2}\{y[\frac{\alpha^3}{(1+\alpha)^3}\exp[-\frac{\pi}{4}y^2\frac{\alpha^2}{(1+\alpha)^2}]\,\mathrm{erf}\,c(\frac{\sqrt{\pi}}{2}y\frac{1}{1+\alpha})+$$

$$\frac{1}{(1+\alpha)^3}\exp[-\frac{\pi}{4}y^2\frac{1}{(1+\alpha)^2}]\,\mathrm{erf}\,c(\frac{\sqrt{\pi}}{2}y\frac{\alpha}{1+\alpha})]+$$

$$\frac{4\alpha}{\pi(1+\alpha)^2}\exp[-\frac{\pi}{4}y^2\frac{1+\alpha^2}{(1+\alpha)^2}]\},$$

where $\alpha = \frac{<D_{J_1}>}{<D_{J_2}>}$, $g_1 = \frac{2J_1+1}{2(2I+1)}$, $g_2 = \frac{2J_2+1}{2(2I+1)}$. Both distributions take into account possible existence of two systems of resonances with spins J_1, J_2 and $< D_{J_1} >$, $< D_{J_2} >$ accordingly. In case of one system of resonances they become the well known Porter-Thomas[7] and Wigner[8] distributions.

Resonance spacings distributions for one and two systems of levels differ considerably (see Fig.1). Resonances of the same spin are pushed apart, hence probability for resonance spacing for such resonances decreases as the latter decreases to zero. In the case of two spin level systems the resonances of different spins are not forced from each other, so you find no zero probability even for zero spacing value. This may result in much greater experimental resonance missing for odd nuclei.

The probability to resolve resonances in the experiment $\Psi(x,y,E)$ is modeled by:

$$\Psi(x,y,E) = \frac{1+a}{a+\exp[\frac{c\Delta(E)}{x^s y<D>}]} \frac{1}{(\frac{x_0}{x})^p+1} ,$$

where $\Delta(E)$ is experimental energy resolution, x_0-threshold of width discrimination, p-determines the slope of the threshold, s-correlation factor between weak resonance and poor resolution level missing, c -a constant, close to unity, a-normalization constant. Model function $\Psi(x,y,E)$ describes typical experimental situation. It decreases to zero when x , y , $x^s y$, $\frac{1}{x_0}$ or $\frac{<D>}{\Delta(E)}$ urge towards zero, and becomes unity when x, y,$x^s y$, $\frac{1}{x_0}$ or $\frac{<D>}{\Delta(E)}$are growing. $< D >, < g\Gamma_n^0 >$ and resolution function parameters are found by adjusting theoretically expected reduced neutron widths and level spacings distributions to experimental ones within framework of the best likelihood method with the computer code created on the base of the suggested approach.

Figures 2-5 show comparison of experimental and adjusted expected reduced neutron widths and level spacings distributions for ^{238}U and ^{237}Np nuclei. They were chosen as a test. Table gives evaluated values S_0 and $< D >$ for these nuclei and comparison with other evaluations. For the reasons already discussed $< D >$ for ^{237}Np is overestimated by other evaluators, as they do not take into account shadowing of the resonances of one spin by the other.

Table. Comparison of the evaluated <S_0> and <D> values with the data from other libraries

Nucleous	Exp.energy interval,keV	Portion of missed	Evaluated	
			$S_0 \times 10^4$,eV$^{-1/2}$	<D>,eV
^{238}U	0 - 6.0	0.100	1.033±0.087	19.29±0.57
^{237}Np	0 - 0.390	0.331	0.962±0.072	0.485±0.028
^{243}Cm	0 - 0.1	0.294	1.458±0.21	0.679±0.056
^{245}Cm	0 - 0.1	0.416	1.253±0.21	0.698±0.080
^{246}Cm	0 - 0.385	0.227	0.89±0.30	17.5±4.0*
^{241}Am	0 - 0.150	0.387	0.864±0.131	0.505±0.042

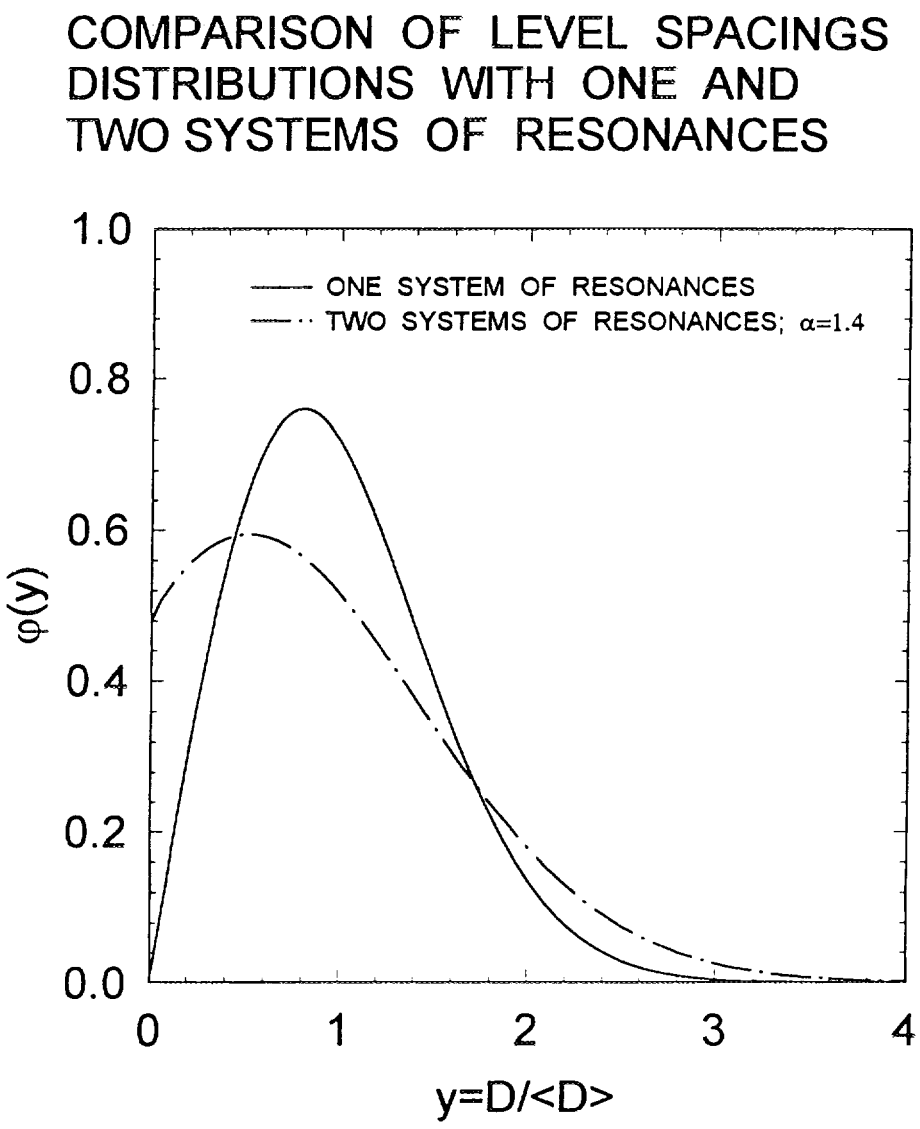
COMPARISON OF LEVEL SPACINGS DISTRIBUTIONS WITH ONE AND TWO SYSTEMS OF RESONANCES
ONE SYSTEM OF RESONANCES
TWO SYSTEMS OF RESONANCES; α=1.4
φ(y)
1.0
0.8
0.6
0.4
0.2
0.0
0
1
2
3
4
y=D/<D>

Figure 1:

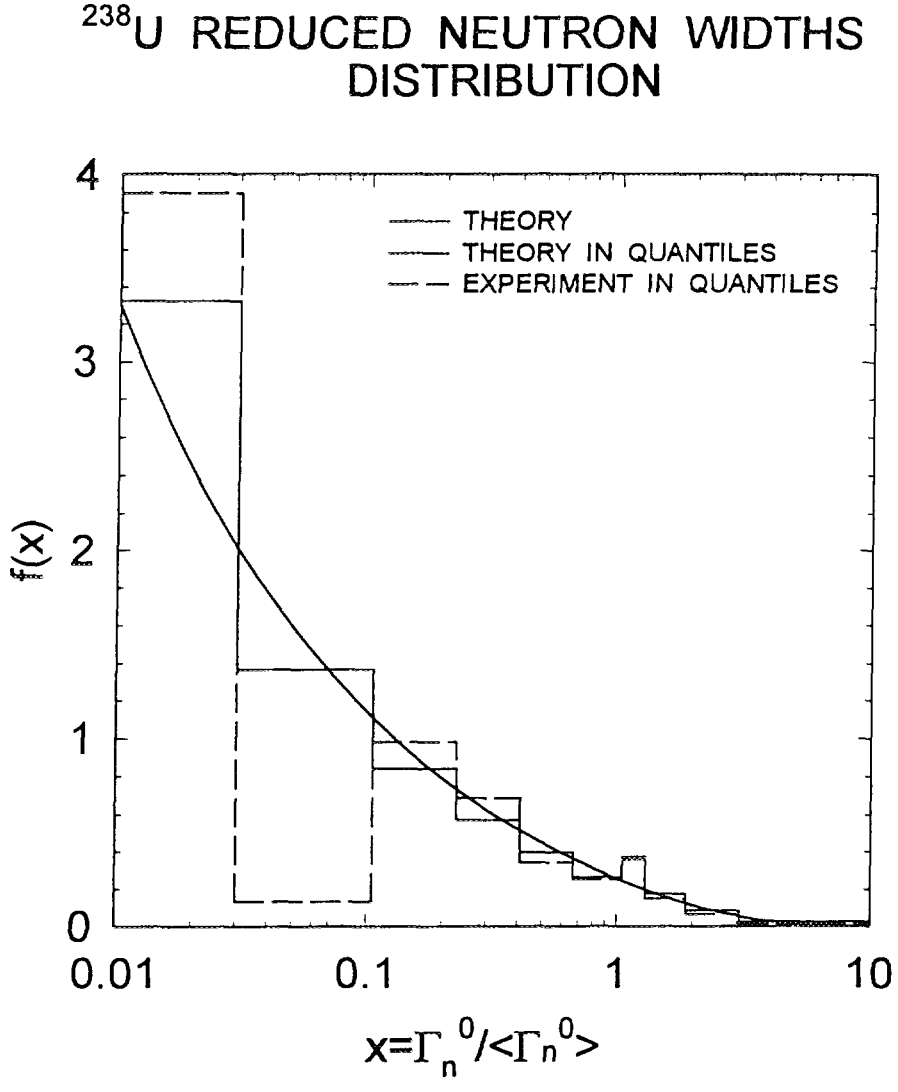
238U REDUCED NEUTRON WIDTHS DISTRIBUTION
THEORY
THEORY IN QUANTILES
EXPERIMENT IN QUANTILES
f(x)
0
1
2
3
4
0.01
0.1
1
10
x=Γn0/<Γn0>

Figure 2:

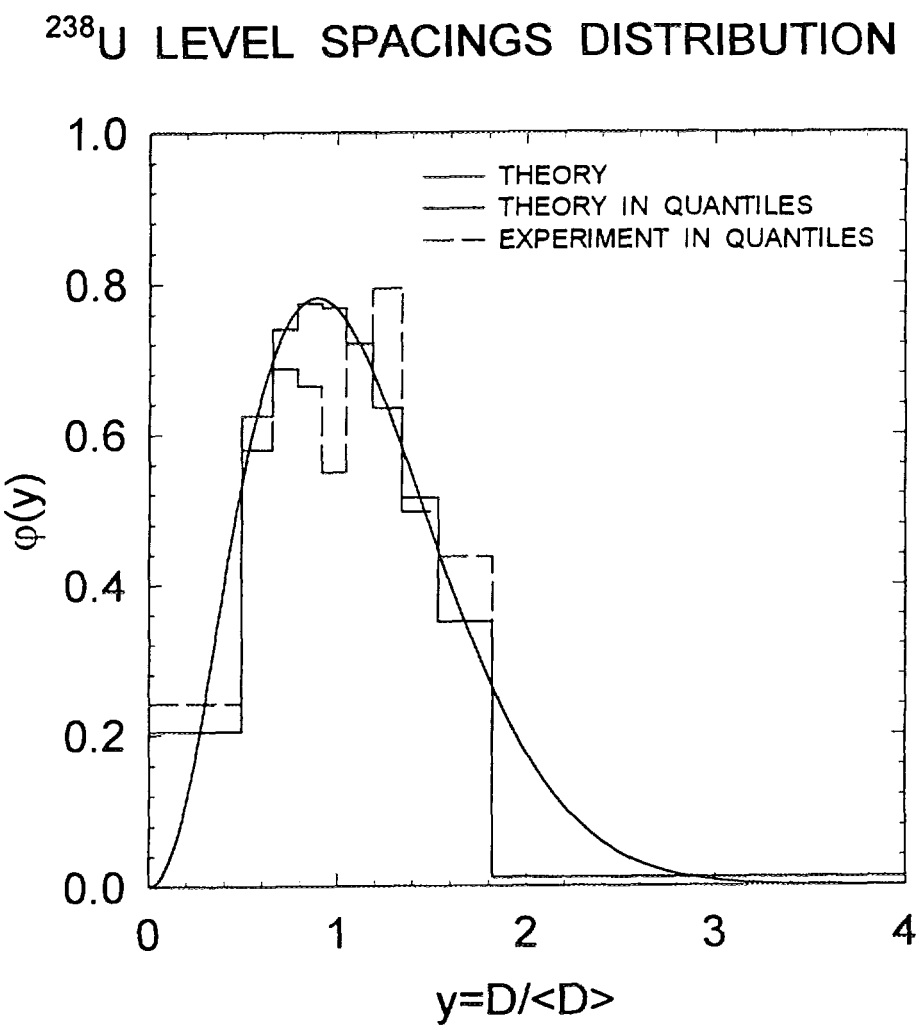
238U LEVEL SPACINGS DISTRIBUTION
THEORY
THEORY IN QUANTILES
EXPERIMENT IN QUANTILES
φ(y)
y=D/<D>
1.0
0.8
0.6
0.4
0.2
0.0
0
1
2
3
4

Figure 3:

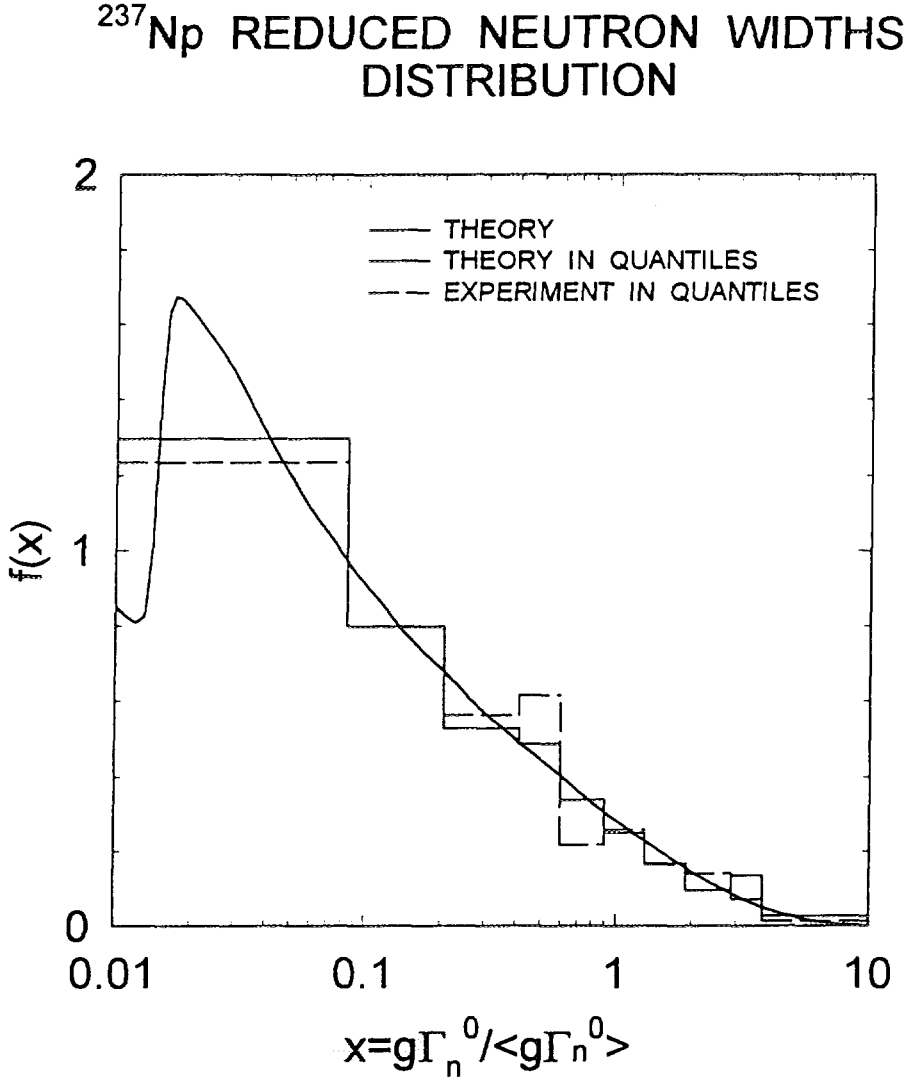
^{237}Np REDUCED NEUTRON WIDTHS DISTRIBUTION
THEORY
THEORY IN QUANTILES
EXPERIMENT IN QUANTILES
f(x)
2
1
0
0.01
0.1
1
10
x=gΓn0/<gΓn0>

Figure 4:

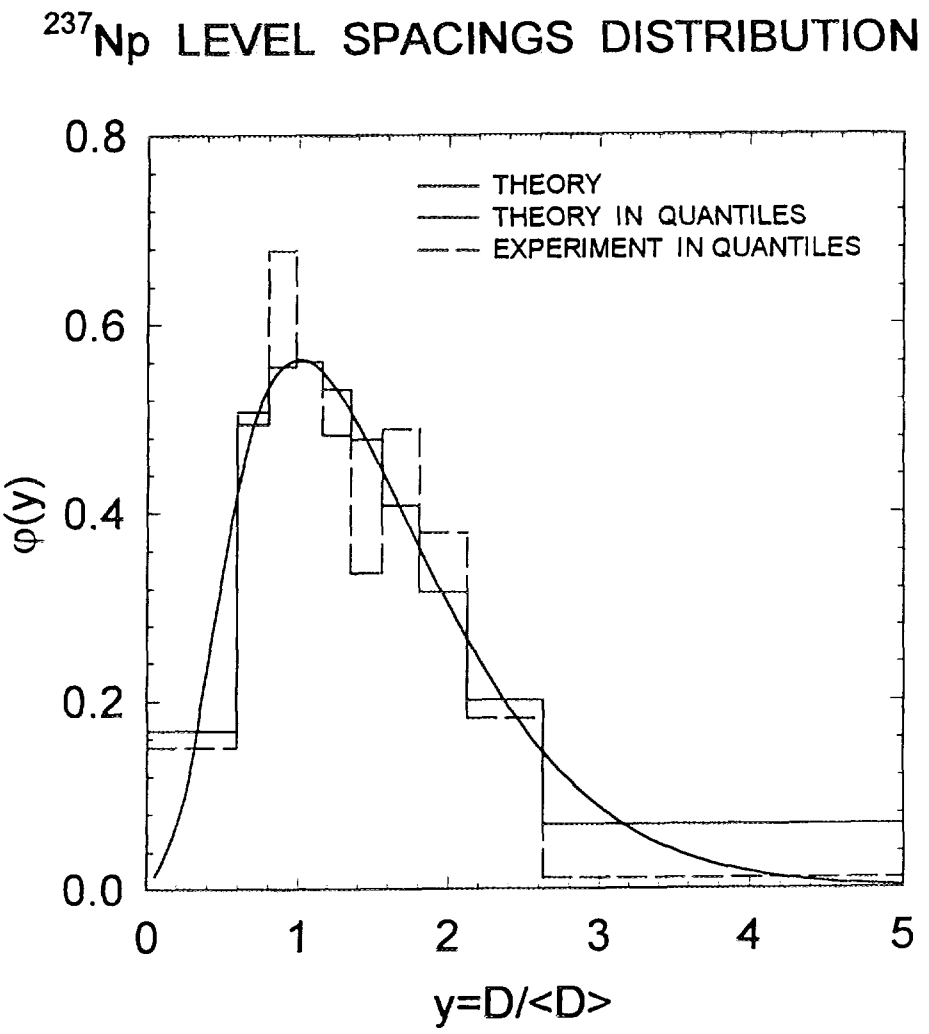
^{237}Np LEVEL SPACINGS DISTRIBUTION
THEORY
THEORY IN QUANTILES
EXPERIMENT IN QUANTILES
φ(y)
0.0
0.2
0.4
0.6
0.8
0
1
2
3
4
5
y=D/<D>

Figure 5:

BNL-235		JENDL-3		Obninsk	
$S_0 \times 10^4$,$eV^{-1/2}$	<D>,eV	$S_0 \times 10^4$,$eV^{-1/2}$	<D>,eV	$S_0 \times 10^4$,$eV^{-1/2}$	<D>,eV
1.2±0.1	20.9±1.1			1.15±0.12	21.7±0.9
1.02±0.06	0.52±0.04			0.99±0.12	0.56±0.05
1.30±0.26	1.1±0.2	1.5	0.8	1.3±0.4	0.81±0.10
1.18±0.27	1.4±0.1	1.18	1.4	1.1±0.2	1.38±0.10
0.50±0.16	34±7	0.94	31.7	0.6±0.2	30±5
0.90±0.09	0.55±0.05	0.967	0.432**	0.93±0.10	0.58±0.04

*with the account of the shadowing by the contamination isotopes in the sample.
**adjusted to $\sigma_{n\gamma}$ in the unresolved energy region.

Table also gives S_0 and $< D >$ values from nuclear data files requested by JAERI General Manager Y. Kikuchi and evaluated for the ISTC Project B-03.

One can see considerable differences. Our results seem to be more reliable as we use simultaneously both reduced neutron widths and level spacings distributions, transformations of which are considered correlating; account of missing allows to enlarge the involved data base, hence to improve statistics (data with up to 50% resonances missed can be taken into account); for odd nuclei it is more correct using right distribution for level spacings.

References

[1]Coceva C., Stefanon M., Nucl. Phys.,315, 1 (1979).

[2]Dyson P. H., Menta M. L., J. Math. Phys., 4, 701, (1963).

[3]Fröhner F.H., Proc. of the IAEA Consultants Meeting on Uranium and Plutonium resonance Parameters (Vienna,1981): IAEA, p.103, 1981.

[4]Ignatyuk A.V., Proc.1st Research Co-ordination Meeting on Development of Reference Input Parameter Library for Nuclear Model Calculations of Nuclear Data (Ravenna,1994): INDC (NDS-335), p.137, 1995.

[5]Reffo G. , Ibid, p.105.

[6]Jaynes F. J., Trans. Systems Sci. and Cybern., 4, 227, (1968).

[7]Porter C. E., Thomas R. G., Phys. Rev.., 104, 483, (1956).

[8]Wigner E. P., Proc. Conf. Appl. Math., Toronto, 483, (1959).

1. 4 Soft Rotator Model and ^{246}Cm Low-Lying Level Scheme

Yu.V. Porodzinskij & E.Sh. Sukhovitskij
Radiation Physics & Chemistry Problems Institute
220109, Minsk-Sosny, Belarus

Abstract

Non-axial soft rotator nuclear model is suggested as self-consistant approach for interpretation of level schemes, γ−transition probabilities and neutron interaction with even-even nuclei.

Non-axial $\beta-$ and γ−soft rotator model [1] was suggested to predict low-lying collective excitations of even-even nuclei. This model is based on the assumption that such excitations can be found as the energy eingenvalues of the nuclear Hamiltonian:

$$\widehat{H} = \frac{\hbar}{2B}\{\widehat{T}_\beta + \frac{1}{\beta^2}[\widehat{T}_\gamma + \widehat{T}_r]\} + \frac{\beta_0^4}{\beta^2}V(\gamma) + V(\beta),$$

while

$$\widehat{T}_\beta = -\frac{1}{\beta^4}\frac{\partial}{\partial\beta}(\beta^4\frac{\partial}{\partial\beta}), \widehat{T}_\gamma = -\frac{1}{\sin^3\gamma}\frac{\partial}{\partial\gamma}(\sin^3\gamma\frac{\partial}{\partial\gamma}) \text{ and } \widehat{T}_r = \frac{1}{4}\sum_{\lambda=1}^{3}\frac{\widehat{I}_\lambda^2}{\sin^2(\gamma-2\pi\lambda/3)}.$$

The solution is obtained in the flow of Davydov-Chaban [2] idea that soft nucleus is stretched due to rotations, hence equilibrium oscillator deformations change for different excited rotational states. These equilibrium oscillator deformations are usually growing as spin J of excited level is growing. In our case we managed to take into consideration soft quadrupole $\beta-$ and $\gamma-$ vibrations, and existence of rigid hexadecapole deformation. An attempt is also made to take into account (in a rather rough approximation) octupole nuclear deformability ξ [3]. Formulas for collective excitation energies and wave functions are too complicated to show them here, all the details can be found in [1,3]. Figures 1, 2 demonstrate comparison of experimental and levels calculated within the framework of our method for ^{238}U and ^{76}Se nuclei. It is seen that all the levels of positive parity up to the

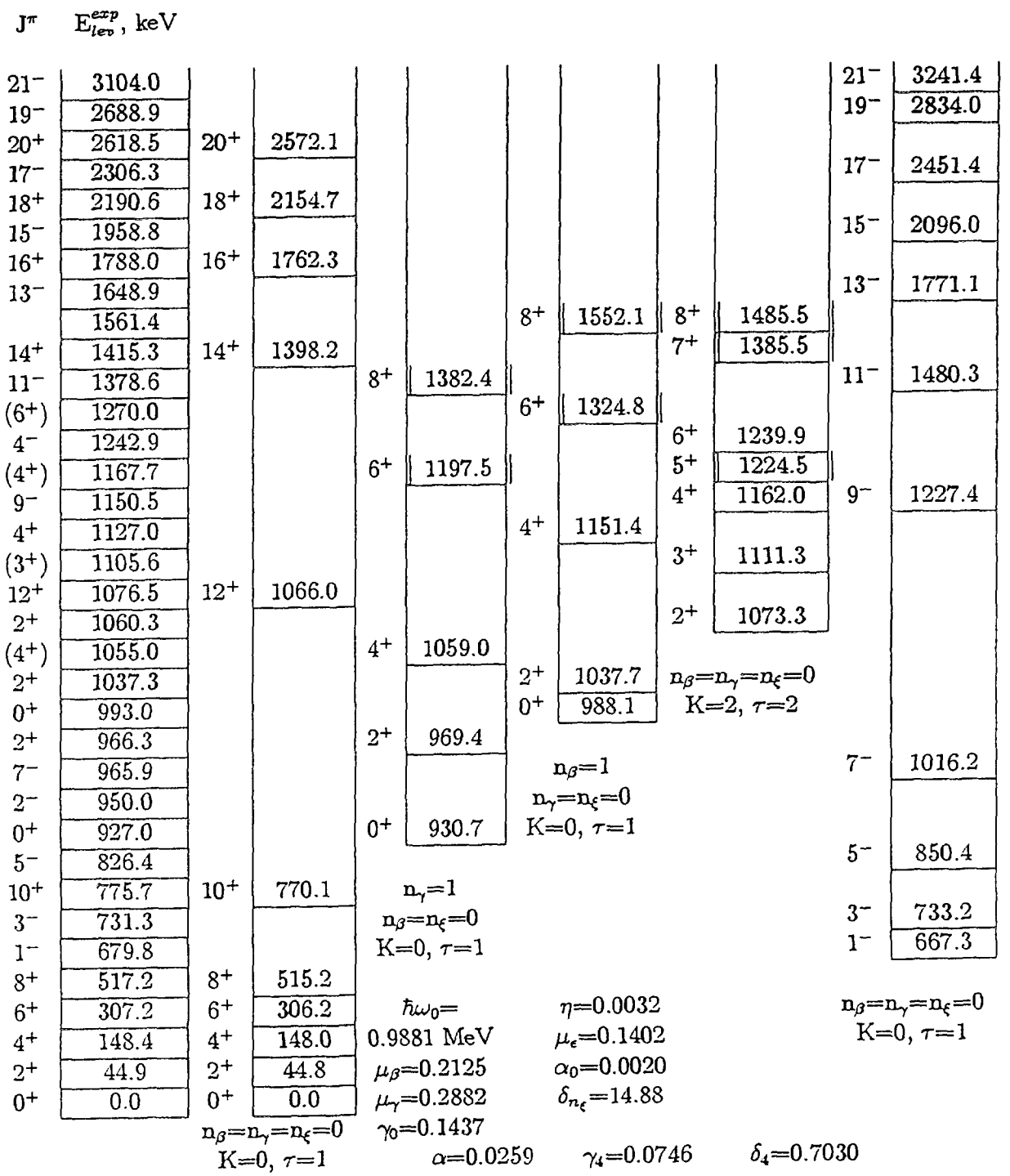

Figure 1. Comparison of experimental and predicted ^{238}U level scheme.

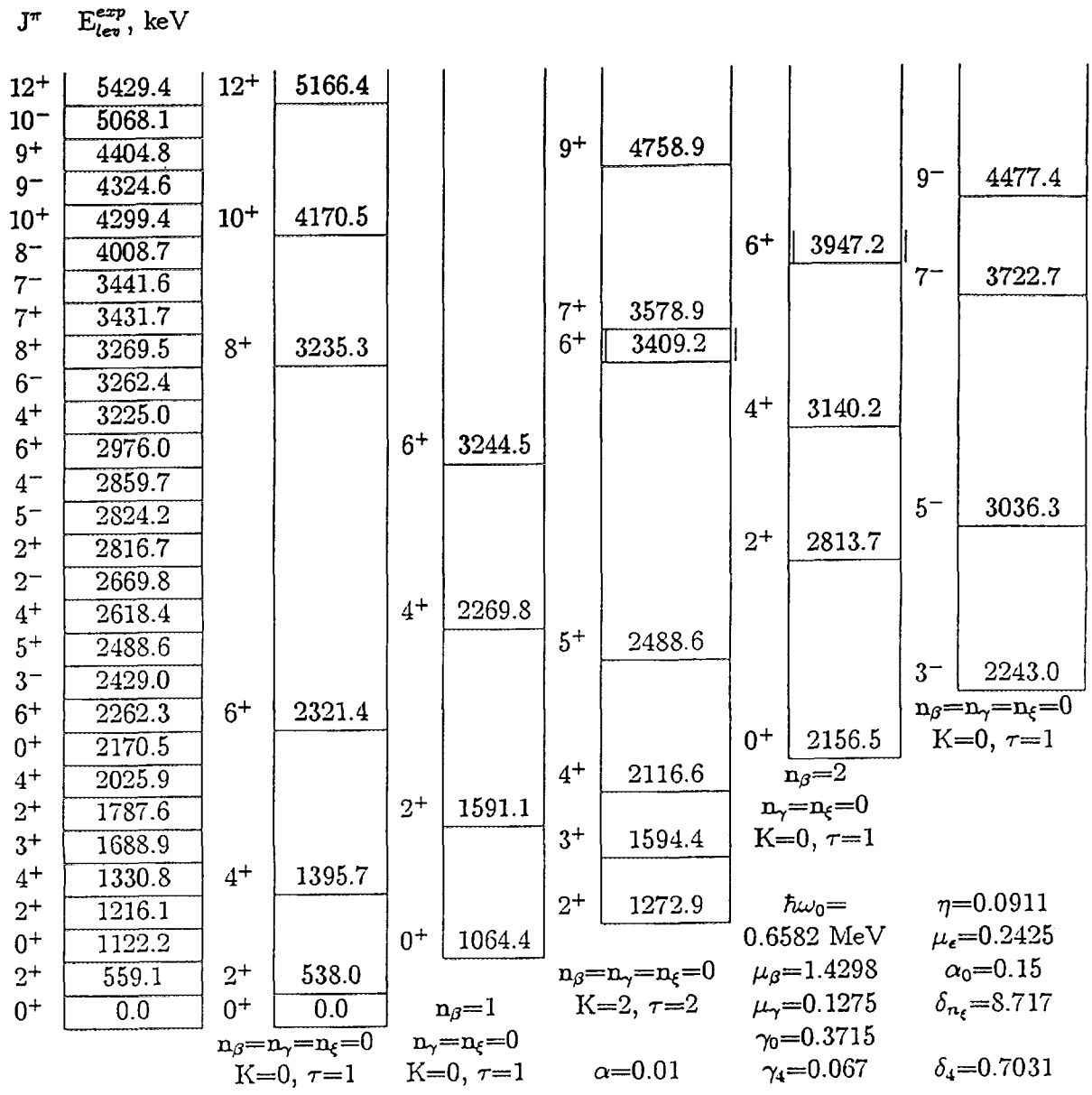

Figure 2. Comparison of experimental and predicted ^{76}Se level scheme.

2 MeV and 5 MeV excitation energies accordingly (at least 4 rotational bands) are predicted with good accuracy. Account of octupole vibrations is very rough in our model, hence we can describe only K=0^- band levels of negative parity (energy sequence of K=2^- band levels is also predicted, but the energy of the K=2^- head is usually not right). Table 1 gives the comparison of experimental and calculated γ−transition probabilities. They were calculated in homogeneously charged soft ellipsoid approximation. One can see that agreement is not so bad.

Table 1. Comparison of experimental and calculated γ−transition probabilities.

^{238}U					
B(E2;i-f),e^2b^2		B(E3;i-f),e^2b^3		B(E4;i-f),e^2b^4	
$0^+(0.0)$-$2^+(44,9)$		$0^+(0.0)$-$3^-(731.3)$		$0^+(0.0)$-$4^+(148.4)$	
experim.	calc.	experim.	calc.	experim.	calc.
11.7±0.8	11.15	0.50±0.06	0.112	0.69±0.0.37	0.62
11.7±0.15		0.54±0.07			
12.30±15		0.64±0.06			
12.70±0.17		0.49±0.07			
$6^+(307.2)$-$8^+(517.2)$					
4.7±0.6	5.00				
$8^+(517.2)$-$10^+(775.7)$					
5.2±0.5	5.07				
$24^+(3534.4)$-$26^+(4017.4)$					
5.6±0.13	7.38				
$0^+(0.0)$-$2^+(1037.7)$					
0.1150±0.0164	0.15				

^{76}Se			
B(E2;i-f),e^2b^2		B(E3;i-f),e^2b^3	
$0^+(0.0)$-$2^+(559.1)$		$3^-(2429.0)$-$0^+(0.0)$	
experim.	calc.	experim.	calc.
0.4230±0.0050	0.4103	0.0057±0.0007	0.0049

We think all this proves that nuclear wave functions of our model are reliable enough to be used to build coupling scheme for coupled-channels calculations.

Such code was created by us. Deformed optical potential of the model is expanded in the power series of deformed radius to get it's $\beta-$, $\gamma-$ and

ξ−deformation parameters dependence. Comparing arising coupling scheme with that from standard oscillator approach [4] one can see that effective deformations are changed in our model by matrix elements $\langle i|\beta^{\lambda}|f\rangle$, $\langle i|\gamma^{\lambda}|f\rangle$, $\langle i|\xi^{\lambda}|f\rangle$. In these matrix elements $|i\rangle$ and $|f\rangle$ are nuclear Hamiltonian wave functions for initial and final states, λ−is the power of expansion. Of course matrix elements are different for different states and they are usually growing with the spin J of the level. This results in predicted redistribution of scattered neutrons. A possibility of reliable ^{238}U experimental optical data interpretation within the framework of the suggested approach was demonstrated elsewhere [5]. Figs. 3-9 show comparison of experimental and calculated angular distributions of neutrons scattered by ^{76}Se nuclei. Coupling of five lower levels (0^+, 2^+, 0_2^+,2_2^+, 4^+) plus negative parity level (3^-) is considered in our calculations. Scattering with excitation of negative parity level of ^{76}Se is also in agreement with experiment(Fig. 9).

Suggested model takes into account complicated collective motions that are combinations of rotations and vibrations, while in the standard approach two models (rigid rotator and oscillator) exist separately. Parameters of nuclear Hamiltonian in our approach are adjusted to predict experimental level scheme and γ−transition probabilities. Hence we consider our coupled-channels scheme much more realistic.

Let us discuss the principal advantages of our approach. Table 2 presents the results of coupled-channels optical cross section calculations in the standard rigid rotator approach with the optical potential parameters [6] for ^{238}U

Table 2. Results of coupled-channels optical cross section calculations with different coupling.

Coupling	S_0	S_1	σ_t,b		σ_{abs},b	
scheme	$\times 10^4$		250keV	1.3MeV	250keV	1.3MeV
0^++2^+	0.802	0.737	9.30	6.35	1.74	2.28
0^++2^++4^+	0.962	1.963	10.28	7.02	3.35	3.34
0^++.....+6^+	1.216	2.231	10.81	7.06	3.53	2.98
0^++....+8^+	1.216	1.979	10.37	6.94	3.36	3.04
0^++....+10^+	1.217	1.978	10.38	6.96	3.36	3.06

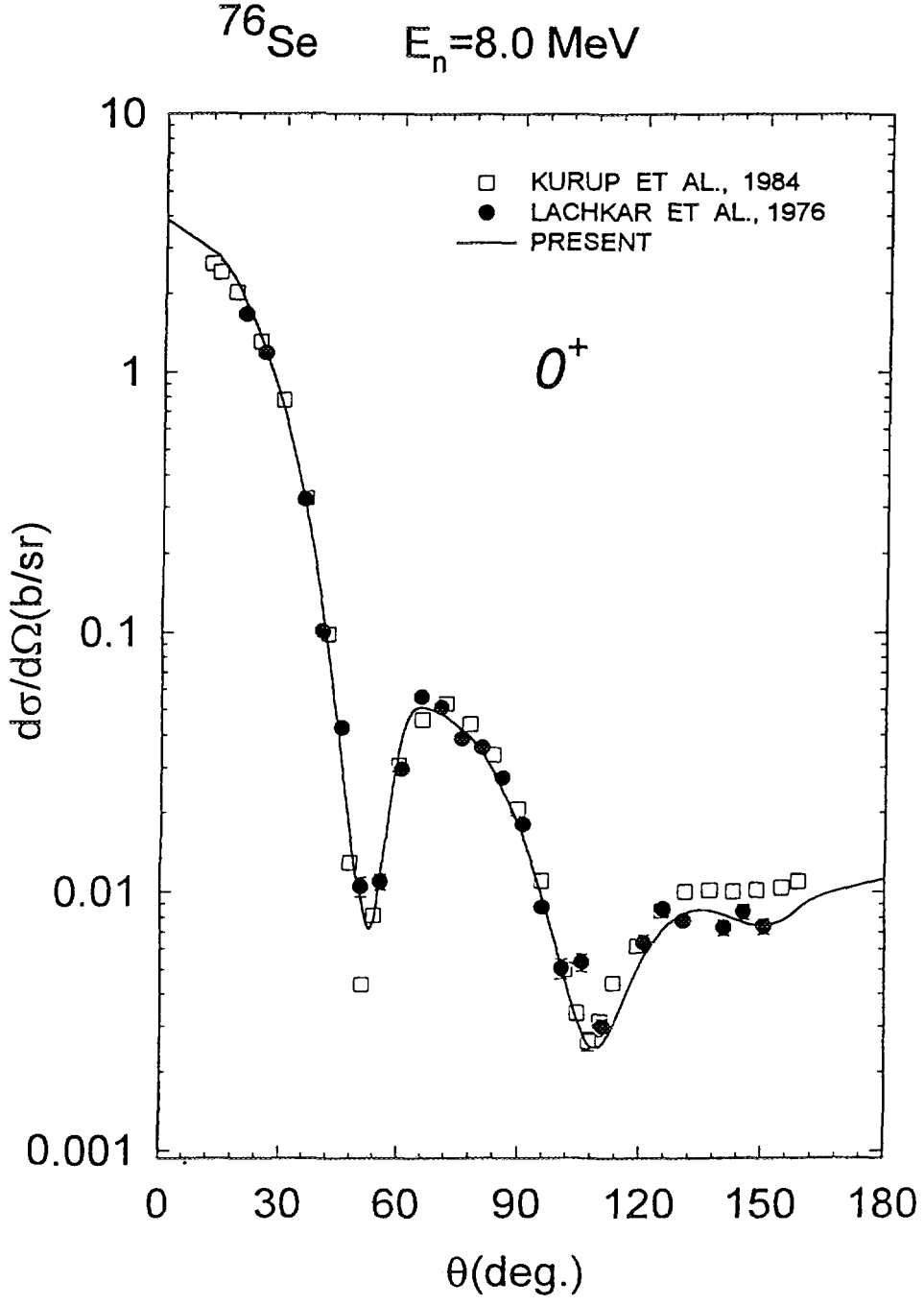
^{76}Se E_n=8.0 MeV
KURUP ET AL., 1984
LACHKAR ET AL., 1976
PRESENT
0^+
10
1
0.1
0.01
0.001
dσ/dΩ(b/sr)
0
30
60
90
120
150
180
θ(deg.)

Figure 3.

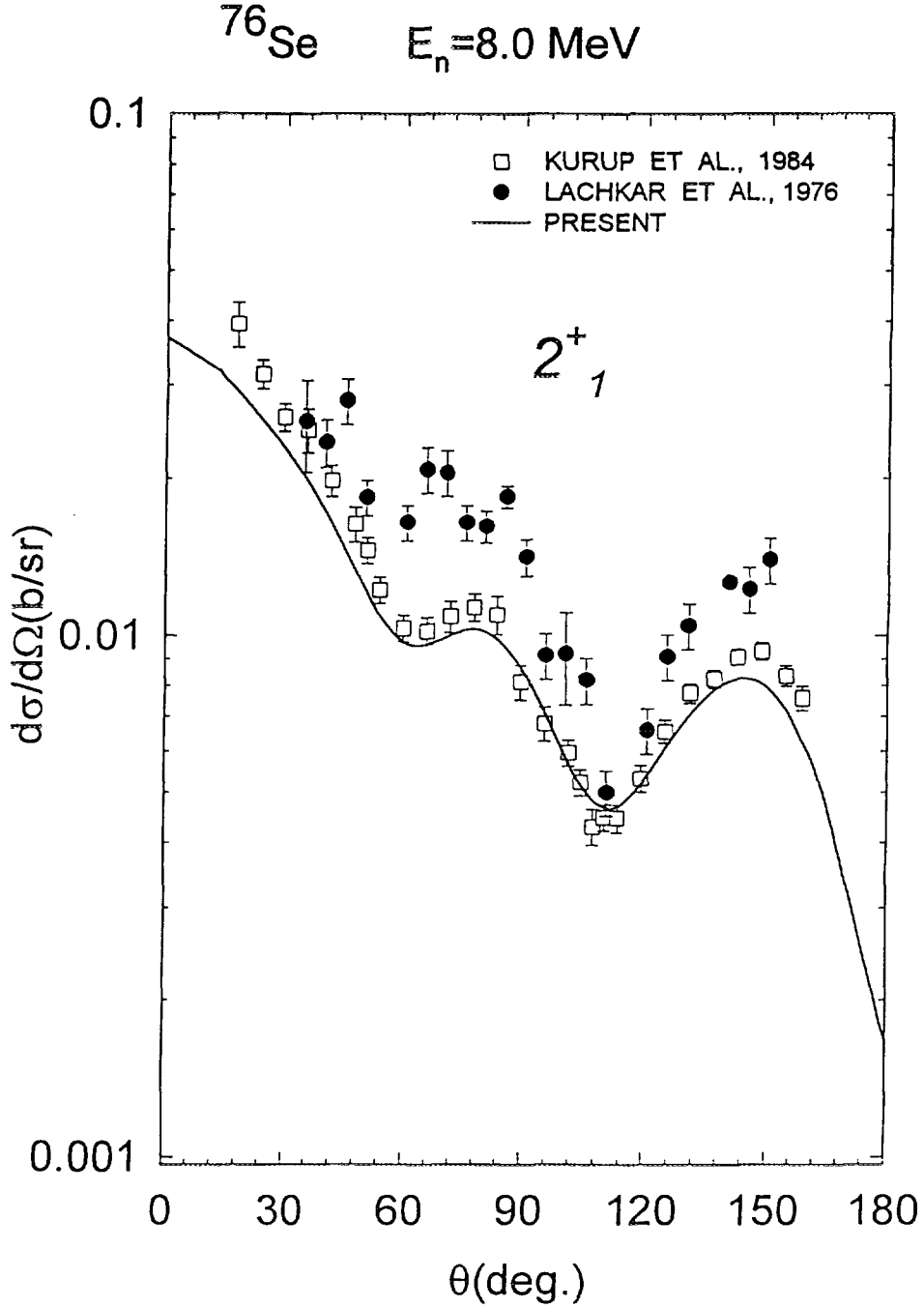
^{76}Se E_n=8.0 MeV
KURUP ET AL., 1984
LACHKAR ET AL., 1976
PRESENT
2^+_1
0.1
0.01
0.001
dσ/dΩ(b/sr)
0
30
60
90
120
150
180
θ(deg.)

Figure 4.

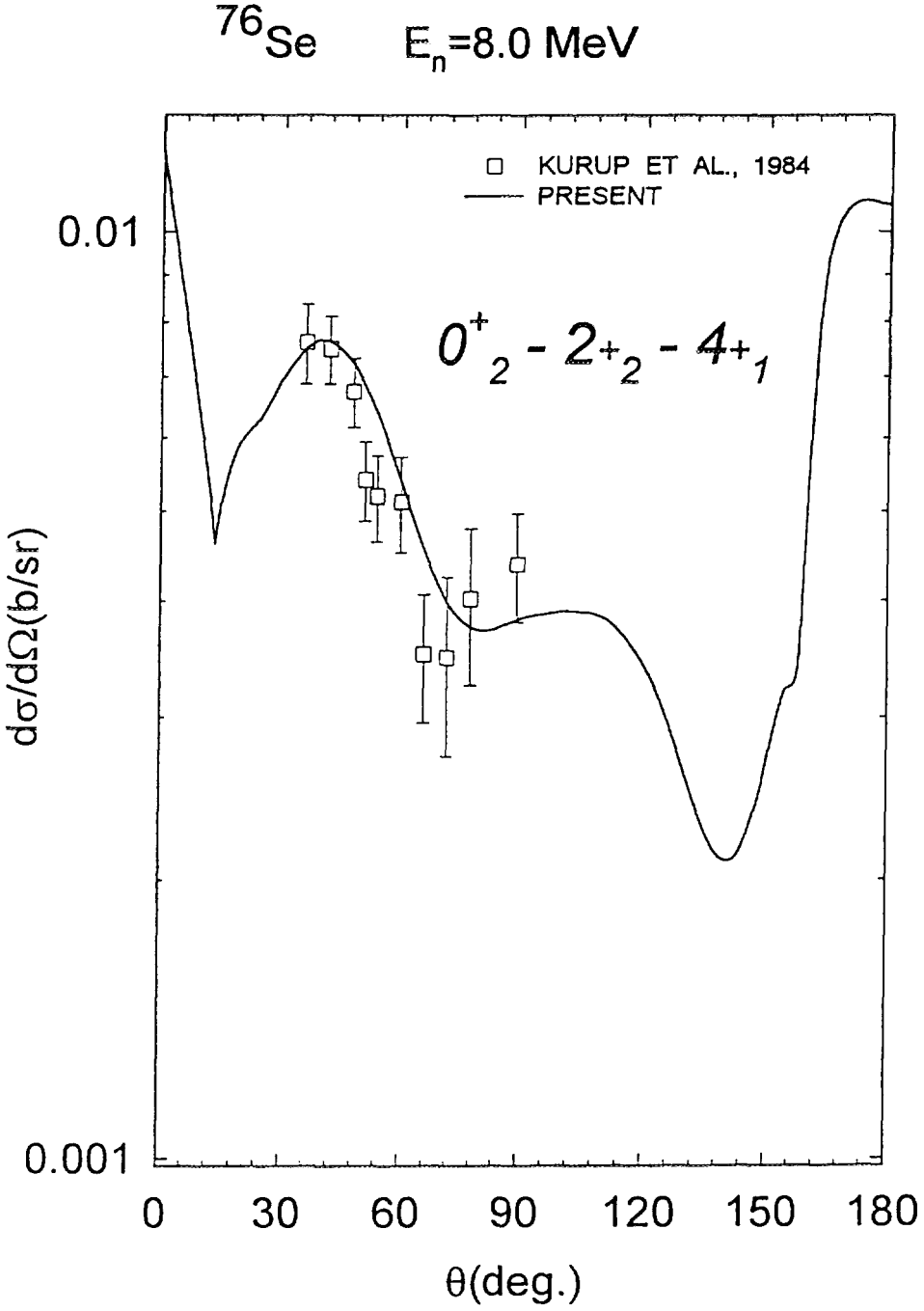
^{76}Se E_n=8.0 MeV
KURUP ET AL., 1984
PRESENT
0^+_2 - 2^+_2 - 4^+_1
0.01
0.001
dσ/dΩ(b/sr)
0
30
60
90
120
150
180
θ(deg.)

Figure 5.

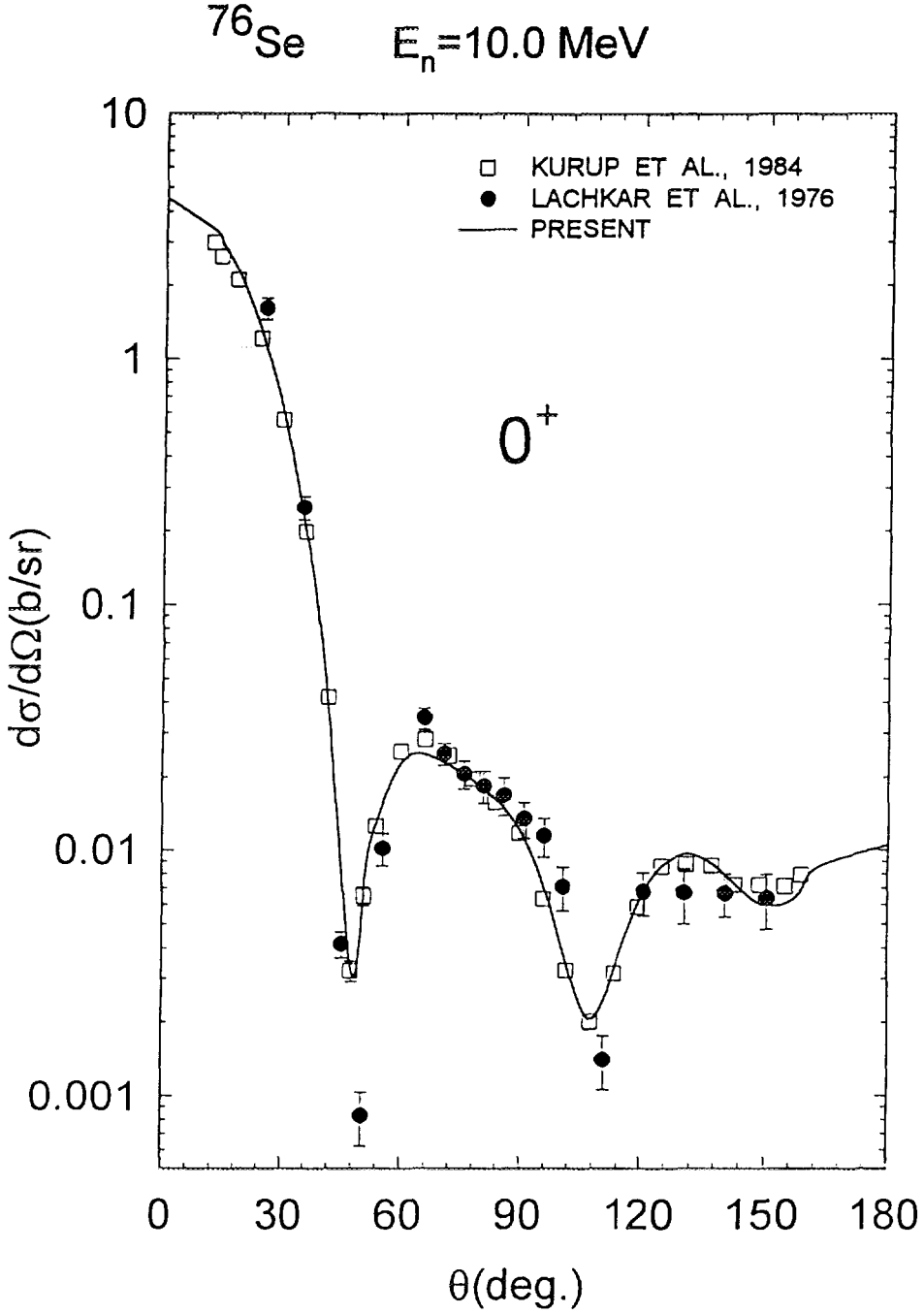
^{76}Se E_n=10.0 MeV
KURUP ET AL., 1984
LACHKAR ET AL., 1976
PRESENT
0^+
dσ/dΩ(b/sr)
θ(deg.)
10
1
0.1
0.01
0.001
0
30
60
90
120
150
180

Figure 6.

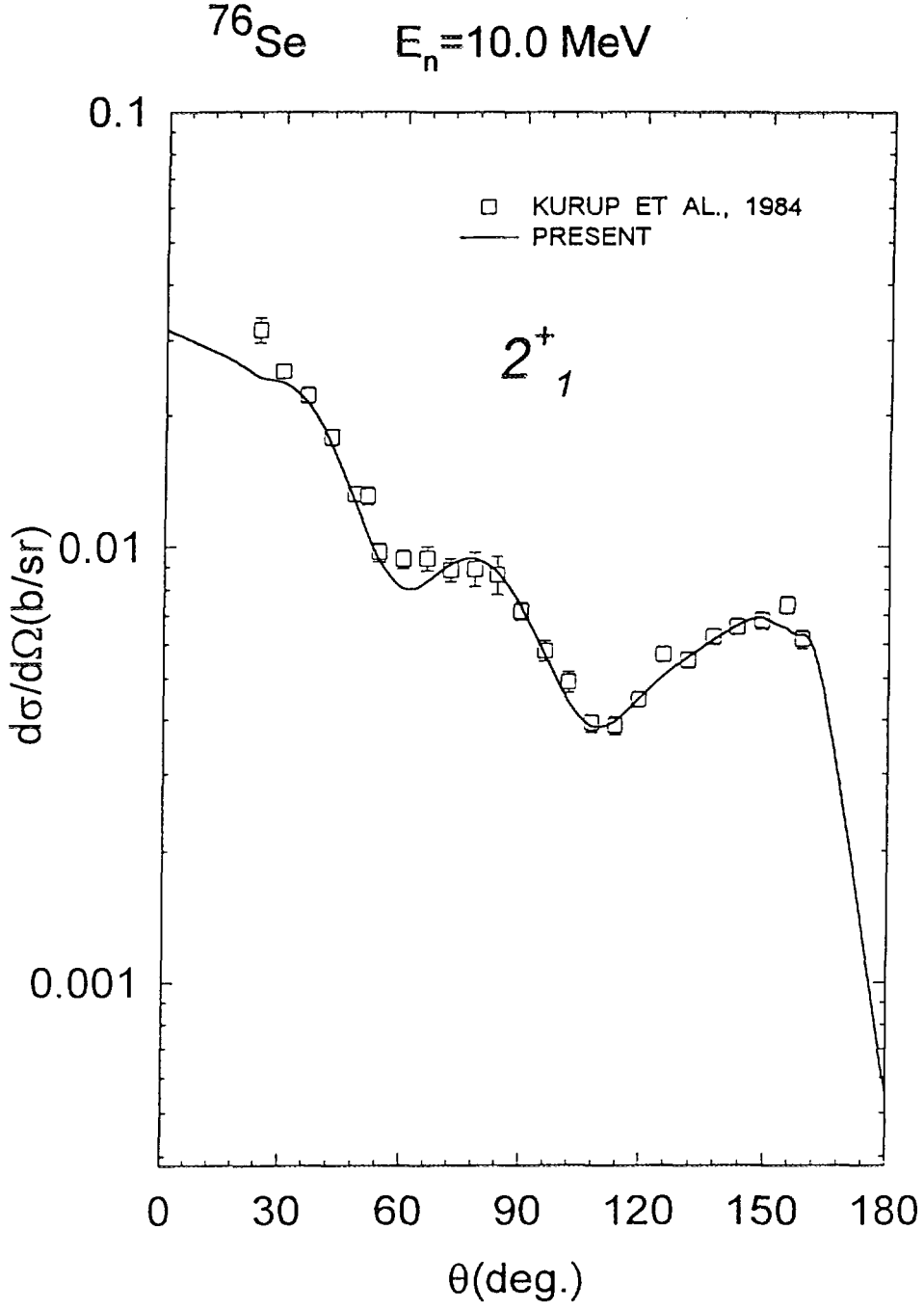
^{76}Se E_n=10.0 MeV
KURUP ET AL., 1984
PRESENT
2^+_1
0.1
0.01
0.001
dσ/dΩ(b/sr)
0
30
60
90
120
150
180
θ(deg.)

Figure 7.

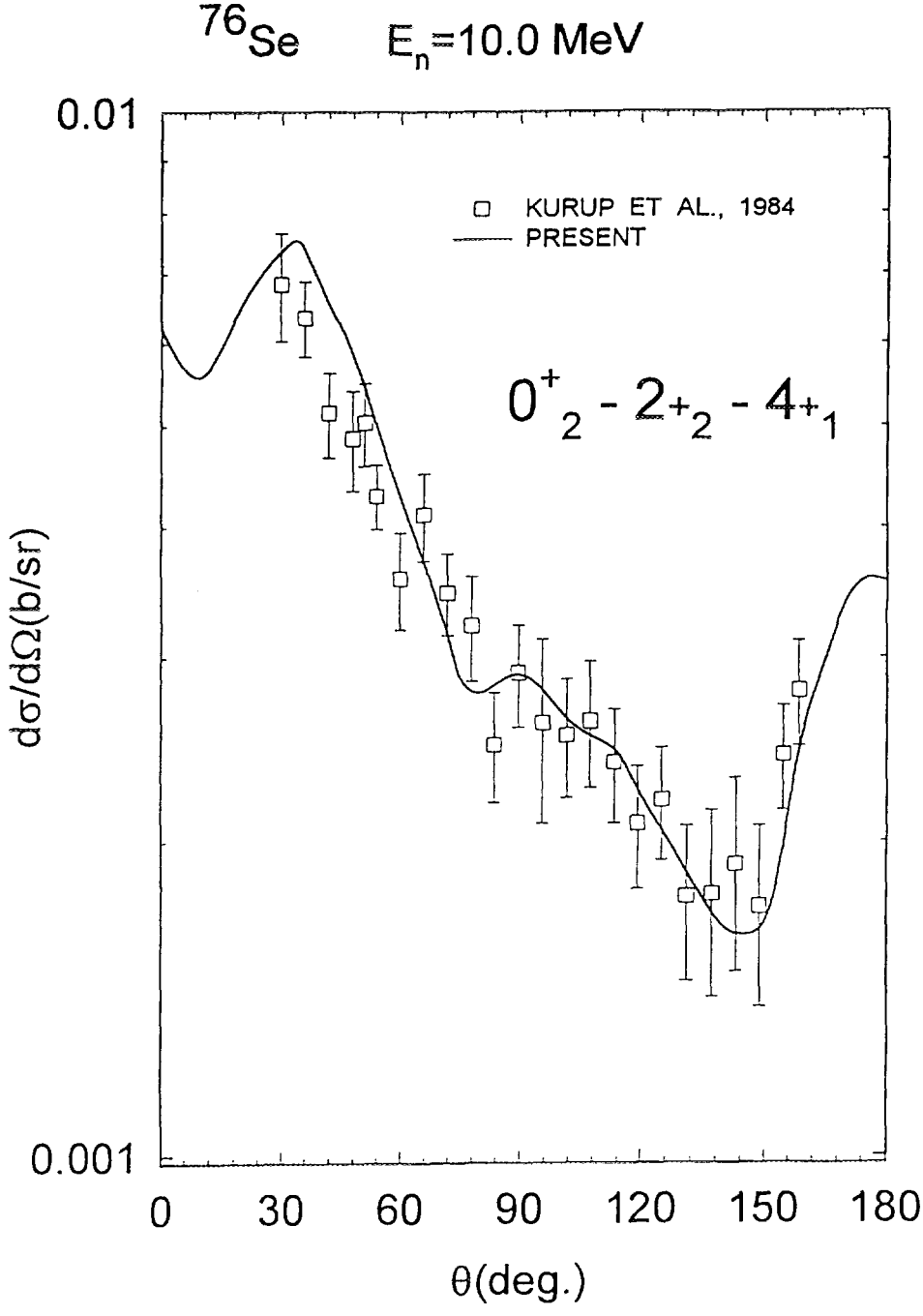
^{76}Se E_n=10.0 MeV
0.01
0.001
KURUP ET AL., 1984
PRESENT
0^+_2 - 2^+_2 - 4^+_1
dσ/dΩ(b/sr)
0
30
60
90
120
150
180
θ(deg.)

Figure 8.

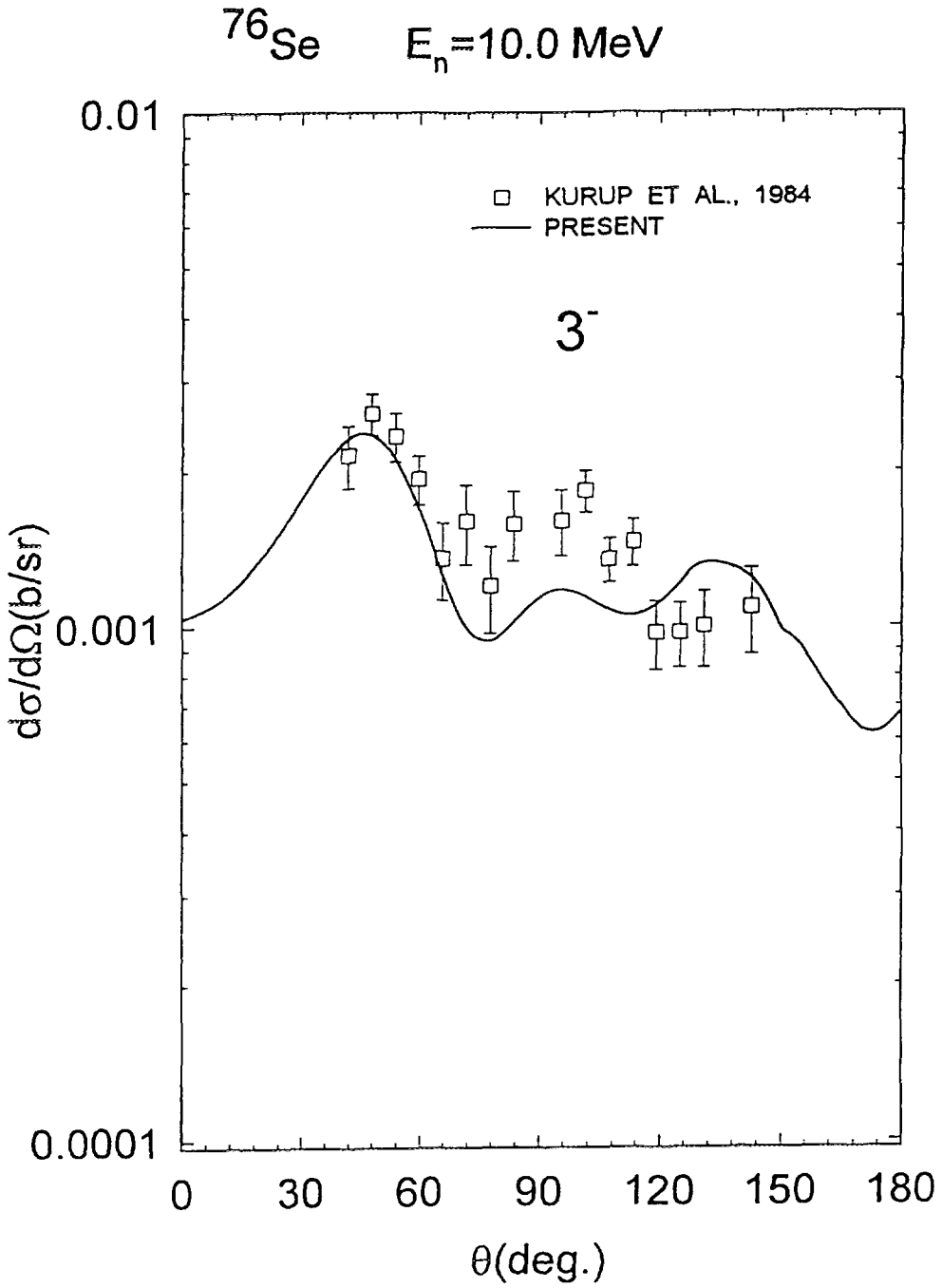
^{76}Se E_n=10.0 MeV
KURUP ET AL., 1984
PRESENT
3$^-$
0.01
0.001
0.0001
dσ/dΩ(b/sr)
0
30
60
90
120
150
180
θ(deg.)

Figure 9.

Results for three and five or six levels coupling scheme differ while differences are greater than experimental errors of calculated values. That means that three level coupling scheme recommended for calculations with the involved potential parameters is not saturated. Nevertheless it predicts experimental data with high accuracy. As we understand rejected coupling is compensated by correlated changes of veritable optical potential parameters that become to be not unique. That means recommended potential parameters cannot be used for optical calculations that request changes in coupling scheme, such as prediction of neutron transmissions for rotational band excited levels of ^{238}U.

It seems that optical potential for saturated coupling can solve the problem. But in standard rigid rotator model it is impossible to couple $K = 2^+$ band levels with the ground state rotational band, as it does not allow to couple levels with different K. While non-axial soft rotator model predicts (and their is some experimental evidence) that they are coupled with the ground state as strong as $J = 4, K = 0^+$ level, coupling of which can't be ignored (see Table 2). That means coupling cannot be saturated without at least $J = 2, K = 2^+$ level.

Model of soft non-axial rotator solves the problem as $K = 2$ band levels and others can be coupled with the ground state within the framework of the model. And what is more gives very effective tool for correct calculations of direct excitations of a number of collective levels of even-even nucleus up to $\sim$ 2 MeV.

Let me return to the application of the model. The low-lying levels of ^{246}Cm scheme of Nuclear Data Sheets [7] appears incomplete at excitation energy above 0.780 MeV (see Fig.10). We used our model to predict energies for all positive parity levels of even-even ^{246}Cm nucleus up to the excitation energies $\sim$ 2 MeV (assuming five rotational bands). The gap in cumulative number of ^{246}Cm levels $N(U)$ between 0.5 and 0.8 MeV is due to rather high position of the $K^\pi = 0^-$ band, as compared with other actinides. We generated the unobserved positive parity levels of ^{246}Cm with high spin values and levels of negative parity rotational band with $K^\pi = 0^-$ up to 1.22 MeV. The parameters of the model were adjusted, fitting experimental energies of band-heads: $K^\pi = 0^+(n_\beta = n_\gamma = n_\xi = 0)$, $K^\pi = 2^+(n_\beta = n_\gamma = n_\xi = 0)$, $K^\pi = 0^+(n_\beta = 1, n_\gamma = n_\xi = 0)$, $K^\pi = 0^+(n_\beta = 0, n_\gamma = 1, n_\xi = 0)$, $K^\pi = 1^-(n_\beta = n_\gamma = n_\xi = 0)$, here n_β, n_γ, n_ξ- are quantum numbers of $\beta-, \gamma-$quadrupole, and $\xi-$octupole vibrations. Rotational levels for bands with $K^\pi = 2^-; 1_1^-; 1_2^-$ were built as $E_J^{K^\pi} = E^{K^\pi} + A(J(J+1) - K(K+1))$, the values of rotational constant A were adjusted to describe the measured level energies. We assigned spin and parity $J^\pi = 6^-$ for the level $E = 1340.16keV$, previously unidentified. Adopted level scheme is compared with the experimental (see Fig.10). One can see that 3 levels up to 1.22

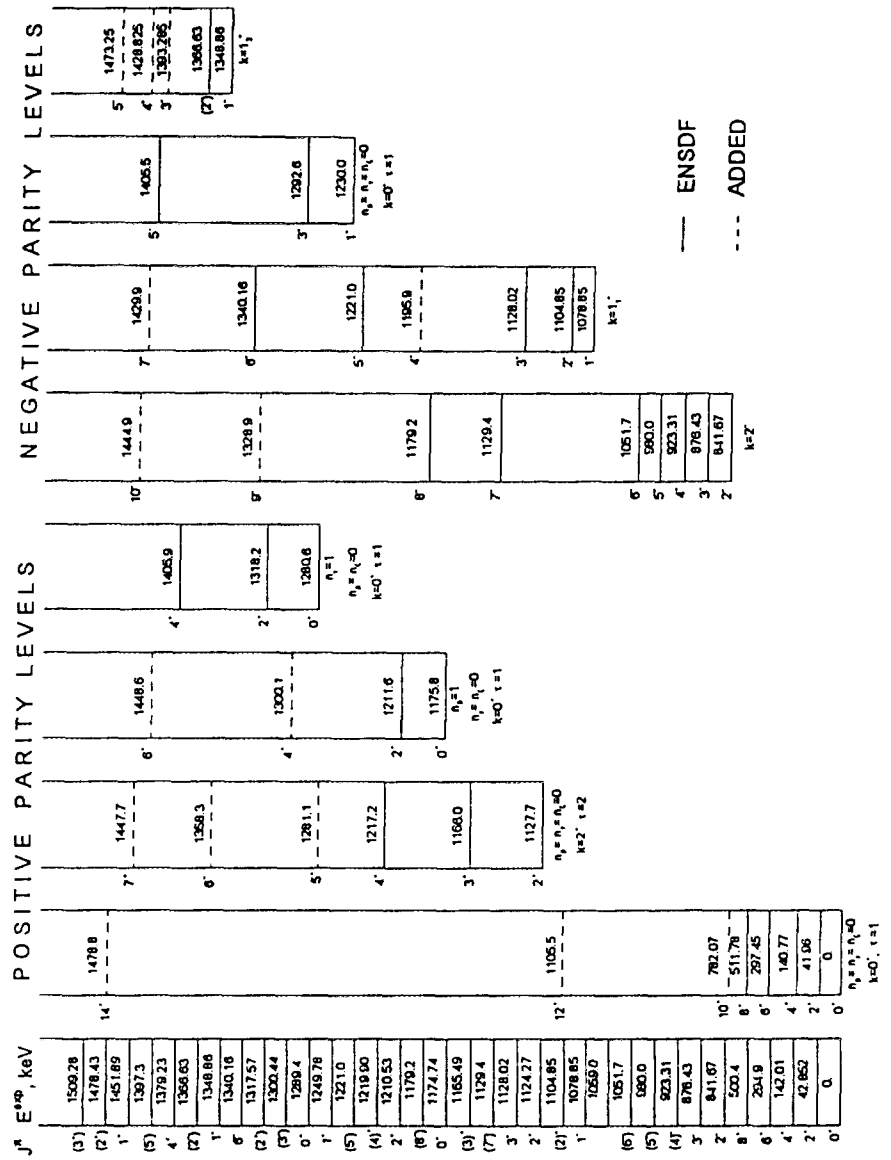
POSITIVE PARITY LEVELS
NEGATIVE PARITY LEVELS
ENSDF
ADDED

Figure 10.

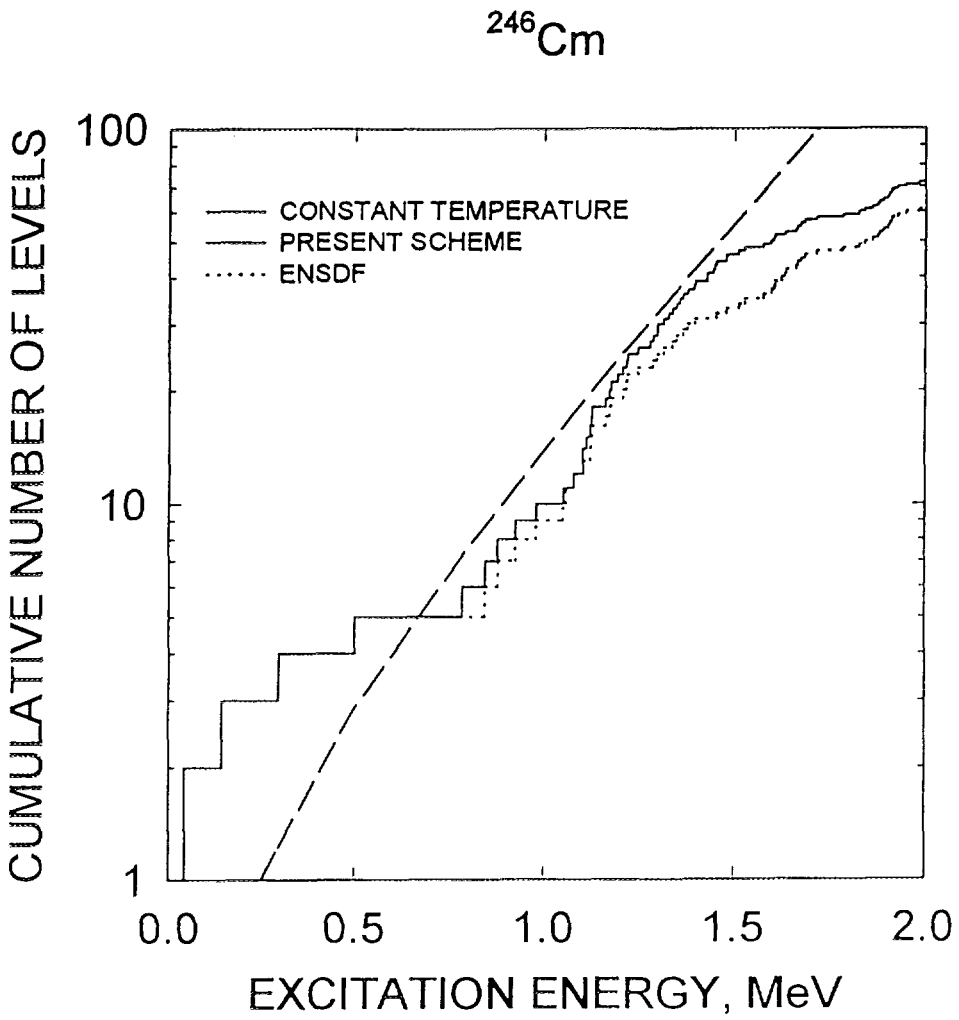

Figure 11.

MeV were added.

In JENDL-3 evaluation there are 29 discrete excited levels up to 1.509 MeV, i.e. the missing of at least 15 collective levels above $\sim$ 0.78 MeV is ignored. Fig. 11 demonstrates that this estimate of level missing is consistent with the adopted constant temperature approximation of cumulative number of levels.

References

[1]Porodzinskij Yu.V., Sukhovitskij E.Sh.,Yadernaja Fizika, 53, 64 (1991) (in Russian)

[2]Davydov A.S., Chaban A.A., Nuclear Physics, 20, 499 (1960)

[3]Porodzinskij Yu.V., Sukhovitskij E.Sh., Physics of Atomic Nuclei, 59, 228 (1996)

[4]Tamura T., Rev. Mod. Phys., 37, 679, (1965)

[5]Porodzinskij Yu.V., Sukhovitskij E.Sh.,Yadernaja Fizika, 56, 64 (1993) (in Russian)

[6]Porodzinskij Yu.V., Sukhovitskij E.Sh., Papers of 2^{nd} RCM on Development of Reference Input Parameters Library for Nuclear Model Calculations of Nuclear Data, Vienna, Austria, 30 October-3 November, 1995 (to be published by IAEA)

[7]ENDSF, 1995

1. 5 Above-threshold structure in ^{244}Cm neutron-induced fission cross section

V.M. Maslov
Radiation Physics and Chemistry Problems Institute, 220109,
Minsk-Sosny, Belarus

Abstract

The quasi-resonance structure appearing above the fission threshold in neutron-induced fission cross section of ^{244}Cm(n,f) is interpreted. It is shown to be due to excitation of few-quasiparticle states in fissioning ^{245}Cm and residual ^{244}Cm nuclides. The estimate of quasiparticle excitation thresholds in fissioning nuclide ^{245}Cm is consistent with pairing gap and fission barrier parameters.

The pairing correlation effects in fission have been studied rather extensively. In case of even-even fissioning nuclei the step-like structure of the K_o^2 parameter, defining the angular anisotropy of fission fragments, is interpreted to be due to few-quasiparticle excitations.[1] The modelling of the few-quasiparticle state excitations in the level density of the even-even fissioning nuclide ^{236}U was employed recently to fit the step-like structure in neutron-induced fission cross section of ^{235}U around ~1 MeV incident neutron energy.[2] The broad quasi-resonance structure in fission cross sections of N-even curium target nuclei occurs at incident neutron energies above the fission threshold, i.e. in the plateau region. The observed well-pronounced structures in bomb-shot data on neutron-induced fission cross section of ^{244}Cm, ^{246}Cm, ^{248}Cm by Fomushkin et al.[3,4] and Moore et al.[5] (see Figs.1,2) also could be attributed to the interplay of a few-quasiparticle excitations in the level density of the fissioning nuclide and residual nuclei. We suggest that the intrinsic quasiparticle state densities in fissioning even-odd as well as residual even-even Cm nuclei play an essential role.

We will discuss ^{244}Cm(n,f) reaction data analysis. We suppose that the structure appearing in the neutron-induced fission cross section of even-even target nucleus ^{244}Cm could be interpreted as follows. In the vicinity of the fission threshold and at higher excitations the main competing reactions are fission and inelastic scattering. In a double-humped fission barrier model the main factor, defining the competition of fission and neutron emission is

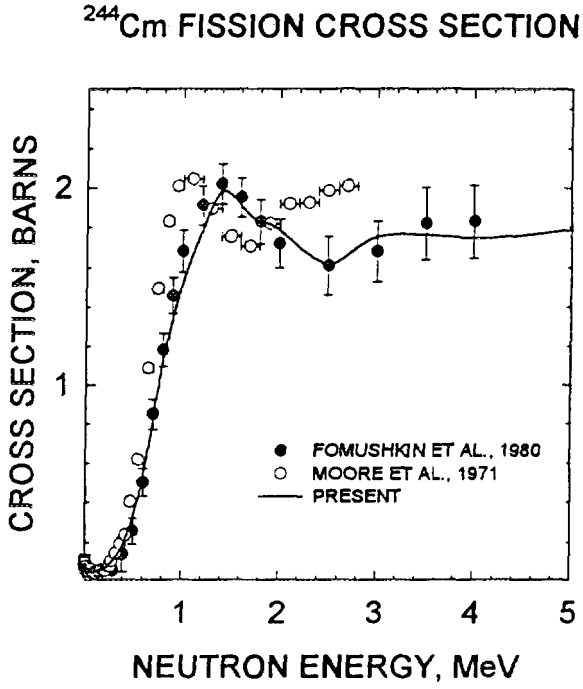

Figure 1:

the total level density of fissioning nuclide ^{245}Cm at inner and outer saddles and residual ^{244}Cm nuclide at equilibrium deformation.

The total nuclear level density could be represented as the factorized contribution of quasiparticle and collective states within a phenomenological model by Ignatyuk et al.[6], which takes into account the shell, pairing and collective effects in a consistent way

$$\rho(U, J, \pi) = K_{rot}(U, J) K_{vib}(U) \rho_{qp}(U, J, \pi), \qquad (1)$$

where $\rho_{qp}(U, J, \pi)$ is the quasiparticle level density, and $K_{rot}(U, J)$ and $K_{vib}(U)$ are factors of rotational and vibrational enchancement of level density, respectively. The Eq.1 holds in an adiabatic approximation, when the intrinsic and collective states contributions to the total level density $\rho(U, J, \pi)$ are factorized.

For deformed axially symmetric nucleus, which is characteristic for equilibrium deformations of actinides

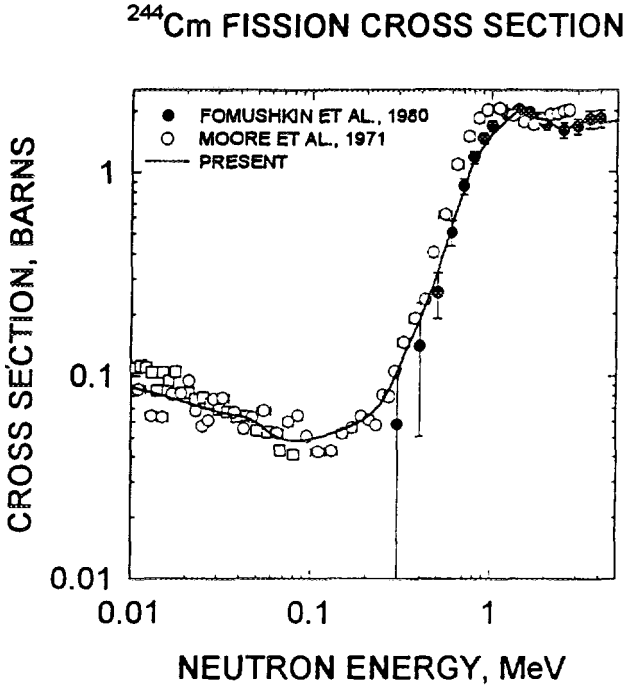

Figure 2:

$$K_{rot}(U) = \sum_{K=-J}^{K=J} exp(-K^2/K_o^2) \approx \sigma_\perp^2 = F_\perp t, \tag{2}$$

$$K_o^2 = (\sigma_\parallel^{-2} - \sigma_\perp^{-2})^{-1},$$

where $\sigma_\perp$ and $\sigma_\parallel$ are the angular momentum distribution parameters, K is the spin J projection on the symmetry axis. The momentum of inertia $F_\perp$ (perpendicular to the symmetry axis), equals rigid body value at high excitation energies, when pairing is destroyed,

$$F_\perp = 2/5 m_o r_o^2 A^{5/3}(1 + 1/3\varepsilon), \tag{3}$$

where $r_o = 1.24$ fm, m_o - nucleon mass, ε− quadrupole deformation parameter, at zero temperature it equals experimental value F_o and is interpolated in between, using pairing model equations[6].

The respective parameters for inner and outer saddle and equilibrium deformations: shell correction δW, pairing correlation function Δ, quadrupole

deformation ε, and momentum of inertia at zero temperature $F_o/\hbar^2$ are given in Table 1. For ground state deformations the shell corrections were calculated as $\delta W = M^{exp} - M^{MS}$, where M^{MS} denotes liquid drop mass (LDM), calculated with Myers-Swiatecki parameters[7], and M^{exp} is the experimental nuclear mass.

According to shell-correction method calculations of Howard and Moller[8] the inner barrier of Cm nuclei is triaxially symmetric during fission process. The outer barrier retains axial symmetry, while being mass asymmetric.

Table 1

Level density parameters of fissioning nucleus and residual nucleus

Parameter	inner saddle	outer saddle	neutron channel
δW, MeV	2.5	0.6	LDM
$\triangle$, MeV	$\triangle_o + \delta^*$	$\triangle_o + \delta^*$	$\triangle_o$
ε	0.6	0.8	0.24
$F_0/\hbar^2$, MeV^{-1}	100	200	73

*)δ value is defined by fitting fission cross in the plateau region.

The mass asymmetry doubles the $K_{rot}(U)$ factor as defined by Eq.2. For triaxially symmetric nuclides the rotational enchancement factor is

$$K_{rot}(U) = 2\sqrt{2\pi}\sigma_\perp^2\sigma_\parallel. \tag{4}$$

The quasiparticle level density $\rho_{qp}(U, J, \pi)$ is defined as follows

$$\rho_{qp}(U, J, \pi) = \frac{(2J+1)\omega_{qp}(U)}{4\sqrt{2\pi}\sigma_\perp^2\sigma_\parallel} \exp\left(-\frac{J(J+1)}{2\sigma_\perp^2}\right), \tag{5}$$

here $\omega_{qp}(U)$ is the intrinsic quasiparticle state density.

Now we will address the main item of our discussion - intrinsic state density of quasiparticle excitations $\omega_{qp}(U)$, which could be represented as a sum of n-quasiparticle state densities $\omega_{nqp}(U)$:

$$\omega_{qp}(U) = \sum_n \omega_{nqp}(U) = \sum_n \frac{g^n(U-U_n)^{n-1}}{((n/2)!)^2(n-1)!}, \tag{6}$$

where $g = 6a_{cr}/\pi^2$ is a single-particle state density at the Fermi surface, n is the number of quasiparticles. The value of the main a−parameter of the model at excitation energy $U = U_{cr}$, a_{cr}, is defined by fitting neutron resonance spacing.[9] The shell correction dependence of a_{cr} is defined using

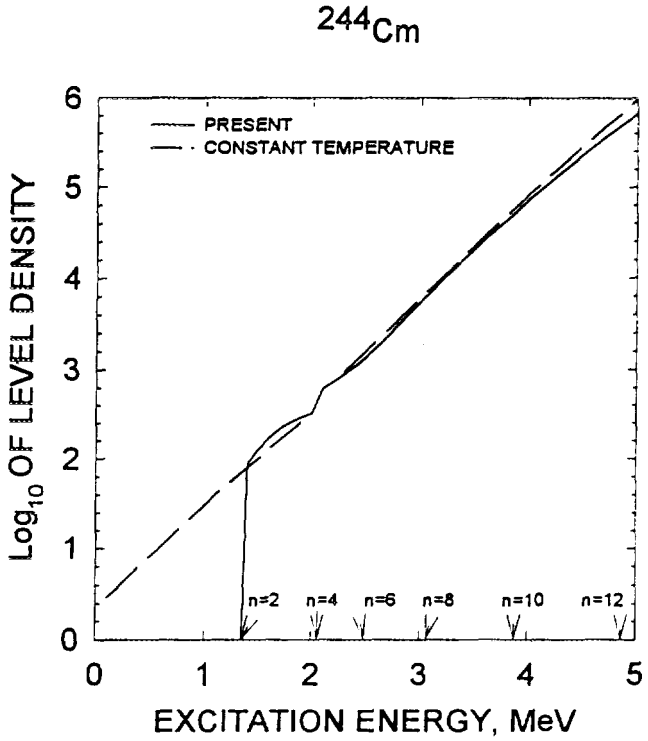

Figure 3:

the following equation[6]:

$$a(U) = \begin{cases} \tilde{a}(1+ \delta W f(U - E_{cond})/(U - E_{cond})), & U > U_{cr} = 0.47 a_{cr}\Delta^2 - m\Delta \\ a(U_{cr}) = a_{cr} & U \leq U_{cr} = 0.47 a_{cr}\Delta^2 - m\Delta, \end{cases} \quad (7)$$

here m = 0,1,2 for even-even, odd-A and odd-odd nuclei, respectively; $f(x) = 1 - exp(-\gamma x)$, is the dimensionless function, defining the shell effects dumping; condensation energy $E_{cond} = 0.152 a_{cr}\Delta^2$, where Δ is the correlation function, which equals $12/\sqrt{A}$ for ground state deformations, $\tilde{a}$ is the asymptotic a-parameter value at high excitation energies.

The partial n-quasiparticle state densities $\omega_{nqp}(U)$ depend critically on the threshold values U_n for excitation of the n-quasiparticle configurations, $n = 1, 3...$ for odd-A nuclei and $n = 2, 4...$ for even-even nuclei. The values of U_n could be defined as follows from[10]:

$$U_n = \begin{cases} E_{cond}(3.23n/n_{cr} - 1.57n^2/n_{cr}^2), & \text{if } n < 0.446 n_{cr} \\ E_{cond}(1 + 0.627n^2/n_{cr}^2), & \text{if } n \geq 0.446 n_{cr}. \end{cases} \quad (8)$$

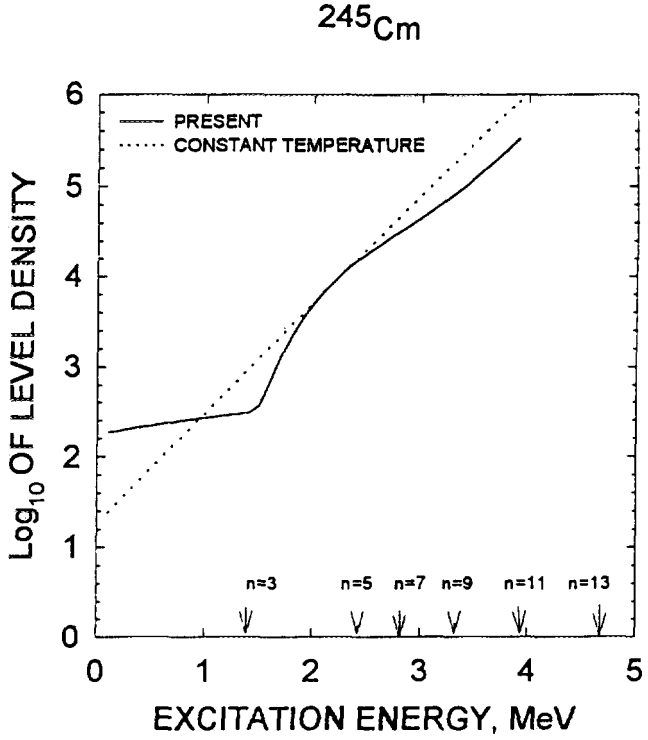

Figure 4:

Here, $n_{cr} = 12/\pi^2(ln2)gt_{cr}$, critical temperature $t_{cr} = 0.571\Delta$. This U_n value estimate embodies the energy dependence of the correlation function $\Delta(U)$ as well as a modified Pauli correction to the excitation energy. The angular momentum distribution parameter $\sigma_{\parallel}^2$ could be represented as

$$\sigma_{\parallel}^2 = \sum_n n\langle m^2\rangle \omega_{nqp}(U) / \sum_n \omega_{nqp}(U), \tag{9}$$

where $\langle m^2\rangle = 0.24A^{2/3}$ is the average value of the squared projection of the angular momentum of the single-particle states on the symmetry axis.

In case of even-even nuclides the partial contributions $\omega_{nqp}(U)$ of n-quasiparticle states to the total intrinsic state density $\omega_{qp}(U)$ produce "jumps" only for n =2 and n =4 (see Fig.3). The intrinsic state density $\omega_2(U)$, for the residual nuclide ^{244}Cm could be represented by equation, modifying $\omega_2(U) = g^2(U - U_2)$ with a Woods-Saxon expression at excitations below four-quasiparticle excitation threshold:

$$\omega_2(U) = g^2(U_4 - U_2 - 0.25)(1 + exp((U_2 - U + 0.1)/0.1))^{-1}. \quad (10)$$

This estimate of $\omega_2(U)$ was obtained by modelling the structure of ^{238}Pu intrinsic state density to interprete the step-like structure in ^{239}Pu(n,2n) reaction data near threshold.[11] Within the pairing gap the experimental collective levels should be employed. Since the scheme of ^{244}Cm collective levels, lying within the pairing gap, is rather incomplete, we employed the spectra of collective states for ^{246}Cm, taken from the recent version of Nuclear data Sheets. Fig.3 shows the ^{244}Cm total level density

$$\rho(U) = K_{rot}(U)K_{vib}(U)\frac{\omega_{qp}(U)}{\sqrt{2\pi}\sigma_{\|}}, \quad (11)$$

calculated with Eqs.1-10, as compared with the Gilbert-Cameron-type approximation of $\rho(U) = T^{-1}\exp((U - U_o)/T), U_o = -m\Delta$, where m=0,1,2 for even, odd and odd-odd nuclei, matched to the pairing model with unconstrained number of quasiparticles.[6] The arrows on the horizontal axis of Fig.3 indicate the excitation thresholds of n-quasiparticle configurations. Below the excitation threshold U_2 the constant temperature model fits the cumulative number of levels for ^{246}Cm nuclide.

In case of even-odd nuclei the partial contributions $\omega_{nqp}(U)$ of n-quasiparticle states to the total intrinsic state density $\omega_{qp}(U)$ produces "jumps" only for n =1 and n =3 (see Fig.4). The level density of the fissioning nuclide ^{245}Cm was calculated with Eq.(1-10), introducing odd-even excitation energy shift: $\hat{U} = U + \Delta$, where Δ is the correlation function for the saddle point deformations (see Table 1). We suppose that the ^{244}Cm(n, f) cross section magnitude is governed by the inner fission barrier parameters, which are fixed by fission data fit for incident neutron energy above 10 keV. Fig.2 shows the comparison of deep subthreshold data by Maguire et al.,[12] measured with linac and bomb-shot data by Fomushkin et al.[3] and Moore et al.[5] The incident neutron energy $E_3 = U_3 + E_{fA} - B \simeq$2.35 MeV, where B is the neutron binding energy, E_{fA} is the inner saddle height, corresponds to three-quasiparticle state excitation threshold U_3 at the inner saddle deformation. The intrinsic state density for the lowest number of quasiparticles n =1, is $\omega_1 \sim g$, there is no explicit excitation energy dependence. It defines the decreasing trend of fission cross section up to the incident neutron energy of E_3 ~2.35 MeV. At higher incident neutron energies the three-quasiparticle state excitations with intrinsic excitation state density $\omega_3 \sim g^3U^2$ came into play. Five-quasiparticle excitation threshold occurs at $E_5 \simeq$3.37 MeV. Hence, the fission cross section starts to increase once again. To fit the fission data we just scaled the ω_1 and ω_3 intrinsic states densities by a factor of 1.5. It seems to be a realistic estimate of level density at low

excitation energies, although it depends on the fission barrier parameter values. However, good description of fission data below threshold (see Fig.2) is the sign of consistency between level density and fission barrier estimates. The same kind of structure occurs in case of neutron-induced fission[3,4,5] of ^{246}Cm and ^{248}Cm targets. The measured cross section data also could be described with present approach in deep subthreshold and plateau region. The detailed description of ^{246}Cm(n,f) and ^{248}Cm(n,f) fission cross sections will be given in the forthcoming paper.

The modelling of the intrinsic state density structure of fissioning ^{245}Cm nuclide and residual ^{244}Cm has enabled the qualitative analysis of the quasi-resonance structure in ^{244}Cm(n,f) measured data well-above fission threshold. This irregularity is the consequence of threshold excitation of ^{245}Cm three-quasiparticle configurations. The excitation threshold is consistent with measured data below fission threshold.

Acknowledgements

This work was performed under the Project Agreement No. CIS-03-95 with International Science and Technology Center and Research Contract No. 8832/RB with International Atomic Energy Agency.

References

1. Shpack D.L., Ostapenko Yu.B., Smirenkin G.N. Yadernaya Fyzika, 13, 950, 1971.
2. Ignatjuk A.V., Maslov V.M., Proc. Int. Symp. Nuclear Data Evaluation Methodology, Brookhaven,USA, October 12-16, 1992, p.440, World Scientific, 1993.
3. Fomushkin E.F., Novoselov G.F., Vinogradov Yu.I., Gavrilov B.B., Zherebtsov G.F., Sov. J. Nucl. Phys. 31, 19 (1980).
4. Fomushkin E.F., Novoselov G.F., Vinogradov Yu.I., Gavrilov B.B. Sov. J. Nucl. Phys. 36, 338 (1982).
5. Moore M.S., Keyworth G.A. Phys. Rev. C, 3, 1656 (1971)
6. Ignatyuk A.V., Istekov K.K., Smirenkin G.N. Sov. J. Nucl. Phys. 29, 450 (1979).
7. Myers W.O., Swiatecky W.J., Ark. Fyzik, 36, 243 (1967).
8. Howard W.M., Moller P. Atom. Data and Nucl. Data Tables 25, 219 (1980)
9. Maslov V.M., Porodzinskij Yu.V., Sukhovitskij E.Sh., Klepatskij A.B., Morogovskij G.B. INDC(BLR)-3, IAEA, Vienna, 1996.
10. Fu C. Nucl. Sci. Engng. 86, 344 (1984).
11. Maslov V.M. Zeit. Phys. A, Hadrons & Nuclei, 347, 211 (1994).
12. Maguire Jr. H.T., Stopa C.R.S., Block R.C. et al. Nucl. Sci. Eng. 89, 293 (1985)

1.6 EVALUATION OF NEUTRON DATA FOR AMERICIUM-241

Maslov V.M., Sukhovitskij E.Sh., Porodzinskij Yu.V.,
Klepatskij A.B., Morogovskij G.B.
Radiation Physics & Chemistry Problems Institute,
220109, Minsk-Sosny, Belarus

May 8, 1996

Abstract

The evaluation of neutron data for ^{241}Am is made in the energy region from 10^{-5} eV up to 20 MeV. The results of the evaluation are compiled in the ENDF/B-VI format .

This work is performed under the Project Agreement CIS-03-95 with the International Science and Technology Center (Moscow). The Financing Party for the Project is Japan. The evaluation was requested by Y. Kikuchi (JAERI).

1 Introduction

The advanced nuclear fuel cycle studies request the nuclear data of transplutonium isotopes.[1] The neutron data for americium isotopes are especially important in this respect. Recently we have evaluated the data for ^{243}Cm, ^{245}Cm and ^{246}Cm. In this work the evaluation of ^{241}Am neutron data is performed. The next isotope, which neutron data would be evaluated is ^{243}Am. The curium and americium isotopes data to be evaluated were requested by the General Manager of Japan Nuclear data Center Dr. Y. Kikuchi. The quantities evaluated are resolved and unresolved resonance parameters, total, elastic and inelastic scattering, fission, capture, (n,2n) and (n,3n) reaction cross sections, angular and energy distributions of secondary neutrons, including partial (n,xn) and (n,xnf) reaction spectra, fission spectra and number of neutrons per fission. The incident neutron energy range covered is from 10^{-5} eV up to 20 MeV. The evaluated quantities are compared with JENDL-3 evaluation.[2]

2 Resolved resonance region

The measured data base has not changed essentially since the JENDL-3 and ENDF/B-VI evaluations were completed. Although the high level of subthreshold fission cross section of Seeger et al.[4] was discarded, the recent data of Kobayashi et al.[5] attracted attention to this problem once again. The latter data are still unaccessible up to now, maybe because they need more sophisticated analysis of ^{241}Am sample impurities.

2.1 Previous evaluations of resolved resonance parameters

The evaluated single-level Breit-Wigner resonance parameters of ENDF/B-VI[3] are based on the resonance parameters by Derrien and Lucas[6], Weston and Todd[7] and Kalebin et al.[8] from 10^{-5} eV up to 150 eV. Since the first few resonance parameters given by these authors are quite compatible, the evaluated resonance parameters are the average values of initial resonance parameters.[6,7,8] The weights take into account the appropriate measurement errors. The resulted 195 resonance parameters, including 5 negative resonances, are obtained assuming radiation width Γ_γ = 44.2 meV for 70% of the resonances. The scatter of radiation width values is from 10 meV up to 94 meV. In the energy region 142.5-150 eV a background radiative capture cross section of 12.2 barns is employed. The average resonance parameters,

thermal cross sections and resonance integral data are given in Table 2.1. Thermal total cross section is compatible with Kalebin et al.[8] data.

The multi-level Breit-Wigner resonance parameters of JENDL-3 evaluation[2] are actually parameters, provided by Derrien and Lucas.[6] Since the fission width values are provided by Derrien and Lucas[6] only up to 40 eV, at higher energies average fission width value of 0.229 meV was adopted. The radiation width Γ_γ = 43.77 meV was assumed for 102 resonances out of total number of 194 resonances. In the energy interval of 55 - 67 eV the radiation width Γ_γ was increased arbitrarily by 100 meV, this leads to severe discrepancies of ENDF/B-VI and JENDL-3 evaluated capture cross sections. Thermal total and capture cross sections are compatible with Lynn et al.[9] evaluation.

2.2 Measured data fitting

The purpose of current resonance parameter evaluation is to extract resolved resonance parameters up to 150 eV by consistent analysis of available data on total, fission, absorption and capture data. The incident neutron energies range is divided rather arbitrarily into two intervals: 10^{-5} - 0.1 eV and 0.1 - 150 eV. The energy point of 0.1 eV was chosen because the negative resonances define the cross sections below 0.1 eV, while contributing mainly to the thermal cross section values. The multi-level Breit-Wigner formalism is employed. The assigning of resonance spins was done as follows. Two assumptions were adopted: the number of resonances with spin J is proportional to $(2J+1)$, reduced neutron width distribution should obey that of Porter-Thomas, neutron resonance spacing distribution should obey that of Wigner.

2.2.1 Total cross section

The total cross section data of Derrien and Lucas[6] are available in the energy region of 0.785 eV - 150 eV, Adamchuk et al.[10] data are available in the energy region of 0.0063 eV - 82 eV and Belanova et al.[11] data are available in the energy region of 0.0212 eV - 150 eV. Two former data sets[6,10] are compatible in the energy interval of 0.785 eV - 1 eV, while the latter data set is systematically higher by about 40÷50 barns below 1 eV (see fig. 2.1). The same is true at higher energies (see fig. 2.2), however the data shapes are similar. Moreover, the thermal total cross section of Belanova et al.[11] is essentially higher than other available data. We suppose that there is a systematic error in data of Belanova et al.[11], so we omit them henceforth from the analysis.

2.2.2 Fission cross section

Fission cross section was measured in the energy region of 1 eV - 40 eV by Derrien and Lucas[6], in the energy region above 0.01883 eV by Dabbs et al.[12], in the energy region of 0.0321 eV - 150 eV by Bowman et al.[13] and in the energy region of 0.0231 eV - 50 eV by Gerasimov et al.[14] All data sets, excluding data of Dabbs et al.[12], were normalized to the thermal fission cross section value of ~3.13 eV.

2.2.3 Radiative capture cross section

Radiative capture cross section was measured in the energy region of 0.68 eV - 150 eV by Vanpraet et al.[15]

2.2.4 Absorption cross section

Absorption cross section was measured in the energy region of 0.01 eV - 370 keV by Weston and Todd.[7] The cross section was normalized at thermal neutron energies (0.2-0.3 eV).

2.2.5 Energy region below 0.1 eV

The negative resonances define the cross section values in this energy region. We adopted the following thermal values of: total $\sigma_t = 599.5$ barns, absorption $\sigma_a = 582.78$ barns and fission $\sigma_f = 3.136$ barns cross sections, evaluated from the measured data. The potential scattering radius, calculated with the coupled channel approach $R_p = 9.157$ fm. The resonance contribution to the thermal scattering cross section is about 1 barn, the absorption cross section data of Weston and Todd[7] should be renormalized to the value of thermal absorption cross section $\sigma_a = \sigma_t - \sigma_n \simeq 588$ barns. Consistent fitting of total, absorption and fission data gives the appropriate values, given in Table 2.1

The negative resonance parameters due to Lynn et al.[9]are adopted. Thermal cross section values and cross section data below 0.1 eV are fitted with present resonance parameters.

2.2.6 Energy region 0.1 ÷ 150 eV

There is a systematic difference in the energy interval of 15 eV - 39.8 eV between fission data by Derrien and Lucas[6] and by Dabbs et al.[12], the latter being ~30% higher. However, for narrower intervals (~5 eV), the difference may exceed ~40%. To "reconcile" both data sets we assumed the total error of data of Dabbs et al.[12] ~3 times as large as original total error. The resolution function of Dabbs et al.[12] measurement was modelled[16], while the resolution parameter was extracted from the comparison of the original

data and reconstructed with modelled resolution function of data by Dabbs et al.[12]

The resolution function of Vanpraet[15] capture cross section measurement was also modelled[16], while the resolution parameter was extracted from the data shape analysis. It was increased ~5 times in the interval 56.5 - 79 eV, ~4 times in the interval 79 eV - 110.7 eV, ~3 times in the interval 110.7 eV - 150 eV. We suppose that the total error must be about that of the absorption measurement by Weston and Todd.[7] Hence, the original error was increased ~2.3 times.

2.2.7 Resonance parameter analysis

We have got parameters for 195 resonances up to 150 eV. They describe the measured data on total, fission and capture cross sections within the attributed errors. The average resonance parameters, thermal cross sections and resonance integrals are presented in Table 2.1. Figures 2.3, 2.4, 2.5

Table 2.1

	ENDF/B-VI	JENDL-3	This evaluation
$\langle\Gamma_n^0\rangle$, meV	0.1462	0.1467	0.1451
$\langle\Gamma_f\rangle$, meV	0.301	0.229	0.324
$\langle\Gamma_\gamma\rangle$, meV	45.06	54.62	48.33
$\langle D\rangle$, eV	0.771	0.775	0.771
$S_0 \times 10^4$	0.9528	0.9535	0.9345
σ_t , barn	633.20	614.584	599.469
σ_γ , barn	618.758	600.436	584.802
σ_f , barn	3.1385	3.018	3.1358
σ_n , barn	11.303	11.130	11.531
g_γ	1.00357	1.00287	1.00722
g_f	1.01646	1.01665	1.02783
I_γ , barn	1387.69	1305.80	1351.20
I_f , barn	14.994	13.862	14.508

demonstrate the data fits below 0.1 eV. Figures 2.1 and 2.2 demonstrate the measured total data fits up to 8 eV. The fig. 2.6 shows the comparison of distribution of radiative capture widths for positive resonances with Porter-Thomas distribution. The resonance missing as well as reduced neutron width $\langle\Gamma_n^0\rangle$ and neutron resonance spacing $\langle D\rangle$ distributions are discussed below. Table 2.1 shows that for different evaluations s−wave neutron strength function S_0 and reduced neutron width $\langle\Gamma_n^0\rangle$ values are close to each other. It is not the case for average fission width, which are rather

discrepant. Present average fission width value is appreciably higher than that of JENDL-3 evaluation, since for all resonances above 40 eV the value of 0.229 meV was adopted. In ENDF/B-VI evaluation the radiative width was kept constant (44.2 meV) for most of the resonances. In JENDL-3 evaluation the radiative width is rather high for resonances in the interval 55 - 67 eV. Thermal cross sections and resonance integrals are fairly compatible with respective measured data.

The thermal total σ_t, capture σ_γ, and scattering σ_n cross sections, $g_\gamma-$, and g_f-factors, as well as resonance integrals $I\gamma$ and I_f values are calculated with a code INTER.[17] In case of JENDL-3 and present evaluations the multi-level Breit-Wigner formalism was used, while for ENDF/B-IV evaluation single-level formula was employed.

3 Unresolved resonance region

3.1 Review

Unresolved resonance region of ^{241}Am is supposed to be from 0.15 keV up to 41.3483 keV. The lower energy is the end-point of resolved resonance region. the upper energy is the threshold energy of the inelastic scattering. We suppose $s-$, $p-$ and $d-$wave neutron-nucleus interactions to be effective.

3.2 The s-wave average resonance parameter evaluation

3.2.1 Estimate of resonance level missing influence on $\langle D_{obs}\rangle$ and $\langle S_0\rangle$

The preliminary estimates of average partial widths were obtained by averaging the evaluated resolved resonance parameters. Figure 3.1 shows the cumulative sum of resolved resonance levels. The averaged parameters for positive resolved resonances are as follows:

$$\begin{aligned}\langle\Gamma_n^0\rangle &= 1.444\times10^{-4}\ (\mathrm{eV})^{1/2}\\ \langle\Gamma_f\rangle &= 0.327\ \mathrm{meV}\\ \langle D_{obs}\rangle &= 0.787\ \mathrm{eV}\\ \langle\Gamma\gamma\rangle &= 48.4\ \mathrm{meV}\end{aligned}$$

Due to missing of weak resonances these average values overestimate actual reduced neutron width $\langle g\Gamma_n^0\rangle$ and neutron resonance spacing $\langle D_{obs}\rangle$. To get a physically justified values of $\langle g\Gamma_n^0\rangle$ and $\langle D_{obs}\rangle$ we employ a method, which is described elsewhere.[18] Both reduced neutron width and neutron resonance spacing distributions are obtained in a unified approach. We take into account the correlation of weak resonance missing and resonance missing

due to poor experimental resolution. The resolution function parameters as well as $\langle g\Gamma_n^0 \rangle$ and $\langle D_{obs} \rangle$ values are obtained by maximum likelihood method when comparing experimental distributions of reduced neutron width and resonance spacing with Porter-Thomas and Wigner distributions, modified for the resonance missing. The latter distributions will be called expected distributions.

3.2.2 Evaluation of $\langle D_{obs} \rangle$, $\langle S_0 \rangle$, $\langle \Gamma_\gamma \rangle$ and $\langle \Gamma_f \rangle$ based on the resonance parameters

To evaluate average neutron resonance spacing $\langle D_{obs} \rangle$ and s-wave neutron strength function S_0 we apply our method[18] to the resolved resonance data base. We suppose that data up to 150 eV should be taken into account. Figure 3.1 shows the cumulative sum of resolved resonance levels. Dashed lines above and below the solid line show the dependence of the error of $\langle D_{obs} \rangle$ and the number of resonances. The missing of levels is evident at very low energies. Energy intervals denoted as I and II, corresponding to different experimental resolution are shown. Figure 3.2 demonstrates cumulative sum of reduced neutron widths. Here again, dashed lines above and below the solid line show the $s-$wave neutron strength function error. The evaluated values are:

$$\langle S_0 \rangle = (\ 0.864 \pm 0.131) \times 10^{-4}\ (\mathrm{eV})^{-1/2}$$
$$\langle D_{obs} \rangle = (0.505 \pm 0.042)\ \mathrm{eV}$$

Figure 3.3 shows the comparison of expected and experimental reduced neutron width distributions. Figure 3.4 shows the comparison of distributions for neutron resonance spacing. All the figures are obtained for energy interval 0-150eV. The expected distributions shown on the figures 3.2 and 3.3 demonstrate the effect of resonance missing. There is evidence that the expected distributions are consistent within statistical errors with the experimental data for energy interval 0-150 eV. That is the reason to consider the $\langle D_{obs} \rangle$ and S_0 estimates reliable.

3.3 The s-, p- and d-wave average resonance parameter evaluation

3.3.1 Neutron width

Average neutron width is calculated as follows

$$\langle \Gamma_n^{J,l} \rangle = S_l \langle D_J \rangle E_n^{1/2} P_l,$$

where P_l is the transmission factor for the lth partial wave, which was calculated within black nucleus model. The p-wave neutron strength function $S_1 = 2.204 \times 10^{-4}$ (eV)$^{-1/2}$ was calculated with the optical model, using the deformed optical potential, described below. According to the results of optical model calculations S_0 was assumed to decrease linearly to the value of S_0=0.807×10^{-4}(eV)$^{-1/2}$ for neutron energy of 41.3483 keV. The d-wave neutron strength function was taken from optical model calculations: S_2 = 1.022×10^{-4} (eV).$^{-1/2}$ Since the d-wave contribution is rather small, the impact of any reasonable approximation on calculated values is negligible

3.3.2 Neutron resonance spacing

Neutron resonance spacing $\langle D_J \rangle$ was calculated with the phenomenological model[19], which takes into account the shell, pairing and collective effects. The main parameter of the model $\tilde{a}$ was normalized to the observed neutron resonance spacing $\langle D_{obs} \rangle$ =0.505 eV.

3.3.3 Fission width

Fission widths are calculated within a double-humped fission barrier model. Energy and angular momentum dependence of fission width is defined by the transition state spectra at inner and outer barrier humps. We constructed transition spectra by supposing the triaxiality of inner saddle and mass asymmetry at outer saddle. They will be described below. The calculated fission widths $\langle \Gamma_f^{2-} \rangle$ and $\langle \Gamma_f^{3-} \rangle$ for s−wave neutrons are normalized to the average fission width $\langle \Gamma_f \rangle$ =0.38 meV at 0.15 keV incident neutron energy, which allows to describe fission measured data. This value of $\langle \Gamma_f \rangle$ is somewhat higher than average resolved resonance fission width.

3.3.4 Radiative capture width

Energy and angular momentum dependences of radiative capture width are calculated within a two-cascade γ-emission model with allowance for the (n,γf) and (n,γn') reaction competition to the (n,$\gamma\gamma$) reaction. In this energy region (n,γ) reaction appears to be a radiative capture reaction. The radiative capture width is normalized to the value of $\langle \Gamma_\gamma \rangle$ =48.4 meV. (For details see Chapter IV).

3.4 Cross section evaluation in the region 0.15-41.3483 keV

3.4.1 Fitting of fission cross section structure

Experimental fission cross-sections in the unresolved resonance region are measured by Bowman et al.[20], Shpak et al.[21], Gayther and Thomas[22], Wisshak and Kappeler[23], Hage et al.[24], Knitter and Budtz-Jorgensen[25], Dabbs et al.[12] and Kobayashi et al.[5] Data of Wisshak and Kappeler[23], Hage et al.[24] and Dabbs et al.[12] are fitted in present evaluation. Dabbs et al.[12]data were chosen to be the base of fission cross section evaluation in the unresolved resonance region (for details see Chapter IV). An argument in the support of data by Dabbs et al.[12] gives calculation with fission width normalized to the resolved resonance fission value of $\langle\Gamma_f\rangle$ =0.327 meV. The resulted cross section values are even somewhat lower than data of Dabbs et al.[12] In our evaluation we described data by Dabbs et al.[12] with fission widths normalized to $\langle\Gamma_f\rangle$=0.38 value at 0.15 keV. Structure observed in data by Dabbs et al.[12] is fitted by adjusting fission width in l=0, J=2^- entrance channel. Comparison of evaluated and experimental fission cross sections in the unresolved resonance energy region is given on Fig3.5. Below 10 keV the problem of discrepancies between earlier and recent data was addressed by Kobayashi et al.[5] This data tend to support Gayther and Thomas[22] data, which are ~3 times higher than data of Dabbs et al.[12] below 10 keV. The data of Knitter and Budtz-Jorgensen[25] are lying ~10 times lower than data of Dabbs et al.[12] around 1 keV. The most disturbing is the discrepancy of evaluated curve with data of Knitter and Budtz-Jorgensen[25], since they were obtained with different technique as compared with measurements of Wisshak and Kappeler[23] and Hage et al.[24] That means at least new measurements are highly desirable below ~100 keV.

3.4.2 Capture cross section energy dependence

Capture cross section in the energy region of interest is measured by Gayther and Thomas[22], Wisshak and Kappeler[23] and Vanpraet et al.[15]. Absorption data of Weston and Todd[7] can be also used as fission cross-sections is very small in this region. All the experimental data sets are compatible with each other below 10 keV, although Vanpraet et al.[15] data are lying somewhat higher than others. Above 10keV data of Wisshak and Kappeler[23] are in good agreement with data of Gayther and Thomas[22] while the data of Weston and Todd[7] and Vanpraet et al.[15] are essentially lower. In present evaluation we adopted capture data of Gayther and Thomas[22] and Wisshak and Kappeler[23] since the data trends above 10 keV are consistent with our calculated cross sections with the adopted average resonance paremeters. Comparison of evaluated and measured capture cross-sections in unresolved resonance region is given on Fig 3.6. We consider non-feasible the repro-

duction of structure, observed in data of Gayther and Thomas[22] below ~1.5 keV.

3.4.3 Comparison of current and JENDL-3 and ENDF/B-IV evaluated data

Evaluated fission cross sections of this work is consistent with JENDL-3 and ENDF/B-VI in the unresolved resonance region as they are based on the same data of Dabbs et al.[12] Figure 3.5 shows the comparison of fission cross sections σ_f for both evaluations. The discrepancies are noticed when comparing the (n,γ) reaction cross sections (see fig. 3.6) Current evaluated capture cross section is $\approx$ 25% lower at the lower edge of unresolved resonance region then JENDL-3 and ENDF/B-VI evaluations and almost coincide above 10keV. Fig 3.6 gives comparison of evaluated capture cross section with measured data. Comparison of the evaluated fission and capture cross-sections is given in Table 3.1.

Table 3.1 Comparison of the evaluated fission and capture cross sections

Energy,	$\sigma\gamma, b$			σ_f, b		
keV	present	JENDL-3	ENDF/B-VI	present	JENDL-3	ENDF/B-V
0.175	25.26	31.24	26.07	0.165	0.161	0.168
0.350	17.47	22.98	22.29	0.147	0.147	0.152
0.550	13.78	17.55	14.29	0.084	0.093	0.078
0.650	12.59	15.70	13.80	0.100	0.084	0.079
0.850	10.93	13.20	11.27	0.065	0.071	0.069
1.250	8.9	10.73	11.16	0.065	0.053	0.064
1.750	7.46	9.01	8.43	0.041	0.043	0.043
3.5	5.24	6.10	5.92	0.037	0.037	0.035
4.5	4.65	5.00	4.85	0.031	0.031	0.033
8.5	3.53	3.73	3.72	0.021	0.022	0.021
12.5	3.06	3.11	3.25	0.020	0.019	0.019
17.5	2.76	2.81	2.85	0.017	0.017	0.016
22.5	2.58	2.58	2.54	0.016	0.016	0.016
27.5	2.45	2.39	2.38	0.016	0.016	0.015
41.3483	2.22	2.08	2.11	0.014	0.015	0.014

4 Fast neutron cross sections

The measured neutron data in fast energy region, i.e. above ~41 keV are available for total, capture, fission and (n,2n) reaction cross sections. There is a lot of discrepancies in fission data in a deep subthreshold region, in a

plateau region and at higher energies, especially around 14.6 MeV. Nonetheless, the available fission and capture data fit would be used as constraint for (n,n') and $(n,2n)$ reaction cross sections calculation. We reproduce also the average resonance fission width within double-humped fission barrier model. To fix fission channel parameters the systematic trends are used.

4.1 Optical potential

The deformed optical potential for n+^{241}Am interaction is employed. The data of Phillips et al.[26] on total cross section are fitted, having in mind the systematic error of 0.6 barn. The starting values for the potential parameters were those for n+^{238}U interaction.[27] The isotopic dependences of real and imaginary parts of the potential were calculated using the optical potential parameter systematics.[28] Previously we modified the original potential geometry parameters[27] to fit total cross section and differential scattering data for N-odd and even targets above 10 MeV. This procedure of parameter fitting is well tested in case of and ^{233}U, ^{239}Pu, ^{235}U, ^{232}Th and ^{238}U targets. Four levels of the ground state rotational band ($5/2^-$,$7/2^-$,$9/2^-$,$11/2^-$) are coupled. The deformation parameters β_2 and β_4 are obtained by fitting $s-$wave neutron strength function S_0 value of 0.864×10^{-4} $(\mathrm{eV})^{-1/2}$ and p-wave neutron strength function S_1 value of 2.00×10^{-4} $(\mathrm{eV}).^{-1/2}$ The p-wave neutron strength function S_1 was obtained by fitting capture cross section data of Gayther and Thomas[22] and Wisshak and Kappeler[23] in 20 - 300keV energy region. This low value of S_1 was obtained by slight changing of V_R and W_D values to get low compound reaction cross section. The potential parameters are as follows:

$$
\begin{aligned}
& V_R = 46.15 - 0.3E, MeV, r_R = 1.26\ fm, a_R = 0.615\ fm \\
W_D = & \begin{cases} 3.56 + 0.4E, MeV, & E \leq 10 MeV, r_D = 1.24\ fm, a_D = 0.5\ fm \\ 7.56\ MeV, & E > 10\ MeV \end{cases} \\
& V_{SO} = 6.2\ MeV, r_{SO} = 1.12\ fm, a_{SO} = 0.47\ fm, \beta_2 = 0.181, \beta_4 = 0.076
\end{aligned}
$$

The s-, p-, and d-wave neutron strength functions and potential scattering cross section, calculated with this potential parameters in a coupled channel approach at incident neutron energy of 150 eV are:

$$S_0 = 0.851 \times 10^{-4}(\mathrm{eV})^{-1/2} \quad , \quad R' = 9.157 \text{ fm}$$

and at 41.3483 keV are:

$$S_0 = 0.807 \times 10^{-4}(\mathrm{eV})^{-1/2} \quad S_1 = 2.204 \times 10^{-4}(\mathrm{eV})^{-1/2} \quad S_2 = 1.022 \times 10^{-4}(\mathrm{eV})^{-1/2}$$

The reaction cross sections, calculated with deformed optical potential and spherical optical potential, which is used in JENDL-3 evaluation, are

compared on fig. 4.1. The significant differences below 1 MeV and above 10 MeV would be manifested in inelastic scattering cross section and $(n, 3n)$ cross section. The total cross section seem rather different (see fig. 4.2), especially at low energies, although they fit the data of Phillips and Howe[26] within errors. The discrepancy of elastic scattering cross sections, shown on fig. 4.2 is similar to that, observed in case of total cross section. The differences at low energies are due to rather low value of $s-$wave strength function adopted in present evaluation.

4.2 Fission cross section

4.2.1 Status of the experimental data

A number of measurements are available for fission cross section, but most of them are discrepant with each other. We will divide the data into four groups: deep subthreshold region, threshold region, plateau region and region above emissive fission threshold (see figs. 4.4, 4.5, 4.6, 4.7).

Fission cross section of ^{241}Am was measured by Seeger et al.[4] from 20 eV to 1 MeV at the bomb-shot. Above 10 keV ratio of fission cross sections of ^{241}Am and ^{235}U was obtained. Fission cross section of ^{241}Am was measured at linac[20] as a ratio to fission cross section of ^{239}Pu. BF_3-counter was used as a flux monitor.

Shpack et al.[21] defined fission cross section of ^{241}Am in the energy region from 3 keV to 4 MeV. They have measured shape of fission cross sections ratio of ^{241}Am and ^{239}Pu. Then the shape of ^{241}Am fission cross section was defined, using fission cross section of ^{239}Pu. Eventually absolute fission cross section of ^{241}Am was obtained by normalizing to data of Fomushkin et al.[29] The anomalous trend of fission cross section deep below threshold, observed by Seeger et al.[4] was discarded by these data as early as in 1969.

Fission cross section ratio of ^{241}Am and ^{235}U was defined by Fomushkin et al.[29] in the range of incident neutron energy from 0.44 MeV to 3.62 MeV. They have used mica detectors. The sample weight was defined using $T_{\alpha_{1/2}}$ =458.1 years, so their results should be renormalized to new value of $T_{\alpha_{1/2}}$ =432 years.

The ratio of fission cross sections of ^{241}Am and ^{239}Pu was measured in the energy range from 0.13 to 7.0 MeV by Kupriyanov et al.[30] The energy dependence of fission ratios was defined using ionization fission chambers. The absolute values of fission ratios were obtained using mica detectors. The ratios of fission cross sections of ^{241}Am and ^{235}U we obtained from the original data with the aid of ratio of fission cross sections of ^{239}Pu and ^{235}U by Fursov et al.[31]

The absolute fission cross section was obtained by Aleksandrov et al.[32] at 2.5 MeV neutron energy with the time-correlated associated particle method.

Neutrons were produced via D(d,n)^{3}He reaction.

The fission cross section ratio of ^{241}Am and ^{235}U was measured by Knitter and Budtz-Jorgensen[25] in the energy range from 100 eV to 5.3 MeV. Fission events of ^{241}Am were registered by fragment detection using an ionization chamber with intrinsic suppression of alpha background. Monoenergetic neutrons were produced via ^{7}Li(p,n) (0.153-1.3 MeV), T(p,n) (1-4.5 MeV), D(d,n) (4.5-5.3 MeV). Below 300 keV down to 5 keV the measurements were executed with pulsed Van de Graaff accelerator. Neutrons of energies from 1.28 eV to 2.5 MeV were produced with the linac. Absolute values of the ^{241}Am fission cross section were obtained using ^{235}U reference fission cross section of ENDF/B-VI.[3]

Gayther and Thomas[22] have measured average fission cross section in the range of incident neutron energy from 50 eV to 10 keV by observing prompt fission neutrons at 45 MeV linac. The ^{235}U measurement was used to establish an absolute scale for the ^{241}Am fission cross section. The average ^{235}U fission yield in the 1 keV to 2 keV range of incident neutron energies of 7.167 barns was used to normalize the ^{235}U fission cross section measurement.

Subthreshold fission cross section was measured in the energy range from 10 to 250 keV, using ^{235}U as a standard, by Wisshak and Käppeler.[23] Neutrons were produced via ^{7}Li(p,n) (10-150 keV) and the T(p,n) (50-150 keV) reaction with the Van de Graaff accelerator. Fission events were detected by a fission neutrons detector (liquid scintillator). The fission ratio was converted into absolute fission cross section using ^{235}U fission cross section of ENDF/B-VI.[3]

Fission cross section was measured by Hage et al.[24] in the energy range from 10 keV to 1030 keV, using ^{235}U as a standard. Continuous spectrum neutrons were produced via the ^{7}Li(p,n) (10-140 keV) and quasi-monoenergetic spectra neutrons also via the ^{7}Li(p,n) (120-1030 keV) reaction with the Van de Graaff accelerator. In other respects the experimental setup is similar to that of Wisshak and Käppeler.[23] The resulted fission cross section agrees quite good with the data of Wisshak and Käppeler[23], while both data sets lay about 2 times lower than the data of Knitter and Budtz-Jorgensen[25] below 250 keV. At higher energies the data of Knitter and Budtz-Jorgensen[25], Hage et al.[24], Shpack et al.[21] and Kupriyanov et al.[30] agree with each other.

The fission cross section ratios were measured by Behrens and Browne[33] from 0.2 MeV to 30 MeV using ionization fission chambers and a threshold cross section method. To avoid alpha pileup problems ^{241}Am sample of 4 mg was used. The most severe discrepancy is observed in the first plateau region with previous data of Knitter and Budtz-Jorgensen[25] and Kupriyanov et al.[30], which are up to ~10% lower.

The widest energy range covered in one measurement is from 0.02 eV

to 20 MeV by Dabbs et al.[12] They have measured cross sections ratio of ^{241}Am and ^{235}U above 101 keV, while at lower energies ^{6}Li(n,α) cross section, normalized to ^{235}U fission cross section in the 7.8-eV to 11-eV interval served as a standard. The reduction of the effects of intense alpha-particle background was achieved with the "honeycomb" fission ionization chamber. Below 101 keV the data of Dabbs et al.[12] are the lowest in the cross section level (14± 0.6 mbarns at 52 to 58 keV.) In the threshold region the data of Dabbs et al.[12] agree with data of Hage et al.[25], the data of Knitter and Budtz-Jorgensen[26] being higher than both data sets up to 600 keV. At higher energies, especially in the first plateau region, the data of Dabbs et al.[12] appear to be consistent with data of Knitter and Budtz-Jorgensen[25], but remain systematically lower than data of Behrens and Browne.[33] Above the emissive fission threshold the shapes of the data by Dabbs et al.[12] and Behrens and Browne[33] are drastically different.

A number of measurements exists around 14 MeV energy point, which are rather discrepant. Protopopov et al.[34], Kazarinova et al.[35]and Fomushkin et al.[36], have measured fission cross section at 14.6 MeV. The sample weight was defined using $T_{\alpha_{1/2}}$ =458.1 years, so their results should be renormalized to new value of $T_{\alpha_{1/2}}$ =432 years. The absolute fission cross section measurement was made at 14.6 MeV with a gaseous scintillator using associated particle method by Cance and Grenier.[37] Prindle et al.[38] have obtained an estimate of fission cross section 2.32±0.09 barn at 14.8 MeV by comparative analysis of mass-yields of ^{241}Am and ^{238}U neutron-induced fission. They have observed a 13% discrepancy of absolute yields defined using ^{241}Am and ^{238}U fission cross section ratio and summing mass-yield curve, when the fission cross section of ^{241}Am is obtained using data of Behrens and Browne.[33]

The problem of consistency of ^{241}Am fission cross section looks like that. In the plateau region the data of Knitter and Budtz-Jorgensen[25], Kupriyanov et al.[30] and Dabbs et al.[12] practically coincide, while the data of Behrens and Browne[33] are lying systematically higher(~6 %).

The severe discrepancies again occur below ~0.250 keV up. The data of Dabbs et al.[12] define the lowest cross section level, while the data of Knitter and Budtz-Jorgensen[25] define the highest level. The data of Wisshak and Kappeler[23] and Hage et al.[24] tend to support the data of Dabbs et al.[12] tendency to lower cross section values.

4.2.2 Statistical model calculation of fission cross section

We choose to fit primarily data of Dabbs et al.[12] describing measured data base. That means the lowest cross section level from 10 keV up to 250 keV. From 250 keV up to 2 MeV the measured data are virtually consistent. From 2 MeV up to emissive fission threshold the data of Dabbs et al.[12], Knitter and Budtz-Jorgensen[26] exhibit a distinct slope with incident neutron energy

($d\sigma_f/dE \sim 0.06$ barn/MeV). This is at variance with the trend of data by Kupriyanov et al.[30] which exhibit perfect "plateau" shape. The most peculiar feature of data by Dabbs et al.[12] is the broad bump around the threshold of (n,2nf) reaction, while there is a wild scatter of available data around 14.6 MeV. This bump can not be reproduced within the current statistical model calculations, mostly due to adopted reaction cross section (see fig. 4.1). To predict the fission cross section above 14 MeV, we choose to fit the ^{241}Am(n,2n) reaction cross section.[39] The comparison of calculated fission cross section with measured data is shown in figs. 4.4, 4.5, 4.6 and 4.7. The statistical theory calculation of fission cross section was accomplished within the double-humped fission barrier model. The approach employed in code STAT for fission cross section calculation is described in more details elsewhere.[40,41] The procedure of calculating fission transmission coefficients is briefly described below.

4.2.3 Fission transmission coefficient, level density and transition state spectrum

The intrinsic two-quasiparticle state spectrum of odd-odd nuclide ^{242}Am at equilibrium deformation are modelled by Sood and Singh.[42] The expected location of still unobserved two-quasiparticle states was predicted. Using these intrinsic states as the bandhead energies we have built the rotational bands, i.e. transition state spectra of fissioning nuclide ^{242}Am. The discrete transition spectra, as well as continuous level contribution to the fission transmission coefficient are dependent upon the order of symmetry for ^{242}Am fissioning nucleus at inner and outer saddles. Due to the axial asymmetry at the inner saddle[42] we additionally assume $(2J+1)$ rotational levels for each J value. The rotational band levels at outer saddle are assumed to be doubly degenerate due to mass asymmetry.[42] With transition state spectra defined in the first 0.2 MeV excitation energy range (see Table 4.1) the fission barrier parameters (see Table 4.2) are obtained by fitting fission data (see figs. 4.4, 4.5). The fission width for $s-$wave neutrons $\langle\Gamma_f\rangle$, calculated at incident neutron energy of 0.15 keV is consistent with average fission width value, obtained in unresolved resonance region.

The discrete character of few-quasiparticle excitations is virtually unimportant for level density modelling in case of odd-odd ^{242}Am fissioning nuclide. We will model the level density above 0.2 MeV in the following approximate way. The level density of axially symmetric fissioning nucleus is calculated in constant temperature approximation, i.e. $\rho(U) = T_f^{-1}\exp((U-U_o)/T_f)$. The respective parameters, nuclear temperature T_f and excitation energy shift U_o are defined at the matching energy U_c =2.4 MeV. At excitation energies above U_c the continuum part of the transition state spectrum is represented with the phenomenological model[19], which

takes into account pairing, shell and collective effects at saddle deformations. The asymptotic value of the main parameter of the level density for fissioning nucleus ^{242}Am is assumed to be the same, as that of ^{242}Am compound nuclide. After that the effects of non-axiality and mass asymmetry are included. The detailed procedure of calculating fission transmission coefficient is described elsewhere.[40] The respective parameters: shell correction at saddles δW, pairing correlation function Δ, quadrupole deformation ε, and momentum of inertia at zero temperature $F_0/\hbar^2$ are given in Table 4.3.

Table 4.1

Transition spectra band-heads of ^{242}Am

inner saddle		outer saddle	
K^π	E_{K^π}, MeV	K^π	E_{K^π}, MeV
1^-	0.0	1^-	0.0
0^-	0.044	0^-	0.044
5^-	0.049	5^-	0.049
6^-	0.170	6^-	0.170
1^-	0.220	1^-	0.220
3^-	0.242	$3-$	0.242
2^-	0.288	2^-	0.288

Table 4.2

Fission barrier parameters

Nucleus	Barrier	Barrier height, MeV	Curvature, MeV
^{242}Am	inner	6.315	0.6
^{242}Am	outer	5.775	0.4
^{241}Am	inner	6.000	0.8
^{241}Am	outer	5.350	0.5
^{240}Am	inner	6.100	0.6
^{240}Am	outer	6.000	0.4
^{239}Am	inner	6.000	0.8
^{239}Am	outer	5.400	0.6

Table 4.3

Level density parameters of ^{242}Am fissioning nucleus and residual nucleus ^{241}Am

Parameter	inner saddle	outer saddle	neutron channel
δW, MeV	2.5	0.6	-2.402
$\triangle$, MeV	$\triangle_0$ +0.11	$\triangle_0$ +0.11	$\triangle_0$
ε	0.6	0.8	0.24
$F_0/\hbar^2$, MeV^{-1}	100	200	73

Above ~2 MeV incident neutron energy fission cross section data were fitted (see fig. 4.6) by slight increase of pairing correlation function value. The parameters used for calculation of residual nuclide ^{241}Am level density for neutron emission competition are described below. Below incident neutron energy of 0.312 MeV the neutron cross sections are calculated within Hauser-Feshbach approach with a width fluctuation correction taken into account. For width fluctuation correction calculation only Porter-Thomas fluctuations are taken into account. Effective number of degrees of freedom for fission channel is defined at the higher (inner) saddle as $\nu_f^{J\pi} = T_f^{J\pi}/T_{f\,max}^{J\pi}$, where $T_{f\,max}^{J\pi}$ is the maximum value of the fission transmission coefficient $T_f^{J\pi}$. Above incident neutron energy of 0.312 MeV the Tepel et al.[44] approach is employed. The calculations are made with code STAT.[45]

4.2.4 Fission cross section above emissive fission threshold

The first chance fission cross section of ^{241}Am(n,f) reaction above the emissive fission threshold is fixed with the level density and fission barrier parameters systematics[40,41] (see Tables 4.2, 4.3) and secondary neutron spectra parameterization (see fig. 4.7). A consistent description of a complete set of measured data on (n,f), (n,2n) and (n,3n) for ^{238}U and ^{235}U targets was accomplished with the secondary neutron spectra parameterization[46], which is used here. The fission cross section is calculated with the statistical code STAPRE.[47] The fission barrier parameters of ^{241}Am and ^{240}Am are defined by fitting ^{241}Am(n,f) reaction data above emissive fission threshold. The neutron resonance spacing values for target nuclei ^{240}Am and ^{239}Am were taken from evaluation of Fort et al.[48] The calculated fission cross section is drastically different from JENDL-3 evaluated curve above (n,2nf) reaction threshold (see figs. 4.7, 4.8). The calculated fission cross section at 14.8 MeV neutron energy virtually coincides with the data by Prindle et al.[38] and Fomushkin et al.[36] The discrepancy with Dabbs et al.[12] is unavoidable,

since the measured data by Dabbs et al.[12] appear to be just as high as reaction cross section at 14.8 MeV. They are incompatible with the calculated fission cross section.

4.3 Inelastic scattering cross section

The inelastic scattering cross section is calculated with the statistical codes STAT[45] and STAPRE.[47] The discrete level excitation (compound and direct), continuum excitation and pre-equilibrium emission contribute to the inelastic scattering cross section.

4.3.1 Levels of ^{241}Am

The low-lying levels of scheme of Nuclear Data Sheets[49] appears incomplete at rather low excitation energy (see fig. 4.9). In JENDL-3 evaluation there are 16 discrete excited levels up to 0.682 MeV, i.e. the missing of levels above ~0.682 MeV is ignored (see fig. 4.9). Only one level with J^{π} =13/2$^-$ of the ground state band was added to the adopted level scheme of latest edition of ENSDF.[49]

4.3.2 ^{241}Am level density

The continuum level density below excitation energy U_c = 3.6 MeV is calculated with the constant temperature model

$$\rho(U) = T^{-1} \exp((U - U_o)/T),$$

here, energy shift U_0 = -0.96455 MeV, nuclear temperature T = 0.40723 MeV are the constant temperature model parameters. The cumulative number of observed levels is compared with constant temperature approximation on fig.4.9. At higher excitation energies the phenomenological model[19] is used. The main model parameter $\tilde{a}$ for ^{241}Am residual nucleus is obtained by fitting the predicted neutron resonance spacing[48] of ^{240}Am target nuclide $\langle D_{obs} \rangle$ = 0.372 eV.

4.3.3 Compound inelastic scattering

The residual nucleus ^{241}Am level density modelling, adopted in present work changes the inelastic scattering cross section below 5 MeV as compared with JENDL-3 evaluation (see fig. 4.10). Above ~1 MeV incident neutron energy the discrepancy is due to direct excitation of the ground state band levels. The discrete level excitation cross sections (see figs. 4.11 - 4.16) show that adopted optical potential influences appreciably on the shape of inelastic

cross sections. Above 0.3~ MeV incident neutron energy inelastic scattering to the continuum gives a major contribution to the total inelastic scattering cross section. Above 5 MeV incident neutron energy pre-equilibrium emission and direct inelastic scattering are the two reaction mechanisms which define inelastic scattering cross section (see fig. 4.13). The pre-equilibrium model parameters were tested by the statistical model description of ^{238}U+n interaction secondary neutron spectra and consistent description of fission and (n,xn) reaction data for major actinides.[46] Steep decrease of inelastic scattering cross section of JENDL-3 above ~5 MeV (see fig. 4.10) is due to missing of pre-equilibrium emission of neutrons.

4.3.4 Direct inelastic scattering

The direct inelastic scattering changes the shape of ground band levels excitation cross sections above 1 MeV incident neutron energy (see figs. 4.11 - 4.16). This mechanism defines partly the hard-energy tail in total inelastic scattering cross section (see fig. 4.10). The calculations were accomplished with the code COUPLE.[28]

Table 4.4

Level scheme of ^{241}Am

$E^J_{K^\pi}$, MeV	J^π	K	band	
0.000	$5/2^-$	5/2	A	
0.0418	$7/2^-$	5/2	A	
0.0936	$9/2^-$	5/2	A	
0.1580	$11/2^-$	5/2	A	
0.2059	$5/2^+$	5/2	B	
0.2340	$13/2^-$	5/2	A	*
0.2350	$7/2^+$	7/2	B	
0.2390	$3/2^-$	3/2	C	
0.2720	$9/2^+$	7/2	B	
0.2730	$5/2^-$	5/2	B	
0.3120	$15/2^-$	5/2	A	

*) added

4.3.5 ^{242}Am level density

The level density of odd-odd compound nuclide ^{242}Am one needs to calculate radiative capture width and (n,γn') reaction contribution to the compound

inelastic scattering cross section. The continuum level density below excitation energy U_c = 2.4 MeV is calculated with the constant temperature model, the constant temperature model parameters are: energy shift U_0 = -1.6452 MeV, nuclear temperature T = 0.39241 MeV. The cumulative number of observed levels is compared with constant temperature approximation on fig.4.12. At higher excitation energies the phenomenological model[19] is used. The main model parameter $\tilde{a}$ for ^{242}Am residual nucleus is obtained by fitting the evaluated neutron resonance spacing of ^{241}Am target nuclide $\langle D_{obs} \rangle$ = 0.505 eV.

4.4 Radiative capture cross section

Gayther and Thomas[22] have measured average neutron absorption cross section in the range of incident neutron energy from 100 eV to 500 keV using large liquid scintillator. The shape of incident neutron spectrum was determined by comparison with the ^{6}Li(n,α) cross section below 30 keV and the ^{235}U (n,f) cross section at the higher energies. The cross section was normalized in the 1 keV to 2 keV energy range to the value of 9.48 barns of Weston and Todd.[7] There is a systematic difference between data shapes of Gayther and Thomas[22] and Weston and Todd[7] of up to 20% between 10 and 100 keV.

Capture cross section was measured by Wisshak and Käppeler[23] in the energy range from 10 to 250 keV, using ^{197}Au as a standard. Capture events were detected by Moxon-Rae system. The data have been converted to absolute values using the ^{197}Au(n,γ) cross section of ENDF/B-VI. Capture cross section data agree well with absorption data of Gayther and Thomas[22], while Weston and Todd[7] data are systematically lower than both data sets. We will fit the capture cross section data of Wisshak and Käppeler.[23]

The radiative capture cross section is calculated within a statistical approach up to 5 MeV. Radiative capture strength function equals $S_{\gamma 0}$ = 958.42. At higher incident neutron energies we assume radiative capture cross section to be 1 mbarn. The radiative capture width was calculated with (n,γf) and (n,γn') reactions competition against "true" capture reaction (n,$\gamma\gamma$). Notwithstanding rather high fission threshold for ^{242}Am compound nuclide the competition of (n,γf) reaction is stronger than that of (n,γn') reaction. The influence of (n,γn') and (n,γf) reaction competition on radiative capture cross section is illustrated on fig.4.18 by sharp decrease of capture cross section above 1 MeV incident neutron energy, as compared with (n,γx) reaction cross section. The capture cross section of ENDF/B-VI is systematically higher than present evaluation above 200 keV.

4.5 Cross sections of (n,2n) and (n,3n) reactions

The current and JENDL-3 evaluated (n,2n) and (n,3n) cross sections are rather different. The magnitude of (n,2n) cross section below the (n,2nf) reaction threshold is defined by (n,nf) and (n,2n) reaction competition. We described in our approach the (n,2n) reaction data of Filatenkov et al.[39] around 14 MeV incident neutron energy. To calculate the (n,2n) reaction cross section we use an approach, developed for description of the ^{238}U(n,2n) reaction cross section.[46] The present and JENDL-3 evaluated fission cross sections are rather different, as well as reaction cross sections above 10 MeV incident neutron energy (see fig. 4.1). The present and JENDL-3 evaluations are compared in fig. 4.19. There is no hard-energy tail in (n,2n) reaction cross sections both in JENDL-3 and ENDF/B-VI evaluations. In case of (n,3n) reaction the difference in reaction cross section above 11 MeV (see fig. 4.1) contributes essentially to the discrepancy, shown on fig. 4.20.

5 Energy distributions of secondary neutrons

There is no measured data on secondary neutron spectra. To calculate neutron energy distributions of (n,xnγ) and (n,xnf), x=1, 2, 3 reactions we use a simple Weisscopf-Ewing evaporation model[50] taking into account fission and gamma competition to neutron emission. The pre-equilibrium emission of first neutron is included.

5.1 Model calculations of (n,nx) reaction spectra

The first neutron spectra for the (n,nx) reaction is the sum of evaporated and pre-equilibrium emitted neutron contributions. The pre-equilibrium emission contribution is calculated with a parameter systematics tested in case of n+^{238}U and n+^{235}U interactions.[46] We have calculated the 1st, 2nd and 3d neutron spectra for the (n,nγ), (n,2n) and (n,3n), where applicable. According to the ENDF/B-VI format we included the secondary neutron spectra in the following way. The calculated spectra were summed up and tabular spectra for the (n,nγ), (n,2n) and (n,3n) reactions were obtained. To clarify the competition of neutron, γ-emission emission and fission in case of (n,nx) and (n,2nx) reactions we have chosen the following presentation of spectra. Figure 5.1 shows the spectrum of 1st neutron of the reaction (n,nx) and its partial contributions for (n,nγ), (n,2n), (n,nf) (n,2nf) and (n,3n) reactions. Figure 5.2 shows the spectrum of 2nd neutron of the reaction (n,2nx) and its partial contributions for (n,2n), (n,3n) and (n,2nf) reactions. The spectra of 1st and 2nd neutrons are normalized to unity. The partial neutron spectra shown on figs. 5.1, 5.2 are normalized to the contributions of

appropriate cross sections to the (n,nx) and (n,2nx) reaction cross sections, respectively.

Table 5.1 Average energies of secondary neutron spectra

E_n , MeV	1st neutron average energy, MeV								
	(n, n')			(n, 2n)		(n, n'f)	(n, 3n)		(n, 2n'f)
	pres.	B - 6	J - 3	pres.	J - 3	pres.	pres.	J - 3	pres.
2.0	0.54	0.52	0.60						
8.0	3.55	3.59	1.12	0.68	0.69	1.02			
15.0	10.79	9.65	1.53	3.85	1.53	3.44	1.02	1.19	0.91
20.0	15.78	15.64	1.77	9.06	1.77	4.75	3.11	1.77	2.80

E_n , MeV	2nd neutron average energy, MeV					3d neutron	
	(n, 2n)		(n, 3n)		(n, 2n'f)		
	pres.	J - 3	pres.	J - 3	pres.	pres.	J - 3
8.0	0.23	0.65					
15.0	0.86	1.07	0.73	0.98	0.66	0.22	0.77
20.0	0.85	1.38	1.14	1.39	1.12	0.64	0.80

The inclusion of pre-equilibrium emission changes significantly the average energies of emitted neutron spectra. That is shown in Table 5.1, where the average secondary neutron energies for current and JENDL-3 and ENDF/B-VI evaluations are compared. The most significant is the change of neutron spectra of (n,nγ) reaction. Figs 5.3-5.7 demonstrate the discrepancies of secondary neutron spectra in current, JENDL-3 and ENDF/B-VI evaluations. Spectra of our and ENDF/B-VI evaluations are in qualitative agreement, while those of JENDL-3 are much softer.

The 1st neutron spectra of (n,nf) reaction also becomes harder and that influences prompt fission neutron spectra. On the other hand, the spectra of 2nd and 3d neutrons become softer.

5.2 Prompt fission neutron spectra

Prompt fission neutron spectra were calculated within the framework of Madland-Nix model.[51]

5.2.1 Model calculations of prompt fission neutron spectra

The model parameters, which should be defined are the following.

5.2.1.1 Fragment masses. The fragment masses are defined as $A_L = 102$ and $A_H = 140$, in accordance with the data of Asghar et al.[52] Fragment charges are defined using the ratios of

$$\langle A_{L,H}\rangle/(Z_{L,H} \mp 0.5) = A_F/Z_F.$$

The average fragments adopted are ^{102}Nb and ^{140}Xe.

5.2.1.2 Energy parameters. Average total fission energies $\langle E_R\rangle$ and average fission-fragment separation energies are calculated as in Madland-Nix model using mass tables of Audi and Wapstra.[53] Measured total fragment kinetic energy $\langle TKE\rangle$ for ^{242}Am fissioning nucleus differs significantly in limits 179-185 MeV in various measurements. Therefore the value of $\langle TKE\rangle$ for this nuclei had been defined to fit $\nu_p(E)$ from thermal to 5 MeV energy. The resulted $\langle TKE\rangle = 183.02 - 0.08E_n$, for other fissioning nuclei $\langle TKE\rangle$ had been defined as $\langle TKE\rangle(A-1) = \langle TKE\rangle(A) + 0.24E_n$ in accordance with Viola et al.[54] systematics.

5.2.2 Other parameters.

The level density parameter of the fermi-gas model is calculated as $a = A_{L,H}/10.2$, MeV.$^{-1}$ Becchetti-Greenlees[55] spherical optical potential parameters are employed to calculate compound cross section.

5.2.3 Prompt fission neutron spectra evaluation

Below emissive fission threshold prompt fission neutron spectra are calculated with the parameters given in Table 5.2. Figure 5.8 shows the comparison of calculated thermal prompt fission neutron spectrum with maxwellian spectra of JENDL-3 (T =1.389 MeV) and ENDF/B-VI (T = 1.3906 MeV). Average energy of fission spectrum is 2.14 MeV, it is compatible with evaluated values of JENDL-3 and ENDF/B-VI, however the spectra shapes are significantly different. Figures 5.9, 5.10 demonstrate the discrepancy of our calculation and JENDL-3 and ENDF/B-VI evaluations. The discrepancies are due to emissive fission contribution in present evaluation as well as maxwellian fission spectrum presentation in JENDL-3 independent from incident neutron energy.

Above emissive fission threshold the fission neutron spectra $N(E)$ is the superposition of emissive fission spectra, i.e.

$$N(E) = (\tfrac{\sigma_{nf}}{\sigma_{nF}}\nu_1 N_1(E) + \tfrac{\sigma_{nn'f}}{\sigma_{nF}}\left[\Phi_{nn'f}(E) + \nu_2 N_2(E)\right]$$

$$+\frac{\sigma_{n2nf}}{\sigma_{nF}}\left[\Phi^1_{n2nf}(E)+\Phi^2_{n2nf}(E)+\nu_3 N_3(E)\right])/$$

$$\left[\frac{\sigma_{nf}}{\sigma_{nF}}\nu_1+\frac{\sigma_{nn'f}}{\sigma_{nF}}(1+\nu_2)+\frac{\sigma_{n2nf}}{\sigma_{nF}}(2+\nu_3)\right],$$

where σ_{nF}, σ_{nf}, $\sigma_{nn'f}$, σ_{n2nf} are the total and i-th chance fission cross sections (i = 1,2,3); $\Phi_{nn'f}$, Φ^1_{n2nf}, and Φ^2_{n2nf} are emitted neutron spectra: for (n,nf) reaction, 1st and 2nd neutrons of (n,2nf) reaction, respectively; ν_i and N_i are multiplicity and prompt neutron spectra for the i-th fissioning nucleus. The pre-equilibrium emission of the first neutron is included, the $\Phi^i_{n,xnf}$ spectra for the emissive fission are calculated with Weisscopf-Ewing evaporation model.[50]

Table 5.2

Parameters of the Madland-Nix model

Fissioning nucleus	A_L fragm.	A_H fragm.	$\langle E_R \rangle$, MeV	$\langle TKE \rangle$, MeV	B_n, MeV
^{242}Am	^{102}Nb	^{140}Xe	204.963	183.020	5.538
^{241}Am	^{101}Nb	^{140}Xe	204.353	183.260	6.641
^{240}Am	^{100}Nb	^{140}Xe	204.845	183.500	5.957

Table 5.3 Comparison of Madland-Nix and present approach

	E_n = 8 MeV		E_n = 15 MeV	
Quantity	M-N model[50]	Present	M-N model[50]	Present
$\langle E_1 \rangle$	2.333	2.333	2.485	2.485
ν_1	4.241	4.241	5.220	5.220
$\langle E_{n'f} \rangle$	1.179	1.021	1.600	3.436
$\langle E_2 \rangle$	2.158	2.162	2.310	2.269
ν_2	3.117	3.139	4.000	3.757
$\langle E_{2nf} \rangle^1$	-	-	1.600	0.906
$\langle E_{2nf} \rangle^2$	-	-	1.088	0.658
$\langle E_3 \rangle$	-	-	2.147	2.173
ν_3	-	-	2.967	3.105
$\langle E \rangle$	2.230	2.221	2.367	2.475
ν	4.210	4.215	5.140	5.062

Table 5.3 (continued)

E_n = 20 MeV	
M-N model[50]	Present
2.586	2.586
5.900	5.900
1.839	4.753
2.412	2.351
4.620	4.242
1.839	2.804
1.412	1.124
2.254	2.238
3.560	3.470
2.436	2.625
5.764	5.614

The influence of pre-equilibrium pre-fission neutrons on prompt fission neutron multiplicity ν_i and prompt neutron spectra N_i predictions as well as $N(E)$ and $\nu(E)$, is illustrated in Table 5.3 and Fig. 5.11. In Table 5.3 $\langle E_i \rangle$ denotes average prompt fission neutron energy of i-th fissioning nucleus, $\langle E \rangle$ is the average fission neutron energy, $\langle E_{n'f} \rangle$, $\langle E_{2nf} \rangle^1$and $\langle E_{2nf} \rangle^2$are the average energies of neutrons, emitted in (n,nf) and 1st and 2nd neutrons emitted in (n,2nf) reactions, respectively. The Figs. 5.12-5.14 show the partial contributions of i-th chance fission to the total fission neutron spectrum at incident neutron energies of 8, 15 and 20 MeV.

6 Number of neutrons per fission

The number of prompt fission neutrons at thermal energies was measured by Lebedev and Kalashnikova[56] in 1958 (ν_p=3.066±0.05) and Jaffey and Lerner[57] in 1970 (ν_p=3.219±0.021). At higher energies the $\nu_p(E)$ was measured by Khokhlov et al.[58,59], but the the data are unaccessible and only linear energy dependence $\nu_p(E)$=(3.055±0.023)+(0.139± 0.007)E_n fitted to experimental data is provided. Note, that the data points on the figures of refs.[58,59] lie systematically higher than proposed energy dependence. That may be due to different weights for data points while producing the energy dependence estimate. Therefore the present evaluation of $\nu_p(E)$ is based on calculation within Madland-Nix model, fitted in the energy range up to 5 MeV to the energy dependence of Khokhlov et al.[59]: $\nu_p(E)$=3.078+0.146E_n. The calculated number of prompt fission neutrons is consistent with both the data points and the energy dependence of Khokhlov et al.[59] up to ~ 10 MeV incident neutron energy. The comparison of $\nu_p(E)$ with measured data,

JENDL-3 and ENDF/B-VI evaluations is shown on fig. 6.1. The Madland-Nix model calculations predict non-linear increase of $\nu_p(E)$ above emissive threshold. The influence of pre-equilibrium pre-fission neutrons manifests in additional appreciable decrease of $d\nu/dE$ above 12 MeV. The delayed number of neutrons per fission ν_d and the decay constants for six groups of delayed neutrons are taken from Brady et al.[60] Specifically, $\nu_d = 0.00427$ for incident neutron energies up to 4 MeV and $\nu_d = 0.002418$ for $E_n \geq 7$ MeV.

7 Angular distributions of secondary neutrons

The angular distributions of elastically scattered neutrons and those for neutrons, scattered on three levels of ground state band are calculated with the coupled channel method. The isotropic compound scattering contribution is taken into account by renormalizing l-th Legendre polynomial coefficients A_l^{cc}, calculated with coupled channels:

$$A_l = A_l^{cc}\sigma_{dir}/(\sigma_{dir}+\sigma_{comp}),$$

where σ_{dir} and σ_{comp} are the scattering cross section direct and compound contributions, respectively. For the other contributing reactions angular distributions of secondary neutrons are assumed isotropic.

8 Conclusions

The evaluated neutron data file for ^{241}Am is compiled in ENDF/B-VI format and sent to the International Science and Technology Center (Moscow) and Japan Nuclear Data Center at Japan Atomic Energy Research Institute.

Numerous discrepancies of experimental data coupled with possibility of some new data becoming available (for example, ^{241}Am(n,f) data of Kobayashi et al.[5] (Kyoto University, Japan) may urge some revision of data file. Present version of ^{241}Am data file may be revised before 1 March of 1998, the expiration date of Project CIS-03-95.

9 References

1. Nakagawa T., Kikuchi Y., Proc. of the Int. Conf. on Nuclear Data and Technology, Gatlinburg, Tenn., USA, 9-13 May, 1994, Dickens J.K. (Editor), 709, ANS Inc., 1994.
2. Japanese Evaluated Data Library, Version 3, JAERI 1319, 1990.
3. C.L. Dunford, Nuclear Data for Science and Technology, Proc. Int. Conf. Julich, 1991,788.Springer-Verlag,1992, Berlin
4. Seeger P.A., Hemmendinger A., Diven B.C. Nucl. Phys. A96, 605 (1967)
5. Kobayashi K., Yamamoto S., Fujita Y., et al. Nuclear Data for Science and Technology, Proc. Int. Conf., Gatlinburg, 1994, 242, ANS.
6. Derrien H., Lucas B. Nuclear Cross Sections and Technology, Proc. Conf., Washington DC, March 3-7, 1975, p.637, NBS Special Publication 425 (1975).
7. Weston L.W. and Todd J.H. Nucl. Sci. Eng., 61, 356 (1976).
8. Kalebin S. Sov. J. At. Energy, 40, 373, (1976)
9. Lynn J.E., Patrick B.H., Sowerby M.G. and Bowey E.M. AERE-R8528, 1979
10. Adamchuk Yu.V. et al. Conf. on Peaceful Uses of Atomic Energy, Geneva, vol. 4, p. 216, 1955.
11.Belanova T.S., Zamyatnin Yu.S., Kolesov A.G., et al. Preprint NIIAR-307, 1977.
12. Dabbs J.W.T., Johnson C.H., Bemis Jr. C.E. Nucl. Sci. Engng. 83, 22 (1983).
13. Bowman C.D., Coops M.S., Auchampaugh G.F., Fultz S.C. Phys. Rev. B326, 137 (1965)
14. Gerasimov V.F. Yadernaya Fyzika 4, 985 (1966).
15. Vanpraet G., Cornelis E., Raman S., Rohr G. Nuclear Data for Basic and Applied Science, Proc. Int. Conf., Santa Fe, 1985, vol. 1, 493.
16. Maslov V.M., Porodzinskij Yu.V., Sukhovitskij E.Sh., Klepatskij A.B., Morogovskij G.B. INDC(BLR)-3, 1996.
17. Dunford C.L.: "ENDF Utility Codes Release 6.9", IAEA-NDS-29 (1993)
18. Porodzinskij Yu.V., Sukhovitskij E.Sh., Nuclear Constants, 4, p.27, 1987 (in Russian)
19. Ignatjuk A.V., Istekov K.K., Smirenkin G.N. Sov. J. Nucl. Phys. 29, 450 (1979). 1984.
20. Bowman J.C., Auchampaugh G.F., Fultz S C., Hoff R.W. Phys. Rev. 166, 1216 (1968)
21. Shpack D.L., Ostapenko Yu.B., Smirenkin G.N. JETP Lett. 10, 175 (1969)
22. Gayther D.B. and Thomas B.W. Proc. 4th All-Union Conf. Neutron Physics, Kiev, Soviet Union, April 18-22, 1977, III, 3, Atomizdat (1977).

23. Wisshak K., Kappeler Nucl. Sci. Eng. 76, 148 (1980)
24. Hage W., Wisshak K., Kappeler Nucl. Sci. Eng. 78, 248 (1981)
25. Knitter H.-H., Budtz-Jorgensen C. Atomkernenergie. Kerntechnik, 3, 205 (1979).
26. Phillips T.W., Howe R.E. Nucl. Sci. Engng. 69, 375 (1979)
27. Haouat G., Lachkar J., Lagrange Ch., et al., Nucl.Sci. Engng. 81, 491 (1982)
28. Klepatskij A.B., Sukhovitskij E.Sh., private communication.
29. Fomushkin E.F., Gutnikova Sov. J. Nucl. Phys. 10, 529 (1970).
30. Kupriyanov V.M., Fursov B.I., Ivanov V.I., Smirenkin G.N. Sov. J. At. Energy 45, 176 (1979)
31. Fursov B.I., Kupriyanov V.M., Ivanov V.I., Smirenkin G.N. Sov. J. At. Energy 43, 894 (1978).
32. Aleksandrov B.M., Nemilov Yu. A., Selitskii Yu.A., et al. Sov. J. At. Energy 46, 475 (1979).
33. Behrens J.W., Browne J.C. Nucl. Sci. Engng. 77, 444 (1981)
34. Protopopov A.N., Selitskij Yu.A., Solov'ev S.M. Sov. J. At. Energy 6, 36 (1959)
35. Kazarinova M.I., Zamyatnin Yu.S., Gorbachev V.M. Sov. J. At. Energy 8, 125 (1960)
36. Fomushkin E.F., Gutnikova E.K., Zamyatnin Yu.S., Maslennikov B.K., et al. Sov. J. Nucl.Phys. 5, 689,(1967).
37. Cance M., Grenier G., CEA-N-2194, 1981
38. Prindle A.L., Sisson D.H., Nethaway D.R., Kantelo M.V., Sigg R.A. Phys. Rev. C20, 1824 (1979).
39. Filatenkov A.A, Ikeda Y., Smith D.L. Private communication.
40. Ignatjuk A.V., Maslov V.M., Proc. Int. Symp. Nuclear Data Evaluation Methodology, Brookhaven,USA, October 12-16, 1992, p.440, World Scientific, 1993.
41. Maslov V.M. Sov. J. At. Energy 64, 478 (1988).
42. Sood P.C., Singh R.N. Nucl. Phys. A373, 519 (1982).
43. Howard W.M., Moller P. Atomic Data and Nuclear Data Tables,25, 219 (1980)
44. Tepel J.W., Hoffman H.M., Weidenmuller H.A. Phys. Lett. 49, 1 (1974).
45. Klepatskij A.B., Maslov V.M., Sukhovitskij E.Sh., private communication.
46. Ignatjuk A.V., Maslov V.M., Pashchenko A.B. Sov. J. Nucl. Phys. 47, 224 (1988).
47. Uhl M. and Strohmaier B., Report IRK - 76/10 (Vienna,1976).
48. Fort E., Darrouzet M., Derrien H., et al. Proc. Int. Conf. Nucl. Cross Sections for Technology, Knoxville, 22-26 Oct. 1979, NBS Special Publ., p.862, 1980.

49. ENSDF, 1995.
50. Maslov V.M., Porodzinskij Yu.V.,Sukhovitskij E.Sh., Proc. Int. Conf. on Neutron Physics, 14-18 Sept., Kiev, USSR, V.1, p.413, 1988.
51. Madland D.G., Nix J.R., Nucl. Sci. Engng. 81, 213 (1982).
52. Asghar M. et al., Nuclear Physics A, 334, 327 (1980).
53. Audi G., Wapstra A.H., Nuclear Physics A, 565, 1 (1980).
54. Viola V.E., Kwiatkowski K., Walker M., Phys. Rev., 31, 1550 (1985).
55. Becchetti F.D., Greenlees G.W., Phys. Rev. 182, 1190 (1969).
56. Lebedev V.I., Kalashnikova V.I., Atomnaya Energiya 5, 176 (1958)
57. Jaffey A.H., Lerner J.L., Nuclear Physics A, 145, 1 (1970).
58. Khokhlov Yu.A. et al., Nuclear Data for Science and Technology Proc. of the Int. Conf., Julich, Germany, 13-17 May, 1991 (Springer-Verlag, 1992), p. 51.
59. Khokhlov Yu.A. et al., Nuclear Data for Science and Technology, Proc. of the Int. Conf., Gatlinburg, Tennessee, USA, May 9-13, 1994, v.I, p. 272.
60. Brady M.C., Wright R.Q., England T.R., Report ORNL/CSD/TM-226(1991), IAEA-NDS-102, 1992.

10 Figure captions

Fig. 2.1 Total cross section of ^{241}Am in the energy region below 1 eV.
Fig. 2.2 Total cross section of ^{241}Am in the energy region below 8 eV.
Fig. 2.3 Total cross section of ^{241}Am in the energy region below 0.1 eV.
Fig. 2.4 Absorption cross section of ^{241}Am in the energy region below 0.1 eV.
Fig. 2.5 Fission cross section of ^{241}Am in the energy region below 0.1 eV.
Fig. 2.6 Distribution of radiative capture widths for ^{241}Am.
Fig. 3.1 Cumulative sum of neutron resonance levels of ^{241}Am.
Fig. 3.2 Cumulative sum of reduced neutron widths of ^{241}Am.
Fig. 3.3 Distribution of reduced neutron widths for ^{241}Am.
Fig. 3.4 Neutron resonance spacing distribution for ^{241}Am.
Fig. 3.5 Fission cross section of ^{241}Am in unresolved resonance region.
Fig. 3.6 Radiative capture cross section of ^{241}Am in unresolved resonance region.
Fig. 4.1 Compound reaction cross section of ^{241}Am.
Fig. 4.2 Total cross section of ^{241}Am.
Fig. 4.3 Elastic scattering cross section of ^{241}Am.
Fig. 4.4 Fission cross section of ^{241}Am.
Fig. 4.5 Fission cross section of ^{241}Am.
Fig. 4.6 Fission cross section of ^{241}Am.
Fig. 4.7 Fission cross section of ^{241}Am.
Fig. 4.8 Fission cross section of ^{241}Am.
Fig. 4.9 Cumulative number of levels of ^{241}Am.
Fig. 4.10 Inelastic scattering cross section of ^{241}Am.
Fig. 4.11 Cross section of ^{241}Am: 0.0418 MeV, $7/2^-$ level excitation.
Fig. 4.12 Cross section of ^{241}Am: 0.0936 MeV, $9/2^-$ level excitation.
Fig. 4.13 Cross section of ^{241}Am: 0.158 MeV, $11/2^-$ level excitation.
Fig. 4.14 Cross section of ^{241}Am: 0.2085 MeV, $5/2^+$ level excitation.
Fig. 4.15 Cross section of ^{241}Am: 0.235 MeV, $7/2^+$ level excitation.
Fig. 4.16 Cross section of ^{241}Am: 0.272 MeV, $9/2^+$ level excitation.
Fig. 4.17 Cumulative number of levels of ^{242}Am.
Fig. 4.18 Radiative capture cross section of ^{241}Am.
Fig. 4.19 ^{241}Am(n,2n) reaction cross section.
Fig. 4.20 ^{241}Am(n,3n) reaction cross section.
Fig. 5.1 Components of first neutron spectrum of ^{241}Am for incident neutron energy 15 MeV.
Fig. 5.2 Components of second neutron spectrum of ^{241}Am for incident neutron energy 15 MeV.

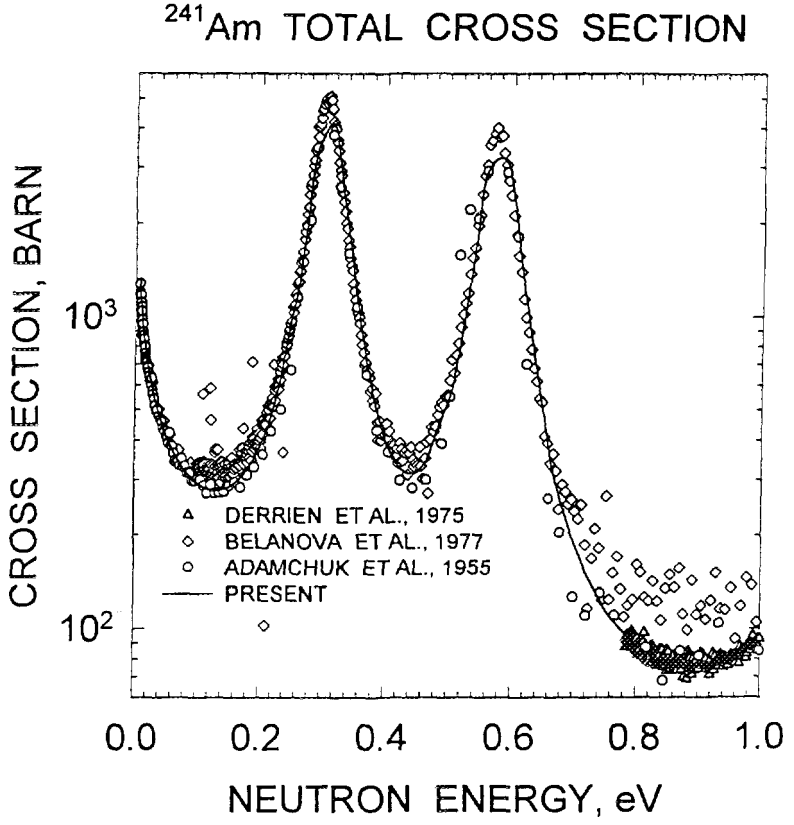
^{241}Am TOTAL CROSS SECTION
CROSS SECTION, BARN
10^3
10^2
DERRIEN ET AL., 1975
BELANOVA ET AL., 1977
ADAMCHUK ET AL., 1955
PRESENT
0.0
0.2
0.4
0.6
0.8
1.0
NEUTRON ENERGY, eV

FIG.2.1

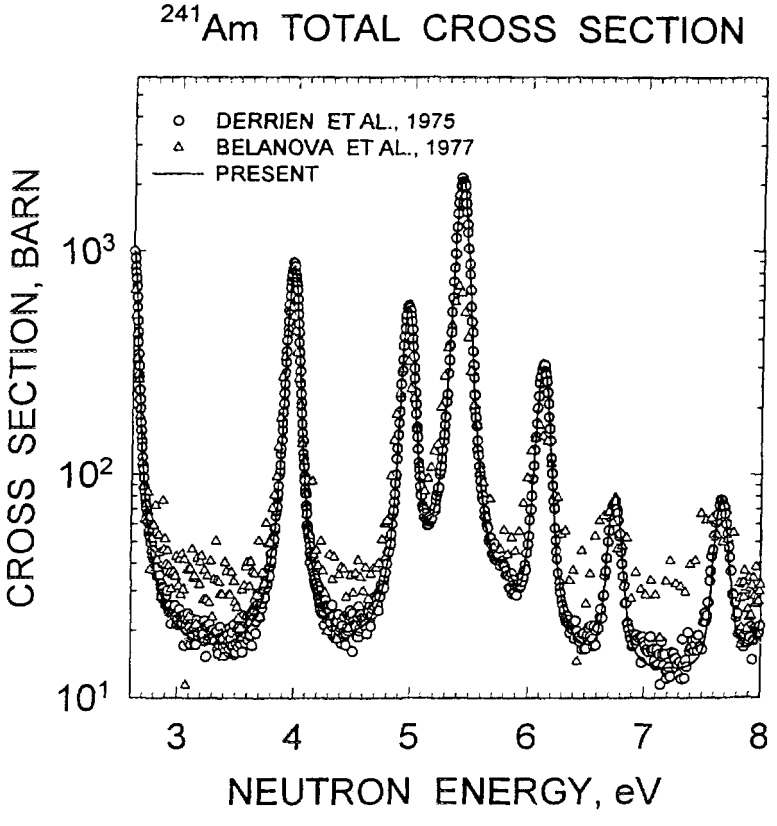
^{241}Am TOTAL CROSS SECTION
DERRIEN ET AL., 1975
BELANOVA ET AL., 1977
PRESENT
CROSS SECTION, BARN
10^3
10^2
10^1
3
4
5
6
7
8
NEUTRON ENERGY, eV

FIG.2.2

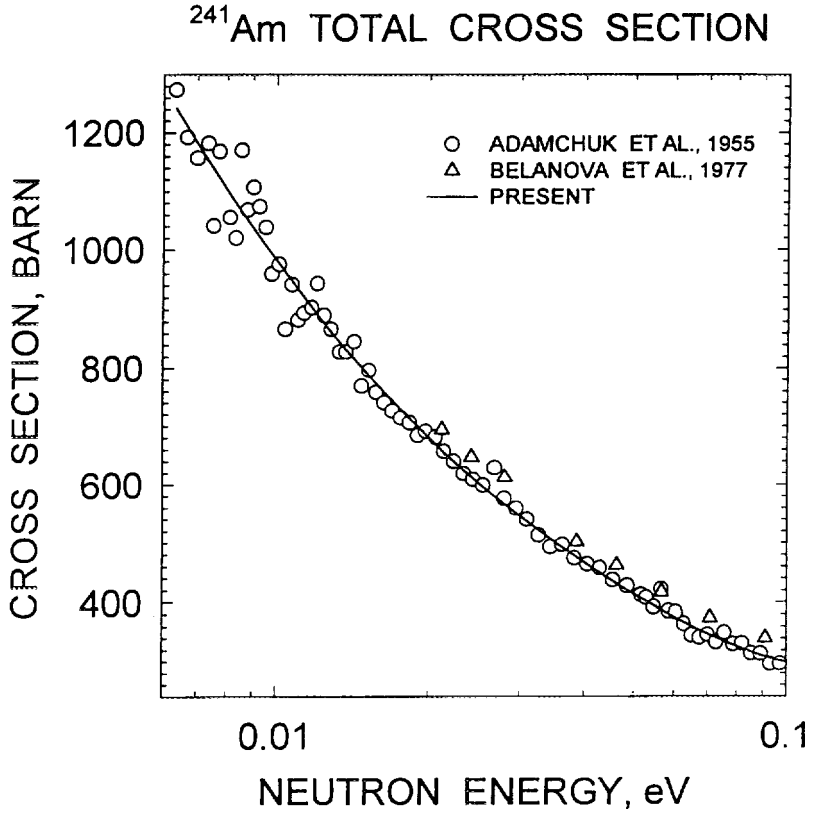
^{241}Am TOTAL CROSS SECTION
ADAMCHUK ET AL., 1955
BELANOVA ET AL., 1977
PRESENT
CROSS SECTION, BARN
1200
1000
800
600
400
0.01
0.1
NEUTRON ENERGY, eV

FIG.2.3

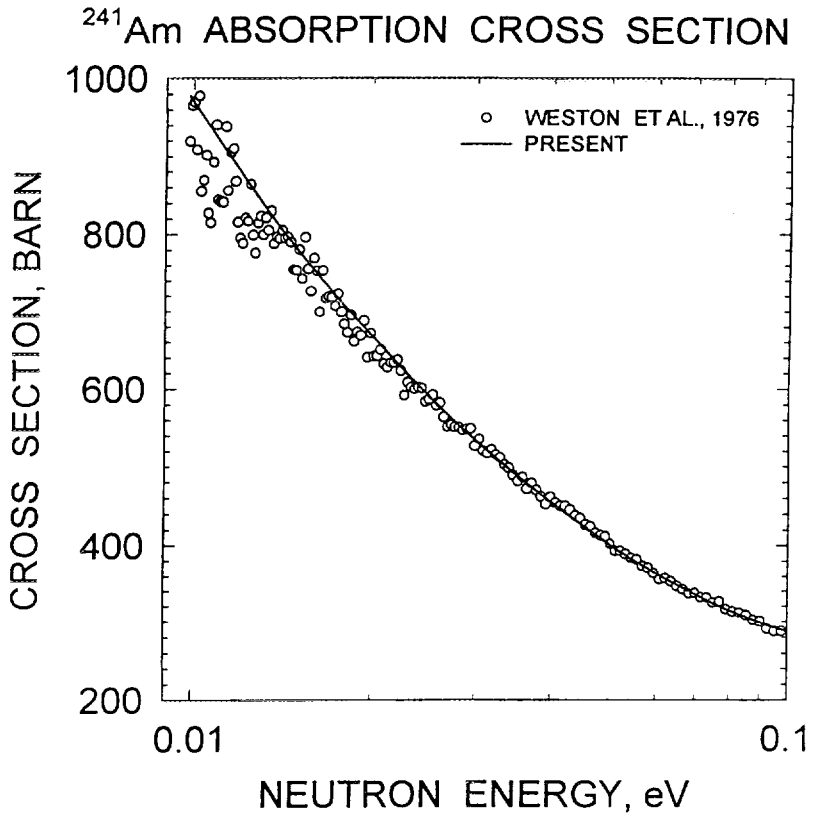
^{241}Am ABSORPTION CROSS SECTION
WESTON ET AL., 1976
PRESENT
CROSS SECTION, BARN
1000
800
600
400
200
0.01
0.1
NEUTRON ENERGY, eV

FIG.2.4

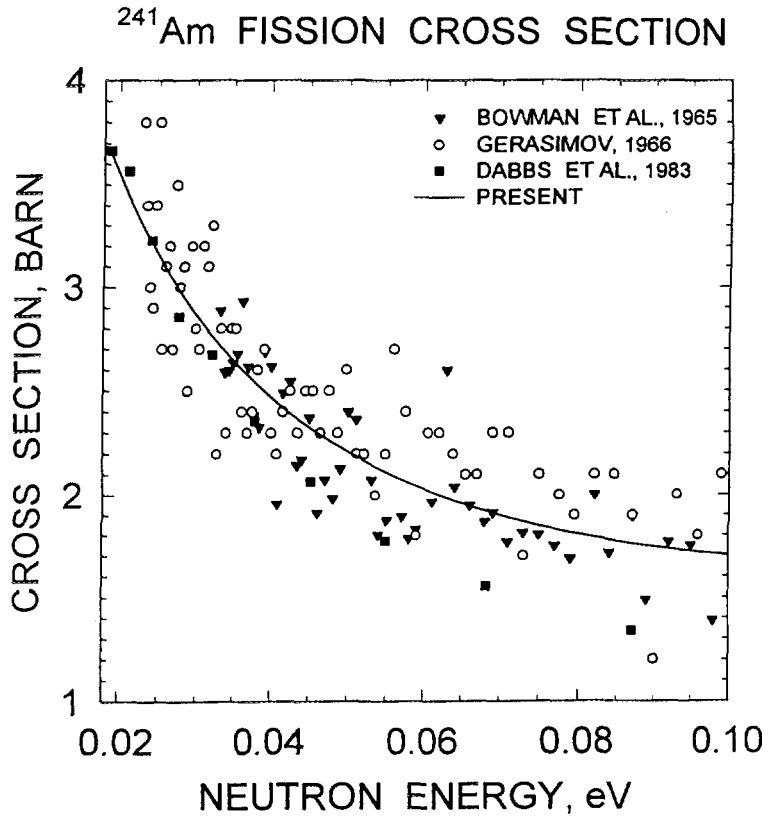
^{241}Am FISSION CROSS SECTION
BOWMAN ET AL., 1965
GERASIMOV, 1966
DABBS ET AL., 1983
PRESENT
CROSS SECTION, BARN
NEUTRON ENERGY, eV
1
2
3
4
0.02
0.04
0.06
0.08
0.10

FIG.2.5

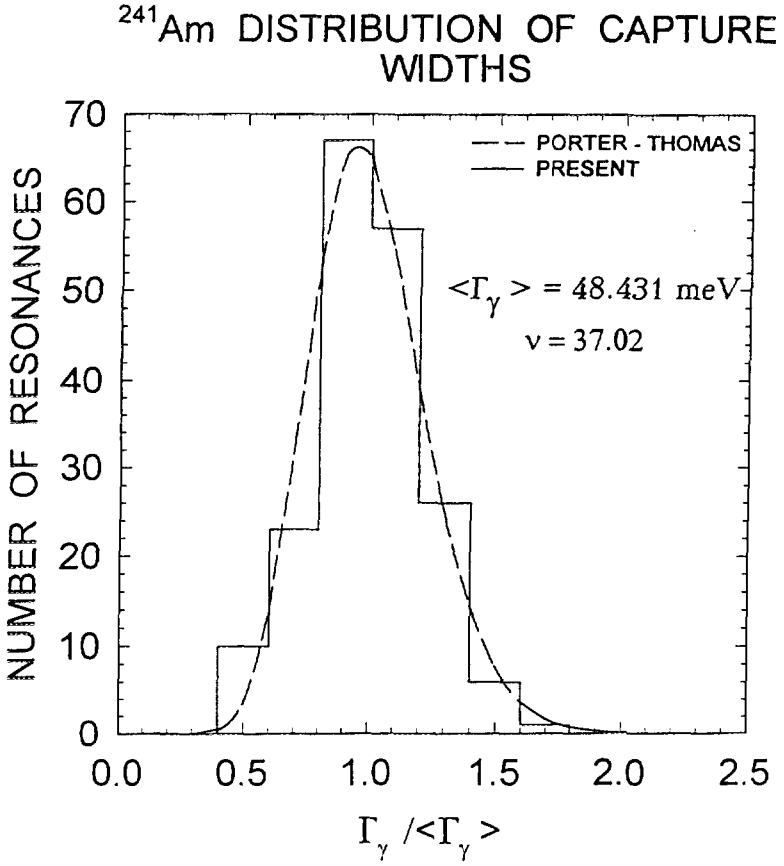
^{241}Am DISTRIBUTION OF CAPTURE WIDTHS
PORTER - THOMAS
PRESENT
$<\Gamma_\gamma>$ = 48.431 meV
ν = 37.02
NUMBER OF RESONANCES
$\Gamma_\gamma / <\Gamma_\gamma>$
0
10
20
30
40
50
60
70
0.0
0.5
1.0
1.5
2.0
2.5

FIG.2.6

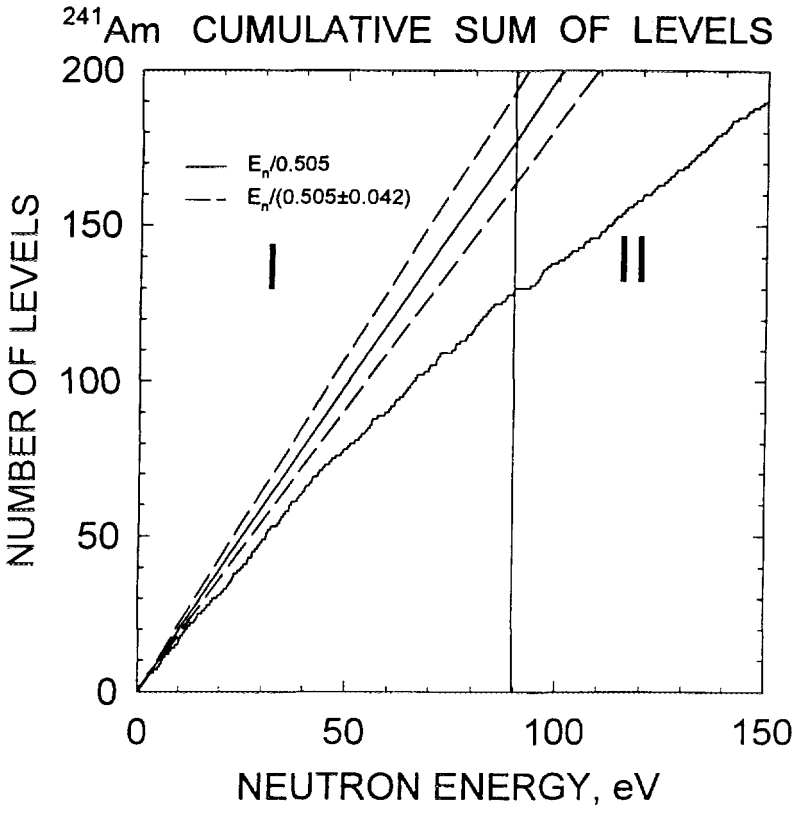
^{241}Am CUMULATIVE SUM OF LEVELS
NUMBER OF LEVELS
NEUTRON ENERGY, eV
E_n/0.505
E_n/(0.505±0.042)
I
II
0
50
100
150
200

FIG.3.1

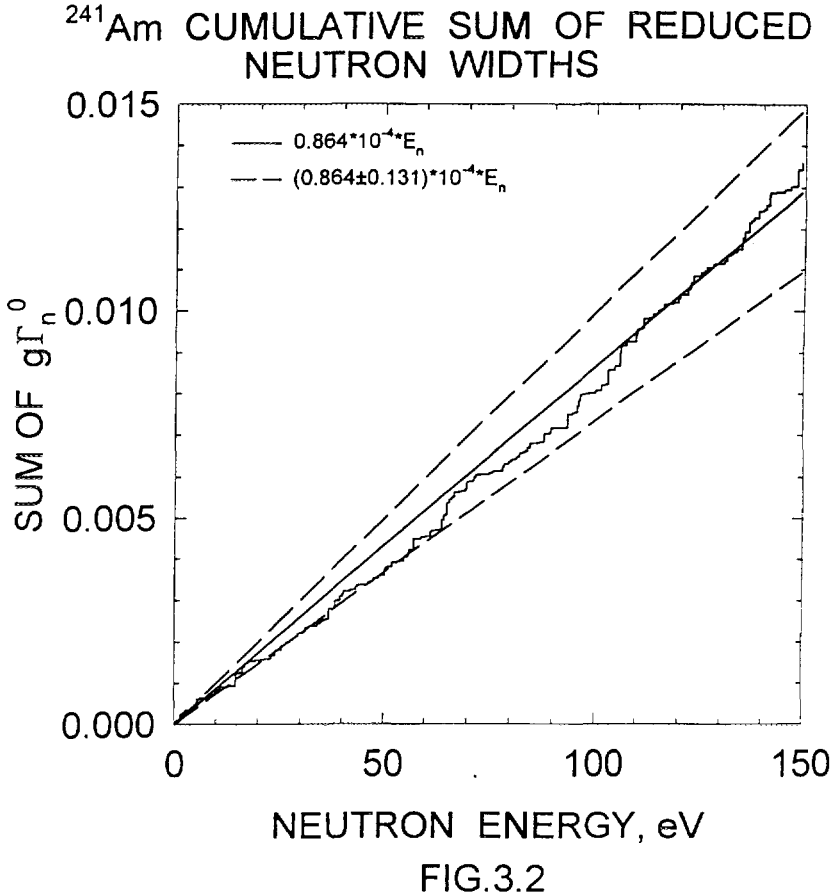
^{241}Am CUMULATIVE SUM OF REDUCED NEUTRON WIDTHS
SUM OF $g\Gamma_n^0$
NEUTRON ENERGY, eV
0.864*10^{-4}*E_n
(0.864±0.131)*10^{-4}*E_n
0.000
0.005
0.010
0.015
0
50
100
150

FIG.3.2

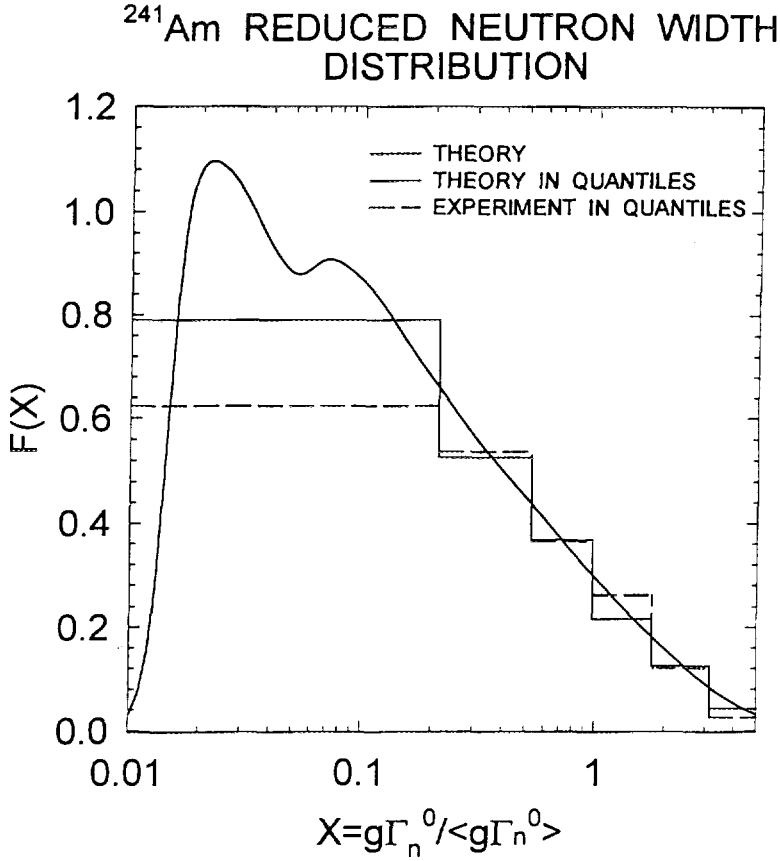
^{241}Am REDUCED NEUTRON WIDTH DISTRIBUTION
THEORY
THEORY IN QUANTILES
EXPERIMENT IN QUANTILES
F(X)
1.2
1.0
0.8
0.6
0.4
0.2
0.0
0.01
0.1
1
X=gΓn0/<gΓn0>

FIG.3.3

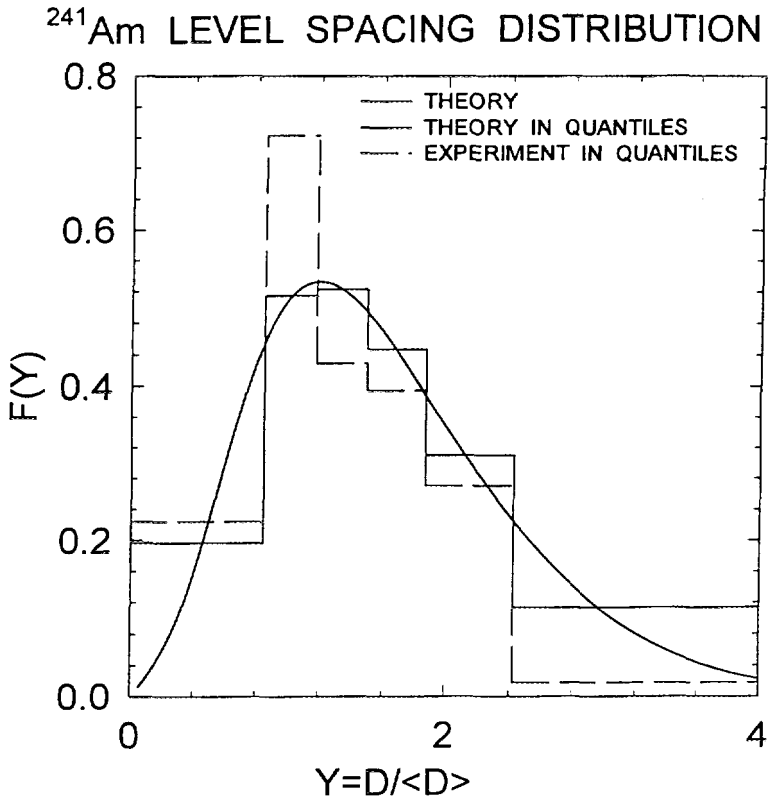
^{241}Am LEVEL SPACING DISTRIBUTION
THEORY
THEORY IN QUANTILES
EXPERIMENT IN QUANTILES
F(Y)
0.8
0.6
0.4
0.2
0.0
0
2
4
Y=D/<D>

FIG.3.4

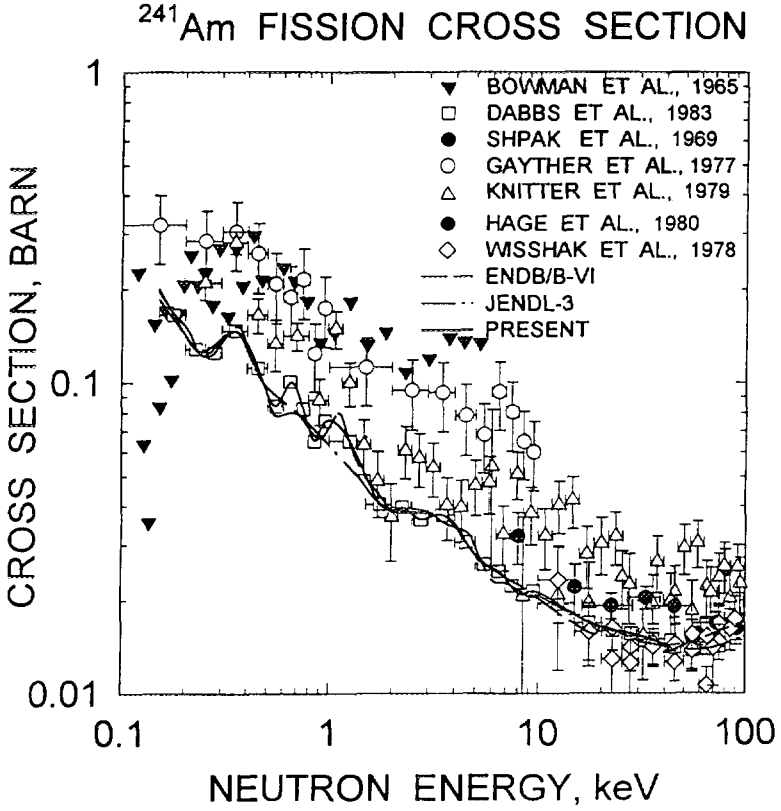
^{241}Am FISSION CROSS SECTION
BOWMAN ET AL., 1965
DABBS ET AL., 1983
SHPAK ET AL., 1969
GAYTHER ET AL., 1977
KNITTER ET AL., 1979
HAGE ET AL., 1980
WISSHAK ET AL., 1978
ENDB/B-VI
JENDL-3
PRESENT
CROSS SECTION, BARN
1
0.1
0.01
0.1
1
10
100
NEUTRON ENERGY, keV

FIG.3.5

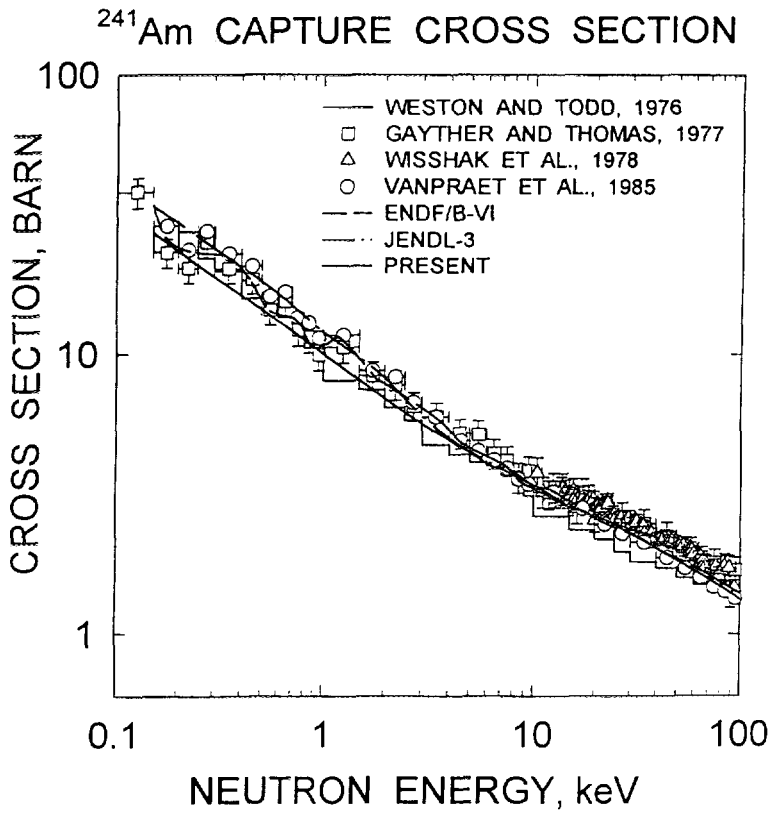
^{241}Am CAPTURE CROSS SECTION
WESTON AND TODD, 1976
GAYTHER AND THOMAS, 1977
WISSHAK ET AL., 1978
VANPRAET ET AL., 1985
ENDF/B-VI
JENDL-3
PRESENT
CROSS SECTION, BARN
100
10
1
0.1
1
10
100
NEUTRON ENERGY, keV

FIG.3.6

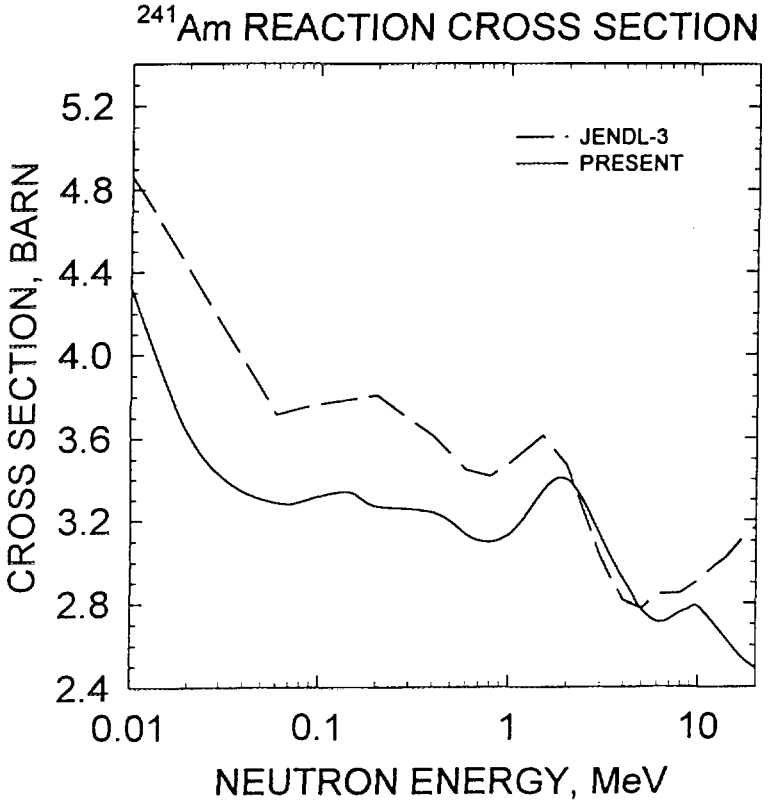
241Am REACTION CROSS SECTION
JENDL-3
PRESENT
CROSS SECTION, BARN
5.2
4.8
4.4
4.0
3.6
3.2
2.8
2.4
0.01
0.1
1
10
NEUTRON ENERGY, MeV

FIG.4.1

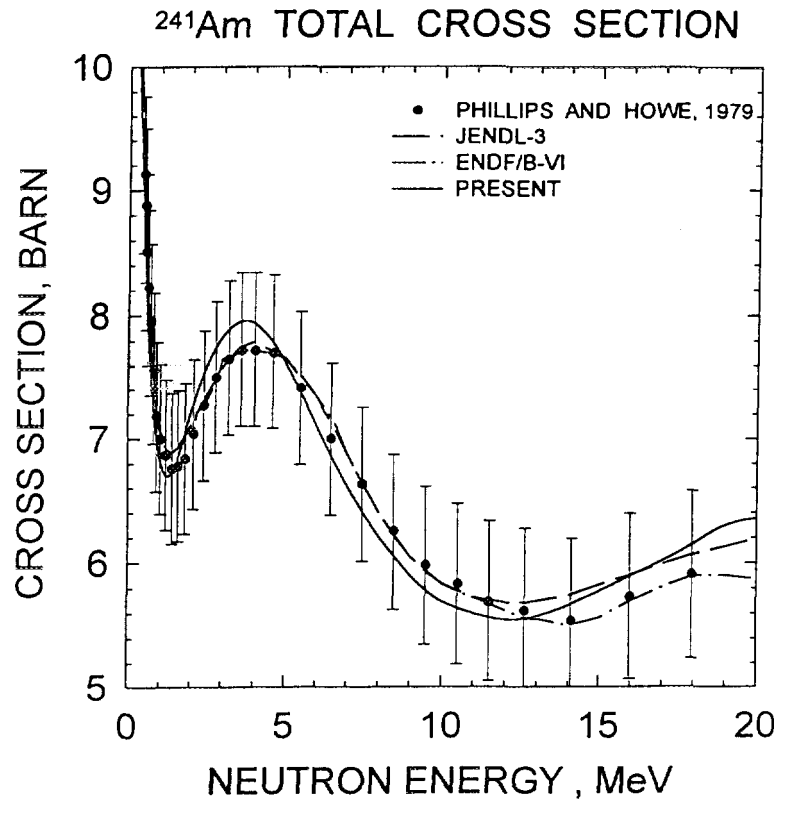
241Am TOTAL CROSS SECTION
PHILLIPS AND HOWE, 1979
JENDL-3
ENDF/B-VI
PRESENT
CROSS SECTION, BARN
10
9
8
7
6
5
0
5
10
15
20
NEUTRON ENERGY , MeV

FIG.4.2

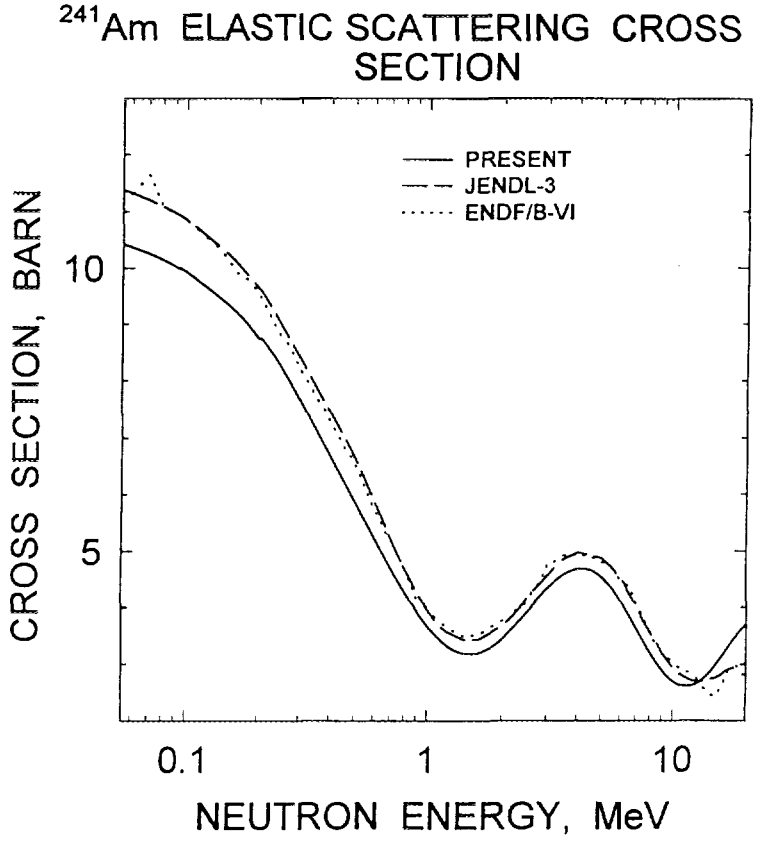
^{241}Am ELASTIC SCATTERING CROSS SECTION
PRESENT
JENDL-3
ENDF/B-VI
CROSS SECTION, BARN
10
5
0.1
1
10
NEUTRON ENERGY, MeV

FIG.4.3

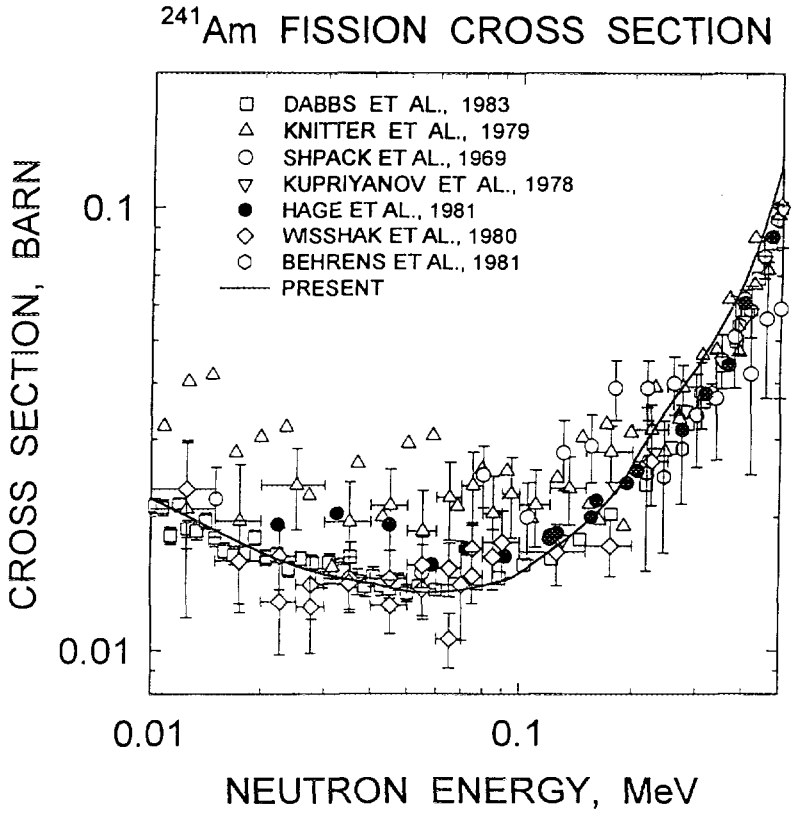
^{241}Am FISSION CROSS SECTION
DABBS ET AL., 1983
KNITTER ET AL., 1979
SHPACK ET AL., 1969
KUPRIYANOV ET AL., 1978
HAGE ET AL., 1981
WISSHAK ET AL., 1980
BEHRENS ET AL., 1981
PRESENT
CROSS SECTION, BARN
0.1
0.01
0.01
0.1
NEUTRON ENERGY, MeV

FIG. 4.4

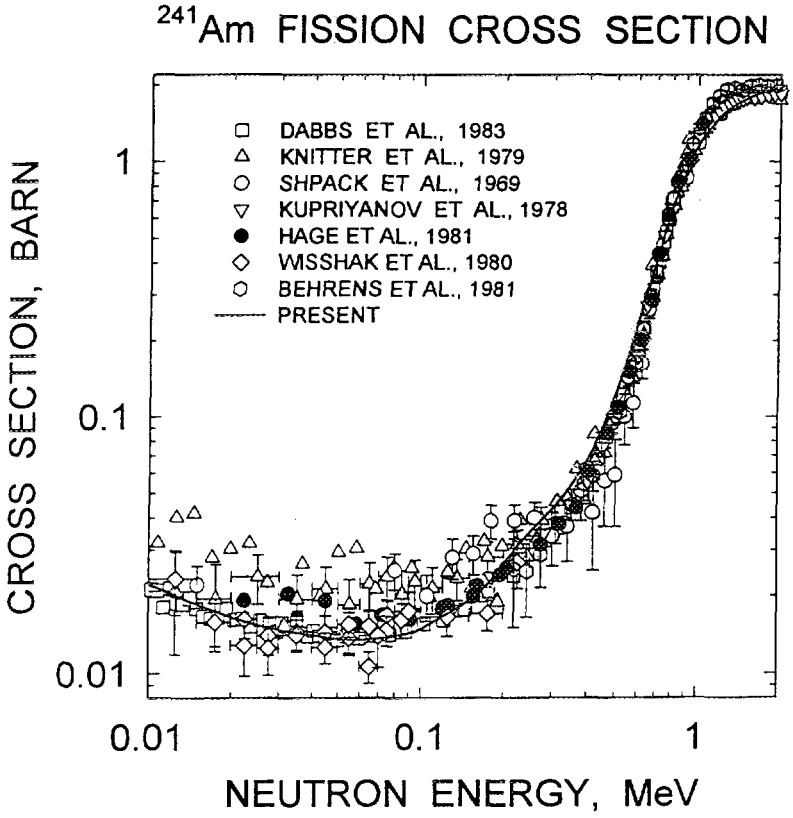
^{241}Am FISSION CROSS SECTION
DABBS ET AL., 1983
KNITTER ET AL., 1979
SHPACK ET AL., 1969
KUPRIYANOV ET AL., 1978
HAGE ET AL., 1981
WISSHAK ET AL., 1980
BEHRENS ET AL., 1981
PRESENT
CROSS SECTION, BARN
1
0.1
0.01
0.01
0.1
1
NEUTRON ENERGY, MeV

FIG. 4.5

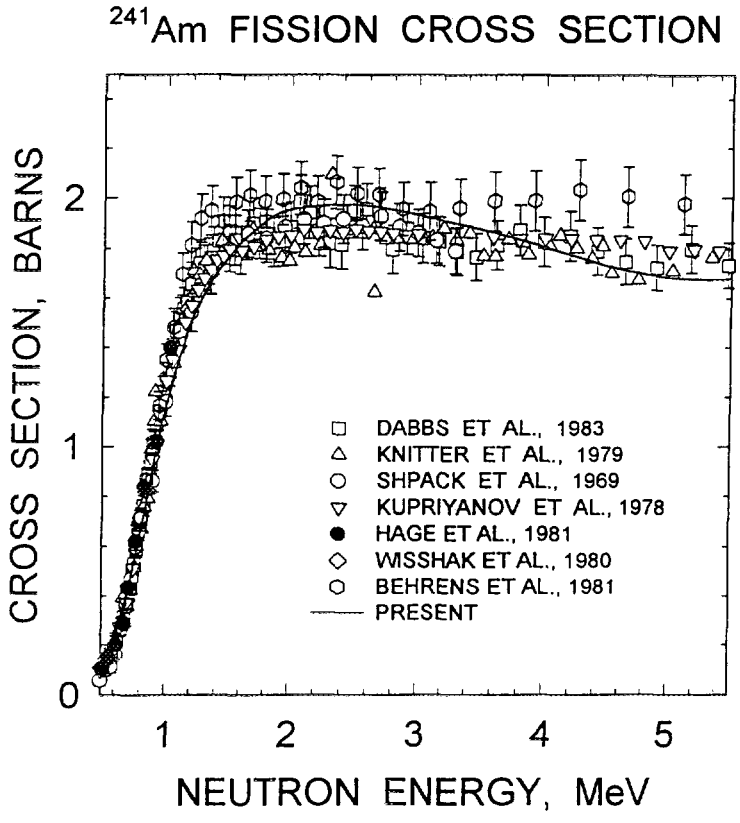
^{241}Am FISSION CROSS SECTION
DABBS ET AL., 1983
KNITTER ET AL., 1979
SHPACK ET AL., 1969
KUPRIYANOV ET AL., 1978
HAGE ET AL., 1981
WISSHAK ET AL., 1980
BEHRENS ET AL., 1981
PRESENT
CROSS SECTION, BARNS
2
1
0
1
2
3
4
5
NEUTRON ENERGY, MeV

FIG. 4.6

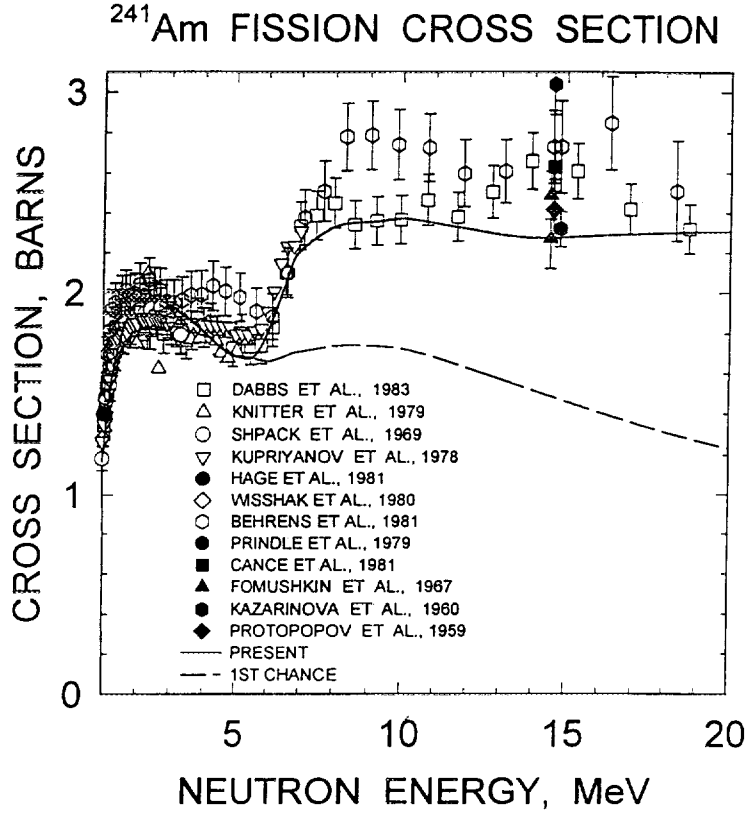
241Am FISSION CROSS SECTION
CROSS SECTION, BARNS
NEUTRON ENERGY, MeV
DABBS ET AL., 1983
KNITTER ET AL., 1979
SHPACK ET AL., 1969
KUPRIYANOV ET AL., 1978
HAGE ET AL., 1981
WISSHAK ET AL., 1980
BEHRENS ET AL., 1981
PRINDLE ET AL., 1979
CANCE ET AL., 1981
FOMUSHKIN ET AL., 1967
KAZARINOVA ET AL., 1960
PROTOPOPOV ET AL., 1959
PRESENT
1ST CHANCE

FIG. 4.7

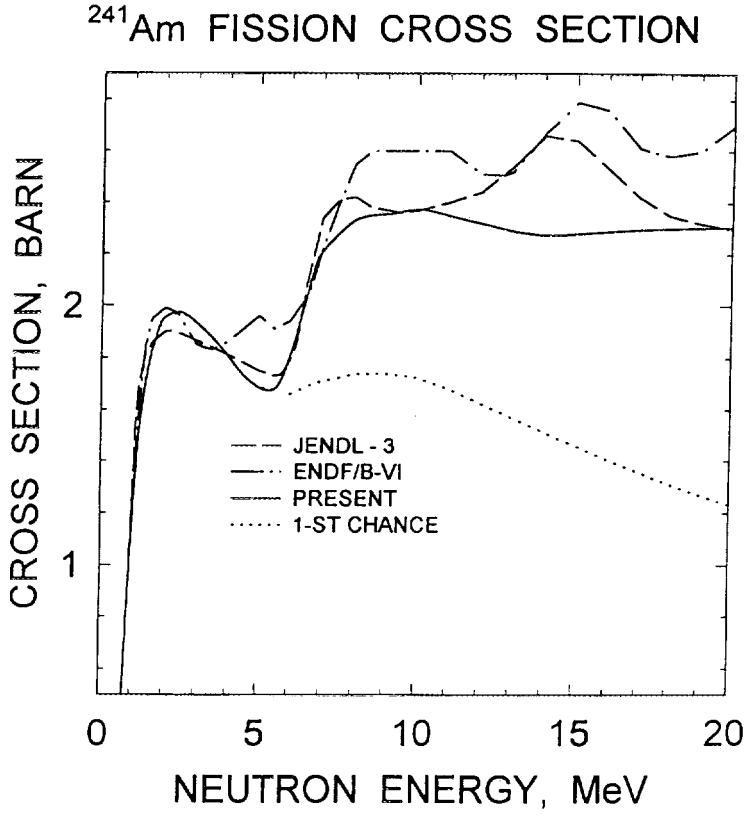
241Am FISSION CROSS SECTION
CROSS SECTION, BARN
NEUTRON ENERGY, MeV
JENDL - 3
ENDF/B-VI
PRESENT
1-ST CHANCE

FIG. 4.8

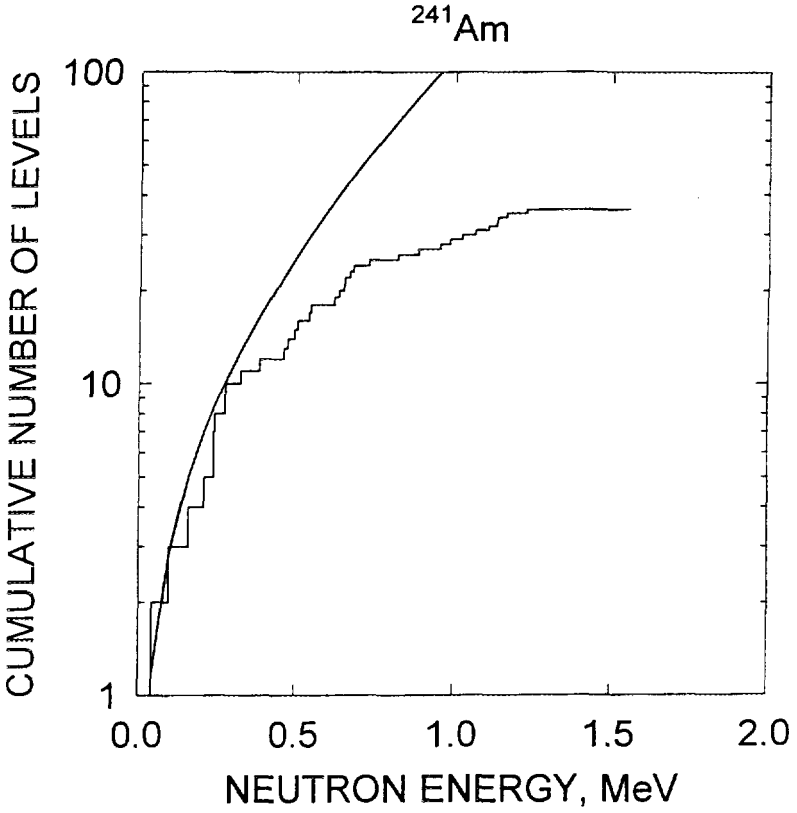

FIG. 4.9

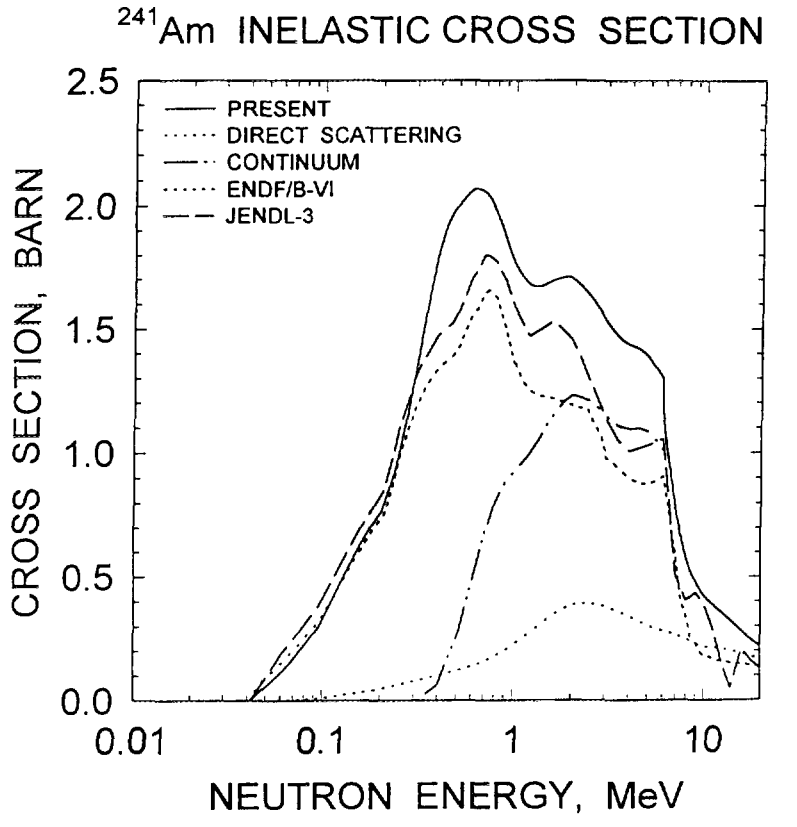

FIG.4.10

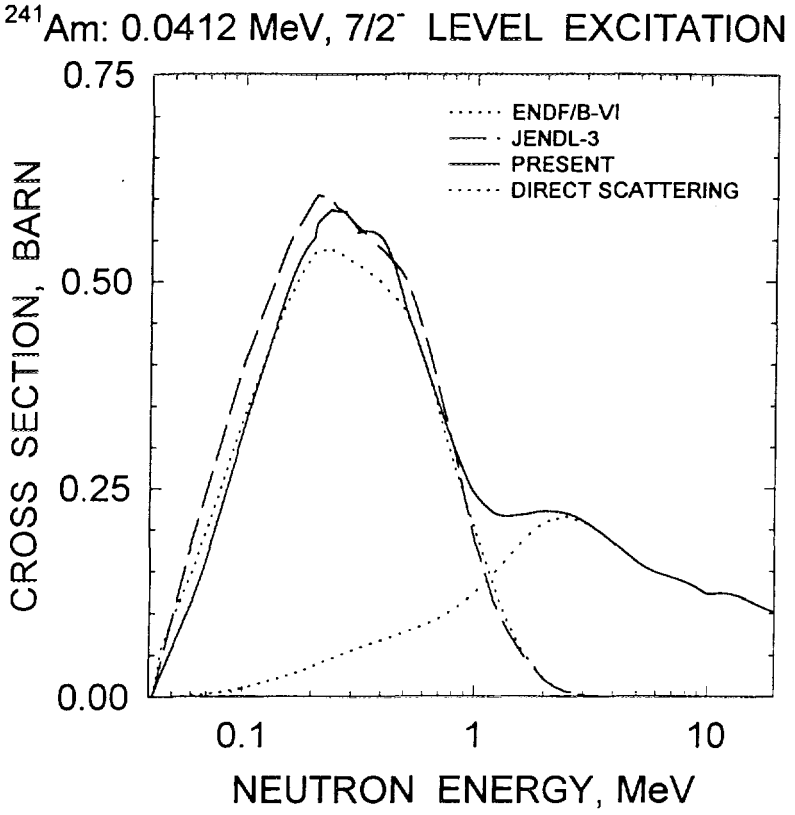

FIG.4.11

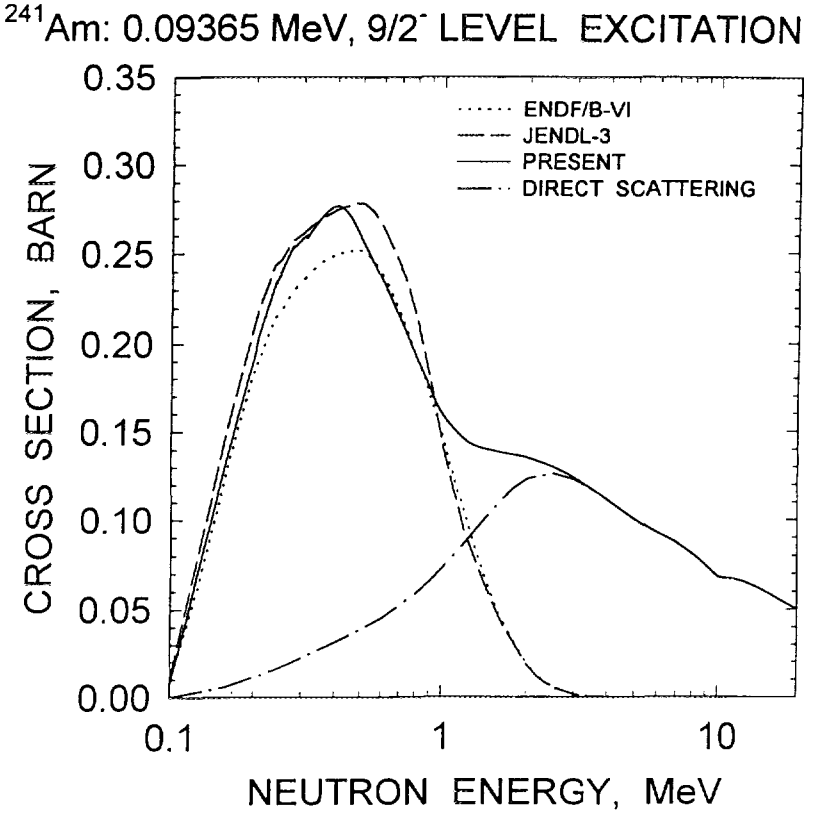

FIG.4.12

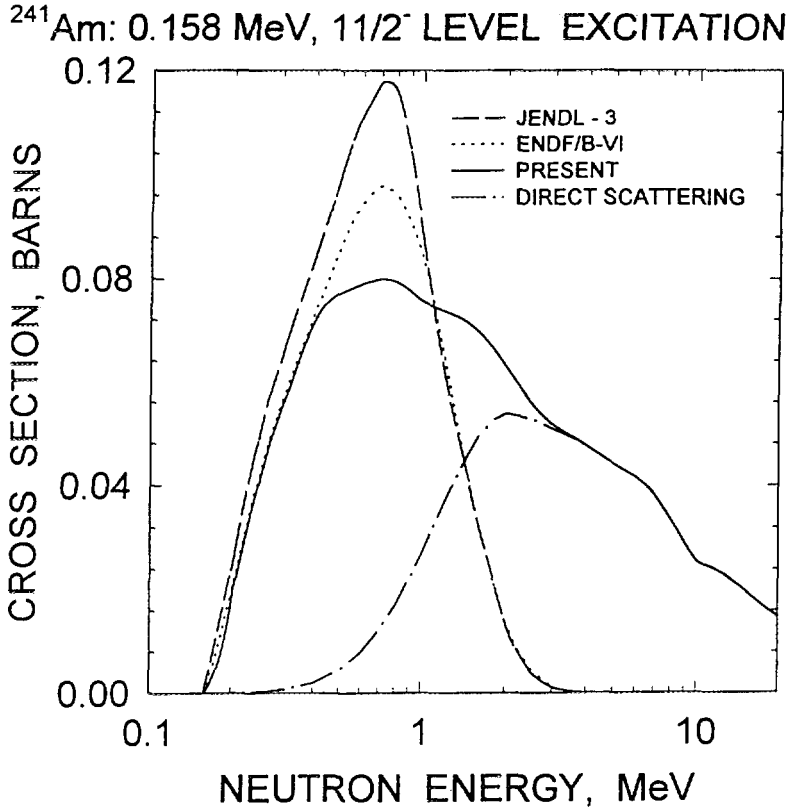

FIG.4.13

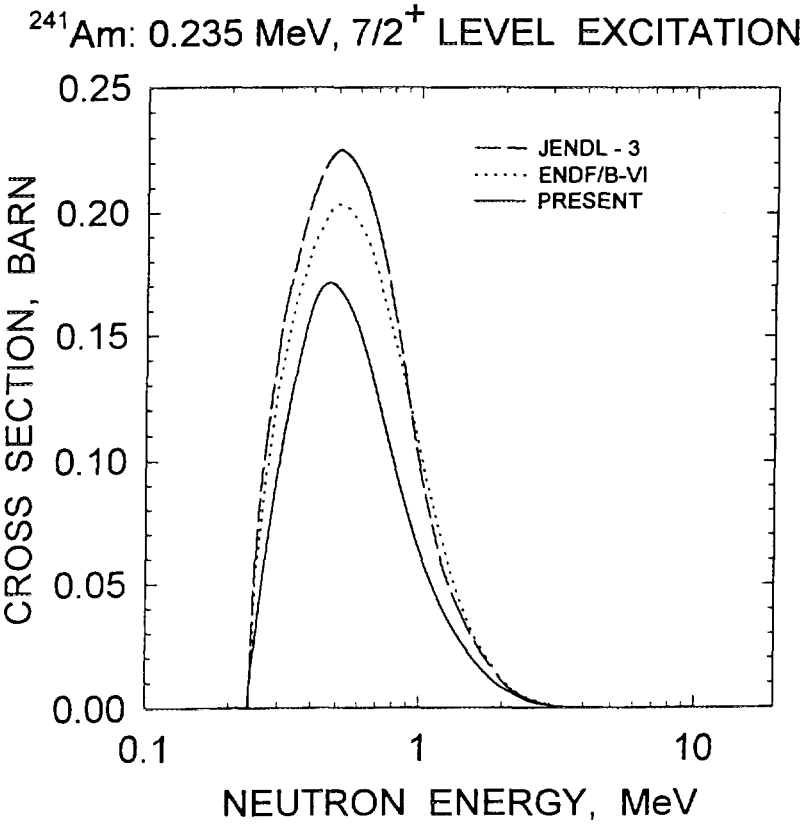

FIG.4.14

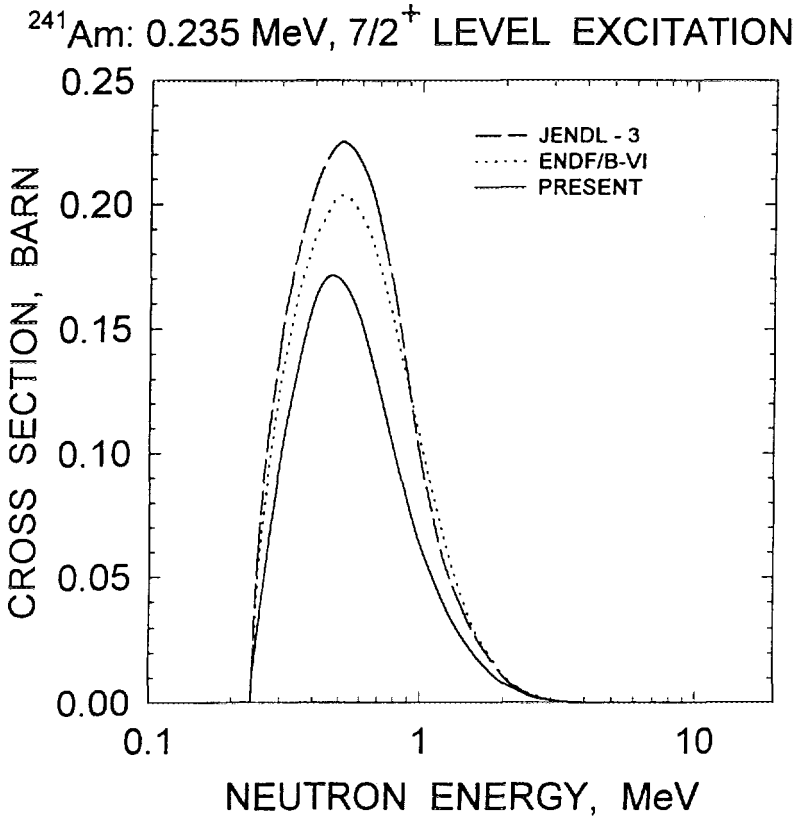

FIG.4.15

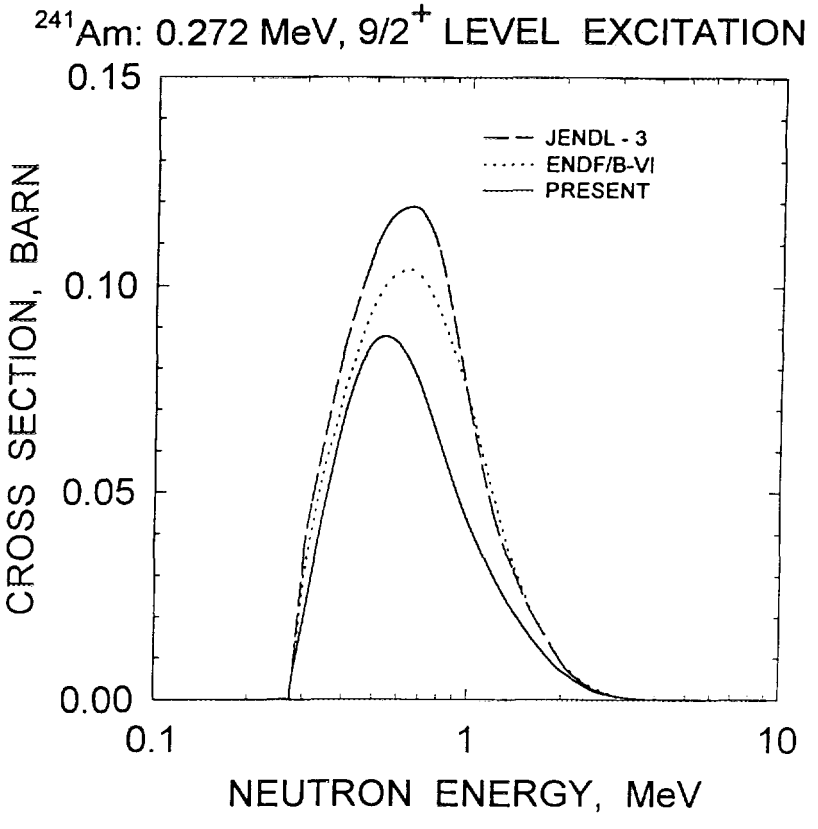

FIG.4.16

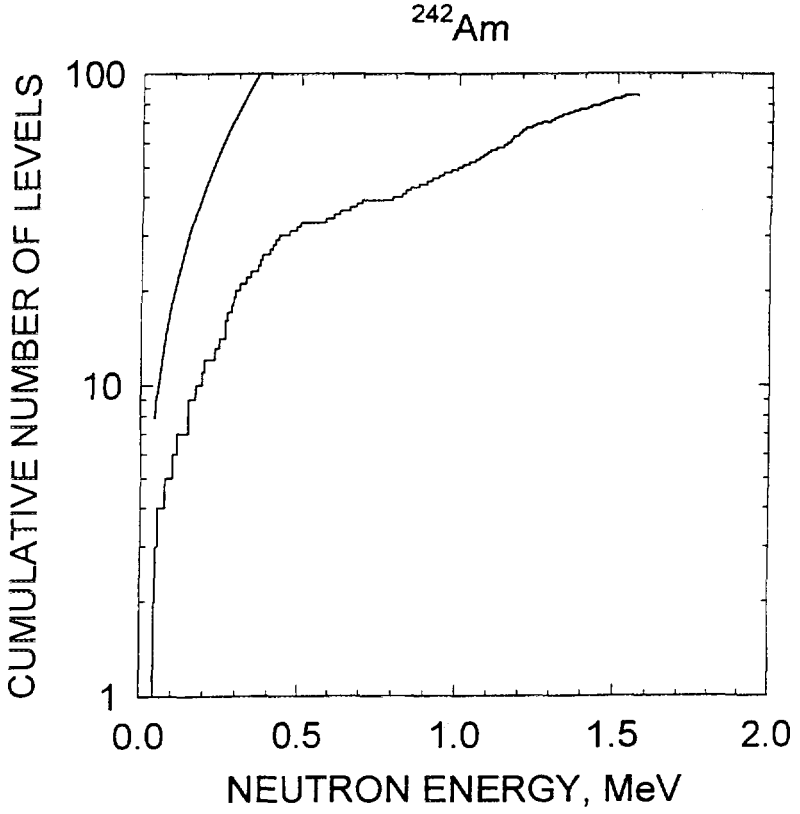

FIG. 4.17

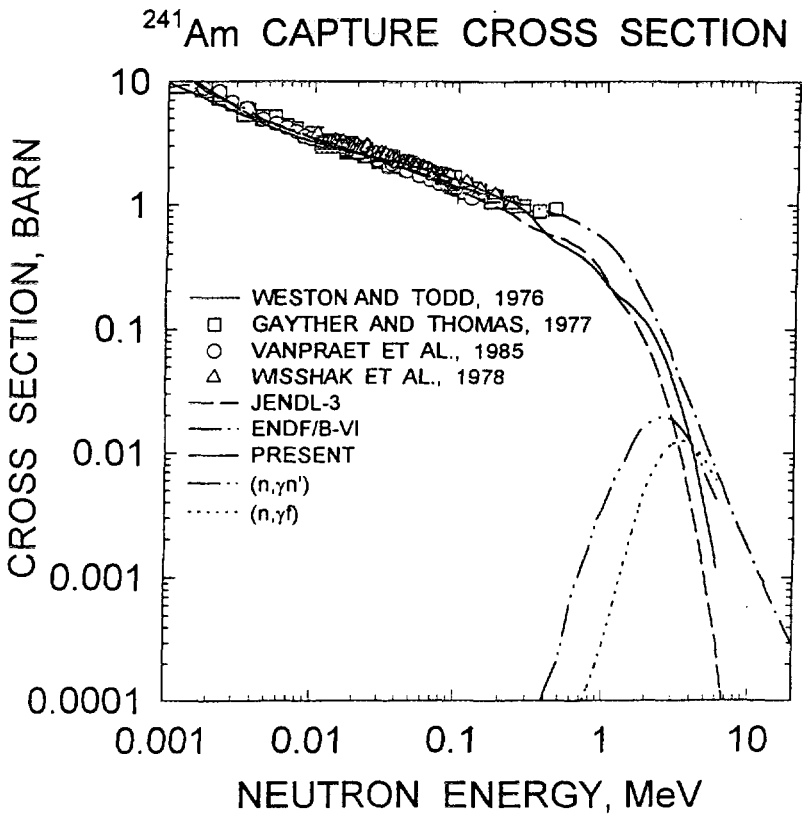

FIG.4.18

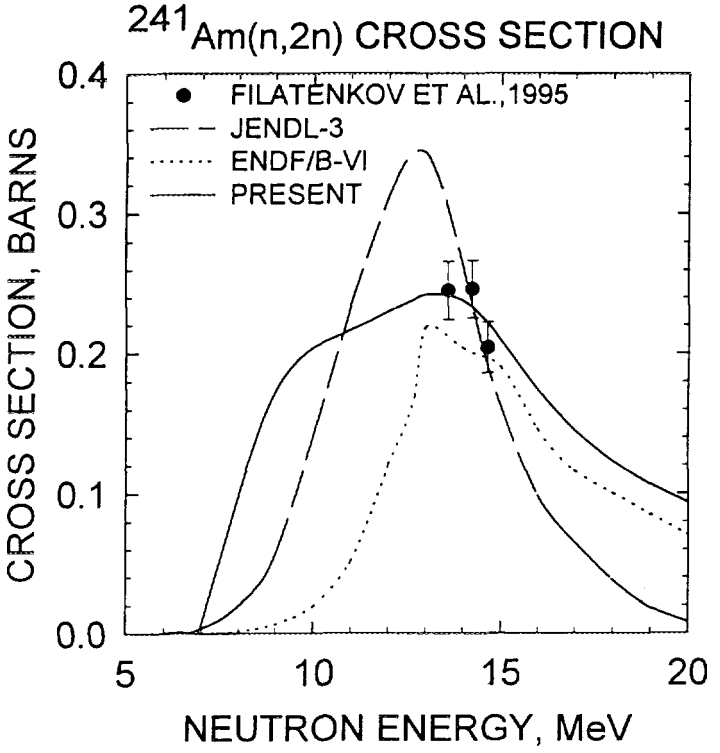

FIG. 4.19

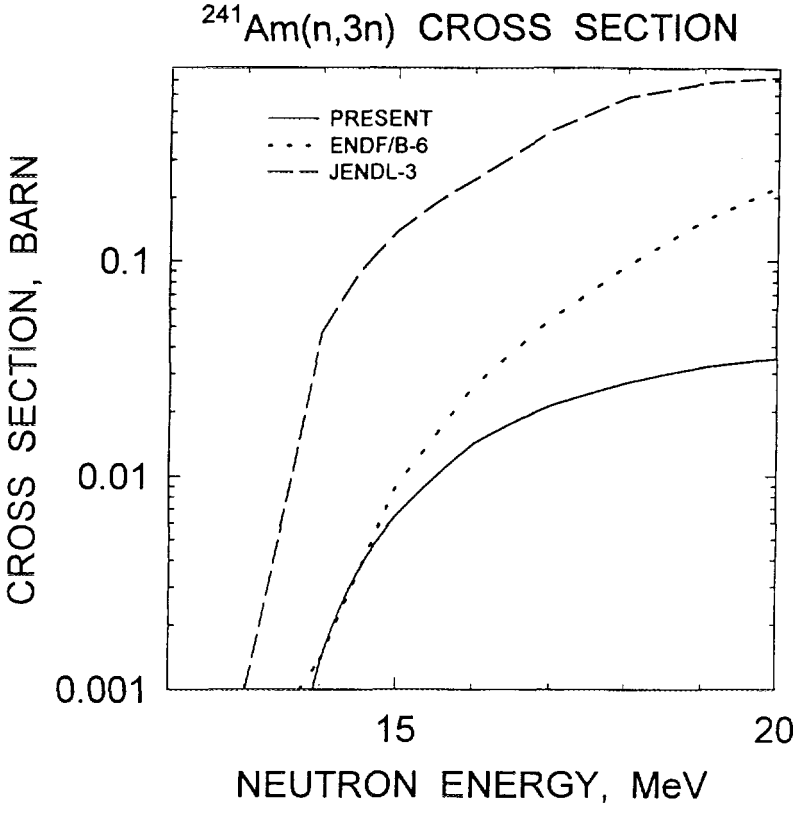

FIG.4.20

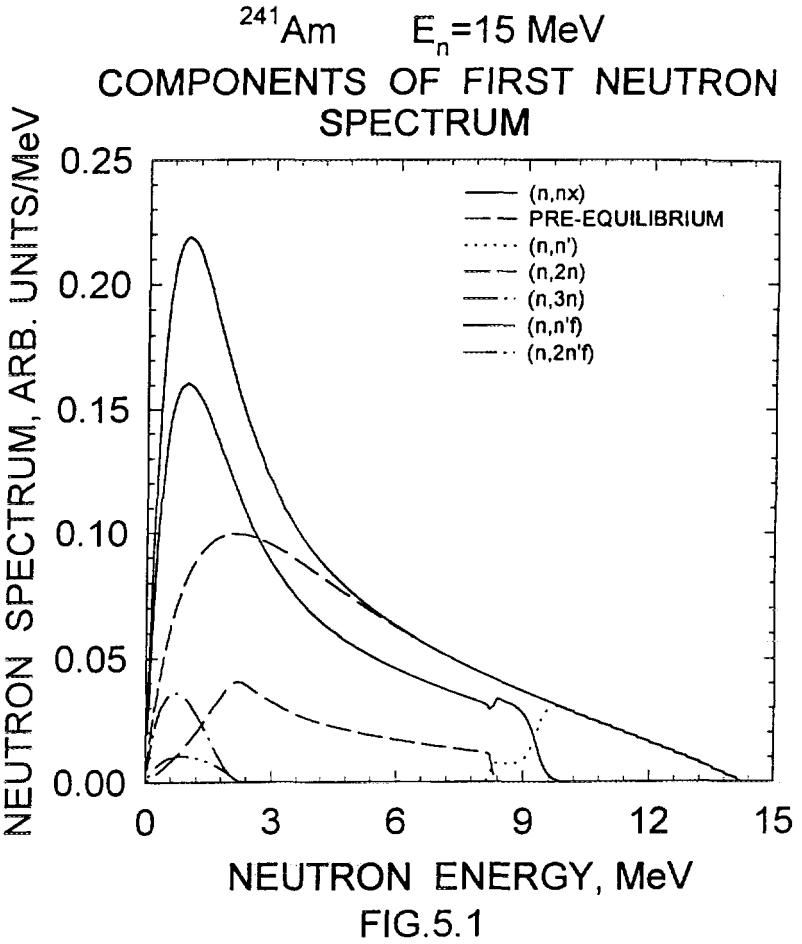
^{241}Am E_n=15 MeV
COMPONENTS OF FIRST NEUTRON SPECTRUM
NEUTRON SPECTRUM, ARB. UNITS/MeV
0.25
0.20
0.15
0.10
0.05
0.00
0
3
6
9
12
15
NEUTRON ENERGY, MeV
(n,nx)
PRE-EQUILIBRIUM
(n,n')
(n,2n)
(n,3n)
(n,n'f)
(n,2n'f)

FIG.5.1

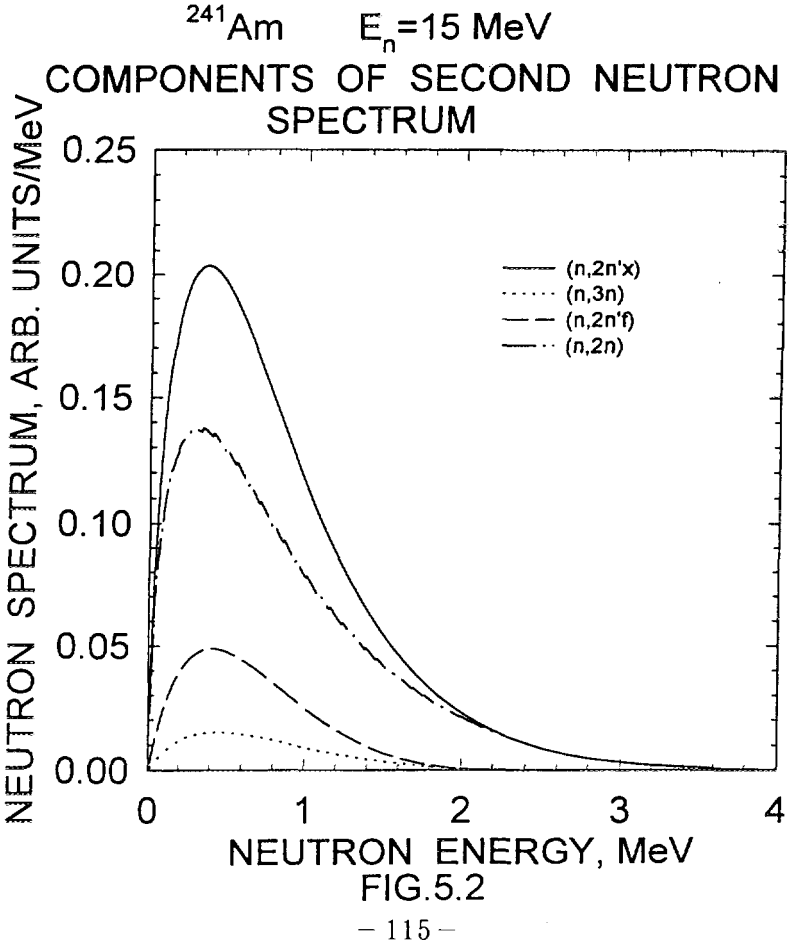
^{241}Am E_n=15 MeV
COMPONENTS OF SECOND NEUTRON SPECTRUM
NEUTRON SPECTRUM, ARB. UNITS/MeV
0.25
0.20
0.15
0.10
0.05
0.00
0
1
2
3
4
NEUTRON ENERGY, MeV
(n,2n'x)
(n,3n)
(n,2n'f)
(n,2n)

FIG.5.2

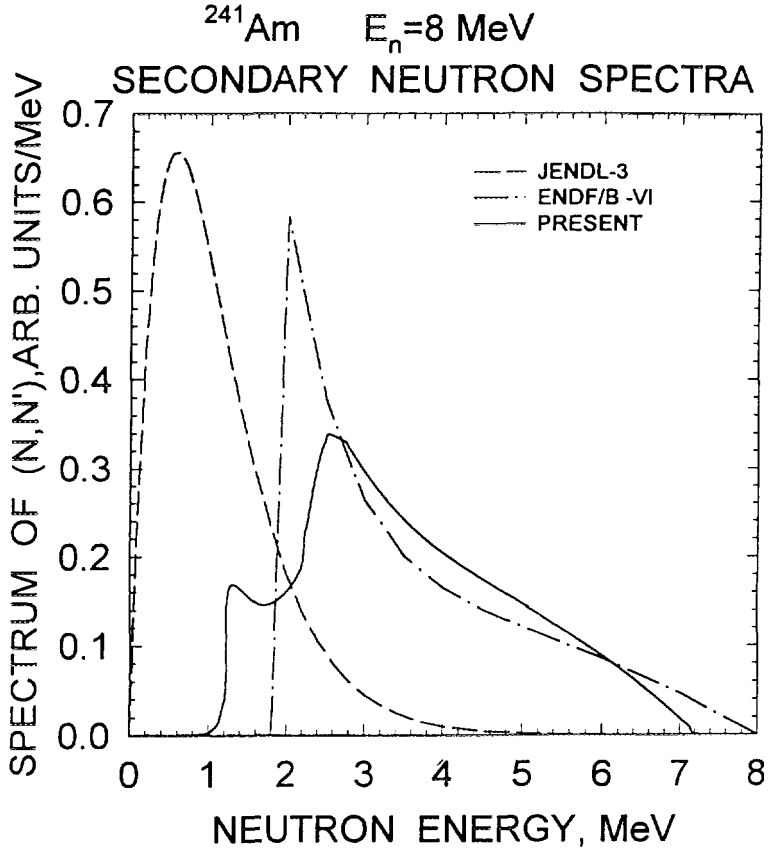
^{241}Am E_n=8 MeV
SECONDARY NEUTRON SPECTRA
JENDL-3
ENDF/B -VI
PRESENT
SPECTRUM OF (N,N'),ARB. UNITS/MeV
NEUTRON ENERGY, MeV
0.0
0.1
0.2
0.3
0.4
0.5
0.6
0.7
0
1
2
3
4
5
6
7
8

FIG.5.3

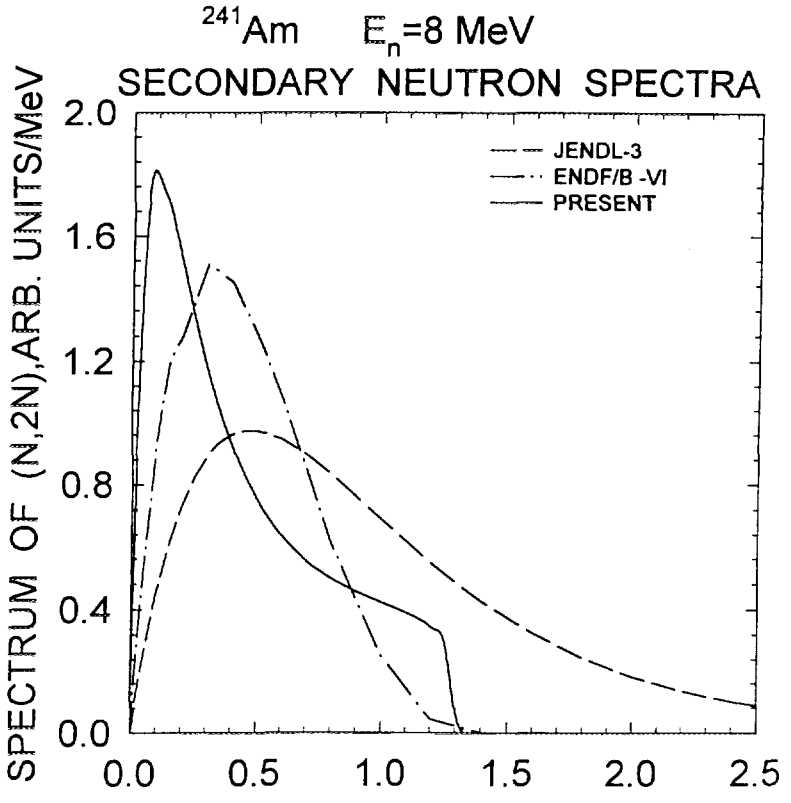
^{241}Am E_n=8 MeV
SECONDARY NEUTRON SPECTRA
JENDL-3
ENDF/B -VI
PRESENT
SPECTRUM OF (N,2N),ARB. UNITS/MeV
NEUTRON ENERGY, MeV
0.0
0.4
0.8
1.2
1.6
2.0
0.0
0.5
1.0
1.5
2.0
2.5

FIG.5.4

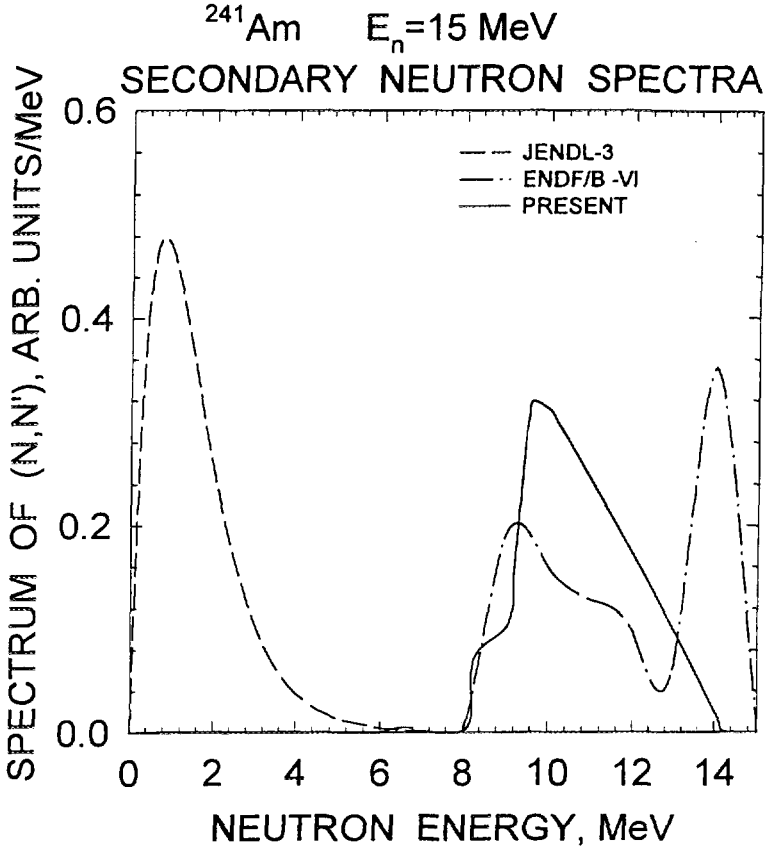
^{241}Am E_n=15 MeV
SECONDARY NEUTRON SPECTRA
JENDL-3
ENDF/B -VI
PRESENT
SPECTRUM OF (N,N'), ARB. UNITS/MeV
0.0
0.2
0.4
0.6
0
2
4
6
8
10
12
14
NEUTRON ENERGY, MeV

FIG.5.5

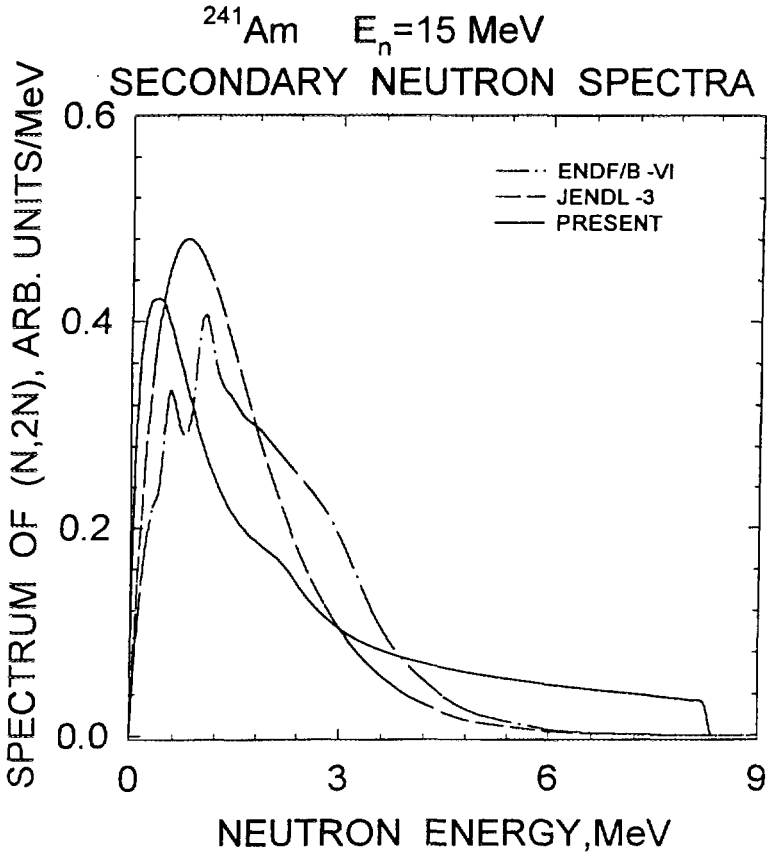
^{241}Am E_n=15 MeV
SECONDARY NEUTRON SPECTRA
ENDF/B -VI
JENDL -3
PRESENT
SPECTRUM OF (N,2N), ARB. UNITS/MeV
0.0
0.2
0.4
0.6
0
3
6
9
NEUTRON ENERGY,MeV

FIG.5.6

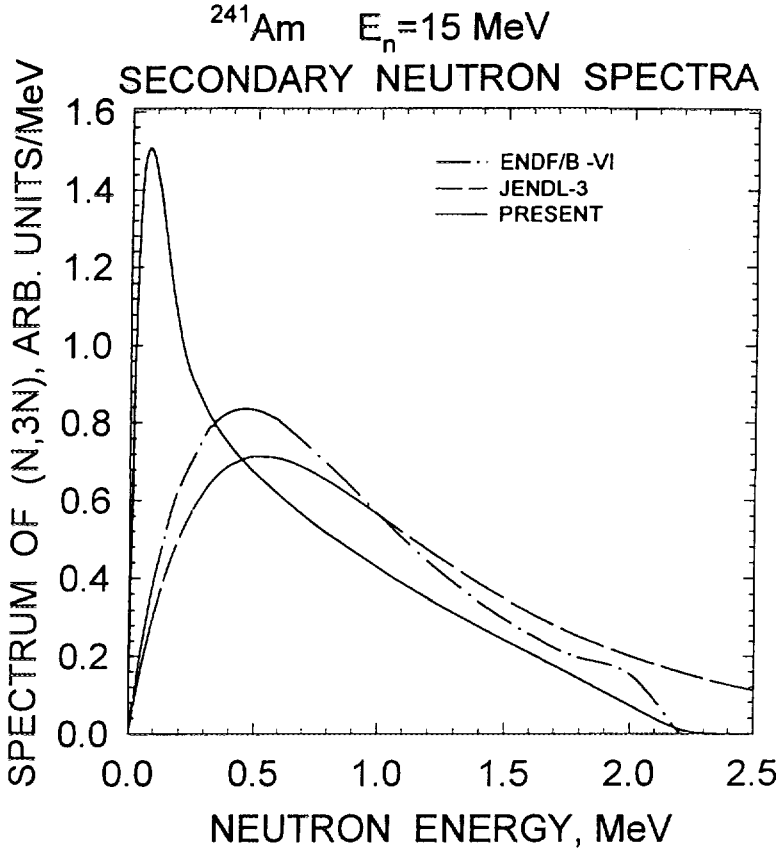
^{241}Am E_n=15 MeV
SECONDARY NEUTRON SPECTRA
ENDF/B -VI
JENDL-3
PRESENT
SPECTRUM OF (N,3N), ARB. UNITS/MeV
1.6
1.4
1.2
1.0
0.8
0.6
0.4
0.2
0.0
0.0
0.5
1.0
1.5
2.0
2.5
NEUTRON ENERGY, MeV

FIG.5.7

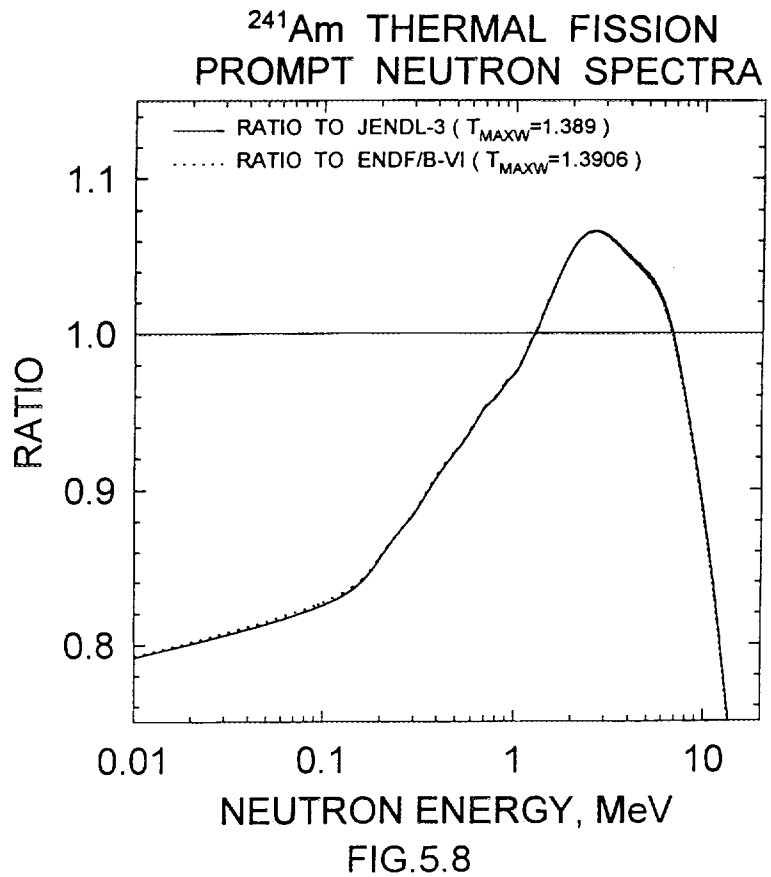
^{241}Am THERMAL FISSION
PROMPT NEUTRON SPECTRA
RATIO TO JENDL-3 (T_{MAXW}=1.389)
RATIO TO ENDF/B-VI (T_{MAXW}=1.3906)
RATIO
1.1
1.0
0.9
0.8
0.01
0.1
1
10
NEUTRON ENERGY, MeV

FIG.5.8

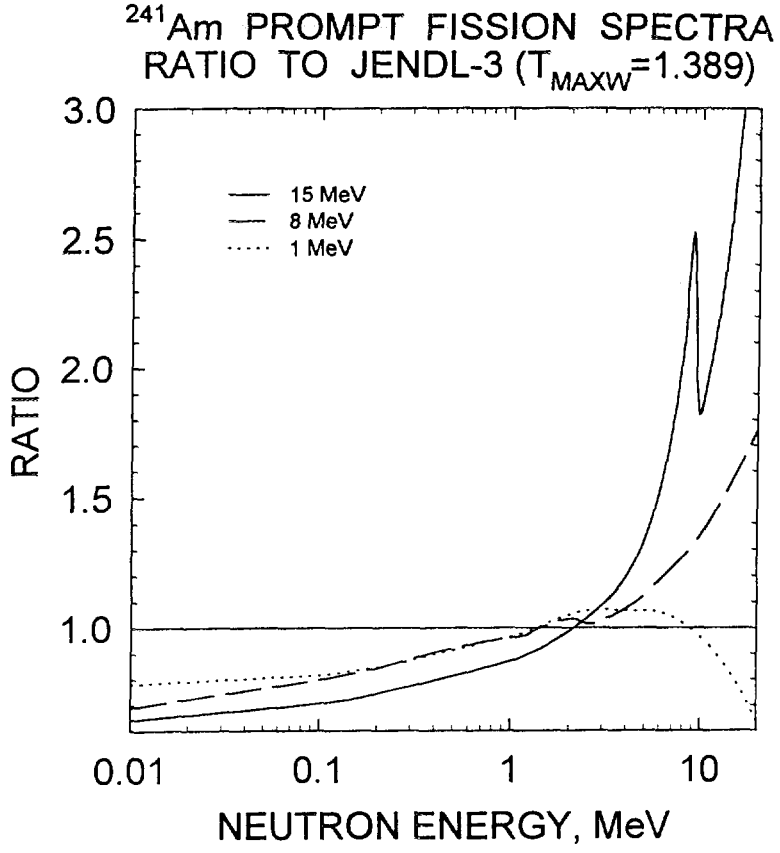

FIG. 5.9

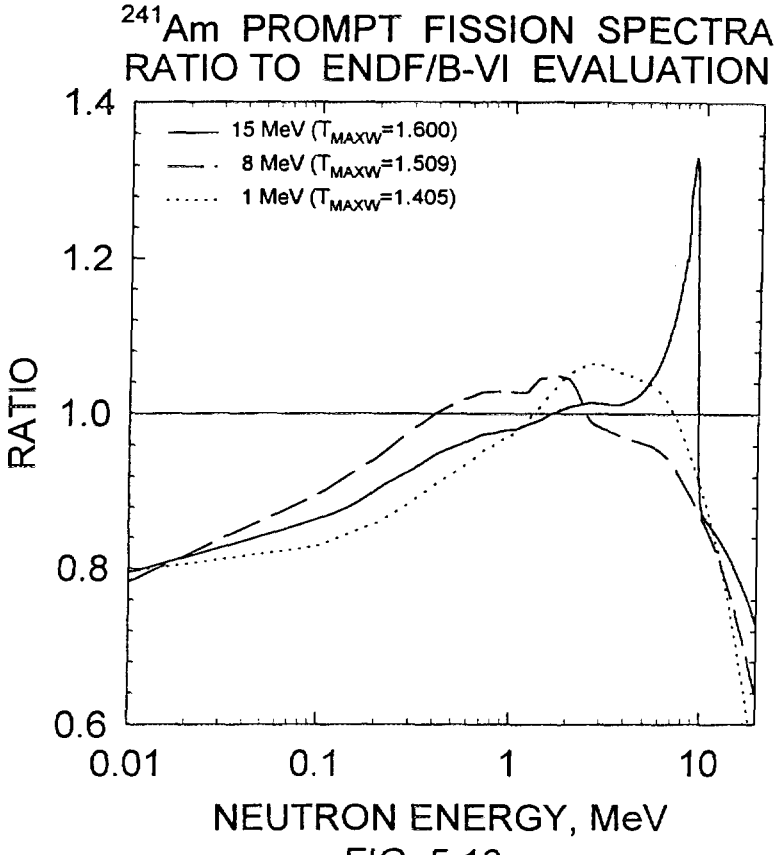

FIG. 5.10

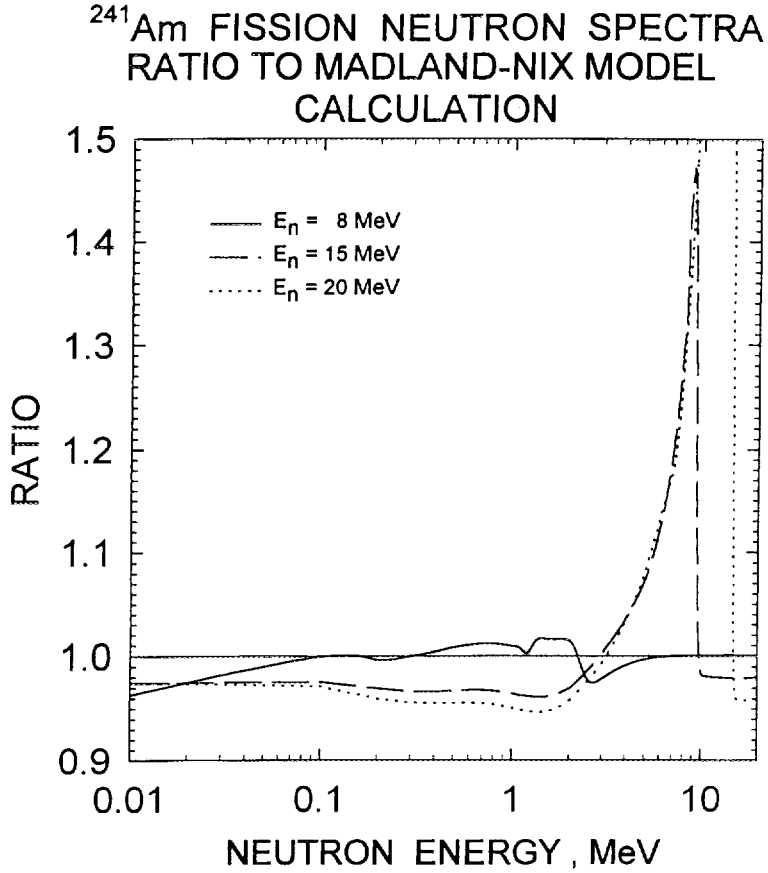

FIG.5.11

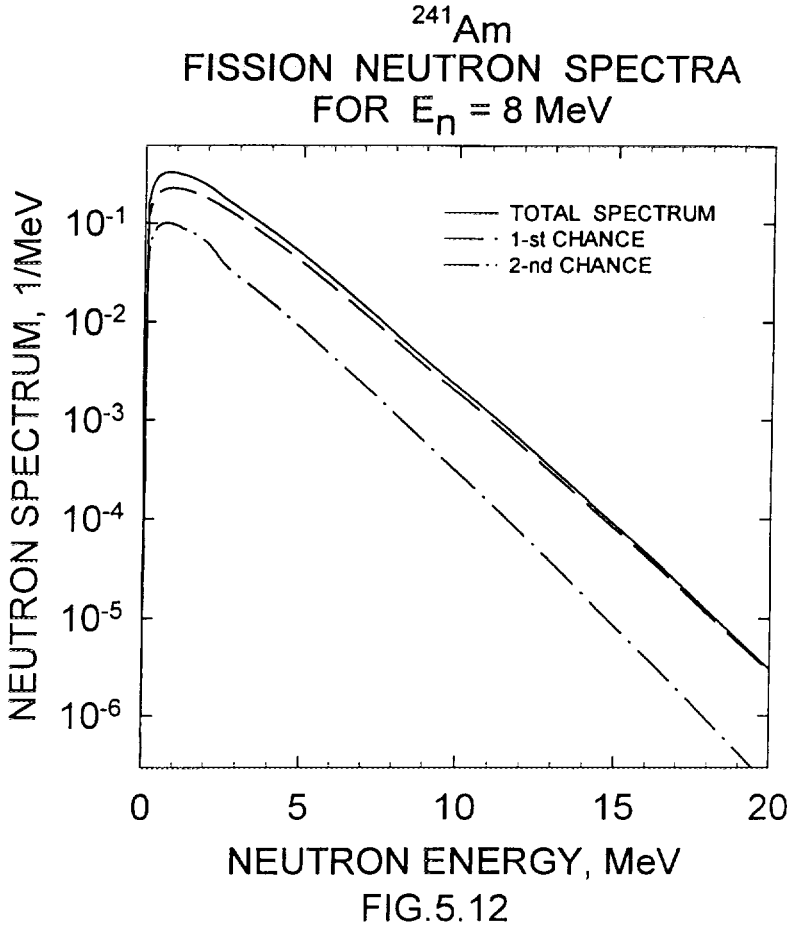

FIG.5.12

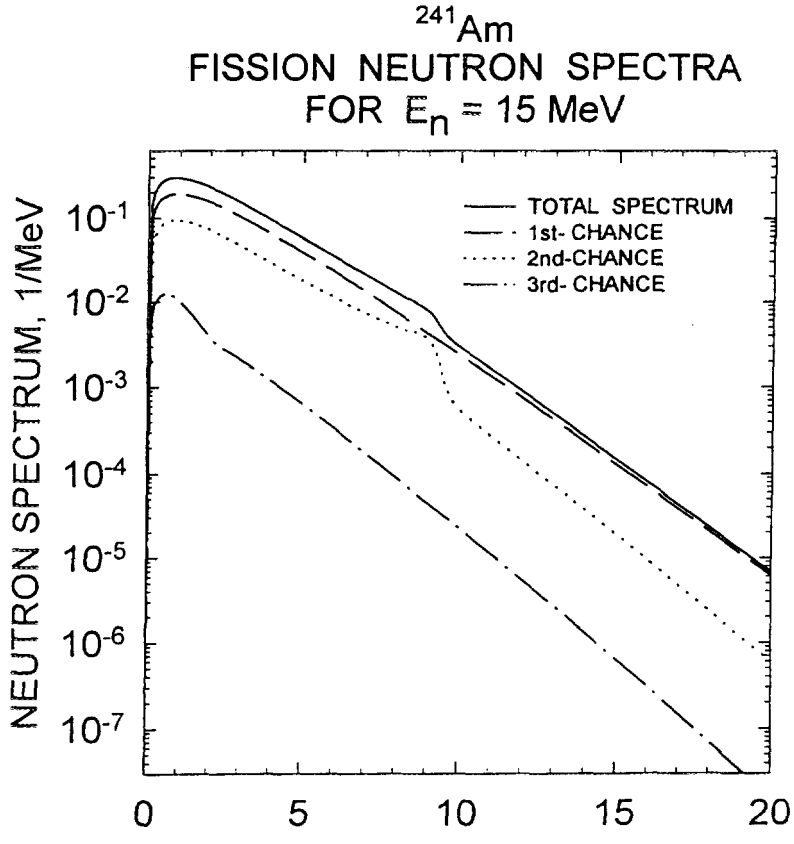

FIG.5.13

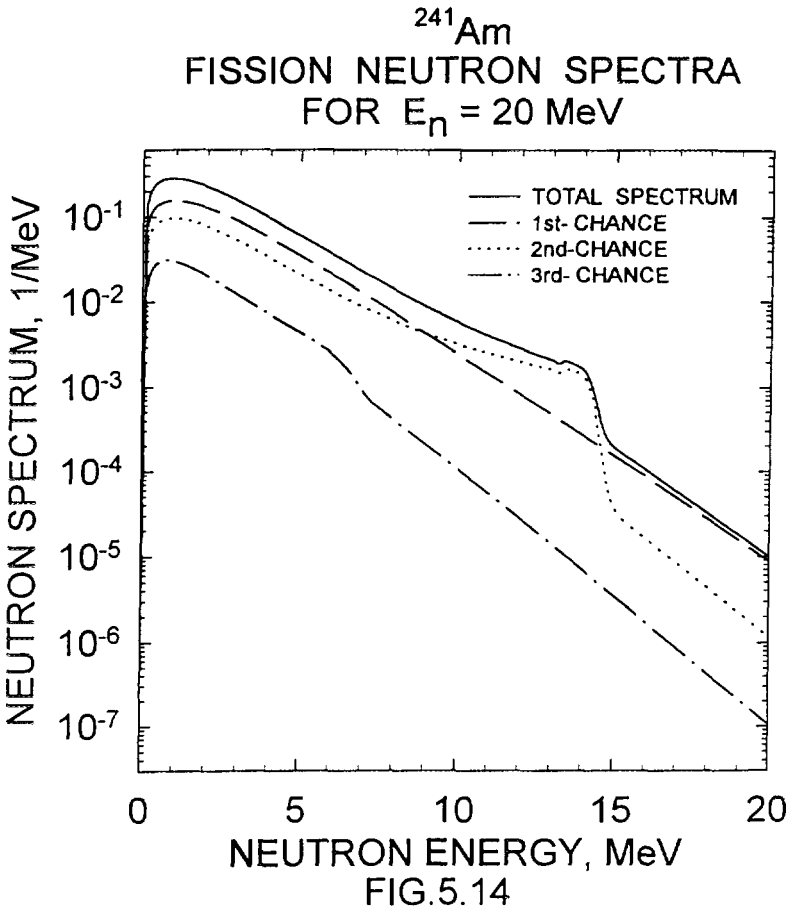

FIG.5.14

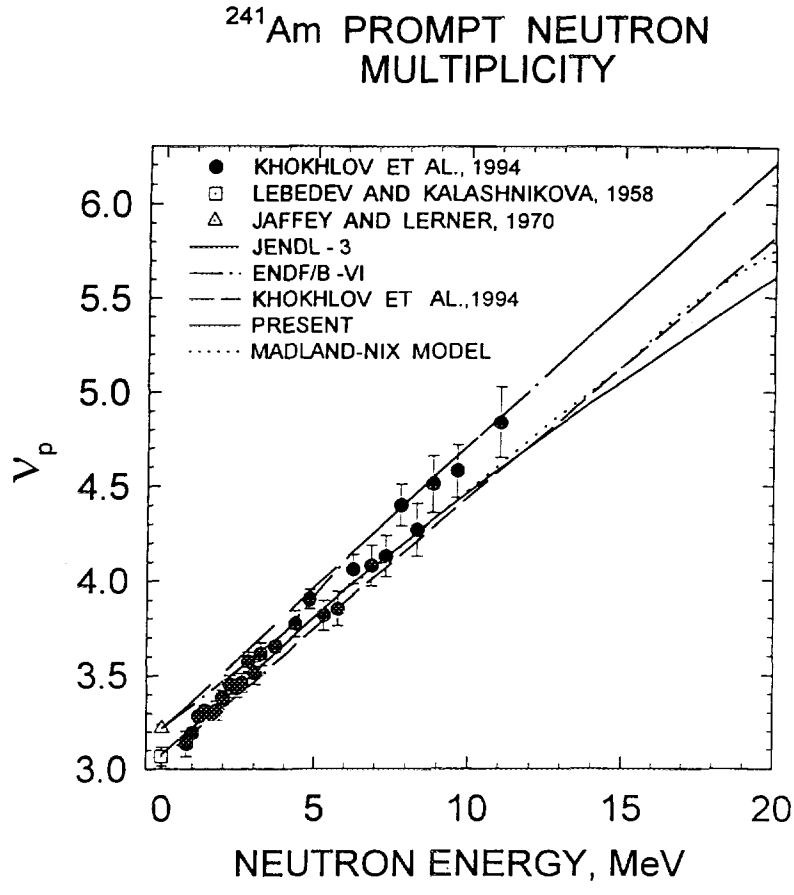
^{241}Am PROMPT NEUTRON MULTIPLICITY
KHOKHLOV ET AL., 1994
LEBEDEV AND KALASHNIKOVA, 1958
JAFFEY AND LERNER, 1970
JENDL - 3
ENDF/B -VI
KHOKHLOV ET AL.,1994
PRESENT
MADLAND-NIX MODEL
ν_p
6.0
5.5
5.0
4.5
4.0
3.5
3.0
0
5
10
15
20
NEUTRON ENERGY, MeV

FIG.6.1

2. Measurements of Fission Neutron Spectra of the Minor Actinides
Spontaneous Fission of Curium Isotopes

(V.G. Khlopin Radium Institute)

2. 1 Status of Measurements of Fission Neutron Spectra of Minor Actinides

L. Drapchinsky, B. Shiryaev

V.G. Khlopin Radium Institute
2nd Murunski Avenue 28, Saint Petersburg, Russia

Abstract

The report considers experimental and theoretical works on studying the energy spectra of prompt neutrons emitted in spontaneous fission and neutron induced fission of Minor Actinides. It is noted that neutron spectra investigations were done for only a small number of such nuclei, most measurements, except those of Cf－252, having been carried out long ago by obsolete methods and imperfectapparatus. The works have no detailed description of experiments, analysis of errors, detailed numerical information about results of experiments. A conclusion is made that the available data do not come up to modern requirements. It is necessary to make new measurements of fission prompt neutron spectra of transuranium nuclides important for the objectives of working out a conception of minor actinides transmutation by means of special reactors.

Status of Measurements of Fission Neutron Spectra of Minor Actinides

L. Drapchinsky, B. Shiryaev

Among other nuclear data necessary for solving the problem of transmutation of actinides using the special Actinide Burner Reactors (ABR) are the data on prompt neutron spectra (PNS) in minor actinide fission.

The Np, Pu, Am, and Cm isotopes are of most interest [1]. The requested accuracy of PNS for this nuclides is the same as for the main fuel nuclides i.e. the accuracy of average neutron energy of spectrum must be 1-2% at high reliability of results.

Meanwhile the measurements of PNS have been carried out only for a few of nuclides of interest in spontaneous fission. In neutron induced fission not numerous measurements have been carried out at a few values of neutron energies only. In most cases the measurements were performed long ago, using imperfect equipment and methods without detailed analysis of possible errors. In a number of cases the results of various authors for the same nuclide differ on the values much greater than the uncertainties quoted.

The data for the ^{252}Cf spontaneous fission and ^{239}Pu thermal neutron induced fission are exceptions. For these nuclides numerous measurements were performed as well as evaluations of integral PNS i.e. the PNS averaged with corresponding weights over the fission fragment mass distributions, emission angles, total kinetic energies of fragments [2,3]. At present the PNS in spontaneous fission of ^{252}Cf is accepted as a standard PNS and widely used in analysis of experimental data and testing and calibration of experimental set-ups.

Monocrystal scintillation spectrometers used in the early works on the PNS measurements made it possible to estimate experimentally the PNS shape. These stylbene spectrometers enabled measuring the PNS in a wide energy range. At the same time the threshold from low energy side was usually 1 - 3 MeV. This resulted in a loss of experimental information and rather large uncertainties in the low energy region of PNS, because this part of PNS was estimated only by

extrapolation of data obtained in accordance with Maxwell [4], Watt [5] or Gurevich and Mukhin [6] distributions. It sould be noted also the definite complexity of transformation of apparatus spectrum into energy one.

During the past 25 years the time-of-flight (TOF) method is exclusively used in PNS measurements in spite of low efficiency of TOF-spectrometers. This method is the most accurate and reliable for neutron energy measurement in a wide energy range. To decrease dead time short properly delayed pulses from fission chamber or formed of an accelerator beam pulse are used as stop signals whereas pulses from neutron detector surve as start signals.

The detection of fission event makes it possible to increase the time resolution of spectrometer, to use an accelerator in permanent regime of operation i.e. to increase the incident neutron flux significantly.

Various fast detectors are used for fission fragment detection: surface-barrier Si-detectors, flat one- and multilayer ionization current pulse chambers, gas scintillation chambers, micro-channel plates, detecting delta-electrons knocked by fragments out of thin aluminium oxide or carbon films set close by the layer of fissile nuclide. It is important to ensure that the fission fragment detection efficiency is close to 100%. That means that the layers of fissile nuclide must be thin enough to avoid the losses of fragments due to self-absorption, the pulses due to alpha-particles and their pile-ups must be well discriminated from those due to the fission fragments.

If the stop pulse formed from accelerator beam pulse is used in TOF-spectrometer the following disadvantages take place: firstly, the finite duration of the accelerator beam pulse decreases the time resolution of spectrometer; secondly, it is impossible to measure PNS in the energy region below the incident neutron energy since the neutron detector will register the incident neutrons both unscattered and scattered. This shortcoming results in the loss of useful information.

At the same time this method has one important advantage: large quantity of fissionable nuclide can be used in the PNS measurement because in this case the fission fragment absorption is of no importance. Nevertheless, the absorption and scattering of neutrons in the sample under study must be taken into account.

Neutron detectors wide used in TOF-spectrometers are of scintillation type based on stilbene crystal, lithium glass, scintillation plastics, liquid scintillators. Good neutron-gamma discrimination by pulse-shape analysis and fast time response are of great importance. That is why stilbene crystals, liquid NE-213, and BC-501 are mainly used lately.

The neutron detector efficiency is determined by measurements of rates of monochromatic neutron fluxes of known intencities and by calculations. The direct determination of neutron detector efficiency can be changed on the measurements of PNS relative to the reference standard PNS, say PNS in spontaneous fission of ^{252}Cf. Namely this method is used in the PNS measurements we are carrying out in the frame of the ISTC, Moscow at the active support of our collaborators, first of all JAERI and Dr. Yasuyuki Kikuchi as JAERI's representative. This method is especially effective if both the PNS of nuclide under study and the reference one are measured simultaneously using the same detectors and measuring channels.

Note, that in most measurements the spectrometer flight bases are 50 to 100 cm and can be varied during the study. Possible PNS distortions due to elastic and inlastic scattering of neutrons by surrounding objects (premise floor, seiling, walls etc.) must be taken into account. It is desirable to perform the measurements in the conditions where these effects can be deminished.

Let us now consider the results of PNS measurements of minor actinides grouping the data in accordance with excitation energies:

- spontaneous fission;
- thermal neutron induced fission;
- fast neutron induced fission.

SPONTANEOUS FISSION

The studies of the PNS in spontaneous fission of minor actinides are performed for a few number of nuclides only. The results are listed in Table 1.

In most experimental works the PNS are compared to the distribution obtained by Terrell [4] on the basis of the evaporation model (the Maxwell one-parameter distribution):

$$N(E) = \frac{2}{(\pi T^3)^{1/2}} \sqrt{E}\, e^{-E/T} \qquad (1)$$

where N(E) is the number of neutrons per unit energy interval, E is the kinetic energy of neutron, T is the "hardness" parameter, or the "temperature". For the Maxwell distribution the spectrum average energy <E> is connected with the temperature by the expression:

$$\langle E \rangle = 3/2\ T \qquad (2)$$

In the earliest measurements of ^{240}Pu by Bonner [7] Bramblett counters [14] were used that allow to obtain the parameter T of the Maxwell distribution by the ratio of the counting rates in two counters of different diameters. The reliability and precision of those measurements are low. The calibration of the counters was done by the PNS in U-235 thermal neutron fission with the parameter T = 1.332 MeV, which by modern data seems to be overestimated.

Measurements of PNS in the ^{240}Pu spontaneous fission by Bolshov et al. [8] and Alexandrova et al. [9], as well as in that of ^{244}Cm [9] were carried out by means of monocrystal scintillation spectrometers based on stilbene crystals. That allowed to broaden the energy interval of measuring the spectrum and to execute a discrimination of gamma-rays. In works [8,9] monochromatic neutrons of the reactions T(p,n), D(d,n) and T(d,n) were used for the calibration of neutron spectrometers. In using monocrystal scintillation spectrometers the neutron registration threshold turns out very high, which causes losses of a great part of the neutron

Table 1. Results of investigations of PNS in spontaneous fission of minor actinides.

Nuclide	Energy (MeV)	Method of measurement	Method of calibration	T (MeV)	Reference
^{240}Pu	0-4	Bramblett counters	Fission neutrons ^{235}U+n (thermal)	1.189± 0.030	[7] 1961
	3-11	Monocryst. spectrometer	Monoenergetic neutrons	1.24 ± 0.03	[8] 1962
	1-17	Monocryst. spectrometer	Monoenergetic neutrons	1.27 ± 0.03	[9] 1974
^{242}Pu	0.3-5	Time-of--flight	Fission neutrons ^{235}U+n (thermal)	1.21 ± 0.07	[10] 1969
^{244}Cm	0.3-6	Time-of--flight	Fission neutrons ^{235}U+n (thermal)	1.37 ± 0.04	[10] 1969
	0.4-6	Time-of--flight	Fission neutrons ^{235}U+n (thermal)	1.38 ± 0.03	[11] 1970
	2-14	Monocryst. spectrometer	Monoenergetic neutrons	1.33 ± 0.03	[9] 1974
^{246}Cm	0.4-6	Time-of--flight	Fission neutrons ^{235}U+n (thermal)	1.39 ± 0.04	[12] 1979
^{248}Cm	0.4-6	Time-of--flight	Fission neutron ^{235}U+n (thermal)	1.43 ± 0.04	[12] 1970
	0.1-10	Time-of--flight	Neutrons of spont. fission of Cf-252	1.379± 0.005	[13] 1991
^{252}Cf	0.02-20	-	Evaluation	1.42	[2] 1986

spectrum. Thus, in initial measurements of ^{240}Pu [8] the neutron registration threshold was about 3 MeV, and the loss in neutron registration accounted for more than 70%. Later the threshold was lowered down, however, remaining quite high (1 MeV). A similar situation is in measurements of the ^{244}Cm fission PNS, where the spectrum was measured in the energy range from 2 to 14 MeV. In this case the loss being over 55%. For the same reason the Maxwell distribution parameters are determined for a very limited region of the spectrum, especially from the low-energy side. Besides, it was assumed in advance that the energy distribution of neutrons corresponds to the Maxwellian. Errors in determining the parameter T are assessed by authors equal to 2-2.5%.

The application of the time-of-flight method in measurements of ^{242}Pu and ^{244}Cm by Belov et al. [10], of ^{244}Cm by Zamyatnin et al. [11], and of ^{246}Cm and ^{248}Cm by Zhuravlev et al. [12] allowed to essentially improve the energy resolution of the measurements and to get rid of complex processing of experimental distributions necessary in previously used methods. In that case, however, the spectrometer light-grasp decreased. Pulses from both a gas scintillation counter detecting fission fragments [11,12], and a scintillation counter detecting fission prompt gamma-quanta [10], were used as stop signals in the spectrometers. In the latter case a thorough development of the method is required, because prompt gamma-quanta correlate with a fragment mass, as well as with the direction of its motion. Scintillation counters based on stilbene crystals and plastic scintillators were used as neutron detectors. The spectrometers time resolution was about 4 ns and better, the flight path used in most works was about 50 cm.

The neutron detectors were calibrated by the PNS in ^{235}U thermal neutron fission with the Maxwell parameter T = 1.29 MeV. In works [10-12] the neutron registration threshold was lowered down to 0.3 - 0.4 MeV, however, without using the neutron/gamma discrimination. The obtained results are shown in Fig. 1a and 1b. They do not disagree with the the Maxwell distribution, however, as seen from the figures, there are few experimental points in energy regions over 3-4 MeV.

Fission layers in all the measurements (except [7]) were thin enough to use the time-of-flight method with fission fragment detection as a time signal. The samples were enriched in the isotope studied. The rates of neutron registration were very low, and this led to the need for prolonged measurements, for a maximum possible decrease of the background and for applying a correction for equipment instability.

The main source of errors in the considered works is inaccuracy of determining of the neutron detector efficiency. A noticeable share of the error may be caused by a number of other reasons: the inaccuracy of the time (or energy) calibration of the spectrometer, the absence of neutron/gamma discrimination, the incorrect account of the background of random coincidences and scattered neutrons, the neutron and gamma-background, etc.

Careful measurements of spectra were carried out in a number of works for ^{252}Cf spontaneous fission [2,15,17] as well as for ^{248}Cm spontaneous fission [13].

The PNS of ^{252}Cf spontaneous fission after making many measurements and evaluations was accepted as an international standard. There are a number of reviews for it (see, for example, [2,15-17]), and therefore it is not considered here in detail. Experimental and calculated PNS in spontaneous fission of ^{252}Cf [19] are shown in Fig. 2. The results are given in relation to the Maxwell distribution with the parameter T = 1.42 MeV accepted at present. One can see that the spectrum has a complex character. There are deviations from the Maxwell distribution in several energy regions, both towards an increase of the N(E) value and towards decrease, especially great at energies over 5 MeV.

Froehner [19] made an evaluation of the PNS of ^{252}Cf and came to conclusion that the Watt distribution

$$N(E) \sim e^{-E/a} \sinh(bE)^{1/2} \qquad (6)$$

at the parameters a = 1.175 and b = 1.040 describes quite well the evaluated PNS. Such a representation of the spectrum, according to Khomyakov et al. [20], may be acceptable for practical application.

The PNS in ^{248}Cm spontaneous fission was measured by Batenkov et al. [13]. Much attention in the measurements was paid to increasing the precision and reliability of the results. For this purpose, for the first time of the works considered the spectrometer was calibrated by the ^{252}Cf spontaneous fission PNS which was being measured simultaneously with ^{248}Cm measurements and using the same equipment. The time reference in the multiparameter neutron spectrometer was done by means of microchannel plates by recording the electrons knocked out by fission fragments from thin films of Al_2O_3 that covered the layers of ^{248}Cm and ^{252}Cf. Neutron detecting was done by a scintillation counter based on stilbene crystal and a photomultiplier FEU-30, using the neutron/gamma pulse-shape discrimination and a two-threshold selection. The high-enrichment (95%) isotope being measured was deposited onto a thin platinum backing on the reverse side of which was applied a layer of ^{252}Cf. As a result the authors succeeded in getting the time resolution less than 0.6 ns for neutron energy over 1 MeV and about 1 ns at low energies, as well as in reducing to minimum the effects of instability of the electronics and the detectors. The uncertainty of determination of the spectrum average energy <E> (relative to the <E> of the ^{252}Cf) was lowered down to 0.4%, and the spectrum was measured in the energy range from 0.1 to 10 MeV. Note, that only a small amount of the ^{248}Cm was used in the measurement. The rate of fissions in curium layer was 2×10^4 fissions/minute. In Fig. 3 the PNS in the form of relation to the Maxwell distribution with the parameter T = 1.38 MeV is shown. The parameter T is determined proceeding from its best correspondence between the Maxwell distribution and the measured PNS in the energy range 0.75 - 6 MeV. It is seen from the figure, that in the energy range below 0.5 MeV is observed an excess of intensity over the Maxwell distribution, and in the energy range 0.5 - 1.0 and over 6 MeV - a decrease.

Terrell [4], and then some other authors, considered the connection of the parameter T (or <E>) with the value of the average number of prompt neutrons emitted in one fission event, the $\langle\nu\rangle$, which also grows in transition to heavier nuclei. A comparison of

the dependence $<E> = a + b[<\nu>+1]^{1/2}$, suggested by Terrell, with experimental data is given in Fig. 4. The values of the $<\nu>$ are taken from the work by Malinovsky et al. [21]. It is seen, that for most transuranium nuclides there is an agreement within experimental error limits with the suggested dependence. However, the value and the character of growth of the <E>, given the existing uncertainties of experimental data and a small number of nuclides studied, are quite indeterminate.

It should be noticed, that all the principal information about neutron spectra in spontaneous fission (^{240}Pu, ^{242}Pu, ^{244}Cm and ^{246}Cm) was obtained long ago [6-11]. And though the errors in determining the Maxwellian parameter T, presented in those works, are relatively small (about 3%), the accuracy of the energy spectrum shape determination remains still rather low. All this is connected with a few reasons. Firstly, the T values are determined only for a limited region of spectra and, consequently, they cannot characterize the T for the whole energy range, and, secondly, (which is principal), careful measurements of the neutron spectra of ^{252}Cf spontaneous fission (and recently also ^{248}Cm) show that spectra shapes essentially differ from the Maxwellian. Therefore the T parameter is mainly used now as an average characteristics of the spectrum shape. It should be noted specially, that works [6-11] do not contain a detailed description of experiments, control tests, analysis of corrections and errors. The works have no numerical material on the results, and the spectra are presented on the logarithmic scale, which does not allow to use even the graphic data. In this connection there is practically no possibility to perform a modern analysis of those works. Therefore all the nuclides considered (^{240}Pu, ^{242}Pu, ^{244}Cm, ^{246}Cm) should be subjected to new measurements on the modern investigation level, as well as should be repeated investigations of the ^{248}Cm spectrum, where, besides, a very weak source of fissions was used.

THERMAL NEUTRON FISSION

Measurements of PNS in thermal neutron fission of transuranium nuclides are also few, except ^{239}Pu for which there are some reviews and evaluations (see, for example, [3, 16, 17]). But the

results of measurements, evaluations and recommendations of main libraries not always agree with one another even for this nucleus, and therefore require an additional specification. Fig. 5 taken from reference [17] shows that the neutron spectrum in ^{239}Pu thermal neutron fission, as well as in the cases of ^{252}Cf and ^{248}Cm spontaneous fission, has a complex character and differs from the Maxwell distribution. According to the recent evaluation by Khomyakov et al. [3], the average energy of PNS in ^{239}Pu thermal neutron fission equals to 2.07 ± 0.03 MeV, and the spectrum shape for neutron-physical calculations within experimental error limits may be satisfactory described by the Watt distribution [see equation (6)] with the parameters a = 1.03 and b = 0.858<ν> - 0.436.

In Table 2 the results of PNS measurements for the thermal neutron fission of minor actinides are given.

Table 2. Results of investigations of PNS in thermal neutron fission of minor actinides.

Nuclide	Energy range (MeV)	Method of measurements	Maxwell distrib. parameter T(MeV)	Reference, year
^{238}Pu	0.4-6.0	Time-of-flight	1.39 ± 0.04	[11],1970
^{239}Pu	-	Evaluation	1.38 ± 0.02	[3],1992
^{241}Pu	0.3-6.0	Time-of-flight	1.335 ± 0.034	[21],1961
^{241}Pu	1.6-7.0	Recoil protons	1.335 ± 0.034	[21],1961
^{242m}Am	0.4-6.0	Time-of-flight	1.42 ± 0.03	[11],1970
^{243}Cm	0.4-6.0	Time-of-flight	1.43 ± 0.04	[12],1973
^{245}Cm	0.4-6.0	Time-of-flight	1.50 ± 0.05	[11],1970
^{247}Cm	0.4-6.0	Time-of-flight	1.46 ± 0.04	[12],1973
^{249}Cm	0.4-6.0	Time-of-flight	1.55 ± 0.04	[11],1970

PNS measurements in thermal neutron fission are more difficult in comparison to spontaneous fission measurements due to neutron and gamma-background. Therefore, much attention in such measurements is paid to a careful collimation and adjustment of the neutron beam, a

good protection of the neutron detector and an effective catching of the beam in order to attenuate the surrounding neutron field and gamma-ray field.

The time-of-flight measurements of PNS in thermal neutron fission of ^{238}Pu, ^{242m}Am and curium isotopes in works by Zamyatnin et al. [11] and Zhuravlyov et al. [12] were carried out on the same equipment as measurements of the PNS at spontaneous fission. A gas scintillation fission chamber with corresponding targets was irradiated with a taken-out horizontal beam (1.5x15 mm) of the SM-2 reactor. The measurements were performed with cadmium and without cadmium on the beam's way. The net effect of thermal neutron fission was determined from these measurements. The obtained experimental results are presented only in the form of dependences $\ln[N(E)/E^{1/2}]$ on the E in the Fig. 1b. The spectra for the measured region agree with the Maxwell distributions. In the cited spectra there are few experimental points for neutron energies over 3.5 MeV, which may be attributed to insufficiient statistics.

In Fig. 6 a dependence of <E> on <ν> for measurements carried out in thermal neutron fission of transuranium nuclides is presented. One can see that, as well as in spontaneous fission, the neutron spectra become harder with a growth of the nucleus mass number or the <ν> value.

Thus, all the spectra for thermal neutron fission of transuranium nuclides (except ^{239}Pu): ^{238}Pu, ^{241}Pu, ^{242m}Am, ^{243}Cm, ^{245}Cm and ^{247}Cm [11,12,21] were measured only once and mainly by one group of authors and over 20 years ago. The measurement results agree with the Maxwellian. Meanwhile practically all modern information on neutron spectra of spontaneous fission (^{252}Cf, ^{248}Cm) and thermal neutron fission (^{233}U, ^{235}U, ^{239}Pu) points to essential deviations from that distribution. Besides, as well as for spontaneous fission, those works not contain a detailed description of the experiments, the methods of applying corrections, the evaluation of errors. The measurements were carried out in quite limited neutron energy ranges, without an account of neutron scattering effect and much else. All this shows that existing data on the energy spectra for the thermal neutron fission of the

considered nuclides do not correspond to modern requirements. Hence follows an unambiguous conclusion of the necessity to perform new measurements on the basis of up-to-date equipment and experimental methods.

FAST NEUTRON FISSION

In measurements of the PNS of transuranium nuclides fission by fast neutrons additional experimental difficulties arise due to the small value of fission cross section and high background because the detection of primary neutrons and the interaction of these neutrons with the environment. Besides, at neutron energies above the threshold of reactions (n,xnf), where x = 1,2,..., the PNS are caused by both the reaction (n,f) and reactions of subsequent fissions, that is after the emission of the pre-fission neutrons. Thus the energy distribution of neutrons is a function of primary neutron energy E_i.

Because of the small fission cross section a comparatively large quantity of the material is necessary in order to obtain an acceptable counting rate of neutrons. In the time-of-flight method this makes it difficult to use the conventional fission chambers. Therefore some works on PNS measurements were run on pulsed accelerators, using the short pulse formed from accelerator beam pulse as a time signal. To use fission event as a time signal fast multilayer pulse fission chambers with a large quantity of the material were developed. Such chambers allow to work on accelerators in the constant regime and, consequently, at comparatively large neutron fluxes.

Note, that even in using multilayer fast fission chambers of special design the PNS measurement in fast neutron fission is a complicated task. The difficulties are largely concerned with an intensive loading of the neutron counter as a result of recording the scattered, both primary and fission, neutrons on the chamber details and surrounding objects, as well as of intensive gamma-radiation. Therefore it is necessary to use an effective shielding of the neutron detector, to make arrangements for decreasing the neutron scattering.

PNS in fast neutron induced fission were measured for the only minor actinide, namely ^{237}Np. These measurements were performed by Trufanov et al. [22, 23] and Boykov et al. [24] by the time-of-flight method with multilayer fast fission chambers , which allowed to use comparatively large amounts of ^{237}Np (especially in work [24]). In Table 3 the data on the results of these spectra investigations are cited.

Table 3. Results of investigations of PNS in ^{237}Np fast neutron fission.

Neutron energy (MeV)	Spectrum range (MeV)	Average energy of spectrum (MeV)	Method of measurements	Year	Reference
2.9	0.25-12	2.06 ± 0.03	Time-of-flight	1994	[24]
4.9	0.7-12	2.19 ± 0.04	Time-of-flight	1992	[23]
6.0	0.7-12	2.23	Time-of-flight	1990	[22]
7.8	1.5-12	2.03 ± 0.08	Time-of-flight	1992	[23]
14.7	0.25-12	2.13 ± 0.04	Time-of-flight	1994	[24]

The fission PNS of ^{237}Np in works by Trufanov et al. [22,23] was measured at energies E_1 = 4.9, 6.0 and 7.8 MeV. The measurements were done at one angle (90 degrees) to the direction of movement of primary neutrons, which could distort the result due to anisotropy of both pre-fission and post-fission neutrons. Note also, that the works do not report about the efficiency of fragment registration. The results of measurements of the spectrum shape, presented on the semilogarithmic scale, are compared to distributions based on calculations by the cascade-evaporation Maerten-Seeliger model [26].

Measurements of ^{237}Np PNS by Boykov et al. [24] were made at energies E_1 = 2.9 and 14.7 MeV, respectively below and over the threshold of emission fission. The flight path was 205 cm, and the calibration of the neutron detector was performed in the course of measuring the spectrum, which allowed to account for the equipment instability connected with the duration of the measurements. The

lower threshold in the spectrum measurement was decreased down to 0.25 MeV. Neutron spectra were measured at the angle 90 degrees to the primary neutron beam, however, corrections were applied into final results for the angular correlation between primary and secondary neutrons. The fragments registration efficiency at the level of discrimination used was 70%. The results of measurements at E_i = 2.9 and 14.7 MeV [24] in the form of ratios of the R_M of measured PNS of fission $N(E,E_i)$ to the Maxwell distribution for ^{252}Cf spontaneous fission (T = 1.42 MeV) are presented in Fig.7. One may see for the E_i = 14.7 MeV an essential increase of $R_M(E,E_i)$ with a sharp enough upper bound at 8.5 MeV, which the authors attribute to the mechanism of non-equilibrium emission of pre-fission neutrons, as well as an increase of the yield of soft neutrons (E < 1.5 MeV) caused, probably, by the dynamics of the process.

Fig. 8 shows a dependence of measured and calculated average energies of PNS for ^{237}Np neutron fission on the E_i value (see [23]). For E_i < 6 MeV a monotonous growth of <E> in dependence on E_i is seen. Near the (n,n'f) reaction threshold, i.e. <E> $\sim$ 6 MeV, there is a decrease of <E> that, according to theory, is caused by the beginning of the emission fission process.

Thus, as a result of investigations of PNS for fast neutron induced fission of minor actinides there are data for ^{237}Np, for five energies of primary neutrons. The registration thresholds were rather high (except [24]). There is a lack of information about the efficiency of fragments registration. Hence, it does not seem possible to evaluate the real uncertainty of measurements on the basis of published data.

CONCLUSIONS

1. There are experimental data on fission prompt neutron spectra for only a small number of transuranium nuclei.

2. Most part of the experimental results were obtained long ago (15-20 years ago and more) by means of imperfect equipment and obsolete methods (quite limited energy range of measurements, low energy resolution, absence of neutron/gamma discrimination,

no account of the neutron scattering effect). In those works there is no detailed description of experiments, no analysis of experimental errors, no numerical information of the results.

3. The indicated in old works comparatively high accuracies of the determination of the Maxwell temperature T for many reasons cannot be considered as an evidence of an accurate determination of the fission PNS shape. First of all, because old measurements of PNS were performed in a limited energy range and that information was extrapolated to the whole spectrum. Besides , by data of measurements in recent years the fission PNS shape considerably differs from the Maxwell distribution.

4. Measurements show, that with an increase of the energy of neutrons inducing fissions grows the hardness of the prompt neutron spectrum. Quantitative conclusions are difficult, however, because of the low quality and a small number of experimental data. Calculations of this dependence by the Maerten-Seeliger model [26] in some cases do not give an agreement with experimental results.

5. Theoretical calculations of prompt PNS on the basis of modern models require a knowledge of the emission mechanism, as well as a great volume of input data. In principle, such calculations may give agreement with experimental results, which takes place for ^{252}Cf spontaneous fission for the spectrum energy region from 0.5 to 10 MeV. However, it is only agreement of theoretical calculations with measurements carried out at high precision for quite a number of nuclides, that can able to use theoretical calculations for predictions of fission PNS characteristics.
6. In connection with the task of long-lived transuranium nuclides transmutation in special burner reactors, the knowledge of neutron spectra shapes is required for isotopes of Np, Pu and Cm with the same accuracy (not worse than 1-2% by the average energy) as for nuclei of the basic fuel in conventional reactors.

7. The task of further investigations is to study the spectra on the modern experimental level, for a wide energy range of a spectrum, with great reliability and for a possibly greater number of nuclides, as was as revealing the regularities of the PNS characteristics in dependence on the A, Z, E^* of fissionable nuclei and the energy of primary neutrons. On the basis of these experimental data it is possible to develop a corresponding systematics of PNS, which will allow, side by side with theoretical calculations, to predict PNS for all cases necessary in practice.

REFERENCES

[1] T.Nishida et al., Nuclear Data Needs Concerning the OMEGA Project, INDC/P(90)-30, Vienna.
[2] W. Mannhart, Properties of Neutron Sources (Proc. of an Advisory Group Meeting on Neutron Sources, Leningrad, June 1986), IAEA-TECDOC-410, IAEA, Vienna, 1987, p.158.
[3] Yu.S. Khomyakov et al., Voprocy Atomnoy Nauki i Techniki, Seriya: Yadernye Konstanty 1 (1992) 70.
[4] J. Terrell, Phys. Rev. 113 (1959) 527.
[5] B.E. Watt, Phys. Rev. 87 (1952) 1037.
[6] Fizika deleniya atomnyh yader, Atomizdat, Moscow, 1957, p.74, (in Russian).
[7] T.W. Bonner, Nucl. Phys. 23 (1961) 116.
[8] V.I. Bolshov et al., Fizika deleniya atomnyh yader, Atomizdat, Moscow, 1962, p.127, (in Russian).
[9] Z.A. Aleksandrova et al., Atomnaya Energiya 36 (1974) 282 (in Russian).
[10] L.M. Belov et al., Yadernaya fizika 9 (1969) 727 (in Russian).
[11] Yu.S. Zamyatnin et al., Nuclear Data for Reactors (Proc. of the 2nd Int. Conf. on Nucl. Data for Reactors, Helsinki, 1970), IAEA, Vienna, vol.2, p.183.
[12] K.D. Zhuravlev et al., Neytronnaya Fizika (Proc. 2nd All-Union Conf. on Neutron Physics, Kiev, 1973), Obninsk, 1974, part 4, p.57 (in Russian).
[13] O.I. Batenkov et al., Atomnaya Energiya, 76 (1991) 566 (in

Russian); Nucl. Data for Science and Technology (Proc. of an Int. Conf., Julich, FRG, 13-17 May, 1991), Berlin, Springer Verlag, 1992, p.523.
[14] R.L. Bramblett et al., Nucl. Instr. Meth. 9 (1960) 1.
[15] M.V. Blinov, Proc. of the IAEA Consultants' Meeting on Neutron Source Properties, Debrecen, Hungary, 1980, INDC(NDS)-114/GT, IAEA, Vienna, 1980, p.79.
[16] A.A. Boytsov et al., Neytronnaya Fizika (Proc. of the 1st Int. Conf. on Neutron Physics, Kiev, 1987), Moscow, 1988, vol.3, p.104 (in Russian).
[17] B.I. Starostov et al., Voprocy Atomnoy Nauki i Techniki, Seriya: Yadernye Konstanty 2(37) (1980) 3 (in Russian).
[18] B.F. Gerasimenko and V.A. Rubchenya , ref. [13], p.208.
[19] F.N. Froehner, IAEA Advisory Group Meeting on Nuclear Theory for Fast Neutron Data Evaluation, Beijing, 12-16 Oct., 1987.
[20] V.V. Malinovskiy et al., Voprocy Atomnoy Nauki i Techniki, Seriya: Yadernye Konstanty 5(54) (1983) 190 (in Russian).
[21] A.S. Smith et al., Phys. Rev. 123 (1961) 140.
[22] A.M. Trufanov et al., Nuclear Data for Neutron Emission in the Fission Process (Proc. of the IAEA. Meeting, Vienna, 22-24 October, 1990), IAEA, Vienna, INDS(NDS)-251, 1990, p.105.
[23] A.M. Trufanov et al., Yadernaya fizika 55 (1992) 298 (in Russian).
[24] G.S. Boykov et al., Yadernaya fizika 57 (1994) 2126; Ann. Nucl. Energy 10 (1994) 585.
[25] I. During et al., Nuclear Data for Neutron Emission in the Fission Process (Proc. of the IAEA Meeting, Vienna, 1990), IAEA, Vienna, INDS(NDS)-251, 1990, p.159.
[26] H. Maerten, D.Seeliger, J. Phys., G: Nucl. Phys. 10 (1984) 349.
[27] J.Terrell, Proc. of the Symp. on Phys. and Chem. of Fission, Salzburg, March 1965, v.2, p.3.

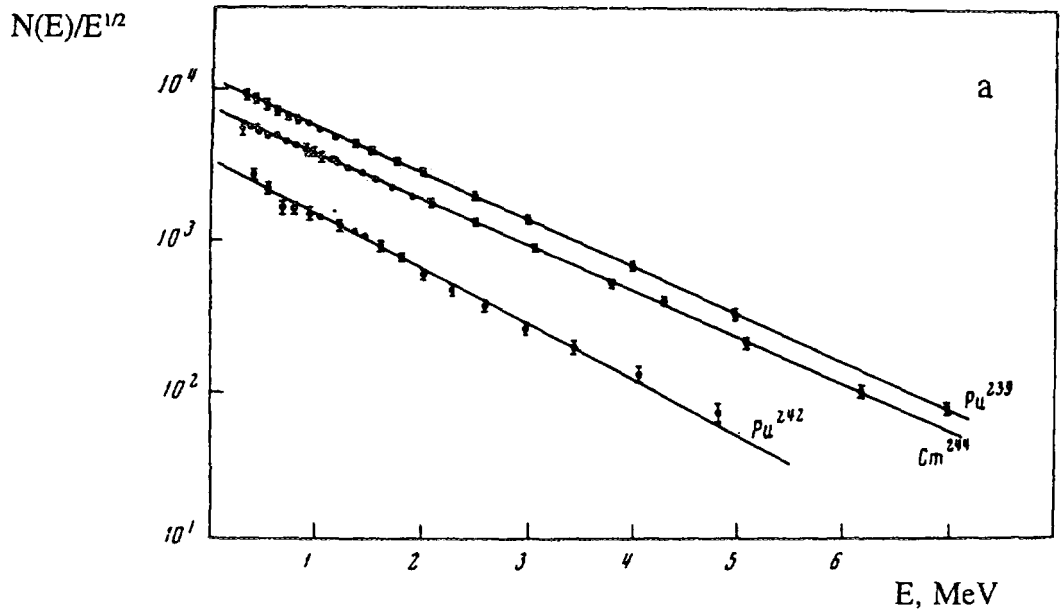

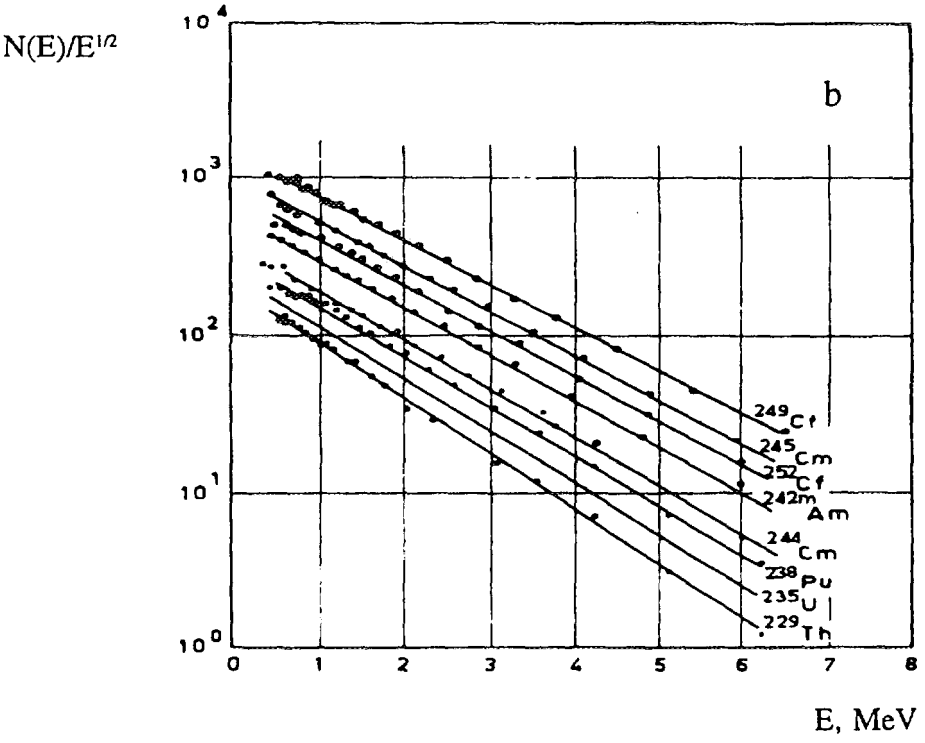

Fig. 1. Fission PNS for some transuranium nuclides.
a - [10]; b - [11].

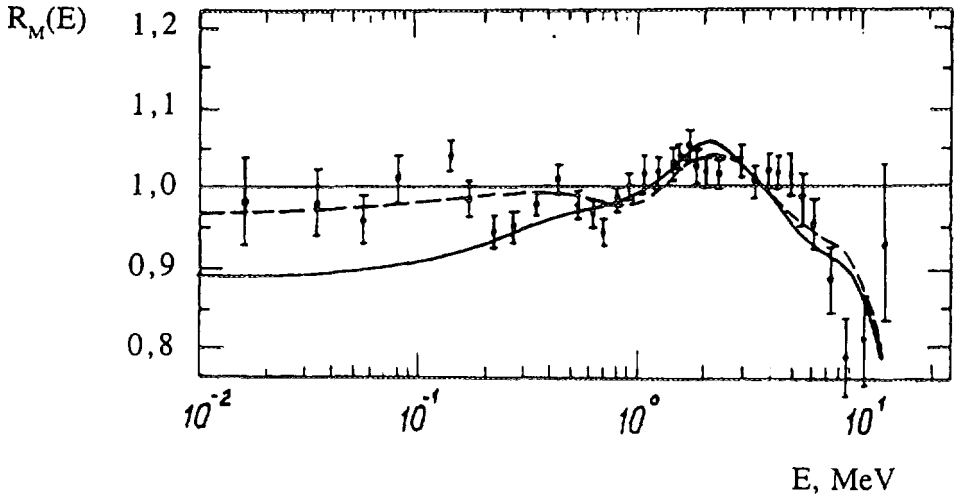

Fig. 2. Evaluated [2] and calculated [19] PNS for Cf-252 spontaneous fission relative to the Maxwell distribution with the parameter T = 1.42 MeV. Calculations using two anisotropy coefficients b of particle emission in the center-of-mass system.
—— - b = 0, - - - - - b = 0.15, ... - experiment.

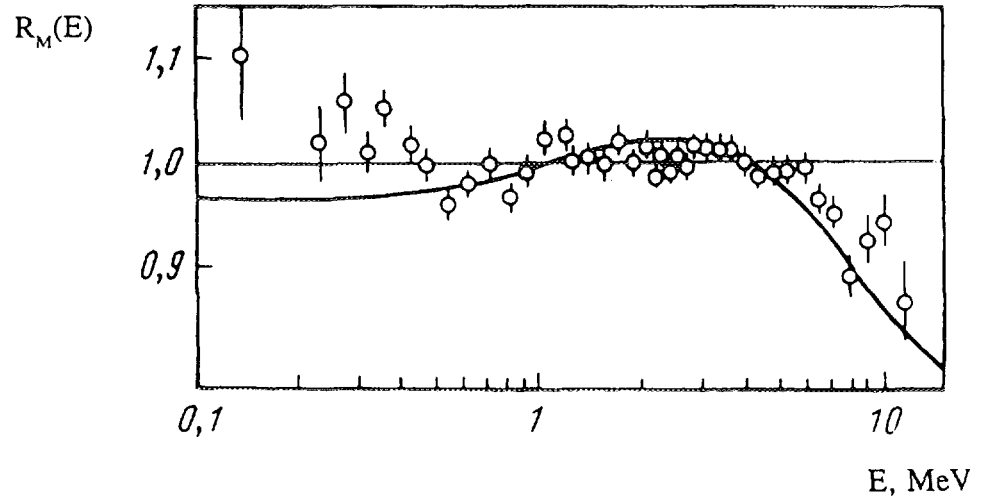

Fig. 3. Deviations of experimental PNS in Cm-248 and Cf-252 spontaneous fission from Maxwell distributions.
o o o - data of work [13] for Cm-248 (T = 1.38 MeV),
—— - evaluation [2] for Cf-252 (T = 1.42 MeV).

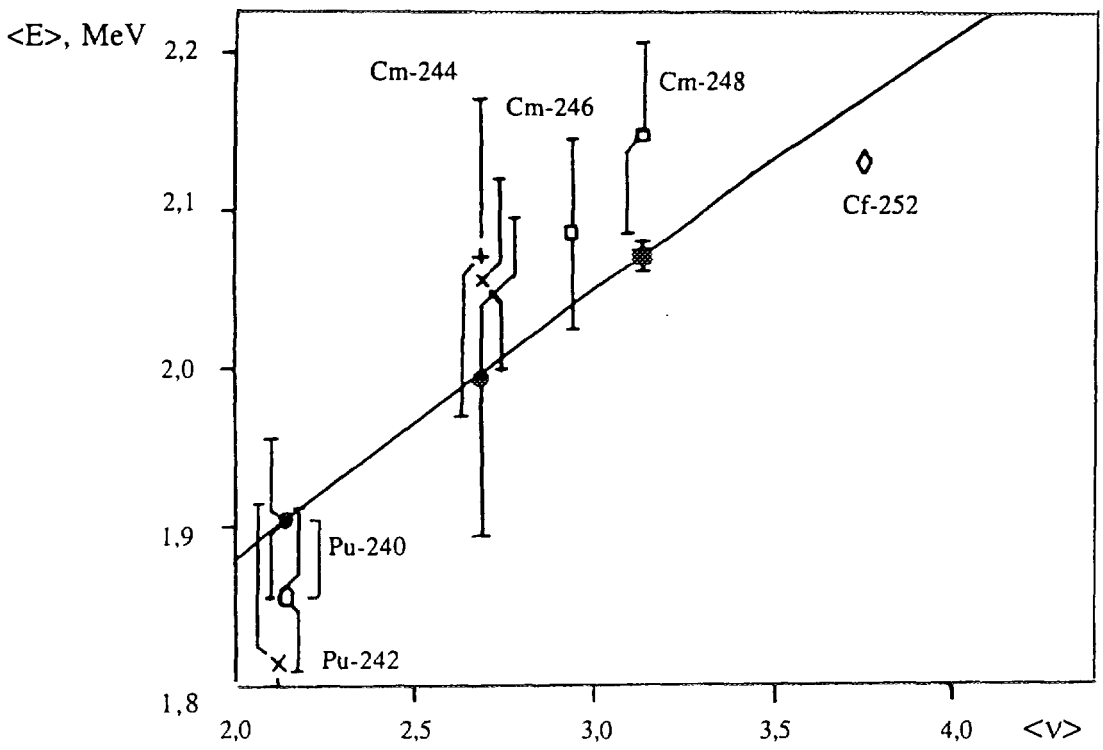

Fig. 4. Dependence of <E> on <ν> for spontaneous fission.
o - Bolshov et al. [8], • - Aleksandrova et al. [9], x - Belov et al. [10],
+ - Zamyatnin et al. [11], □ - Zhuravlyov et al. [12], ■ - Batenkov et al. [13],
◊ - Mannhart [2], —— - Terrell [27].

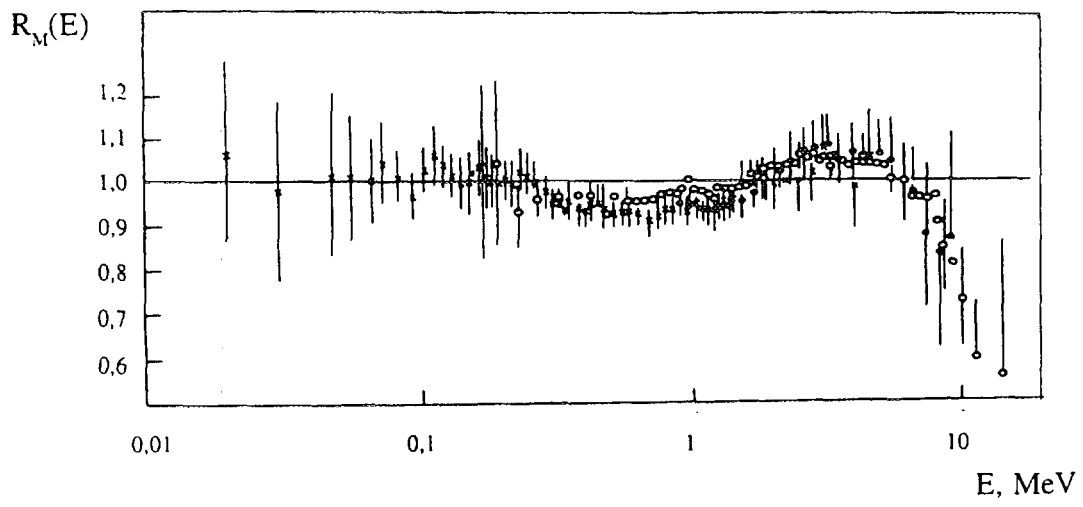

Fig. 5. Relation of PNS in Pu-239 thermal neutron fission [17] to the Maxwell distribution with the parameter T = 1.383 MeV.
• - evaluation, o, x - experimental data.

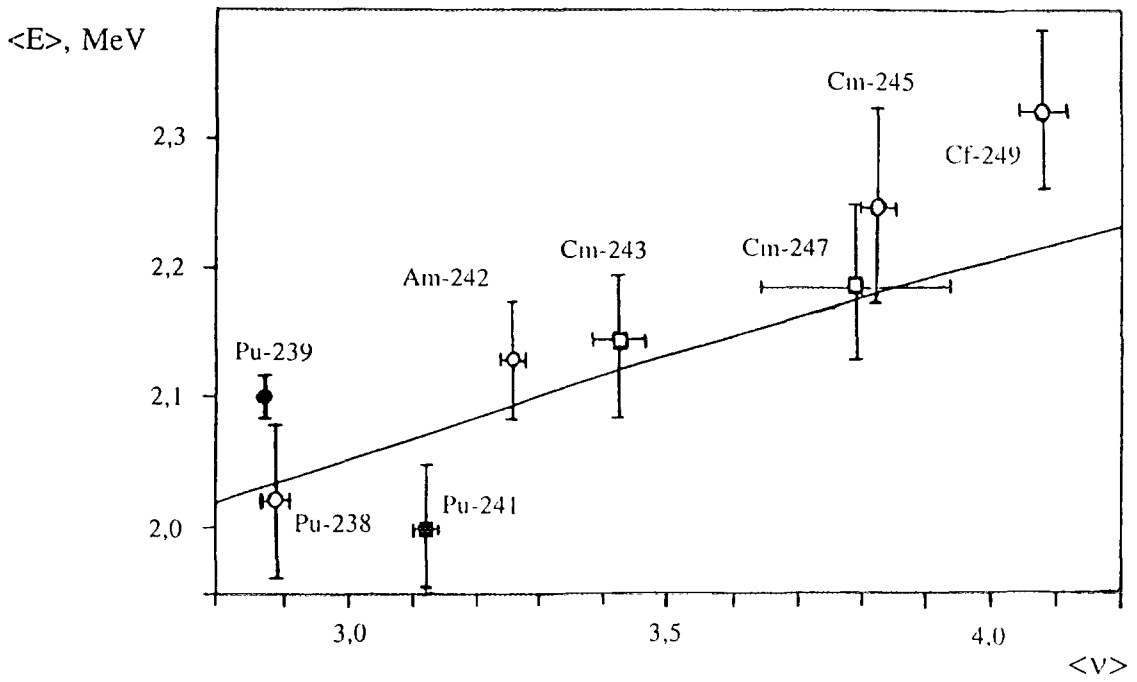

Fig. 6. Dependence of <E> on <ν> for thermal neutron fission.
o - Zamyatnin et al. [11], ◻ - Zhuravlyov et al. [12], ● - Khomyakov et al. [3], ■ - Smith et al. [21], ——— - Terrell [27].

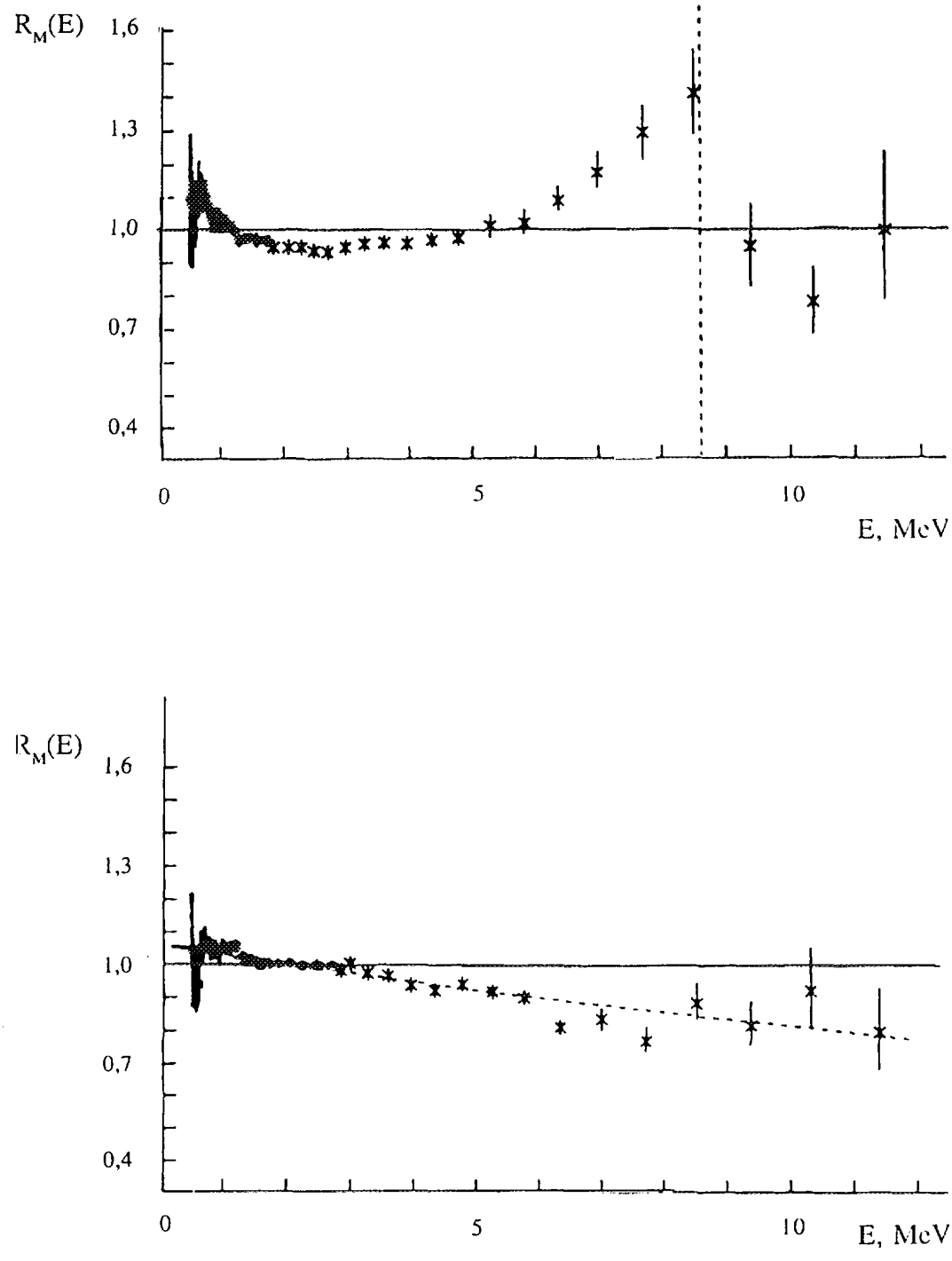

Fig. 7 . Relations of fission PNS in Np-237+n(E_i) reaction at E_i = 2.9 (below) and 14.7 MeV (above) to the Maxwell distribution with the parameter T = 1.42 MeV (Cf-252) [24].

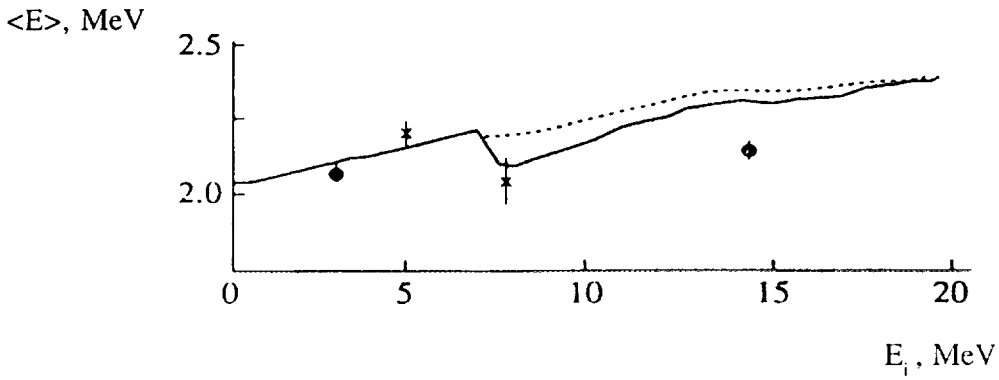

Fig. 8. Dependence of <E> of fission PNS in Np-237+n(E_i) fission on E_i. o - [24], x - [23].

2. 2 The statistical model calculation of prompt neutron spectra from spontaneous fission of ^{244}Cm and ^{246}Cm

B.F.Gerasimenko

V.G.Khlopin Radium Institute,
2nd Murinski Avenue 28, 194021 St.Petersburg, Russia

Abstract

The calculations of integral spectra of prompt neutrons of spontaneous fission of ^{244}Cm and ^{246}Cm were carried out. The calculations were done by the Statistical Computer Code Complex SCOFIN applying the Hauser－Feschbach method as applied to the description of the de－excitation of excited fission fragments by means of neutron emission. The emission of dipole gamma－quanta from these fragments was cosidered as a competing process. The average excitation energy of a fragment was calculated by two－spheroidal model of tangent fragments. The density of levels in an excitated fragment was calculated by the Fermi－gas model. The quite satisfactory agreement was reached between theoretical and experimental results obtained in frames of Project measurements. The calculated values of average multiplicities of neutron number were 2,746 for ^{244}Cm and 2,927 for ^{246}Cm that was in a good accordance with published experimental figures.

THE STATISTICAL MODEL CALCULATION OF PROMPT NEUTRON SPECTRA FROM SPONTANEOUS FISSION OF ^{244}Cm AND ^{246}Cm

B. Gerasimenko
KRI, St. Petersburg, Russia

Introduction

The study of low energy fission has shown that de-excitation of fission fragments is mainly determinated by the statistical emission of prompt fission neutrons (PFN) and gammas [1-3] and the contribution of non - statistic effects is negligible [4[. To calculate PFN spectra the simple cascade evaporation model [5,6] has usually been used. But nowadays it is obviously that more detail investigation of PFN emission phenomena is available only in the frame of exact and consistent approach such as Hauser-Fesebach statistical model.

The method of calculation.

Present calculation have been made assuming that in the case of spontaneous fission the main part of neutrons is connected with equilibrium neutron emission mechanism. It has been shown that this assumption is enough good for the case of spontaneous fission of ^{252}Cf. The neutrons are emitted from fully accelerated excited fragments by the cascade mechanism. It was supposed that neutrons are emitted isotropically in center of mass system (CMS) of fragments. Then PFN spectrum for fragment with A,Z in CMS which moves with E_k will be formed as

$$N(\varepsilon, A, Z, E_k) = \sum_{\nu=1}^{\nu_{max}} (1 - \sum_{i=0}^{\nu-1} W(i)) \cdot n_\nu(\varepsilon, A, Z, E_k), \quad (1)$$

where

ν_{max} - maximum value of neutrons emitted from fragment
$n_\nu(\varepsilon,A,Z,E_k)$ - CMS spectrum of ν-th neutron normalized to 1.
$W(\nu)$ - neutron multiplicity distribution for fragment

CMS spectrum of ν -th neutron can be obtained by averaging of the CMS neutron spectrum $\varphi(\varepsilon,E^*,A-\nu+1,Z)$ from the fragment with excitation energy E^* on the excitation energy distribution

$$\varphi(\varepsilon, E^*, A, Z) = \sum_J \omega(E^*, J, A, Z) \frac{\Gamma_n(E^*)}{\Gamma_n^t(E^*) + \Gamma_\gamma^t(E^*)}, \quad (2)$$

$$n_\nu(\varepsilon, A, Z, E_k) = \int dE^* \cdot P_{\nu-1}(E^*, A, Z) \sum_J \omega(E^*, J, A, Z) \frac{\Gamma_n(E^*)}{\Gamma_n^t(E^*) + \Gamma_\gamma^t(E^*)}, \quad (3)$$

where

$P_{\nu-1}$ - fission fragment excitation energy distribution after ν-1 neutron emission.
ω - fission fragment spin distribution
Γ_n - neutron width
$\Gamma_n^t, \Gamma_\gamma^t$ - total neutron and radiation widths of fragment

$$\Gamma_n^t(E^*, J, A, Z) = 1/2\pi\rho \cdot \int \rho(E^{*\prime\prime}, J'', A-1, Z) \sum_{\ell,j} T_{\ell j}(\varepsilon) dE^{*\prime\prime}, \quad (4)$$

$$\Gamma_\gamma^t(E^*, J, A, Z) = 1/2\pi\rho \cdot \int \rho(E^{*\prime\prime}, J, A, Z) T_\gamma(E^* - E^{*\prime\prime}) dE^{*\prime\prime}, \quad (5)$$

where

ρ - the fragment level density
$T_{\ell j}, T_\gamma$ - neutron and gamma transmission coefficients.

In assuming the isotropic neutron emission the laboratory system PFN spectrum will be described as:

$$\phi(E_n,A,Z,E_K)=\int_{B-}^{B+} N(\varepsilon,A,Z)/[4(\varepsilon\cdot E_f)^{1/2}]\,d\varepsilon, \quad (6)$$

where

E_n - neutron kinetic laboratory system (LS) energy,

$$B_{\pm}=(E_n^{1/2}\pm E_K^{1/2}/A^{1/2})^2, \quad (7)$$

$$E_f=E_K/A. \quad (8)$$

To obtain the total PFN spectrum from (A,Z) -fragment it is necessary to average spectrum (6) on the fragment kinetic energy distribution . Thus the spectrum of the first cascade neutron is expressed as

$$n_{\nu=1}(\varepsilon,A,Z,E_K)=\int_{B_n+\varepsilon}^{E^*_{max}} P_0(E^*,A,Z)\sum_J \omega(E^*,J,A,Z)\,\frac{\Gamma_n(E^*)}{\Gamma_n^t(E^*)+\Gamma_\gamma^t(E^*)}\,dE^* \quad (9)$$

where

B_n - neutron binding energy,

P_0 - the initial fragment excitation energy distribution with parameters $\bar{E}^*$ and σ_{E^*}.

The value of ν_{max} is determined by E^*_{max}. The fragment excitation energy distribution after 1-st neutron emission can be calculated as

$$P_1(E^*,A-1,Z,E_K)=\int_{E^*+B_n(A-1,Z)}^{E^*_{max}-B_n} P_0(E_1^*,A,Z)\cdot\varphi(E_1^*-E^*-B_n,E_1^*,A,Z)\,dE_1^*. \quad (10)$$

The excitation energy distributions at higher stages of evaporation cascade can be calculated by similar way. The neutron multiplicity distribution $W(\nu)$ was determined as shown in [8]. To obtain the integral PFN spectrum for fissioning nucleus (A_c , Z_c) with excitation energy E_c^* the LS neutron spectra from individual fragments must be summarized

$$N(E_n,A_c,Z_c,E^*)=\sum_{A,Z} Y(A,Z,A_c,Z_c,E_c^*)\,dN(E_n,A,Z)/dE_n, \quad (11)$$

where

Y - independent yield of fission fragment.

The PFN multiplicity distribution $P(\nu)$ for the fissioning nucleus (A_c,Z_c) is formed by the same manner.

The statistical model code "SCOFIN" was used systematically in our PFN spectra calculations [10]. In the code were taken into account the level density dependence on fragment excitation energy, the fragment spin influence effect, n-γ competition. The next input data have been used: the average CMS neutron kinetic energies, data on dispersion of the initial excitation energy distribution, and data on average PFN number. The above input data allowed us to calculate the initial average excitation energies of fragments. Because of the experimental information on fission fragment characteristics for spontaneous fission of ^{244}Cm, ^{246}Cm are absent the need of model calculation of E^* was occurred. To solve this problem we use the two-spheroid model [2,11,12]. The average fragment excitation energy is determined in the model as

$$\bar{E}^*(A,Z) = E^*_{sc}(A,Z) + E_{def}(A,Z), \tag{12}$$

where

E_{def} - fragment deformation energy,

E^*_{sc} - fragment excitation energy at scission point.

The fragment deformation energy is described

$$E^*_{def}(A,Z) = \alpha \cdot (b - R_0)^2, \tag{13}$$

where

$R_0 = r_0 A^{1/3}$,

b is one half of long axis of spheroid,

α - fragment deformability connected with fragment rigidity C by expression

$$C = [5/(2\pi)]\alpha \cdot R_0^2. \tag{14}$$

Parameter α is determined [13] by

$$\alpha(A,Z) = \alpha_{LDM}(k - \delta W)/(k + \delta W), \tag{15}$$

where

δW - the fragment shell correction at the scission point,

α_{LDM} - liquid drop model [14] parameter, namely

$$\alpha_{LDM} = (0.16\pi/r_0^2)[a_2(1 - \kappa((A-2Z)/A)^2 - \tfrac{1}{2}c_3 Z^2/A], \tag{16}$$

$$\begin{aligned} k &= 8.0 \text{ MeV}, \\ a_2 &= 18.56 \text{ MeV}, \\ \kappa &= 1{,}79, \\ c_3 &= 0.717 \text{ MeV}. \end{aligned} \tag{17}$$

The length of spheroid axis was found under condition of minimum of potential energy F of fissioning system:

$$\frac{\partial F}{\partial b_1} = 0, \quad \frac{\partial F}{\partial b_2} = 0, \tag{18}$$

where

$$F = V_{coul} + E_{def_1} + E_{def_2}, \tag{19}$$

and

$$V_{coul} = (Z_1 Z_2 e^2)/(b_1 + b_2 + d). \tag{20}$$

Here

e - electron charge,

d - initial distance between fragments formed.
So, the equation system (10) will be

$$-Z_1 Z_2 e^2/(b_1+b_2+d)^2+2\alpha_1(b_1-R_{o_1})+\frac{\partial\alpha_1}{\partial b_1}(b_1-R_{o_1})^2=0$$
$$-Z_1 Z_2 e^2/(b_1+b_2+d)^2+2\alpha_2(b_2-R_{o_2})+\frac{\partial\alpha_2}{\partial b_2}(b_2-R_{o_2})^2=0. \quad (21)$$

Under assumption on small deformations of fragments the above system will be

$$-Z_1 Z_2 e^2/(b_1+b_2+d)^2+2\alpha_1(b_1-R_{o_1})=0$$
$$-Z_1 Z_2 e^2/(b_1+b_2+d)^2+2\alpha_2(b_2-R_{o_2})=0 \quad (22)$$

The solution of above system gives the fragment deformations. It is necessary to take into account the dependence of δW on scission point temperature of fragment. In accordance with [15] this dependence was used in the form

$$\delta W(E^*_{sc})=\delta W\cdot t^2\cdot[ch(t)/sh^2(t)], \quad (23)$$

where

$$t=[2\pi^2/41\cdot A^{-1/3}]\cdot(E^*_{sc}/a)^{1/2}, \quad (24)$$

It was supposed that both fragments temperatures are equal. The energy E^*_{sc} of fissioning nucleus which includes the dissipative energy E_{diss} [16] is devided between the fission fragments according to [12] as:

$$E^*_{sc_1}/E^*_{sc_2}=A_1/A_2. \quad (25)$$

The calculation of $E^*_{sc}(A_c,Z_c)$ was performed in accordance with [12,16]. The solution of equation system (22) permits taking into account (13) and (23), (24) to calculate the deformation energy for each of additional fragments. The next step is the calculation $\bar{E}^*(A,Z)$ of fragment excitation energies.The dispersion of excitation energy distributions for each of additional fragments is calculated with use of dispersions of average kinetic energies of fragment pairs as was described in [10].

Calculations.

On the bases of described approach the PFN spectra for spontaneous fission of ^{244}Cm, ^{246}Cm have been calculated. The total average number of neutrons ν_{tot} emitted was also calculated for both of the nuclei. The data on shell corrections used in the calculation were determined by interpolation of shell corrections of ^{252}Cf fission and of thermal neutron-induced fission of ^{235}U [11,12]. The dissipative energy value was taken from ref. [16]. For r_0 was taken 1.3 Fm and distance d=2 Fm. The average kinetic energies of fission fragment pairs were taken for spontaneous fission of ^{244}Cm from ref. [17] and for spontaneous fission of ^{246}Cm from ref.[18], the independent yields for the case of ^{244}Cm were taken from ref.[19] and for ^{246}Cm from ref. [18]. The level density of excited fragments was calculated on the bases of Fermi-gas model in accordance with ref. [20]. As the optical potential was used the Beccetti-Greenlees potential [21].

Results.

The calculated PFN spectra for spontaneous fission of ^{244}Cm and ^{246}Cm are presented in Fig.1, Fig.2 consequently. The spectra were presented as a ratio to the PFN spectrum of ^{252}Cf spontaneous fission. The last one was also calculated in the frame of the approach described above with use of average fragment kinetic energies and independent yields taken from [22] and [18] accordingly. The spectra under analysis were calculated for two values of initial average spin: J=0 and J=6÷8h. The calculations have shown that increasing of fragment average spin leads to 3%-decreasing of average spectrum energy. It can be seen the satisfactory agreement between theoretical and experimental results. The comparison of calculated and experimentally measured values of total average neutron numbers $\bar{\nu}_{tot}$ is a good criteria of validity of the model used for the PFN spectra calculation. The now available experimental data on $\bar{\nu}_{tot}$ for ^{244}Cm are from 2.61 ± 0.13 [23] to 2.84±0.09 [25] and from 2.86±0.06 [26] to 3.20±0.22 [28] for ^{246}Cm. The following calculated values (2.746 for ^{244}Cm and 2.927 for ^{246}Cm) were obtained in present work. In Fig.3 the calculated and experimentally measured [26] PFN multiplicity distributions for spontaneous fission of ^{246}Cm are presented. The compared results show the satisfactory agreement.

References.

1. H.R.Bowman, J.Milton, S.Thompson, Phys.Rev.,1962,v.126,p.2120.
2. J.Terrell, PHYSICS AND CHEMISTRY OF FISSION. Proc.of the 3rd Symposium on Physics and Chemistry of Fission. IAEA. Vienna.1965. v.2. p.3.
3. H.Maerten,D.Richter, D.Seeliger, NUCLEAR FISSION. Proc. of XV th Intern.Symposium on Nuclear Physics. ZfK-592.,1986, p.1.
4. O.I.Batenkov, A.S.Blinov, M.V.Blinov et al., PROPERTIES OF NEUTRON SOURCES. Proc. of an Advisory Group Meeting on properties of neutron sources. IAEA-TECDOC-410. Vienna, IAEA, 1987, p.201.
5. D.Madland, J.Nix, Nucl. Sci. Eng., 1982, v.81, p.213.
6. R.L.Walsh, Nucl. Sci. Eng., 1989, v.102, p.119.
7. W.Hauser, H.Feshbach, Phys.Rev., 1952, v.52, p.295.
8. B.F. Gerasimenko, V.A.Rubchenya, Atomnaya energiya, 11985, t.59, vip.5, s.335.
9. B.F. Gerasimenko,V.A.Rubchenya, FIFTITH ANNIVERSARY OF NUCLEAR FISSION. Proc. of Intern. Conference. Leningrad, Radium Khlopin Institute, 1992, v.1, p.385.
10. B.F.Gerasimenko, V.A.Rubchenya, Bulleten Tsentra Dannikh LIJaF, 1986, vip.12, s.3.
11. B.D.Wilkins et al., Phys.Rev., 1976, v.14C, p.1832.
12. A.Ruben, H.Maerten, D. Seeliger, Zeitschrift fuer Physik, 1991, p.67.
13. M.Kildir, N.K.Aras, Phys.Rev., 1982, v.25C, p.365.
14. W.Myers, W.Swiatecki, Nucl.Phys., 1966, v.81, p.1.
15. O.Bor, B.Mottelson, STRUKTURA ATOMNOGO YADRA. M. Energoatomizdat, 1983.
16. F.Goennenwein, VANiT, 1988, ser.: Yaderni kohstanti, vip.1, s.14.
17. Yu.A.Barashkov, Yu.A.Vasilyev, A.N.Maslov et al., Yadernaya fizika, 1971, t.13, vip.6, s.1162.
18. J.Unik, J.Gindler et al., see ref. [5[, p.19.
19. F.Caitucoli, M.Asghar, B.Leroux et al., Nucl.Phys.,1983,v.394A, p.360.
20. A.V.Ignatyuk, G.N.Smirenkin, A.S.Tishin, Yadernaya fizika, 1975, t.21, vip.3, s.485.
21. F.Beccetti, G.Greenlees, Phys.Rev., 1969, v.182, p.1190.
22. H.W.Schmitt, J.H.Neiler, F.Walter, Phys.Rev., 1966, v.141, p.1146.
23. W.W.T.Crane, G.H.Higgins, H.R.Bowman, Phys.Lett., 1956, v.101, p.1804.
24. Z.Huanqiao, L.Zuhua et al., Nucl. Sci. Eng., 1984, v.86, p.315.
25. D.A.Hicks, J.Ise, R.V.Pile, Phys.Rev., 1956, v.101, p.1016.
26. R.W.Stoughton, J.Halperin, C.E.Bemis, H.W.Schmitt, Nucl. Sci. Eng., 1973, v.50, p.169.

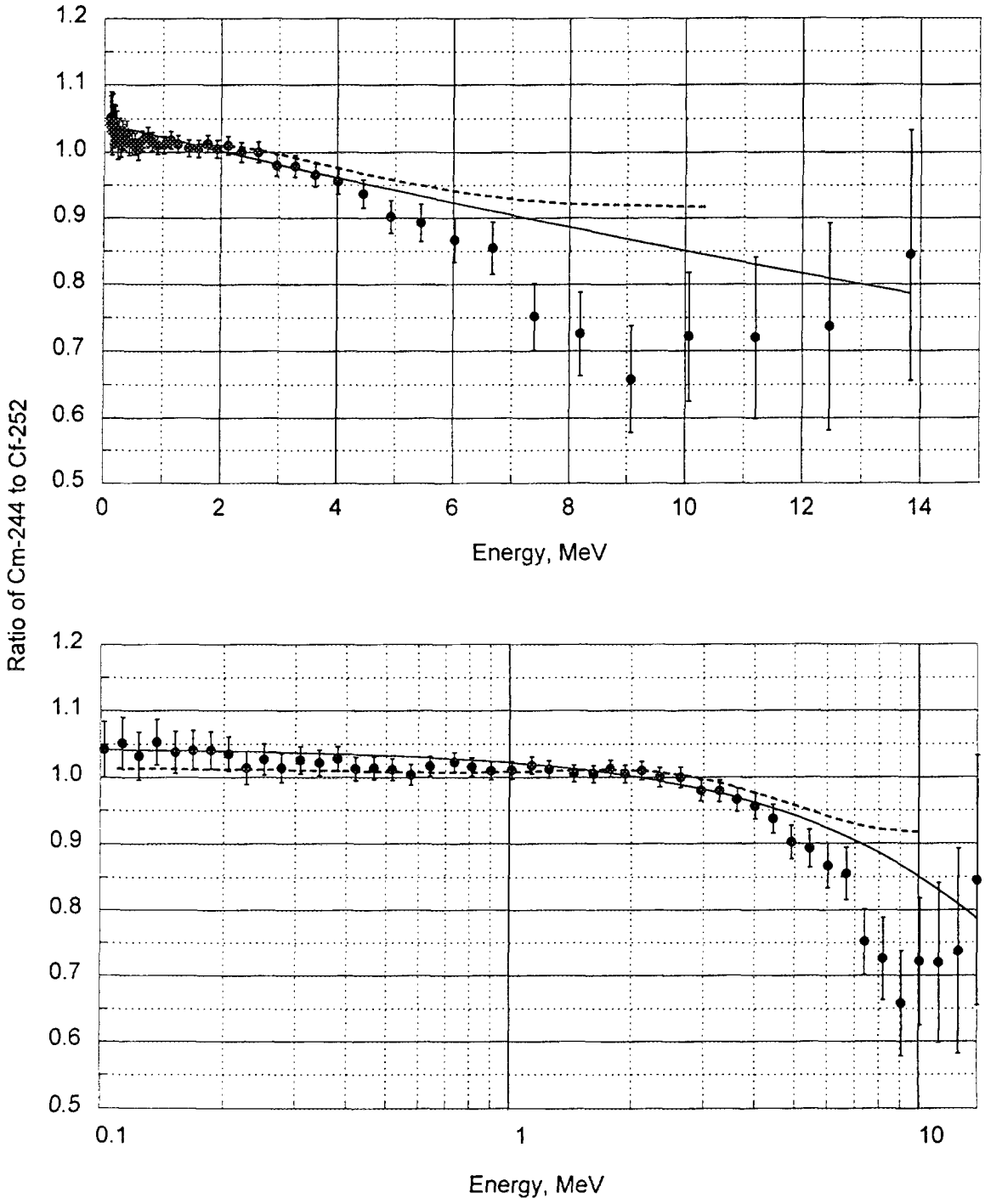

Fig. 1. Resulting ratio of ^{244}Cm to ^{252}Cf neutron spectra. The solid line indicates the results of experimental points fitting to the function $R(E,T_{Cm})=(T_{Cm}/T_{Cf})^{-3/2}\exp(-E(1/T_{Cm}-1/T_{Cf}))$, T_{Cf}=1.42 MeV. he value of the parameter T_{Cm} obtainned by least-squares method was equal to 1.373 MeV (0.005) with Chi^2=0.93 per degree of freedom.
he dashed line - the statistical model caculation (initial fragment spin J=0).

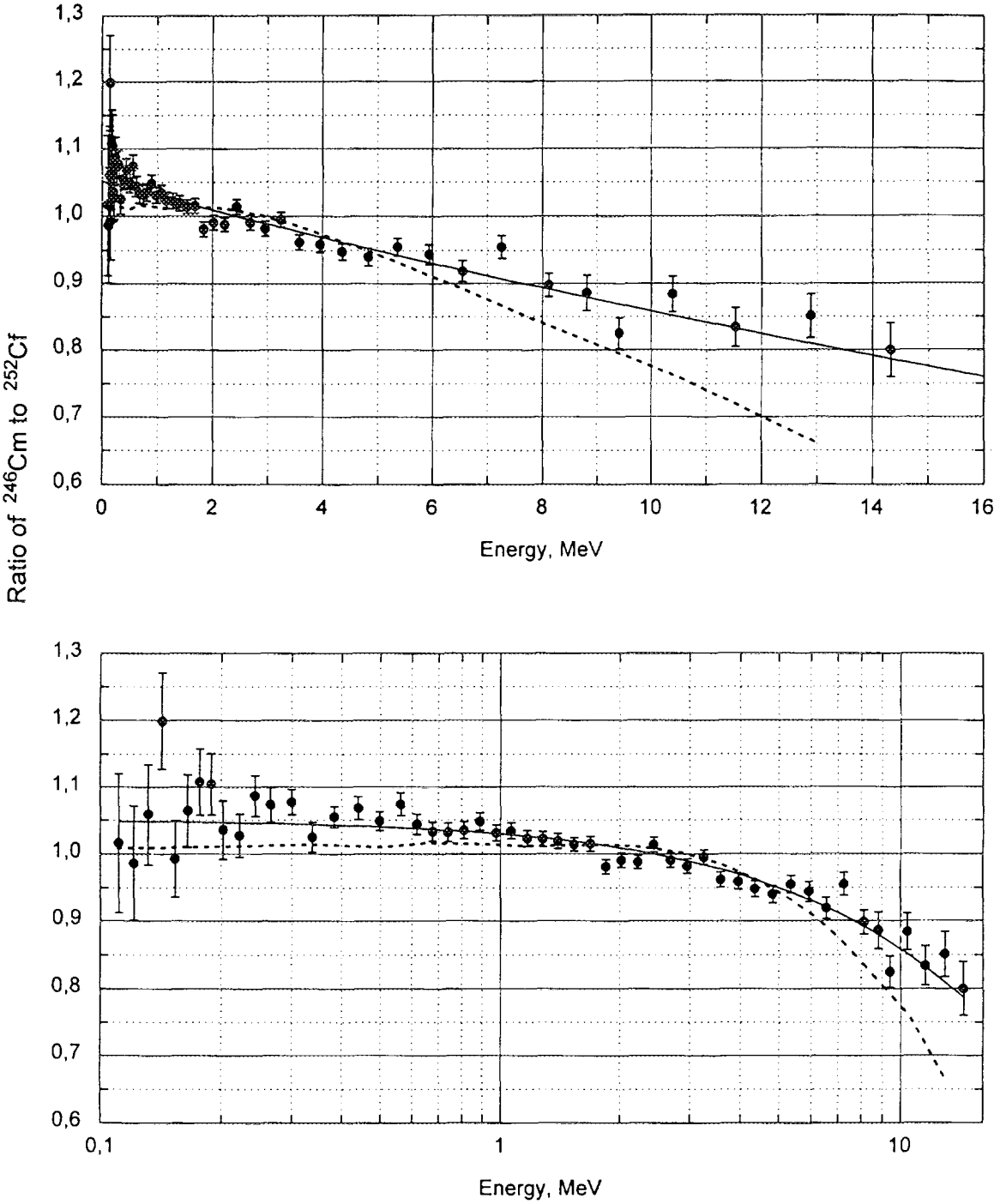

Fig.2. Resulting ratio of ^{246}Cm to ^{252}Cf neutron specta. The solid line indicates the result of experimental points fitting to the function

$R(E_n,T_{Cm})=(T_{Cm}/T_{Cf})^{-3/2}\exp(-E_n/T_{Cm}+E_n/T_{Cf})$, T_{Cf}=1.42 MeV

The value of the parameter T_{Cm} obtained by least-squares method was equal to 1.380 (0.002) MeV with Chi^2 = 1,28 per degree of freedom.

The dashed line presents the statistical model calculation. The value of average initial fragment spin J=0 h.

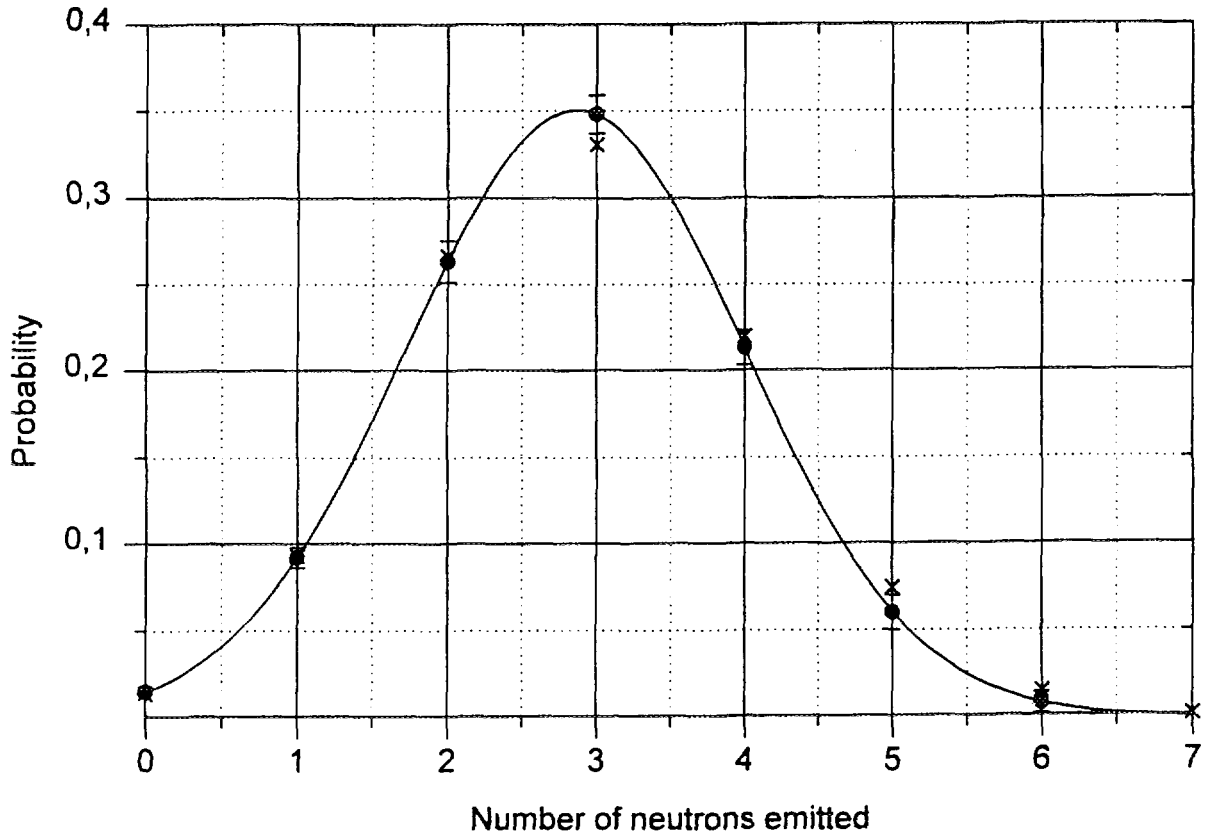

Fig.3 Calculated multiplicity of neutrons in spontaneous fission of ^{246}Cm (×). Experimental points of [18] presented by solid circles.

2. 3 The Measurement of Prompt Neutron Spectrum in Spontaneous Fission of ^{244}Cm

O.I. Batenkov, G.S. Boykov, , L.V. Drapchinsky,
M.Ju. Majorov, V.A. Trenkin
V.G. Khlopin Radium Institute
2nd Murinski Avenue 28, Saint Petersburg, Russia

Abstract

Under the Program of Measurements of Prompt Fission Neutron Spectra of Minor Actinides for Transmutation Purposes the integral neutron spectrum in spontaneous fission of ^{244}Cm has been measured by the time-of-flight method in the energy range of 0.1-15 MeV relative to the standard neutron spectrum in ^{252}Cf spontaneous fission. Essential attention was paid to revealing of possible systematic errors. It is shown, that the ^{244}Cm spectrum shape may be well described by using Mannhart evaluation with appropriate parameter of Maxwell temperature T_M=1.37 MeV.

1. Introduction

The data on energy spectra and the number of neutrons in minor actinide fission are required to work out the transmutation conception using actinide burner reactors. Neutron spectrum measurements in spontaneous and neutron-induced fission of the actinides take a lot of time and efforts. At present those measurements cannot be done at all for a whole number of nuclides. Therefore, it is necessary to carry out the measurements of the fission neutron spectra with an accuracy as high as possible and to create the systematics on the basis of all the measurements available. Those systematics will make it possible to give high accurate predictions for the fission neutron energy spectra of all minor actinides required for reactor transmutation.

The goal of present work is the measurements of prompt neutron spectrum (PNS) from spontaneous fission of ^{244}Cm in the energy range 0.1-15 MeV and determination of average neutron spectrum energy with accuracy better than 2 %. These data are necessary in design process for calculation of the optimum reactor parameters, because the own neutron field of the spent fuel generated mainly by spontaneous fission of *Cm* isotopes must be taken into account in calculations.

In order to solve this task the time-of-flight (TOF) neutron spectrometer measuring the spectrum under investigation with respect to international standard PNS of ^{252}Cf has been designed and built at the V.G. Khlopin Radium Institute. The method of relative measurement is in some preferences to absolute one due to the fact that both spectra are measured simultaneously and in our version of experiment some uncertainties connected with a time instability of apparatus could be excluded. Besides that there is no need to measure the absolute efficiency of neutron detection and to skip of neutron spectrum distortions caused by background from (n,γ)-reactions and neutron scattering on the walls of room, on structural materials of experimental set-up.

To obtain the PNS of ^{244}Cm the experimentally measured ratio $R(E)$ must be multiplied on evaluation [1] of PNS of ^{252}Cf.

$$\frac{dN^{Cm}(E)}{dE} = R(E) \cdot \frac{dN^{Cf}_{eval}(E)}{dE}$$

Then the average value of neutron spectrum energy can be determined as follows

$$\overline{E} = \int E \frac{dN^{Cm}(E)}{dE} dE$$

2. Experimental Arrangement

2.1. Neutron sources

The sources of *Cm* and *Cf* were prepared by thermal evaporation in vacuum and their nonuniformity was no worse than 10% in both cases. To improve the collection of charges targets were covered with a thin (30 mkg/cm^2) layer of Au. The mass-spectrometric analysis made before preparation of sources shows the next contents of initial materials both for *Cm* and *Cf* (see Table 1).

Table 1
The properties of source materials

Source ***Cf***: weight - 0.002 μg
thickness - 0.0015 μg/cm^2
gold cover - 30 μg/cm^2
fission/s - 1255
α-activity - $3.69 \cdot 10^4$ α/s
Backing - stainless steel d=0.1 mm thick

Content, %	fission/s	n/s

^{252}Cf - 73.17	1245	4669
^{251}Cf - 5.49	--	
^{250}Cf - 12.09	10	36
^{247}Cf - 9.21	--	
^{244}Cm < 0.007	--	

Source ***Cm***: weight - 51 μg
thickness - 39 μg/cm^2
gold cover - 30 μg/cm^2
fission/s - 205
α-activity - $1.53 \cdot 10^8$ α/s
Backing - stainless steel d=0.1 mm

Content, %	fission/s	n/s
^{244}Cm - 79.1	187	505
^{245}Cm - 12.6	--	
^{246}Cm - 7.9	18	52
^{247}Cm - 0.4	--	
^{248}Cm - 0.1	< 0.5	

Contribution of ^{246}Cm isotope to the neutron field of source results in negligible correction to the average neutron energy in ^{244}Cm spontaneous fission since the parameters of neutron spectra in both ^{246}Cm and ^{244}Cm fission are very close.

2.2. Fission Fragment Detectors

The main problem in design of fission fragment detector involved by extremely high alpha-activity of ^{244}Cm (10^6 alpha-particles per fission event). The desired statistic accuracy of prompt fission neutron spectra measurements can be achieved by the high activity - more than 10^8 Bq - Cm source application. For such counting rates the time interval between alpha-particles will be about 15 ns that is comparable with pulse length. The above circumstance leads to an increase of pile-up effect and, respectively, the separation between alpha-particles and fission fragments becomes worse.

The shortening of pulse length is one of method to reduce the pile-up effect. The rate of pile-ups N(n) can be estimated as follows

$$N(n) = \frac{n_0}{1 - n_0 t} \cdot \frac{(n_0 t)^{n-1}}{(n-1)!} \cdot \exp(-n_0 t)$$

where:
n_0 - number of alpha-decays

n - number of pile-ups

t - pulse length

If the source intensity is about 150 MBq the rate of 15-fold pile-ups will make up to 1000 per second.

Proceeding from conditions of this experiment an ionization current pulse chamber (IC) was chosen as the fission fragment detector. This type of detectors has a good time resolution, small own mass, is very stable in exploitation and can be manufactured easily. In our case the variant of parallel plate IC was not suitable for the work owing to bad separation between alpha-particles and fission fragments even at the anode to cathode distance of 1mm. We designed and made the IC with hemispherical cathode and anode that permits to limit the alpha-particle ranges. The schematic drawing of IC is shown in Fig.1. The distance between electrodes was chosen 2mm due to the optimum "signal to noise" ratio and, respectively, the best own time resolution of IC. The largest range in the IC is determined by the expression

$$(L_{max}/d)^2 = (R+r)/(R-r)$$

where:

R and r are the radii of anode and cathode respectively,

d is the distance between electrodes

In our case the optimum values were found to be R=10 mm and $L_{max}/d=3$.

The body of the chamber and target backing were made of 0.1 stainless steel, the gross weight of chamber was no more than 2 g. Two identical chambers for *Cm* and *Cf* have been made. The characteristics of the chambers are compiled in Table 2.

Table 2

The characteristics of ionization fission chambers used in present work

Rise time, nc	Pulse length, nc	Intrinsic time resolution nc	Gas	Voltage V	Fragment detection efficiency, % *Cf*	*Cm*
2.5	25	0.4	air	1800	99.9	99.3

The fission fragment amplitude distributions are shown in Fig.2. Arrows indicate the working thresholds. A part of undetected fission fragments was defined using extrapolation of left slope of amplitude distributions to zero and the fragment detection efficiency was determined (see Table 2, last column) as the

ratio of the number of the fragment detected above the threshold to the total estimated number of fragments .

2.3. Neutron Detectors

The detectors based on NE213 liquid and stilbene monocrystal scintillators widely used in neutron TOF measurements due to their fast timing properties and high efficiency were applied in the present experiment. The characteristics of detectors are presented in Table 3.

Table 3. Neutron detectors

Detector			Intrinsic time resolution, ns	Energy threshold, MeV
NE213	∅125×50 mm^2	R1250	1.29	0.2
Stilbene crystal	∅50×50 mm^2	FEU-30	1.03	0.1
Stilbene crystal	∅50×20 mm^2	FEU-30	0.81	0.05

In order to achieve the optimum parameters of neutron detectors the deviders were adjusted especially for each photomultiplier (PM). To reduce the background of low energy gammas the neutron detectors were surrounded with lead 2 mm in thick.

2.4. Electronics Block-Scheme

The main feature of the experimental set-up (see Fig.3) is that common Time to Pulse Height (TPHC) and Amplitude to Digital (ADC) Converters were used for all of four timing channels. Thus, time drift and different kinds of nonliaboutities of TPHC and ADC for all channels will be the same and their influence on the measured ratio R(E) will be significantly decreased. Pulse shape analysis using fast and slow components of the anode pulses of PM's has been carried out to separate neutrons and gamma-quanta. The coefficient of γ-suppression was about 10^2 for the neutron registration threshold 100 keV. Instead of the traditionally used constant fraction discriminators we used usual discriminators with fixed thresholds and time-amplitude compensation was carried out during data processing as will be described later. In order to perform the additional sorting of experimental data the so called "event register" module was used.

The logical scheme of spectrometer was the following . The event flag was formed when TPHC is active. Each ADC as well as Event Register was strobed by

"True-Stop" signal from TPHC. Then data digitized are accumulated by IBM PC and recorded on a hard disk. Thus each event is characterized by four parameters: fission fragment amplitude (*Cm* or *Cf*), fast and slow components of scintillation (1-st or 2-nd neutron detector) and neutron time of flight.

3. Measurements

The neutron spectra have been measured at 3 different flight paths and at angles 0° and 90° versus fission chamber axis. The geometry of measurements is shown in Fig. 4. The information about experimental conditions is presented in Table 6.

Table 6. The experimental conditions and characteristics of measurements

Flight path, cm	Neutron detector	Energy range, MeV	Time resolution, ns	n/γ-rejection	Total number of neutrons	
					Cm	*Cf*
35	Stilbene	0.05	0.9	100	$1.6\ 10^5$	$1.27 \cdot 10^6$
76	Stilbene	0.2	1.1	100	$5.0\ 10^4$	$5.80 \cdot 10^5$
150	NE-213	0.4	1.35	100	$1.2\ 10^5$	$1.00 \cdot 10^6$

4. Data Acquisition System and Data Processing

The software served the experiment was written in Turbo Pascal as Windows 3.x application. It contains the CAMAC- libraries adopted to the various CAMAC controller types and has all common features of modern data acquisition systems like real-time data monitoring, one or 2D histogramming and various filter functions. All data accumulated can be visualized at on-line analysis. The general control of the setup in operation is performed by the analysis of mean count rate in each channel. It is also possible to store the experimental data event-by-event.

The data processing was performed at off-line analysis using the specially developed program. In Fig. 5 the data processing is depicted. Fast and slow components of neutron detector were analyzed to separate neutrons and gammas. Fast and slow components as 2D plot are presented in Fig. The dashed line denotes the boundary between neutrons and gammas.

The neutron time pick-off (time to amplitude correction) has been done by use of leading-edge triggering, but the time of the neutrons flight was software corrected on the Start (neutron detector) and Stop(fission chamber) amplitudes to reduce pulse-height dependent walk. Time to amplitude correction function was determined from 2D plot (Amplitude of fast component versus TOF). Result of

this procedure is illustrated by Fig.7b. as a widths of gamma peak before and after the correction.

High precision measurements of the neutron spectrum are sensitive to the background. High and low time variable thresholds were used to reduce the contribution of (n,n'γ) reaction, neutrons and gammas scattered by air, walls and fragment detector vicinity as shown in Fig.7a. Only events being inside the area limited by thresholds were accepted.

Both Cm and Cf time-of-flight neutron spectra corrected to time-amplitude dependencies and accepted by dynamical thresholds were transformed to laboratory neutron energy scale. Thus a ratio R(E) of neutron of spectrum in spontaneous fission of ^{244}Cm to ^{252}Cf one was obtained (see Fig.8). The final ratio R(E) was obtained by integrating of ratios measured at a various experimental conditions with statistic weights and intrinsic reliability of ratios in given energy range. The resulting ratio is shown in Fig. 9. both in liabout (up) and logarithmic (down) scales.

5. Error Estimation

In the time-of-flight measurements there are two groups of uncertainties: errors in determination of the neutron time of flight and value of neutron spectrum for given time of flight. Separate consideration of the above is presented below.

1. Uncertainties of neutron energy

The neutron time of flight is defined as follows

$$t = (N_\gamma - N_n)\cdot\tau + \frac{L}{C}$$

where N_γ - gamma peak position,
N_n - neutron channel number,
τ - time channel width (0.0535 ns),
L - flight path,
then errors of t and E are

$$\delta^2 t = \delta^2(N_\gamma - N_n)\cdot\tau^2 + (N_\gamma - N_n)^2\cdot\delta^2\tau + \delta^2 L / c^2$$
$$(\delta E / E)^2 = 4\cdot((\delta t / t)^2 + (\delta L / L)^2)$$

uncertainty of channel width $\delta\tau = 2.5\cdot10^{-4}$ ns,
uncertainty of the gamma peak position $\delta(N_\gamma - N_n)\cdot\tau = 1.41\cdot\tau = 0.075$ ns,
uncertainty of flight path δL = 5 mm.

δE/E was from 0.5 to 2 % in the energy range of measurement.

2. Systematic and statistic uncertainties of spectrum

$$(\delta N_{tot})^2 = (\delta N_{st})^2 + (\delta N_{Man})^2 + (\delta N_{diff})^2 + (\delta N_{res})^2$$

δNst - statistic error (change from 0.8 to 18 %)

δN_{man} - error Mannhart evaluation (1.2 - 9.2 %)
δN_{diff} - differential nonliaboutity (0.05 %)
δN_{res} - error of time resolution correction (< 1 %)
$\delta N_{tot}/N$ was from 2.4 to 20 % in the energy range of measurement.

3. The average neutron energy error

$$(\delta\bar{E}/\bar{E})^2 = \sum(E^2 \cdot \delta N_{tot}^2(E) + N^2(E) \cdot 2 \cdot \delta E^2) = 1.3\ \%$$

6. Conclusion

In Fig.10. the results of measurements of prompt neutron spectrum in ^{244}Cm spontaneous fission is presented as the ratio of PNS to appropriate Maxwell distribution with parameter of temperature of 1.373 MeV. Solid line denotes the Mannhart evaluation of PNS in ^{252}Cf SF divided by Maxwellian with temperature of 1.42 MeV.
The average energy of neutron spectrum in the ^{244}Cm spontaneous fission was found to be

$$\bar{E} = 2.055 \pm 0.027\ \text{MeV}$$

where the uncertainty includes both statistic and systematic uncertainties (one standard deviation).

The result obtained well agrees with previous measurements [2-4].

References

1.W. Mannhart, Proc. IAEA Group Meeting on Neutron Sources, (1986, Leningrad, USSR), Vienna, IAEA, p.158, 1986
2. Z. A. Alexandrova et al., Atomnaya Energia, 36, 1974, p. 282 (in Russian)
3. Yu. S. Zamyatnin et al., Nuclear Data dor Reactors, Proc. on 2-nd Int. Conf. on Nucl. data for Reactors, Helsinki, 1970, IAEA, Vienna, vol.2, p.183
4. L.M. Belov et al., Yadernaya Fizika, 9, 1969, p.727 (in Russian)

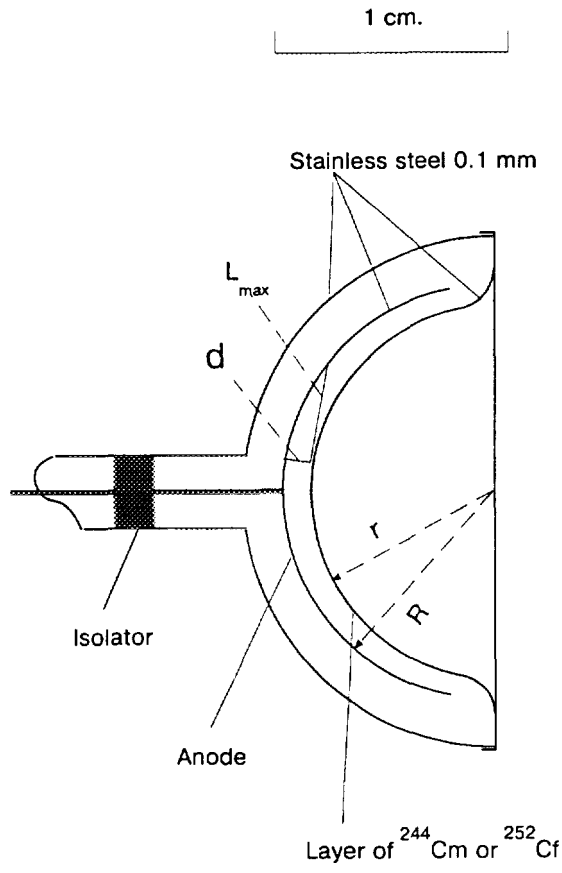

Rise time		2.5 ns
Signal time width		25 ns
Intrinsic time resolution		0.4 ns
Work gas		air
High voltage		1800 V
Weight		2 gr
Fragment detection efficiency	^{252}Cf	99.9%
	^{244}Cm	99.3%

Fig.1 Fission chamber

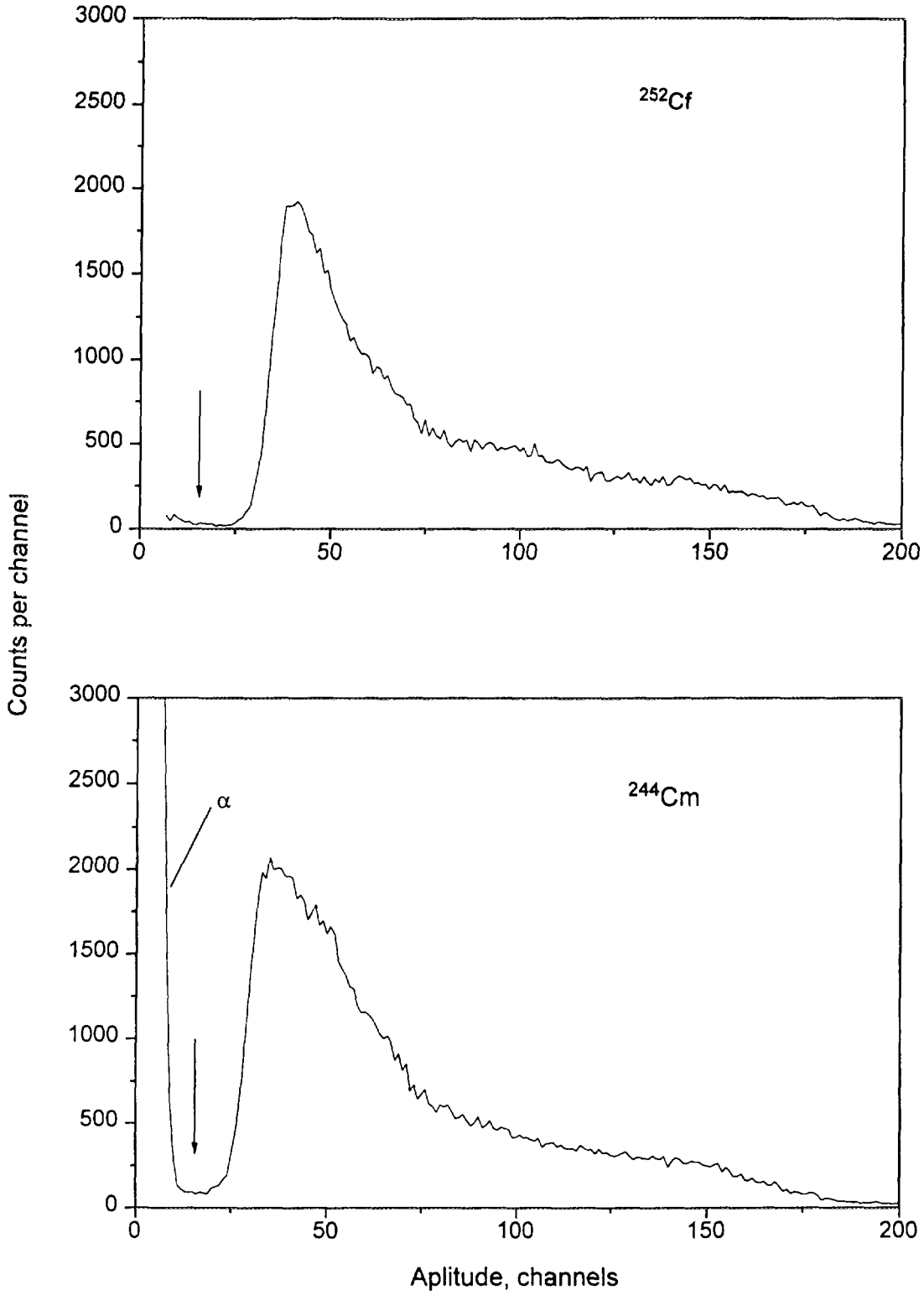

Fig. 2 Apparatus amplitude distributions from Cf and Cm ionization chambers. Arrows show the thresholds used in the measurements.

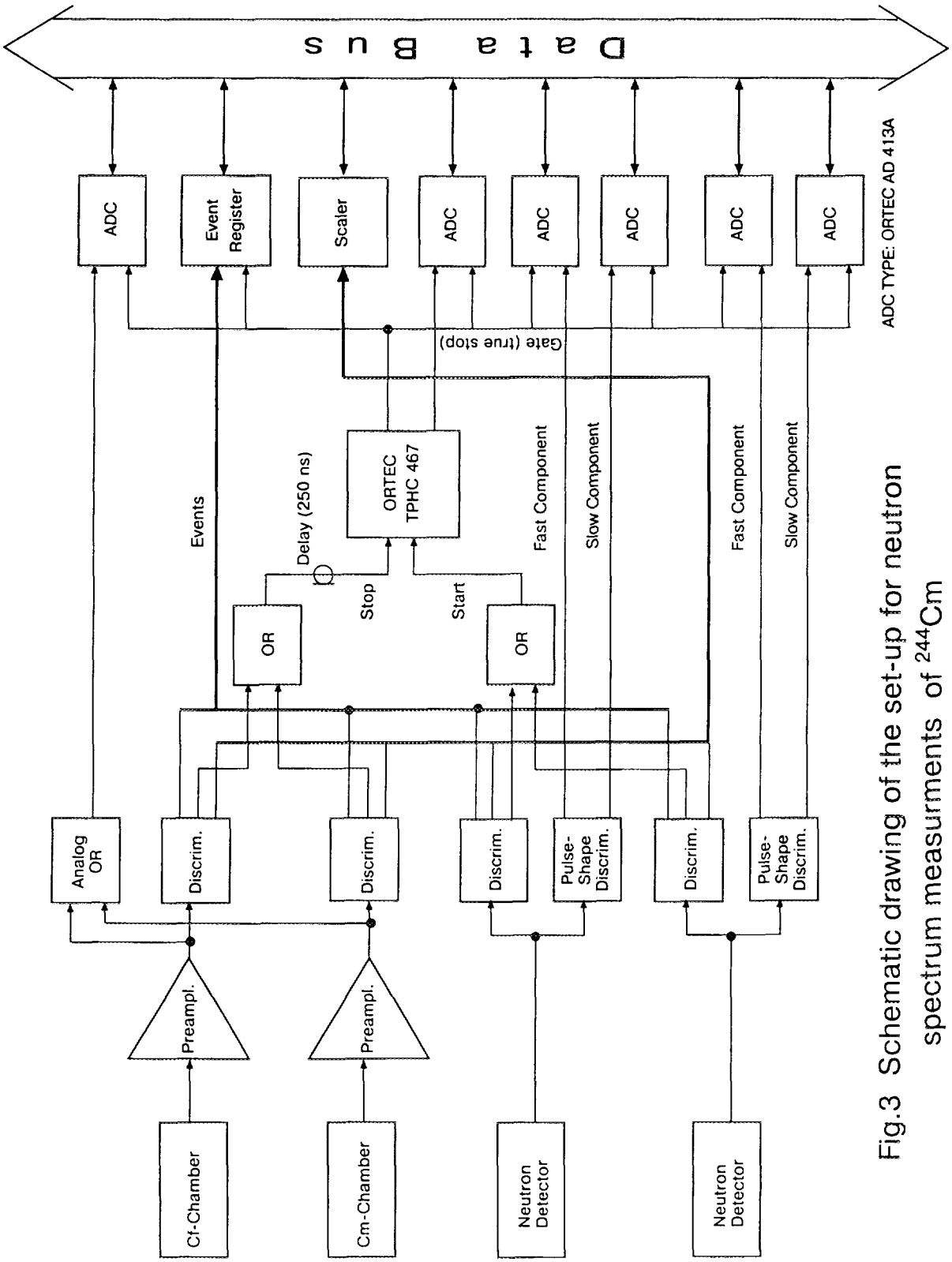

Fig.3 Schematic drawing of the set-up for neutron spectrum measurments of ^{244}Cm

Experimental Geometry

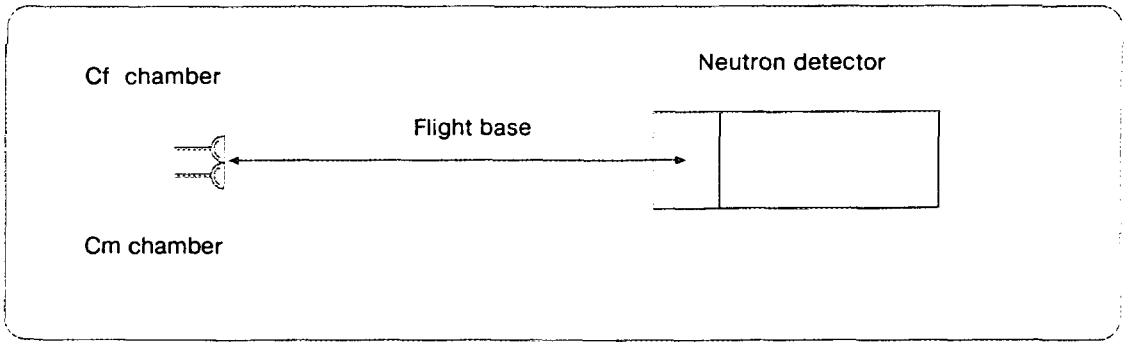

- The wall nearest to neutron detector is 2.7 m. distant
- The volume of experimental room - 112 m^3

Experimental Conditions

Flight base, cm	Neutron detector	Energy range, MeV	Time resolution, ns	N-Y Discrimination	Total number of neutrons detected ^{244}Cm	^{252}Cf
35	Stilbene	0.1-3	0.9	100	$1.6\ 10^5$	$1.27\ 10^6$
76	Stilbene	0.3-7	0.9	100	$5.0\ 10^4$	$5.80\ 10^5$
150	NE-213	0.5-15	1.35	100	$1.2\ 10^5$	$1.00\ 10^6$

- The measurements were carried out by runs.
- The Cm and Cf chambers were changed with each other after each run.
- The time of each run was about 5 hours.
- The total number of runs were 617.
- The instability of gamma-peak positon was not more than 3 channels per 24 hours.

Fig.4 Experimental Conditions and Geometry

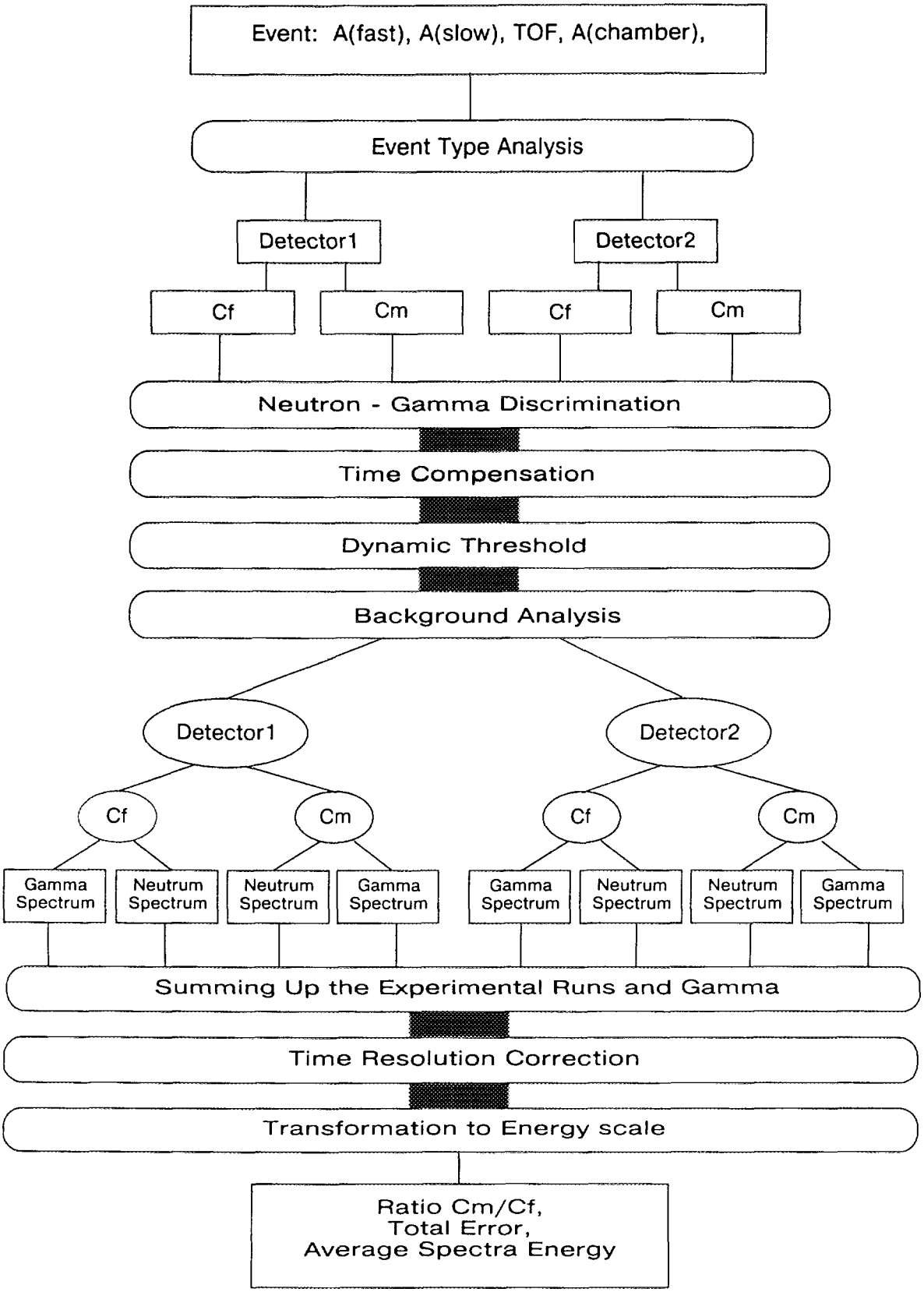

Fig.5 Data Processing

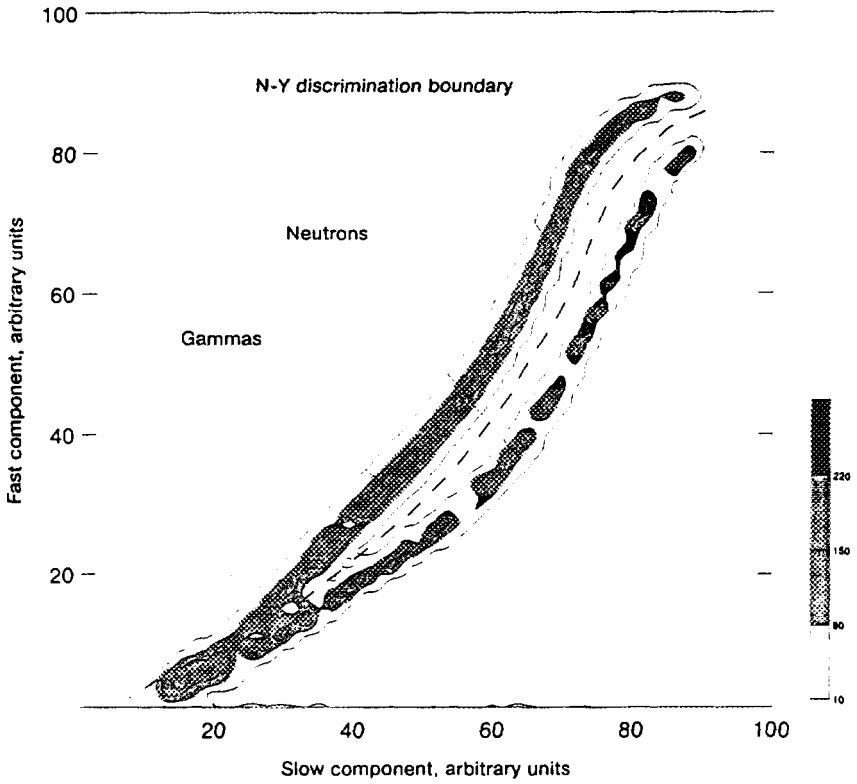

2D distribution of pulse-heights of fast and slow component
of light flash in neutron scintillation detector

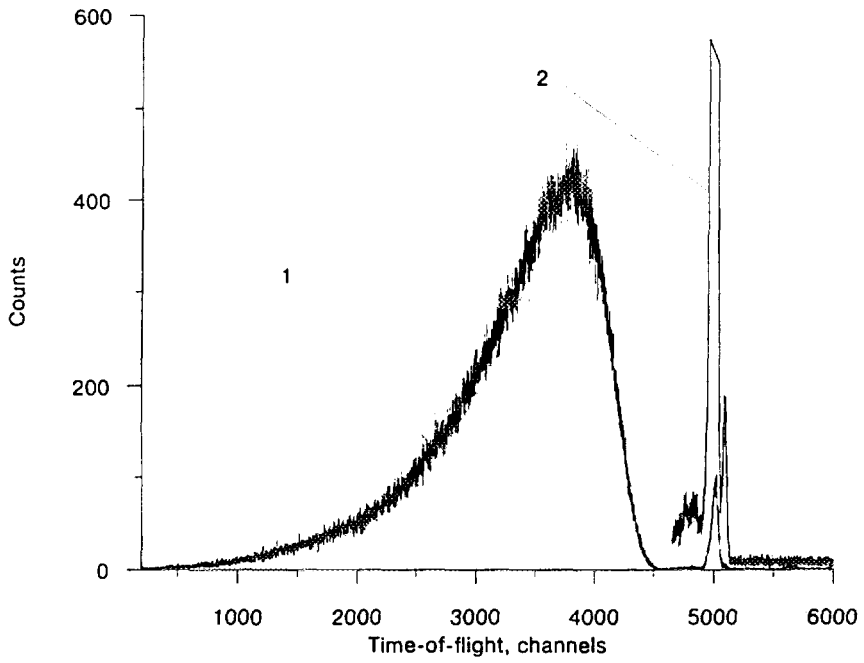

Time-of-flight neutron(1) and gamma(2) spectra after n-y discrimination

Fig. 6

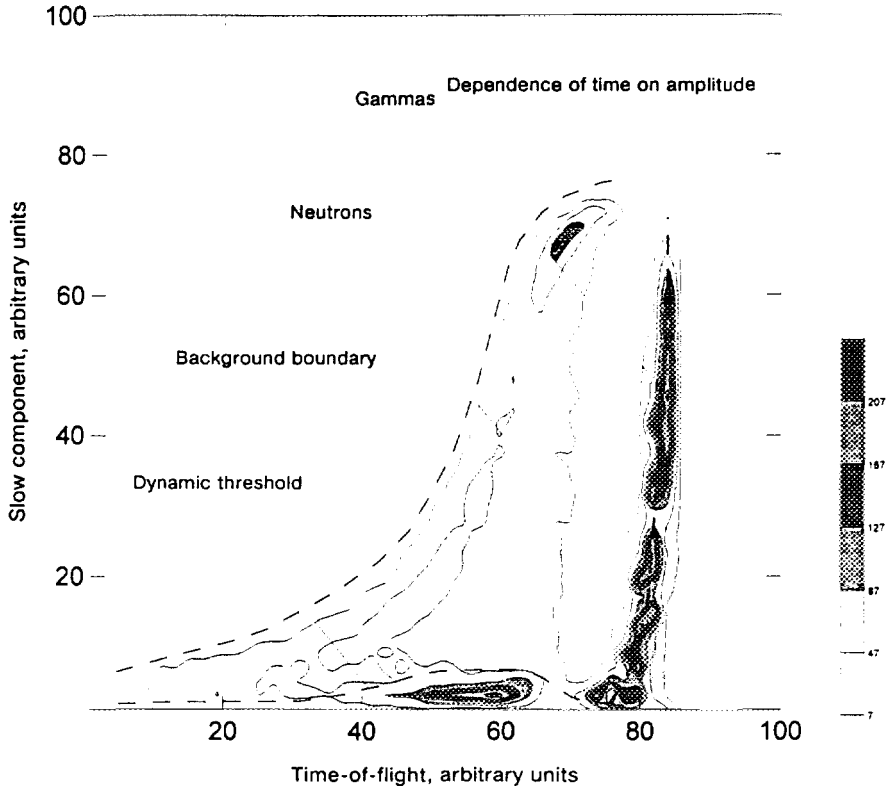

Fig. 7a 2D time-of-flight VS pulse-height distribution of light flash

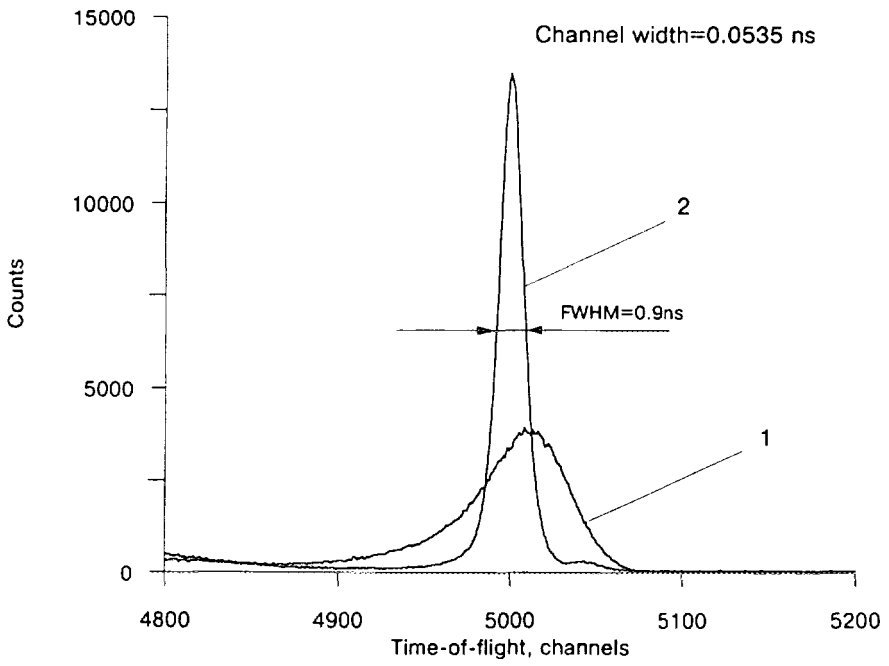

Fig. 7b Gamma peak before (1) and after (2) time compensation

Fig. 7

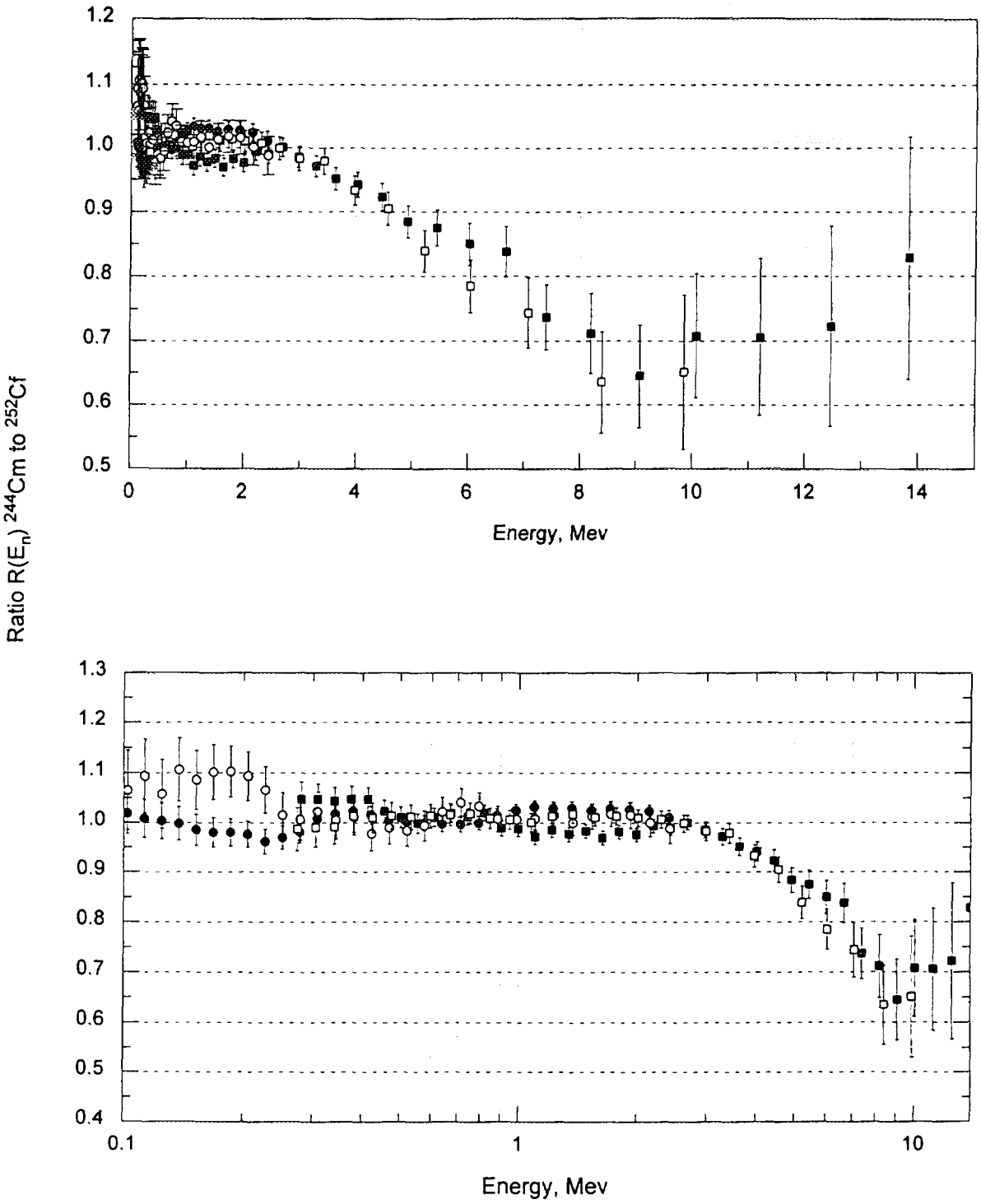

Fig.8 Experimental points obtained at the varios experimental conditions

- ■ Flight base of 150 cm, placed at 0^0
- ● ---------- 35 cm, -------- 0^0
- ○ ---------- 35 cm, -------- 90^0
- □ ---------- 76 cm, -------- 0^0

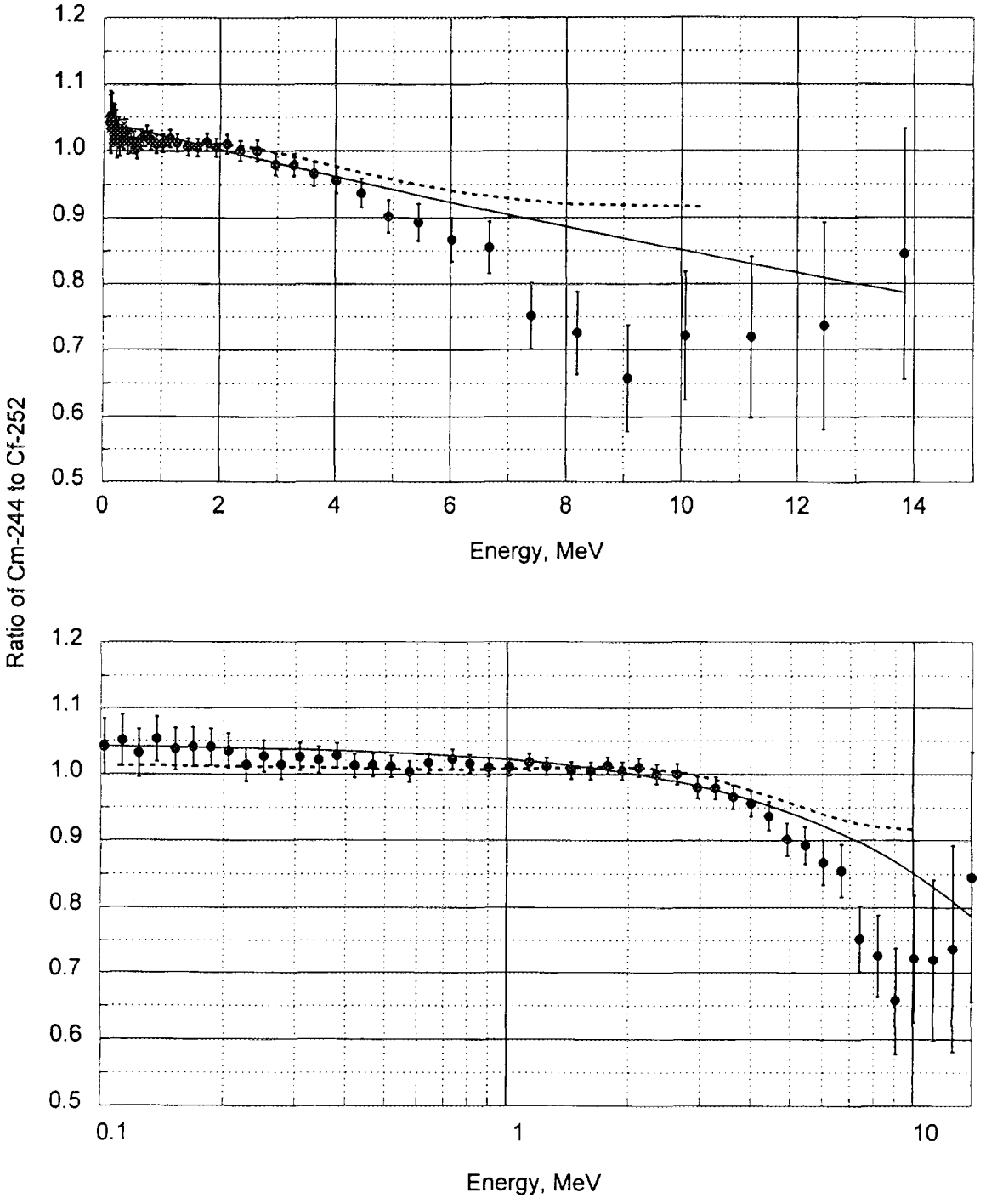

Fig.9 Resulting ratio of ^{244}Cm to^{252}Cf neutron spectra. The solid line indicates the results of experimental points fitting to the function $R(E,T_{Cm})=(T_{Cm}/T_{Cf})^{-3/2}\exp(-E(1/T_{Cm}-1/T_{Cf}))$, T_{Cf}=1.42 MeV. he value of the parameter T_{Cm} obtainned by least-squares method was equal to 1.373 MeV (0.005) with Chi^2=0.93 per degree of freedom.
he dashed line - the statistical model caculation (initial fragment spin J=0).

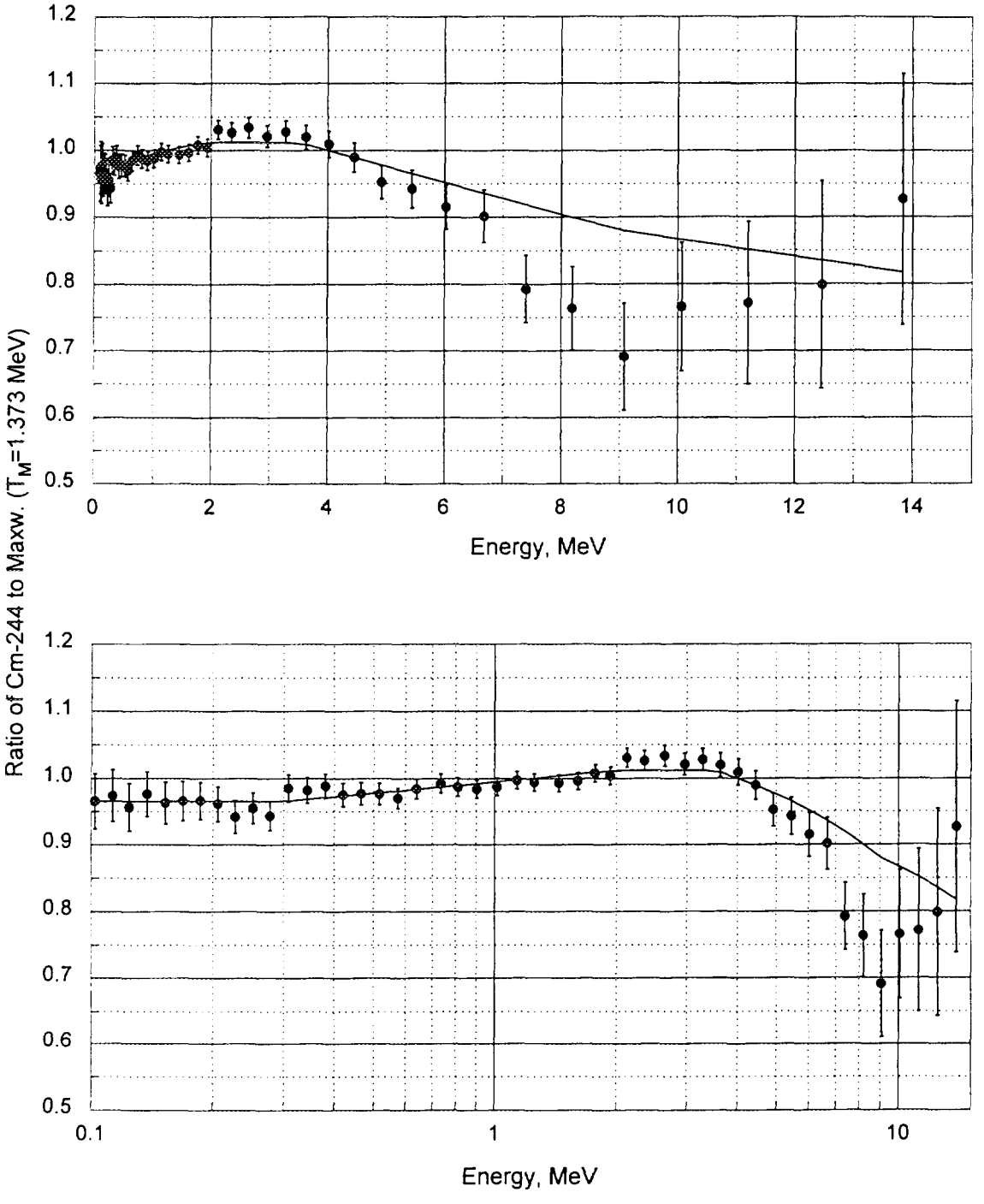

Fig.10 Ratio of integral prompt neutron spectrum of ^{244}Cm spontanneous fission to the Maxwell with temperature of 1.373 MeV.
The line present the ratio of Mannhart evaluation of ^{252}Cf neutron spectrum.

3. Measurements and Analysis of the Basic Nuclear Data for Minor Actinides

(Institute of Physics and Power Engineering)

3. 1 Fission Cross Section Measurements for Minor Actinides

B. Fursov
Institute of Physics and Power Engineering,
Obninsk, Russia

Abstract

The main task of this work is the measurement of fast neutron induced fission cross section for minor actinides of ^{238}Pu, ^{242m}Am, $^{243,244,245,246,247,248}Cm$. The task of the work is to increase the accuracy of data in MeV energy region. Basic experimental method, fissile samples, fission detectors and electronics, track detectors, alpha counting, neutron generation, fission rate measurement, corrections to the data and error analysis are presented in this paper. (Editor)

'FISSION CROSS SECTION MEASUREMENTS FOR MINOR ACTINIDES

Direction-1 (group leader B.Fursov)

I. INTRODUCTION

The main task of the ISTC Project # 304 for D-1 group is the measurement of fast neutron induced fission cross sections for the following set of minor actinides: ^{238}Pu, ^{242m}Am, ^{243,244,245,246,247,248}Cm. The problem of minor actinides transmutation requires data of higher accuracy. Though high accuracy data for ^{242m}Am and ^{245}Cm are available , the disagreements between different experimental data sets still exist. The situation is more difficult for other isotopes. Most of Cm isotopes have short half-lives of alpha-decay or (and) spontaneous fission and therefore the task to measure fission cross sections with good accuracy is very difficult. More detailed data were obtained in USA and USSR using nuclear explosions as the neutron sources, but the accuracy of this data is relatively low. The task of present work is to increase the accuracy of data in MeV-energy region.

II. THE BASIC EXPERIMENTAL METHOD

The idealised form of present experimental method involves placing two monoisotopic samples with accurately known masses in the same monoenergetic neutron flux and measuring their relative fission rates with perfect detectors. Then

$$\frac{F_2(E)}{F_1(E)} = \frac{N_2}{N_1} \cdot \frac{\sigma_2(E)}{\sigma_1(E)}$$

where subscript 1 refers to the reference isotope, 2 to the unknown isotope, F is the fission rate, N is the number of sample atoms, and σ is the fission cross section at neutron energy E.

In practical measurements the samples are not isotopically pure and their composition and the ratio of their masses need to be accurately known. They are placed back-to-back near a localised neutron source and perpendicular to the direction of most of the neutrons. The neutron flux coming primarily from the source is not monoenergetic, although its principal component does have a narrow energy spread. The flux through the two samples is not quite the same due to geometry and transmission effects, and fission rate depends on the order of the sample placement. The observed fission rate ratio due to neutron impinging directly to the sample is

$$\frac{F_{xf}(E) - B_x(E) + \beta_x}{F_{rb}(E) - B_r(E) + \beta_r} = \frac{N_x}{N_r} \cdot \frac{\sigma_x(E)}{\sigma_r(E)} \cdot \frac{G_f \cdot T_f}{G_b} \cdot \frac{L_{xf}(E)}{L_{rb}(E)} \cdot \frac{S_{sf}(E)}{S_{rb}(E)} \cdot \frac{C_x(E)}{C_r(E)}$$

where x - Refers to the unknown sample (Cm)
r - Refers to the reference sample (^{239}Pu)
B_x, B_r - The background corrections
β_x, β_r - Corrections for fissions lying below discriminator level
f - Refers to the sample in the forward position
b - Refers to the sample in the backward position
G_f, G_b - Geometry factors. In the measurements where sample diameters are equal, they are associated with their position only.

T_f - Neutron transmission coefficient for the sample support plates. T_b is always 1.0

L_{xf},L_{rb} - Correction factors for sample thickness, momentum transfer and fission fragment angular distributions.

S_{xf},S_{rb} - Correction factors for neutrons scattered by the fission detector and the neutron source structure

C_x,C_r - Correction factor for the minor isotopes.

III. THE FISSILE SAMPLES

^{235}U is ordinary used as a reference sample, because fission cross section of ^{235}U is standard in the energy range higher than 100 keV. But we used ^{239}Pu as a reference sample. The reasons were as follows. The more accurate method for measurement of the sample masses ratio is α-particle counting, because half-lives and spectra of α-particles for most minor actinides are well known. The half-life and spectrum of α-particles for ^{239}Pu are more suitable in comparison with ^{235}U). The fission cross section of ^{239}Pu in the wide energy range is known with accuracy ~ 2%.

Sample preparation and assay is a crucial part of the experiment. The fissile sample material was twice electromagnetically separated at Arzamas. The samples used in the measurement, their isotopic analyses and their weights are listed in Tables 1,2,3. The fissile layers were prepared by multiple "painting" of organic solvent on the surface of thin (0.1 mm) Al backing and heating during 30 minutes to the temperature 570°C. After polishing the cycle was repeated 30-50 times. Through step by step heating the samples were converted into dioxides. All fissile samples have a diameter 6 mm, the backings diameter is 20 mm.

Table 1. Isotopic analysis of ^{239}Pu samples (atomic percent)

	Mass	^{239}Pu	^{240}Pu	^{241}Pu	^{242}Pu	^{244}Pu
^{239}Pu	55-150 μg	**99.9966**	(2.41±0.04)*10^{-3}	(1.35±0.04)*10^{-3}	1.2*10^{-5}	4.9*10^{-6}

Table 2. Isotopic analysis of ^{242m}Am sample (atomic percent)

	Mass	^{241}Am	^{242m}Am	^{243}Am
^{242m}Am	38 μg	13.870±0.086	**85.616**	0.514±0.04

Table 3. Isotopic analysis of Cm samples (atomic percent)

	Mass	^{242}Cm	^{243}Cm	^{244}Cm	^{245}Cm	^{246}Cm	^{247}Cm	^{248}Cm
^{244}Cm	18μg	-	-	**99.82**	0.15 ± 0.05	0.02 ± 0.01	<2*10^{-3}	<1*10^{-3}
^{245}Cm	84,4μg	-	1.7*10^{-3}	(4.51 ± 0.04)*10^{-3}	**99.9925**	(2.93 ± 0.02)*10^{-3}	1*10^{-5}	5*10^{-7}
^{246}Cm	27μg	1.46*10^{-7}	(3.18±0.6)* 10^{-5}	(1.17 ± 0.40)*10^{-3}	(8.33±0.68) *10^{-5}	**99.8326**	(2.50±0.15) *10^{-4}	-
^{247}Cm	1,65μg	6,66*10^{-4}	0.486 ± 0.005	2.619 ± 0.361	0.084 ± 0.003	5.139± 0.045	**90.316**	1.355 ± 0.009

V. THE FISSION DETECTOR AND ELECTRONICS

The fission detector, shown schematically in Fig.1, is a low-mass double-ionisation chamber with the fissile layers (samples) mounted on both sides of the common cathode. The chamber walls were 0.4 mm thick, the container diameter is 80 mm, length 120 mm. The ionisation chamber was covered by cadmium 0,5 mm thick. Two pairs of fissile samples can be inserted inside the container and two fission cross section ratios can be measured in one experiment (for example $^{242}Am/^{239}Pu$ + $^{247}Cm/^{239}Pu$, $^{244}Cm/^{239}Pu$ + $^{246}Cm/^{239}Pu$). The distance between the neutron target and central electrode for the first pair of samples was 9 mm, for the second pair the distance was 13 mm. The ionisation chamber was filled by gas mixture Ar + 10% CO_2 under pressure 1.8 atm. Most measurements were made with cathode-anode separation 1.5 mm. Voltage gradients were maintained at 1500 volts/cm*atm. The fast rise of the ion chamber current pulse was used to provide good timing characteristics (time resolution was about 3 nsec) and the height of the current pulse was a measure of the electron charge produced in the active volume. Good separation between the alphas and fissions was obtained by keeping the pulse widths small until the pileup alphas were removed by bias levels (Fig.2).

The electronic systems were the same for four channels of ionisation chamber (Fig.3). Signals from anodes went to charge sensitive preamplifiers, which were capable of fast rise-time, then to fast amplifiers. The amplifier outputs were divided and one part triggered fast leading-edge discriminators which provided the start signals for the time-to-pulse-height converters. The stop signal came from a beam-pulse sensor (pick-up electrode) located near the accelerator target. The other part of the clipping amplifier output went to a biased amplifier where the bias levels could be set to reject a large fraction of the alphas and then to a stretcher. The four time signals and the four pulse height signals were routed into separate mixers and sent to the data storage computer along with tags identifying the detector.

V. THE TRACK DETECTORS

The fission fragment registration efficiency of fast ionisation chamber was 92-97% for ^{239}Pu and Cm isotopes, but for ^{242m}Am the efficiency was only 85%. To check the correctness of this value we provide additional fission cross section radio measurement for ^{242m}Am, ^{245}Cm, ^{247}Cm by solid track detectors. The track detectors (mica for ^{247}Cm, cylindrical silicon glass for ^{242m}Am and ^{245}Cm) have well-known fission fragment registration efficiency (it depends on geometry factors only). The pairs of fissile samples and track detectors were irradiated by fast neutrons with energies 0.13, 0.5, 1.0, 4.0, 5.0 MeV as shown in Fig.4. The track numbers were counted under microscope. The results of ionisation chamber and track detectors are in agreement in a limit of statistical errors.

VI. ALPHA COUNTING.

The alpha counting for mass determination was done in "high" geometry alpha counter that was constructed to provide well determined geometry factors (Fig.5). The alphas were detected by silicon detector with a resolution of ~20 keV. The alpha counting ratios for unknown and standard (Pu) samples were constant for different distance between sample and detector and for different azimuthal orientation of samples. The specific activity of the sample was calculated from the isotopic analyses and the half-lives. The mass ratio of samples was then determined by alpha counting.

VII. NEUTRON GENERATION

The measurements were conducted at КГ-2,5 and EG-1 accelerators (IPPE). Direct current was used for ^{242m}Am, ^{245,247}Cm, and pulsed (2 MHz) current (EG-1) was used for ^{244,246}Cm. The monoenergetic neutron sources were Li(p,n), T(p,n), D(d,n) and T(d,n) - reactions on solid targets. The energy is controlled by 90-deg. analysing magnet and slit feedback that was calibrated by observing the threshold of the ^{7}Li(p,n)^{7}Be reaction. The energy distributions of neutrons from the primary source reaction that were incident on the samples were calculated from the incident particle energy, the angular distribution of the source reaction, the target thickness and the source-sample geometry. The dispersion of neutron energy was: ± (20-30) keV for E_n<3 MeV and ± (40-80) keV for E_n>3 MeV.

VIII. FISSION RATE MEASUREMENT

As mentioned above we employed two modes of the fission rate measurement: direct current for samples of low spontaneous fission (^{245}Cm, ^{247}Cm, ^{242m}Am) and pulsed current for ^{244}Cm, ^{246}Cm.

In the first case we provided fission rates measurements "point-by-point" using different reactions for neutron production. Every part of energy range was composed of 6-12 runs for each energy point. The spontaneous fission rates were measured in pauses (the integral time of measurement was about 500 hours). The shares of spontaneous fission were 5-10% for ^{242m}Am and 15-40% for ^{247}Cm. The rate of spontaneous fission of ^{245}Cm was negligible due to the high enrichment of the sample (Tabl.3).

The parasitic neutrons generated in neutron target assembly (Mo + Ti) via (p,n)- and (d,n)- reaction were measured by replacing the real targets with adequate deuterium- and tritium-free templates. These measurements were performed 5-6 times for every energy in the same manner as basic measurement with real neutron target (the same integral charge of accelerated particles at every energy point, the same "history" of irradiating). The results of all runs were averaged. For the (p,n)-reaction the fission cross section ratios were corrected less 1%, for (d,n)-reaction correction was from ~1% (E_n=5 MeV) up to 3,8% (E_n=7,2 MeV).

Correction for fissions due to room returned neutrons was estimated as close to zero (<0.1%) because the distance between sample and neutron target was very small.

The time of flight method (pulse synchronisation method) was used in the fission rate measurement of ^{244}Cm and ^{246}Cm. The experiment was performed using pulsed neutron beam 2 MHz (4 MeV Van-der-Graaf EG 1). The neutron pulse width was about 2 nsec, the averaged current value ~ 8μA. The pulsed neutron beam was controlled with TOF method using stilben scintillation detector, or lithium glass scintillation detector placed on the axis of incident beam line about 3 m from the target. A BF_3 monitor was used to check the stability of neutron generation.

The TOF technique using the fast timing fission chamber(3 nsec) provided a good signal to background ratio. Fig.6 shows typical time spectrum for ^{246}Cm (left) and ^{244}Cm (right) at the E_n=1,26 MeV (top) and E_n=0,65 MeV (bottom). The second peaks in every part of Fig.6 correspond to ^{239}Pu fission events (the backgrounds are close to X--axis). As it is found from Fig.6 a peaks due to the fissions correlated with the pulse beam is clearly separated from the time independent regions which consist of background due to spontaneous fissions, pileup alpha particles and the fissions by room-returned neutrons. The fissions induced by the parasitic neutrons were included in the time depended region and were subtracted after providing a special experiment mentioned above.

The pulse height spectra were obtained simultaneously. In Fig.7, two pulse height spectra for ^{244}Cm are shown; one include alpha-particles (left), the other one is fission fragment signals only.

IV. CORRECTIONS TO THE DATA.

a). Extrapolation to zero bias.
The pulse height spectrum was inspected and cut-off point was selected in the flat region between the alphas and the fission's as illustrated in Fig. The spectrum was extended horizontally to the zero channel. This correction depended on the thickness and uniformity of the deposit. For most of the samples this correction was within the 3-5%, but it increased up to 15% for a sample of ^{242m}Am.

b). Deposit Thickness, Momentum Transfer and Fission Fragment Distribution.
Self-absorption of fission fragment in the sample foil was estimated. The angular distribution of fission fragment was assumed to be isotropic since the data were not available. The thickness of the sample foil was obtained on the assumption the sample was dioxide. The ranges used in the present measurement are: 6,5 mg/cm^2 for Pu, 7,0 mg/cm^2 for Am and 7,5 mg/cm^2 for Cm. The maximum correction was for E_n=20 MeV: ^{244}Cm/^{239}Pu - 3,5%, ^{246}Cm/^{239}Pu -4,5%.

c). Isotopic Impurities.
This correction requires some knowledge of the energy dependent fission cross-section for minor isotopes. The fission cross sections used were those in JENDL-3. For fairly pure samples the minor isotopes are present in such small amounts that there is no need to know cross sections very accurately. For the major isotopes an iterative procedure was used where the fission cross section ratios obtained from one pass through the data were used as input for another pass. This correction was significant for ^{242m}Am sample and ^{244}Cm (impurities of the daughter ^{240}Pu) in the region under threshold.

d). Scattered Neutrons.
Some rough estimation was made of fissions produced by neutrons scattered by target assembly and the fission chamber. The principle (E_n=1 MeV) and multiple scattered neutron energy spectrum are shown on Fig.8. This effect will be corrected by using the Monte-Carlo MCNP code in the nearest future. The cross sections to be used will be the ones FENDL. The typical correction can be expected about 1-2%, the maximum value in subthreshold energy region of ^{244}Cm, ^{246}Cm can reach 10%.

e). Attenuation of Incident Neutron Flux.
The unknown and standard samples are separated by two Al backing (0.1 mm) and stainless steel electrode (0,1 mm). The attenuation of incident neutron flux due to this material will be calculated later. The typical correction is expected to be less 1%.

X. ERRORS

The detail analysis of the errors will be provided after finishing an additional measurements and consistent analysis of total set of experimental results for all Cm isotopes. The systematic error sources are as follows.
- Sample mass ratios:
a). Half lives of alpha decay,
b). Alpha decay rate,
c). Detection efficiency of the alpha counter,
d). Isotopic analysis.
Most of the alpha counting measurements used the same geometry counter so the same sources of error were eliminated. The statistical error was determined as the scatter of

repeated measurements with different geometry factors. The typical statistical error was less than 1% (0,4% for $^{244}Cm/^{239}Pu$, 0,3% for $^{246}Cm/^{239}Pu$).
- Extrapolation to zero pulse height (<1%).
- Thickness corrections (~0,5%0.
- Track detector counting statistics (0,5-1,5%).
- The attenuation of incident neutron flux due to electrode and backing material.
- The difference in solid angle between the forward and backward sample from the neutron target.

All these errors must be included in the normalisation error.
The shape measurement errors are as follows:
- statistical error of fission counts by principle source neutrons,
- statistical errors of spontaneous fissions,
- statistical errors fissions by parasitic neutrons,
- scattered neutron flux by the construction material of the target assembly and the fission chamber,
- error in the corrections associated with angular dependence of source neutrons,
- error in the energy dependent correction associated with self-absorption fission fragment.

The statistical error for $^{245,247}Cm$ and ^{242m}Am was about 1-1,5%. This value for ^{246}Cm was 1-2% in the plateau region and 15-30% under threshold. $^{244}Cm/^{239}Pu$ samples were loaded in ionisation chamber on the second place (distance 13 mm from target). As a result the statistical error was 2,5-4% in plateau region and 20-32% under threshold.

XI. RESULTS

All presented results are preliminary ones. Some additional measurements and calculations are in progress now and we hope the data accuracy will be improved. Data for ^{245}Cm, ^{247}Cm and ^{242m}Am are being reprocessed, beginning with original fission rate measurement, some additional measurements by track detectors are performed.

The results are shown in Fig.9-13. The ENDF/B-6 evaluation for ^{239}Pu fission cross section was used as a standard. The present results show, that JENDL-3 evaluation may be updated and the data accuracy will be improved.

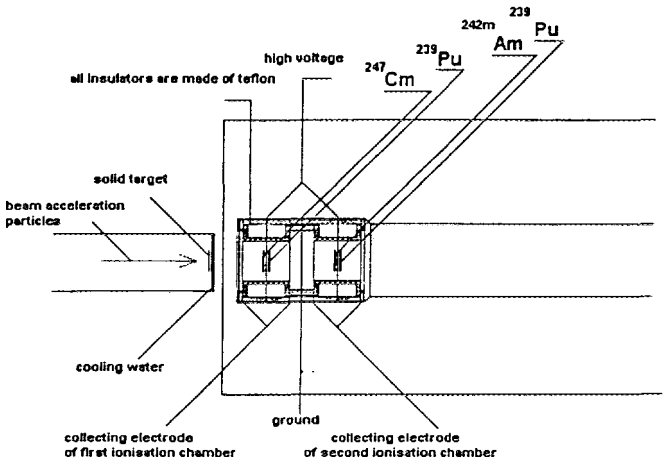

Fig.1 Schematic view of fission chamber.

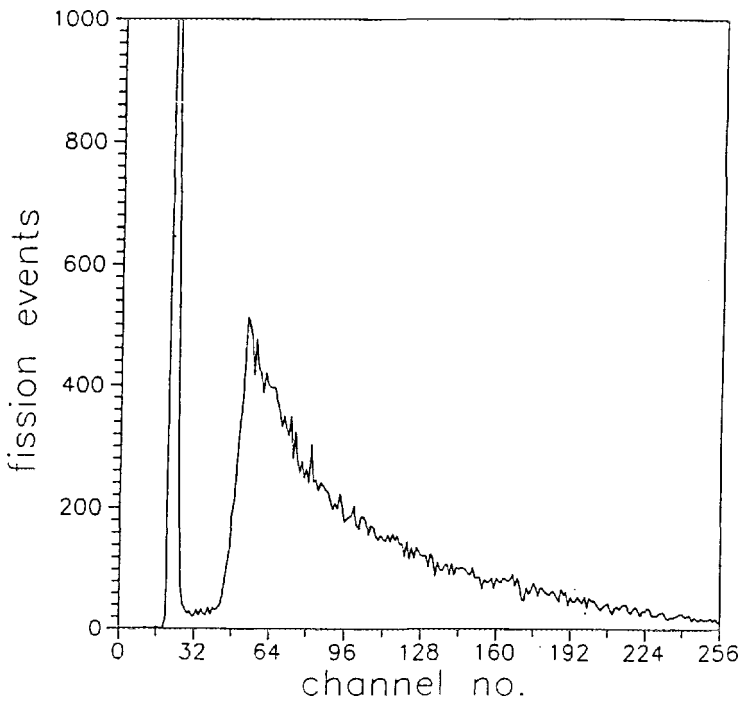

Fig. 2 Pulse height spectrum for ^{247}Cm.

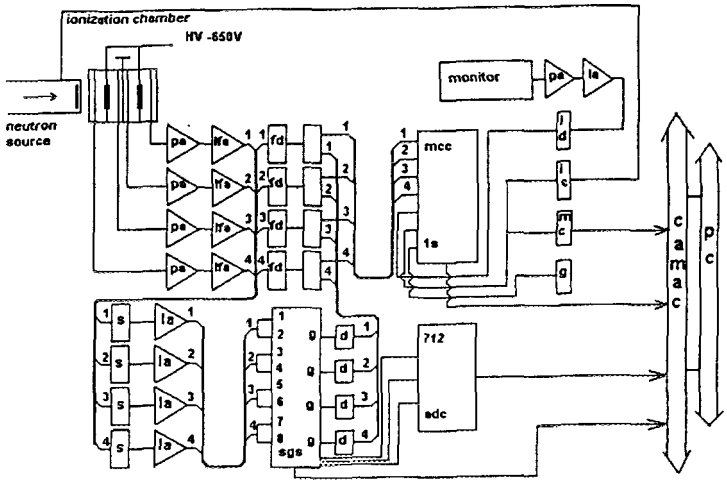

Fig. 3 Electronic set up of fission detector.

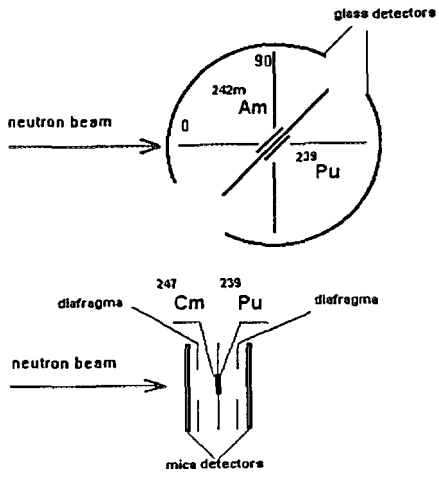

Fig. 4 Track detectors for control measurements of fission cross section ratios.
Top - the silicon glass detectors, bottom - the mica detectors.

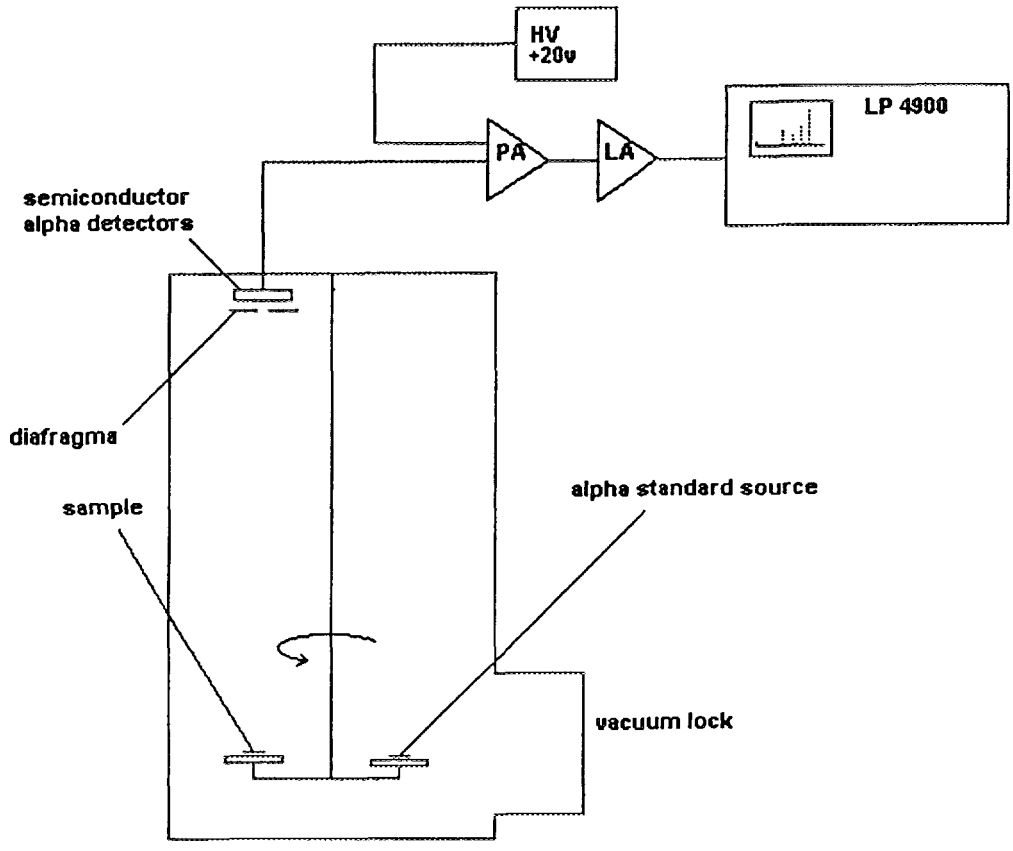

Fig. 5 Schematic arrangement of alpha counter.

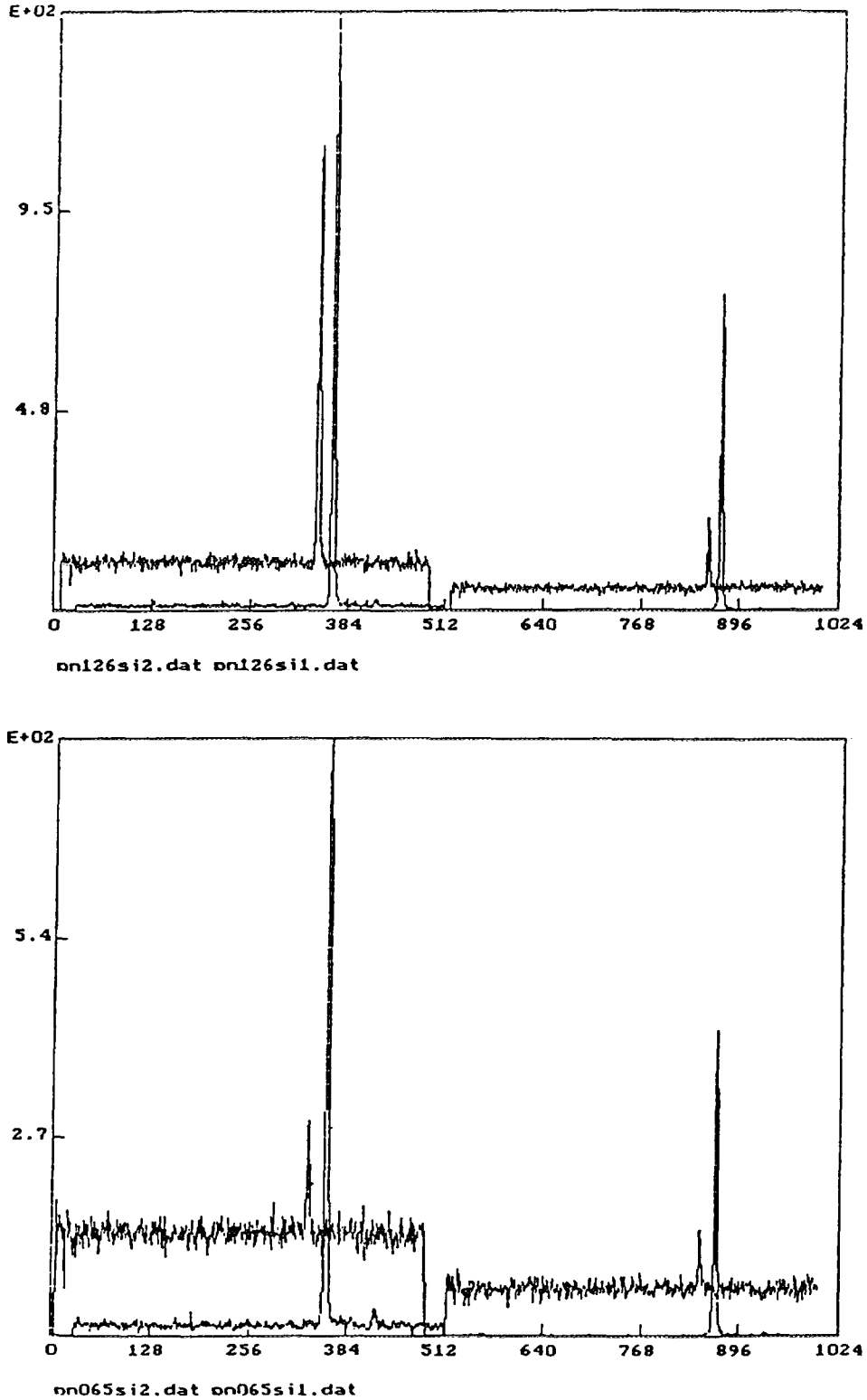

Fig. 6 Typical time spectrum of fission chamber.
X - axis is the channel number (the channel width is about 0.9 ns/channel).
Y - axis is the count/channel.
Left spectrum - $^{246}Cm/^{239}Pu$, right spectrum - $^{244}Cm/^{239}Pu$.
Top - E_n = 1.26 MeV , bottom - E_n =0.65 MeV (subthreshold region).

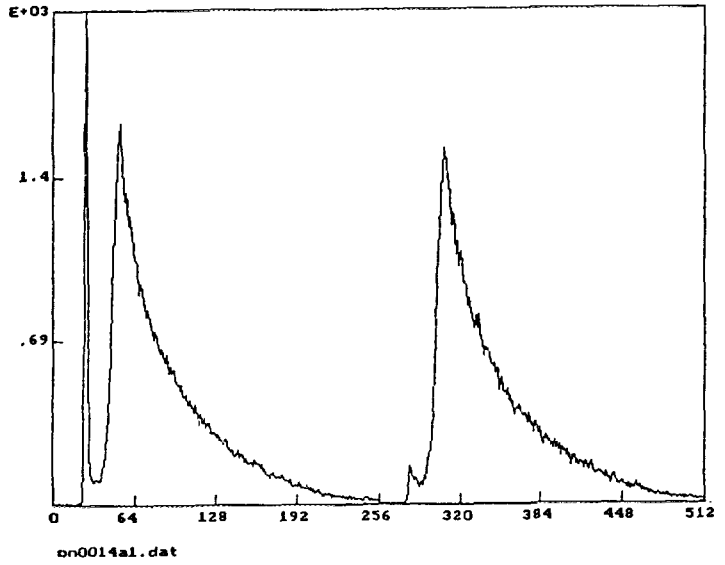

Fig. 7 Pulse height spectra for ^{244}Cm.
Left - total signals, right - fission fragment signals only.

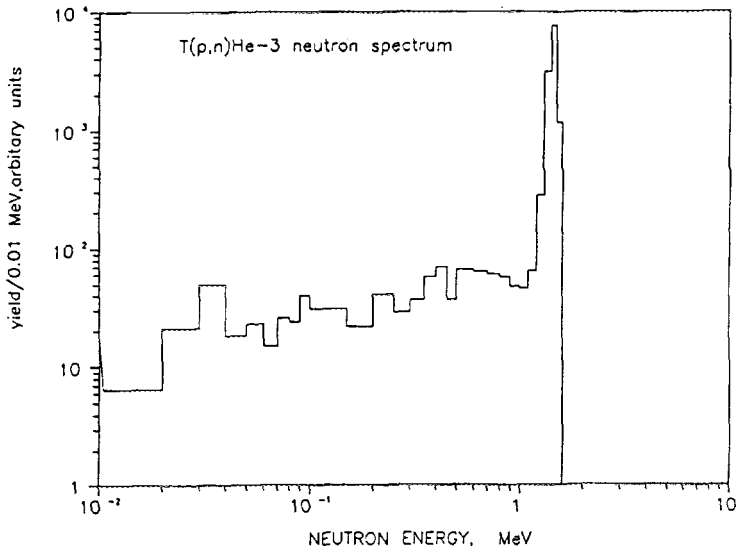

Fig. 8 Monte - Carlo calculation of neutrons scattered by target assembly and fission chamber.
T(p,n) - reaction, E_p = 2.3 MeV, (Mo + Ti) target thickness is 0.6 mg/cm^2.

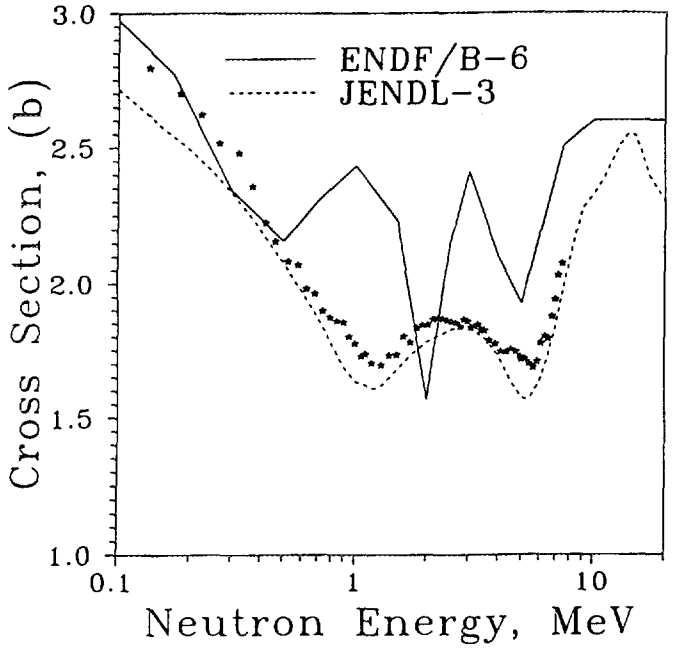

Fig. 9 ^{242m}Am fission cross section.

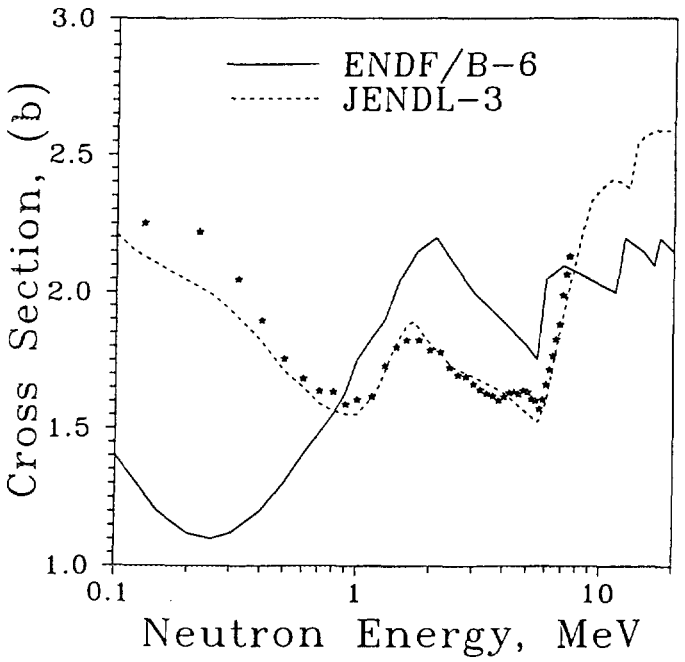

Fig. 10 ^{245}Cm fission cross section.

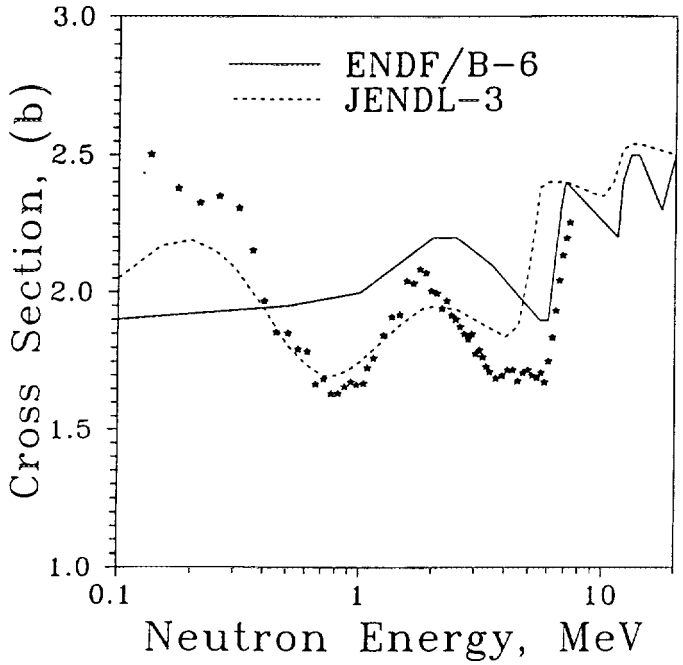

Fig. 11 ^{247}Cm fission cross section.

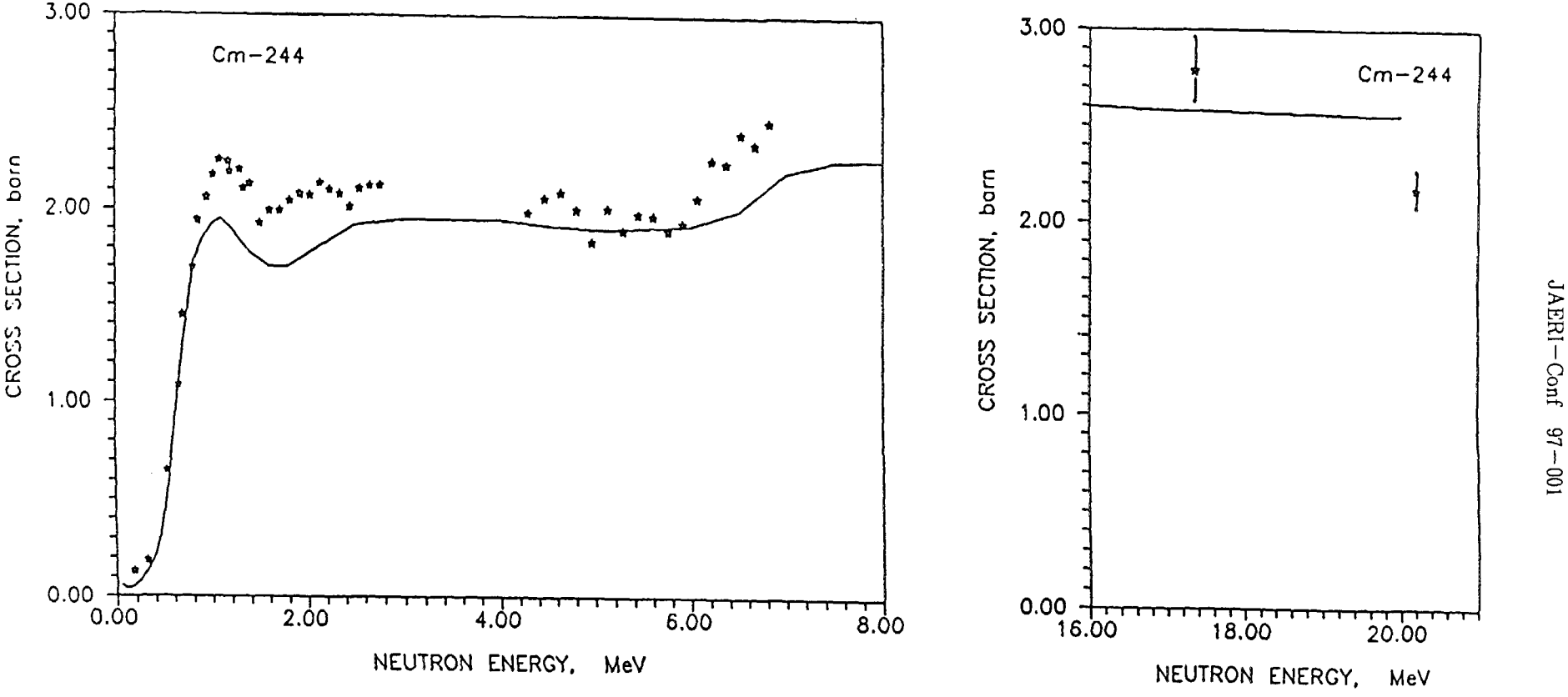

Fig. 12 ^{244}Cm fission cross section.

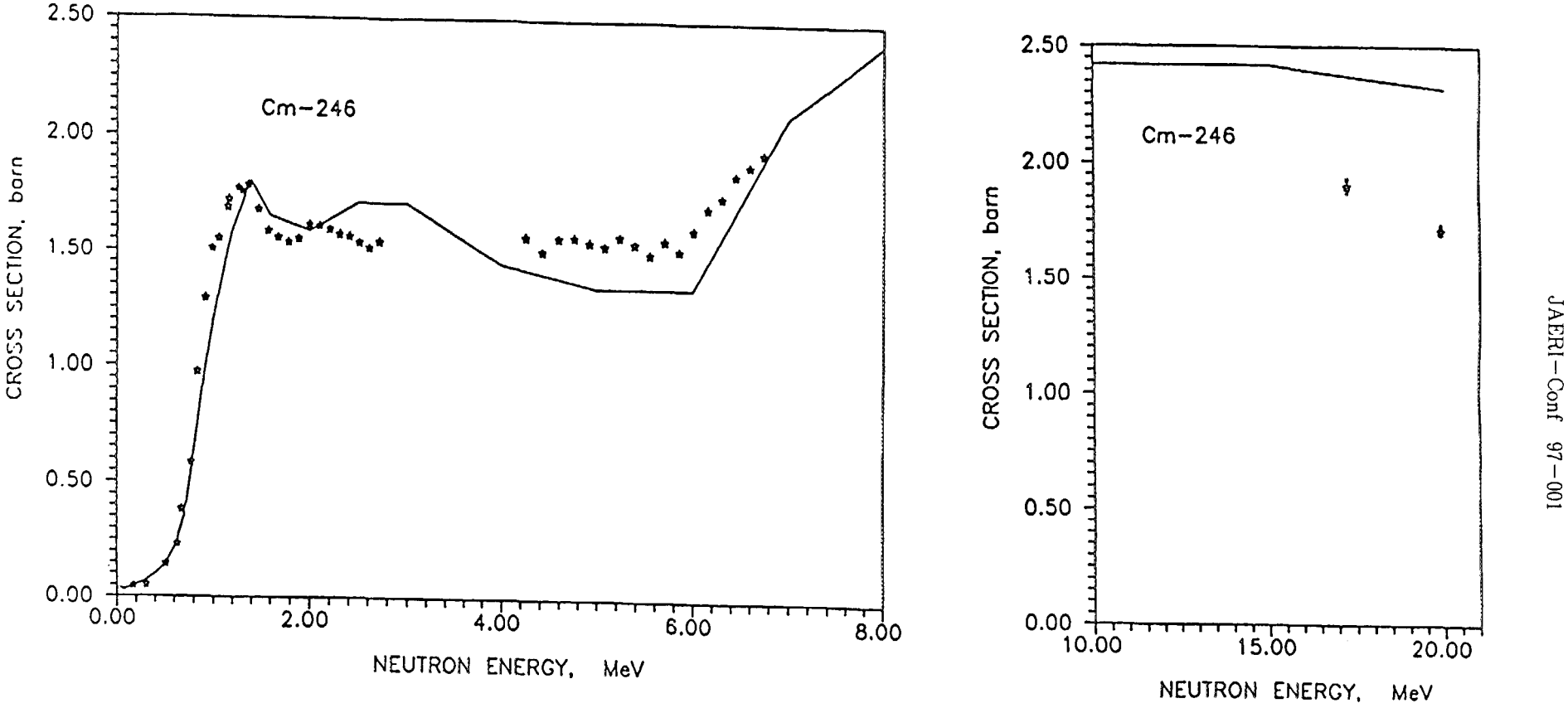

Fig. 13 ^{246}Cm fission cross section.

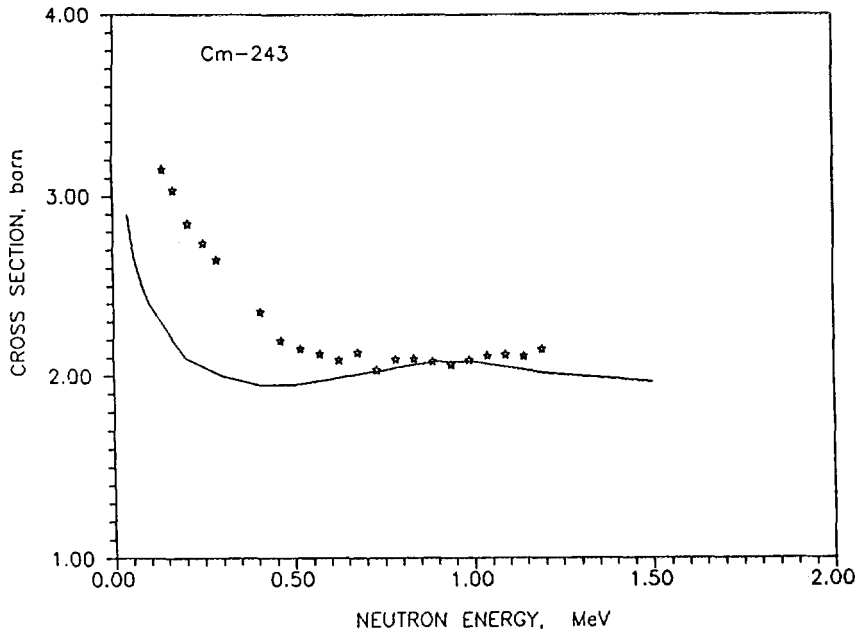

Fig. 14 ^{243}Cm fission cross section. "Hot" points - without any corrections.

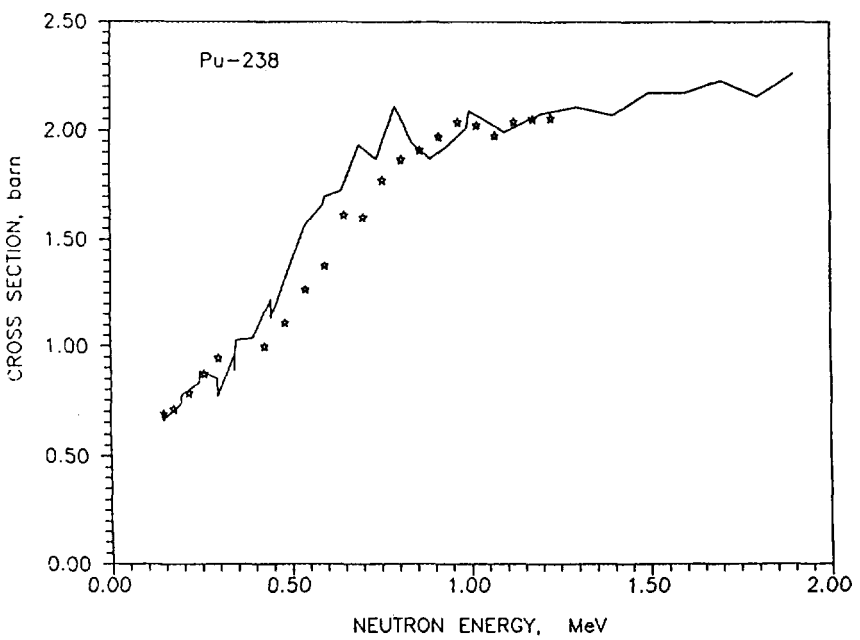

Fig. 15 ^{238}Pu fission cross section. "Hot" points - without any corrections.

3. 2 Development of ionization technique for measurement of fast neutron induced fission products yields of ^{237}Np

A.A. Goverdovski, V.A. Khryachkov, V.V. Ketlerov, V.F. Mitrofanov,
Yu.B. Ostapenko, N.N. Semenova, A.N. Fomichev, L.F. Rodina
Institute of Physics and Power Engineering,
Obninsk, Russia

Abstract

Twin gridded ionization chamber and corresponding software was designed for measurements of masses, kinetic energies and nuclear charges of fission fragments from fast neutron induced fission of ^{237}Np. The ionization detector design, electronics, data aquisition and processing system and the test results are presented in this paper. (Editor)

ISTC Project # 304
Annual report, direction D-2, , 1995-1996

Development of ionization technique for measurement of fast neutron induced fission products yields of ^{237}Np.

A.A.Goverdovski, V.A.Khryachkov, V.V.Ketlerov, V.F.Mitrofanov,
Yu.B.Ostapenko, N.N.Semenova, A.N.Fomichev, L.F.Rodina

Introduction.

^{237}Np fast neutron induced fission cross-section is about 1 barn, therefore dealing with neutron flux of 10^6 n/s, high geometry efficiency fission fragments detector is needed. Frisch gridded ionization chamber was chosen for such a detector. It allows us to determine fragment energy and mass (by 2E method) and nuclear charge (Bragg spectroscopy). It is necessary to use thin spectroscopic target. The information on the particle emission angle will allow us to make corrections in the observed energy for the losses in the layer and the backing, the Frisch grid inefficiency effects and the pulse height defect. The fragment masses will be then calculated by the 2E method. The fragment charge will be determined by comparing the observed Bragg curve with a set of experimental test curves obtained for the fragments with known charges (reference data can be got for thermal neutron induced fission of ^{235}U and spontaneous fission of ^{252}Cf). The accuracy of the data on fragment emission angle and charge is strongly affected by the Bragg curve measurement. The number of points on the Bragg curve is defined by the cathode-grid and grid-anode distances ratio. Described chamber will allow us to improve the accuracy of Bragg curve measurement 4 times in comparison with the ordinary ones.

For our Np target in the beam of fast neutrons with energy 1-5 MeV, we expect to obtain the following parameters: energy resolution of 1-2 MeV, mass resolution of 1.5-2 a.m.u., angular resolution of 0.06 units of cosine, and charge resolution better than 1.5 elementary charges.

I. Ionization detector design.

The ionization chamber is a set of parallel plane electrodes. Negative high voltage (2 kV) is applied to the cathode where a neptunium target is mounted (Fig.1).

The grid is made of gilded tungsten of 30 μm in a diameter with a spacing of 0.3 mm and situated between the anode and the cathode. Anode-grid distance is 2 mm while cathode-grid distance is 40 mm. The guard electrodes are needed for edge effect minimization because of rather large detector working volume. The working gas is a mixture of 90% of Ar and 10% of CH_4 under pressure of 0.65 atm. Experimental data on pulse height defect (PHD) are available from heavy ion beams with energy typical for fission fragments (about 1 MeV/a.m.u.). All electrodes and container were made from stainless steel.

II. Electronics.

Electronic circuit used in the work is shown in fig.2. The current signals from ionization chamber come to inputs of charge-sensitive preamplifiers (CSP) CANBERRA 2001A which integrate them on outputs. The standard CSPs with rise time of τ=60-70 ns were improved to get τ=15-20 ns. It's much less than the integration constant of the chamber (about 30 ns). All signals after CSPs are amplified by fast spectroscopic amplifiers (FSA) CANBERRA 2111 with k_{AMP}=100. In this case differentiation and integration constants were chosen to be zero. The signals after FSA come to Quad Waveform Digitizer (QWD) Le Croy 2262 which gives digital codes with time constant of 12.5 ns. The model 2262 is a high-speed plug-in waveform digitizer providing high resolution, short record solutions to large scale waveform recording requirements needed in fission fragments spectroscopy.

The cathode signal is amplified by CSP and FSA with integration time of 5 ns and differentiation time of 20 ns. Short output signal comes to input of the Constant Fraction Discriminator (CFD) ORTEC 473A. Output signal is delayed on 2-7 μs and is used as a stop signal for QWD. All information is transformed to the host IBM-486 computer.

III. Fast acquisition and processing system.

Schematic view of the acquisition system can be found in fig.3. The system is used for work with the digital units of CAMAC standard which convert signals from the electrodes of the twin gridded ionization chamber. The system is assembly of the computer codes performing three closely connected functions: testing of each information channel in order to carry out correct adjustment of the experimental equipment; acquisitioning and storing experimental data and preparing ones for further

processing; processing of experimental data in "off line" mode or in "on line" mode through the local computer net.

The testing computer code is multichannel analyzer of signals from the amplitude-to-digit converter of CAMAC standard and an oscilloscope based on the information from the wave-form digitizer of CAMAC standard. These computer codes make possible to test and to adjust each channel of the multiparameter spectrometer independently from each other.

The fast experimental data acquisition and storing system is the final component of the multiparameter spectrometer. This computer code performs control of the amplitude-to-digit converters and the wave-form digitizers through the CAMAC crate controller, acquisition of the information from these units and analyzes it in order to single out the real events connected with the physical process under investigation from the continues flux of the background events. One of important functions of the system is to show the data stored. It makes possible to control process and change the experimental conditions if it needed. This computer code allows user to see both one-dimensional and two-dimensional spectra on any logically connected couple of the channels according to experimentalist's wishes. The collected data are stored as consequence of the events, that makes possible, during further processing, to take into account systematic shifts of experimental conditions and process the data as assembly of independent events instead of spectra, because of spectra themselves are processed information.

The experimental data processing system allows us to correct data on the first stage of processing relaying on the information from the different channels of the multiparameter spectrometer in order to eliminate influence of systematic distortions. On the second stage assembly of the independent events can be integrated on any parameter with any conditions according to user's wishes for determination of the physical process under investigation.

IV. Generation of signals.

If the ionization track is oriented at the angle Θ relative to the cathode normal one electron moving between the electrodes of the chamber with velocity v^- will induce the negative charge on the anode with the following amplitude :

$$Q^-_{An} = -\frac{ev^-}{D} * \frac{D - x*\cos(\Theta)}{v^-} = -e\left(1 - \frac{x*\cos(\Theta)}{D}\right)$$

For all of electrons of the track charge signal will be:

$$Q^{-}_{An} = -\int_{0}^{R} \rho(x) * \left(1 - \frac{x * \cos(\Theta)}{D}\right) dx$$

where ρ(x) - ionization density along the track. If total amount of electrons is n_0, the signal is:

$$Q^{-}_{An} = -n_0 e + \frac{\cos(\Theta)}{D} \int_{0}^{R} x * \rho(x) dx = -n_0 e * \left(1 - \frac{\ddot{x}}{D} \cos(\Theta)\right)$$

$$\text{where: } \ddot{x} = \frac{1}{n_0} \int_{0}^{R} x * \rho(x) dx ,$$

In gridded ionization chamber (GIC) expressions for anode and cathode signals can be written in following way:

$$Q^{-}_{An} = -n_0 e$$

$$Q^{-}_{Cat} = n_0 e * \left(1 - \frac{\ddot{x}}{D} * \cos(\Theta)\right)$$

where D is cathode-anode distance. Shapes of both signals determined experimentally with QWD are shown in fig.4 in which angular dependence of cathode pulse height can be seen. Each curve presented is for single α-particle of ^{252}Cf. Time is in channels with the width of 12.5 ns. It means that assumed rise time (approximately 700 ns for argon + methane mixture) is correct.

Practically, any Frisch grid is not ideal hence two specific effects have to be taken into account. There are so-called grid inefficiency (σ) against to shielding of the anode from electrons moving between the cathode and grid and electrons losses on the grid (λ). Therefore the real formula for the anode signal is:

$$P_{An} \approx n_0 (1 - \lambda) * \left(1 + \sigma * \left(1 - \frac{\ddot{x}}{D} \cos(\Theta)\right)\right)$$

To eliminate the electron losses the following condition has to be reached:

$$\frac{V_{Cat} - V_{Grd}}{V_{Grd} - V_{An}} \leq \frac{Y(1+\rho) + 2l\rho}{D(1-\rho) - 2l\rho}$$

Y - distance between the grid and the anode ; $\rho = 2\pi\frac{r}{d}$; r - wire radius; d- grid spacing.
Parameter l is:

$$l = \frac{d}{2\pi}\left(\frac{1}{4}\rho^2 - \ln(\rho)\right)$$

For the detector used the condition presented above is:

$$\frac{V_{Cat} - V_{Grd}}{V_{Grd} - V_{An}} \leq 0.60$$

For the grid inefficiency σ one can be written:

$$\sigma = \frac{d}{2\pi Y} * \ln\left(\frac{d}{2\pi r}\right)$$

Calculated value is σ=0,028.

In practice grid inefficiency has to be determined experimentally. One obvious way is to do analysis of signal's shapes using QWD. For fission fragments (^{252}Cf) this kind of information is presented in fig.5. The curves were obtained for single fragments. For emission angle Θ= 90^0 the rise time is very short and therefore grid inefficiency can be observed very easy. Time T_2 in the figure insert corresponds to the moment when first of electrons moving to the grid reached it. Fig.6 represents the analogous result but for 30 events having the same parameters of energy and therefore ionization power and emission angle. Fig.5 and 6 demonstrate the powerful method of signals analysis.

V. Determination of angular spectra.

Rise time of anode signal T, length of ionization track L, electron velocity v$^-$ and emission angle are dependent from each other: T = L*cos(Θ)/ v$^-$. Two-dimensional data matrix (T_{AN} - T_{CAT} - Y) is presented in fig.7 for α-particles of ^{252}Cf. The constant level of yields can be seen in all region of time difference. It corresponds to isotropic angular distribution. In the case of fission fragments we are dealing with much more complicated situation when the energy spectrum is very broad and corresponds to very different ionization powers in the gas. It can be seen in fig.8. Low energy part is due to high energy losses scattering of the fission fragments on the target assembly. In fig.9 the data matrix cos(Θ)-energy-yield is presented. Isotropic angular distributions are observed again for any fragments kinetic energy like in the case of alpha-particles.

Coincidence of the emission angles of two complementary fragments associated with a single fission event gives the value of angular resolution (fig.10). Fig.11 shows the integral angular spectrum of fission fragments of californium. Pronounced peak around $\cos(\Theta)=0^0$ is the result of backscattering effects of the fragments in the radioactive target. It is obvious that the last effect has to be taken into consideration in fission fragments spectroscopy. In fig.11 a slop on the left side of the spectrum ($\cos(\Theta)=0$) is much smaller relative to that one on the right side ($\cos(\Theta)=1$). It is due to much different rise times and therefore time and angular resolution.

VI. Fission fragments mass and kinetic energy distributions.

After including of all corrections to the experimental charge signals masses of primary fission fragments can be determined using well known and widely used two-energy method (so-called 2E method). Results of this kind of procedure is shown in fig.12. Very good resolution between heavy fragments and light ones can be seen in figure. As a calibration constant the mean total kinetic energy of californium-252 was used. Average energy of light group is 106 MeV. One-dimensional spectra are presented in fig.13. All of parameters are in good agreement with reference ones well known in literature. For example, peak-to-valley ratio in energy spectrum is approximately 2.7(0.1). To correct the data on relatively low energy losses in the target and in the backing, the dependence of light fragments position on inverse cosine was determined. These data are presented in fig.14. The bottom chamber is characterized by the properties of the Al_2O_3 backing and gold layer. For another part of GIC energy losses are negligible .

VII. A spectrometric ^{237}Np target testing by an α-particles analysis.

Fission fragment yields measurement was assumed to be made using spectrometric twin gridded ionization chamber, therefore the neptunium target must be low-active and relatively thin. The target was fabricated from enriched neptunium as NpF_4 layer vacuum-evaporated onto Al_2O_3 backing of 40 $\mu g/cm^2$ thick. The surface of the target was covered with pure gold to make the cathode electrically conductive. Diameter of the target is 32 mm and diameter of the active spot is 20 mm. The thickness, absolute α-activity and isotopic composition of the target were determined by an α-analysis made with the same 4π gridded chamber which will be used for fission

fragments yields investigations. The chamber was filled with the gas mixture of Ar+10% CH_4 under pressure of 1.8 atm.

Two-dimensional analysis was used to suppress backgrounds. Anode amplitude spectrum is presented in fig.15. The main part of the spectrum is associated with the ^{237}Np α-line. Integration of events in corresponding area gave absolute activity and resulting in the thickness of the target : 57.5 ± 0.5 μg/cm^2. Two additional α-lines can be associated with very small contamination of ^{239}Pu and ^{241}Am (or ^{238}Pu). The experimental and reference α-particle energies and the isotopic composition of the target are presented in the Table.

Conclusion.

The main task of the work presented above was to design twin gridded ionization chamber and corresponding software for measurements of masses, kinetic energies and nuclear charges of fission fragments. It's necessary to get detailed data on chain and independent yields of fission products. Investigations have shown wide perspectives of ionization technique in combination with high-quality nuclear electronics and developed software.

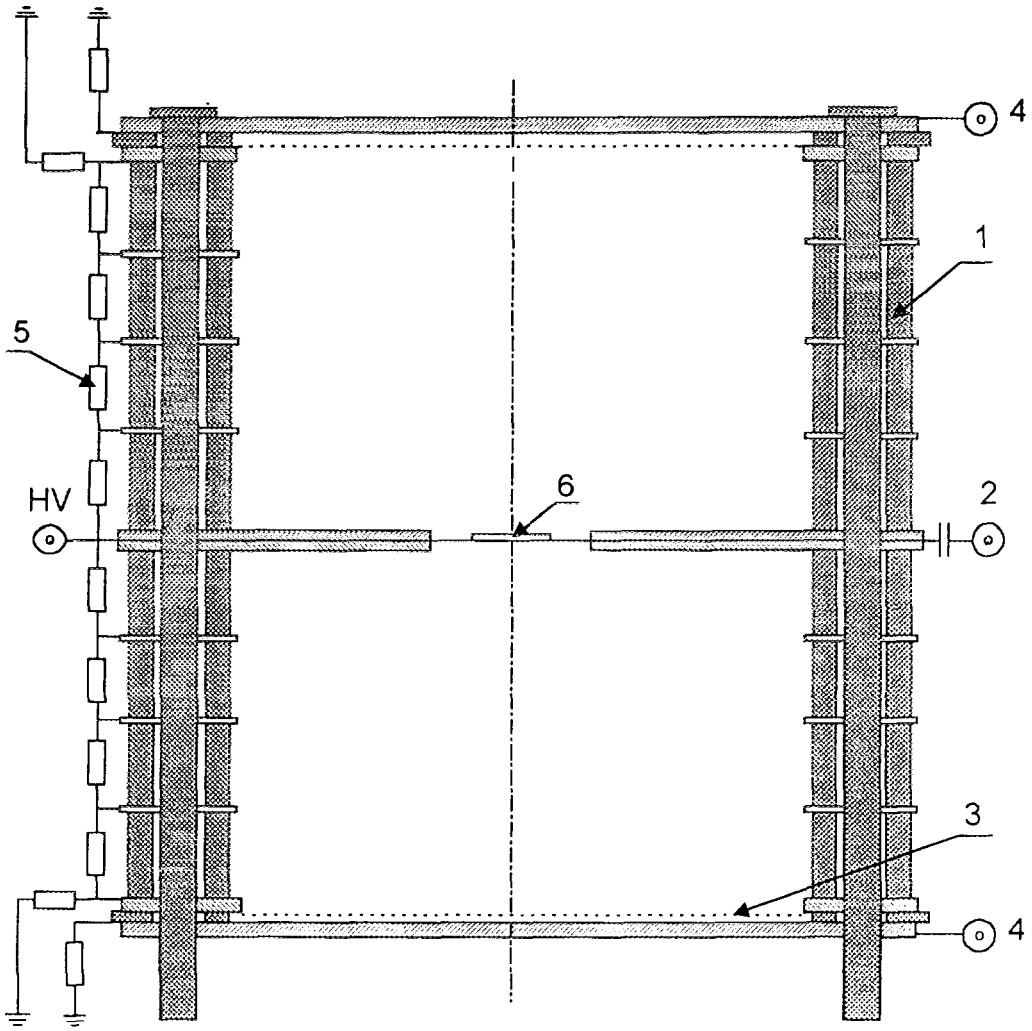

Fig.1. Ionization chamber: 1-insulator; 2-cathode;
3-grid; 4-anode; 5-shilding electrodes; 6-target.

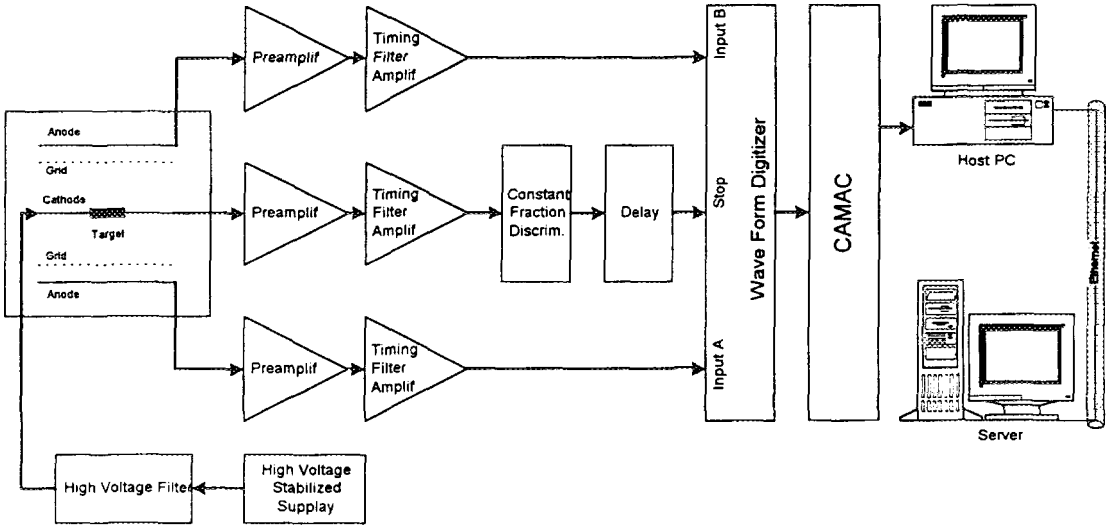

Fig.2. Electronic circuit.

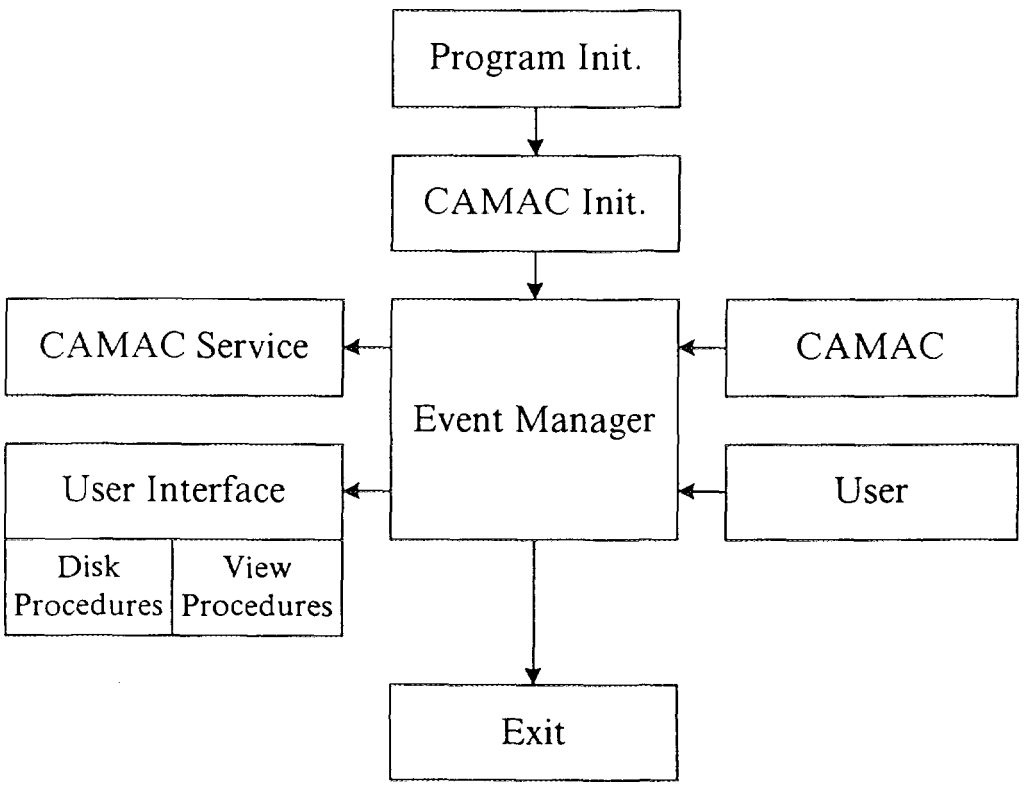

Fig. 3. Fast acquisition system.

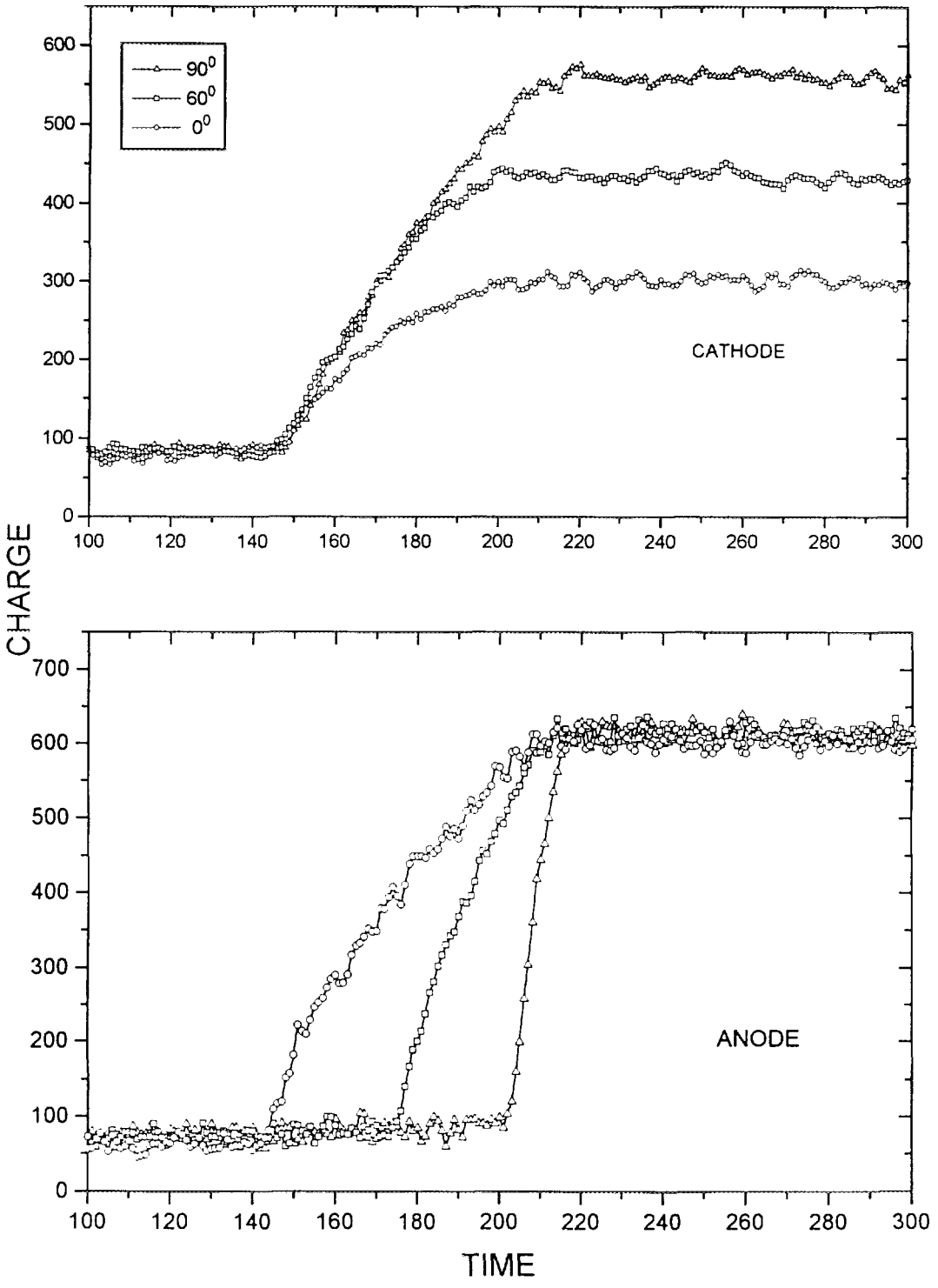

Fig.4. The shapes of anode and cathode signal for different track orientations relative to normal to the cathode (α-particles of ^{252}Cf).

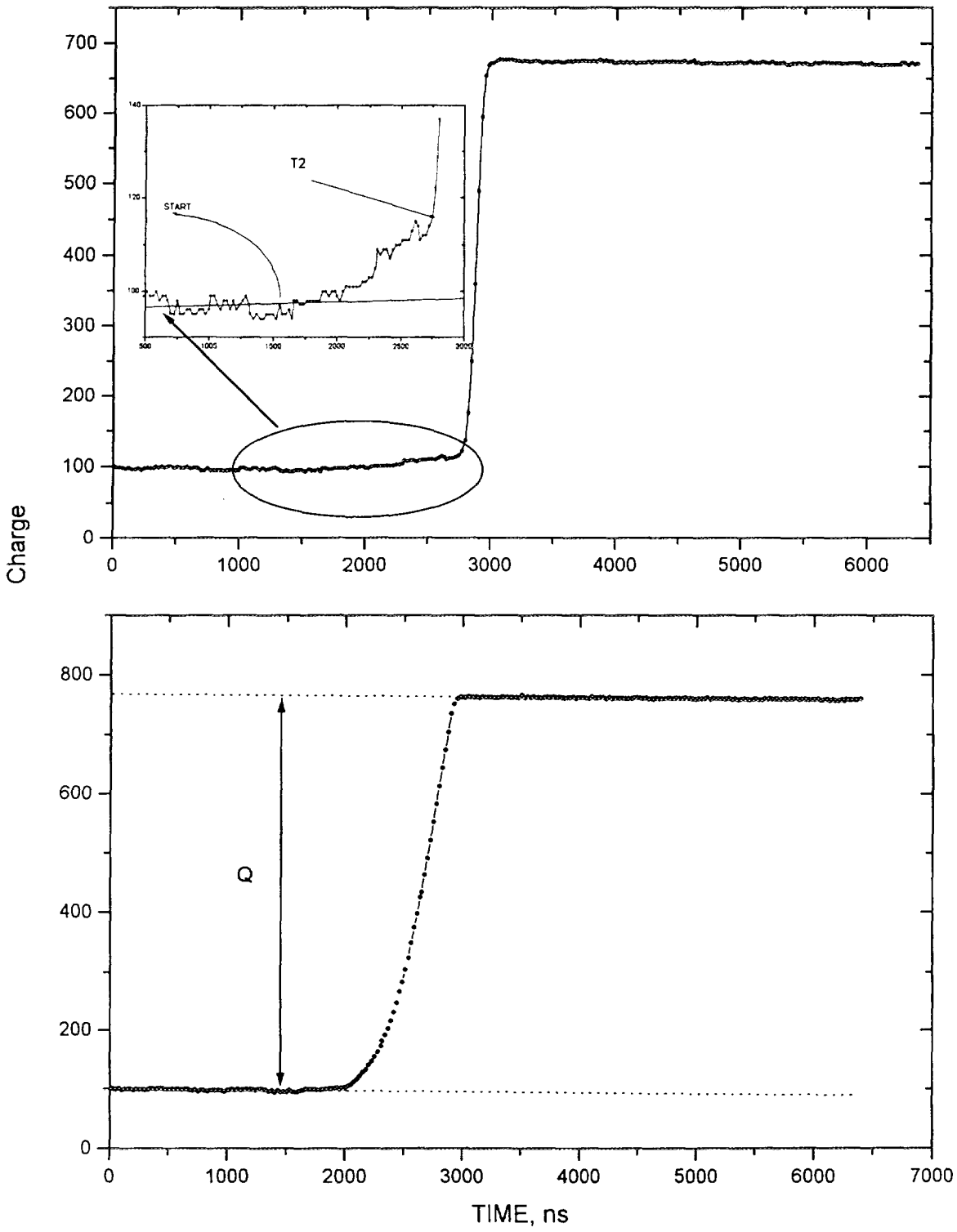

Fig.5. The same as in fig.4 but for single fission fragment. Upper part is for angle θ=90°, and bottom one is forθ=0°.

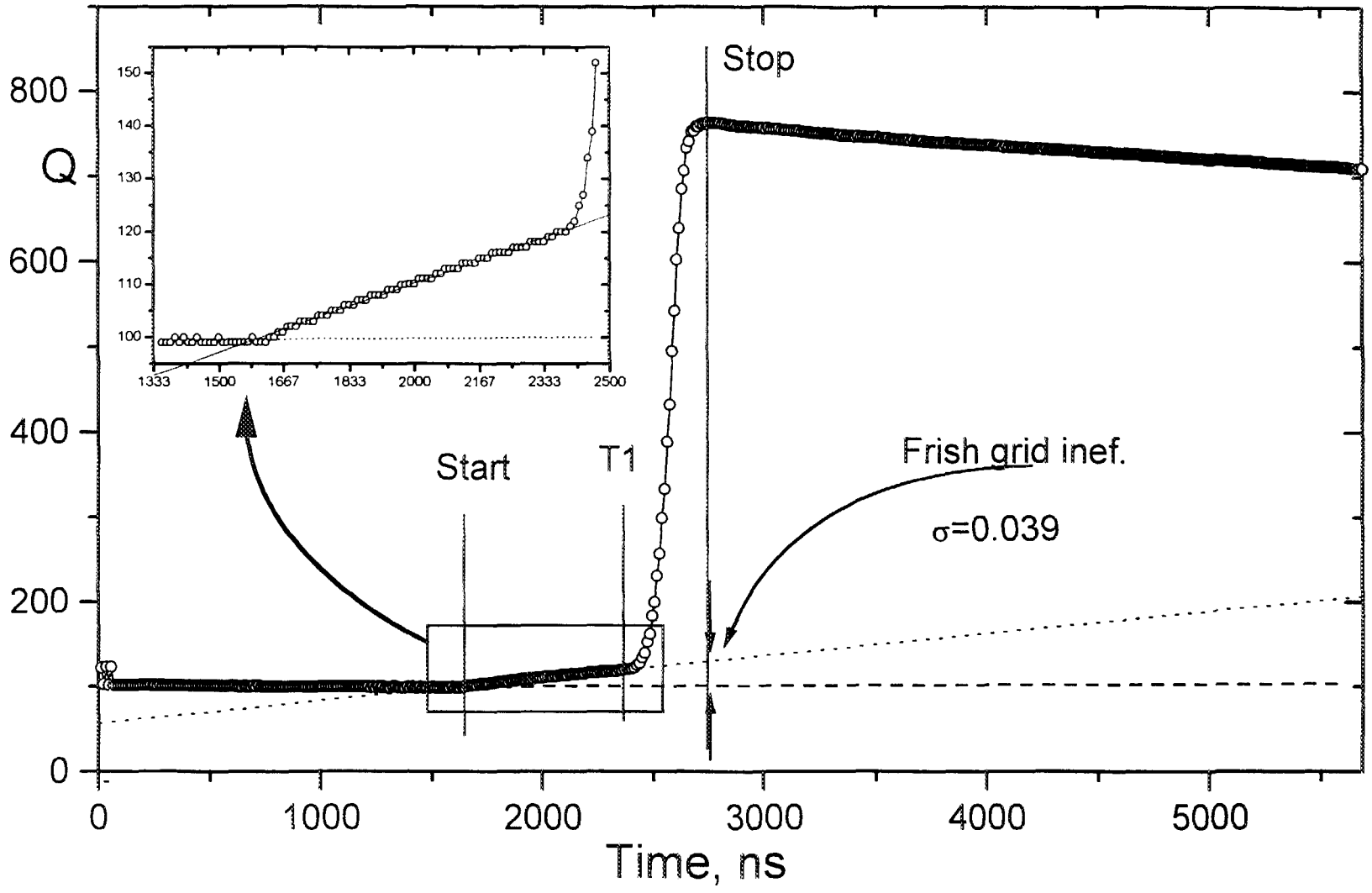

Fig.6. 30 fission fragments signal shape. Determination of the Frish grid inefficiency.

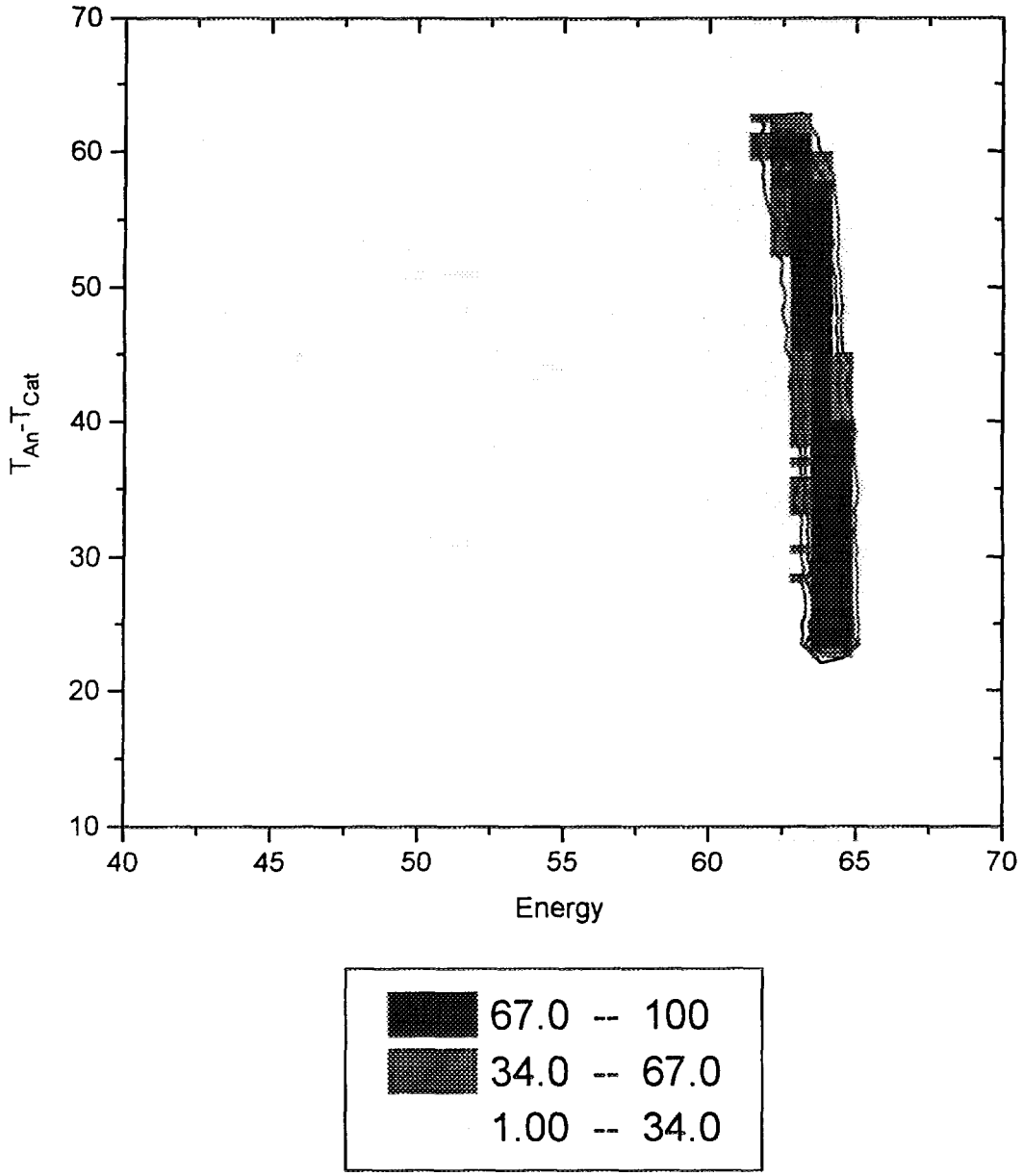

Fig.7. Time difference T_{an} - T_{cat} as a function of α-particles energy (in arbitrary units).

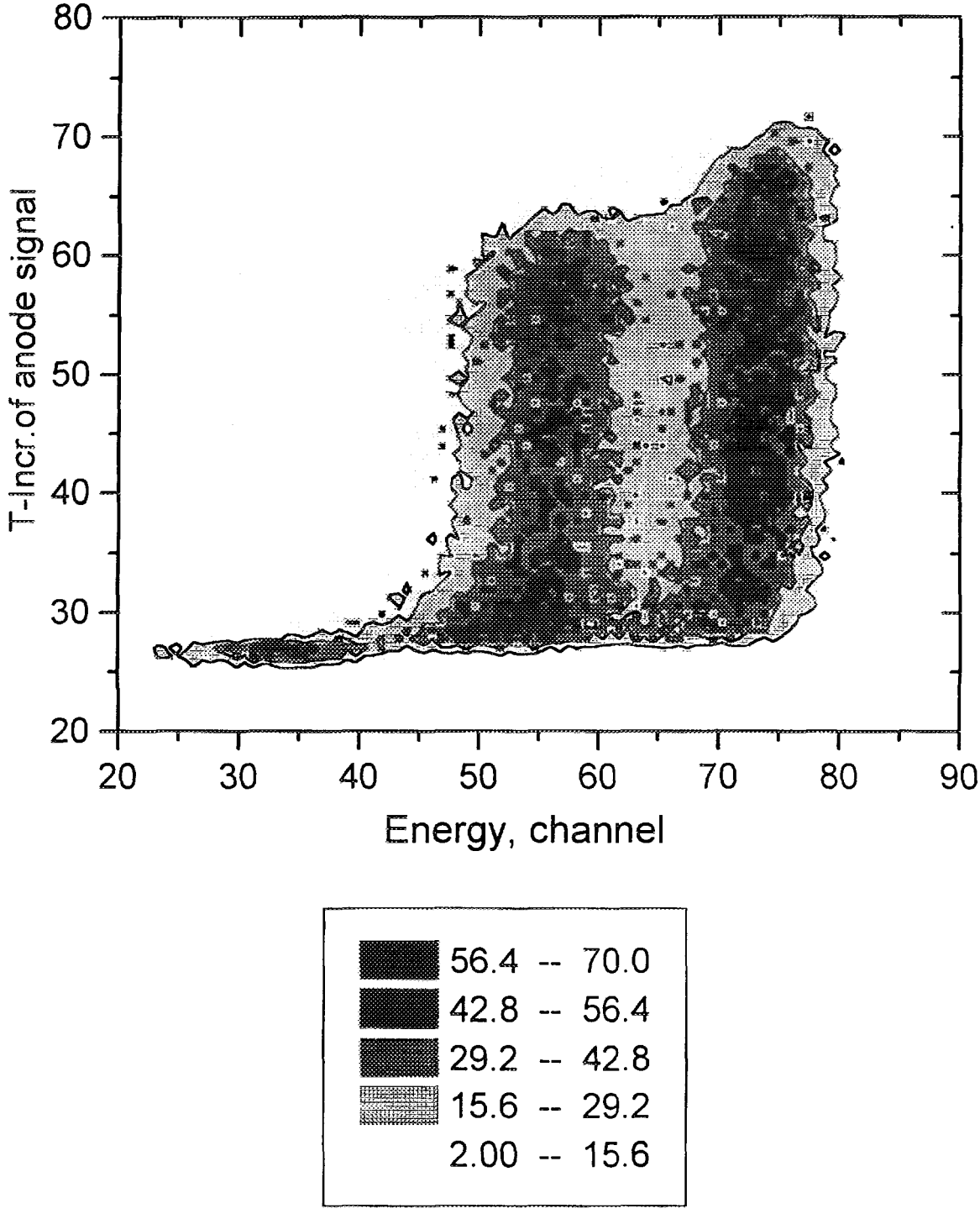

Fig.8. Anode signal rise-time as a function
of fission fragments energy (arbitrary units).

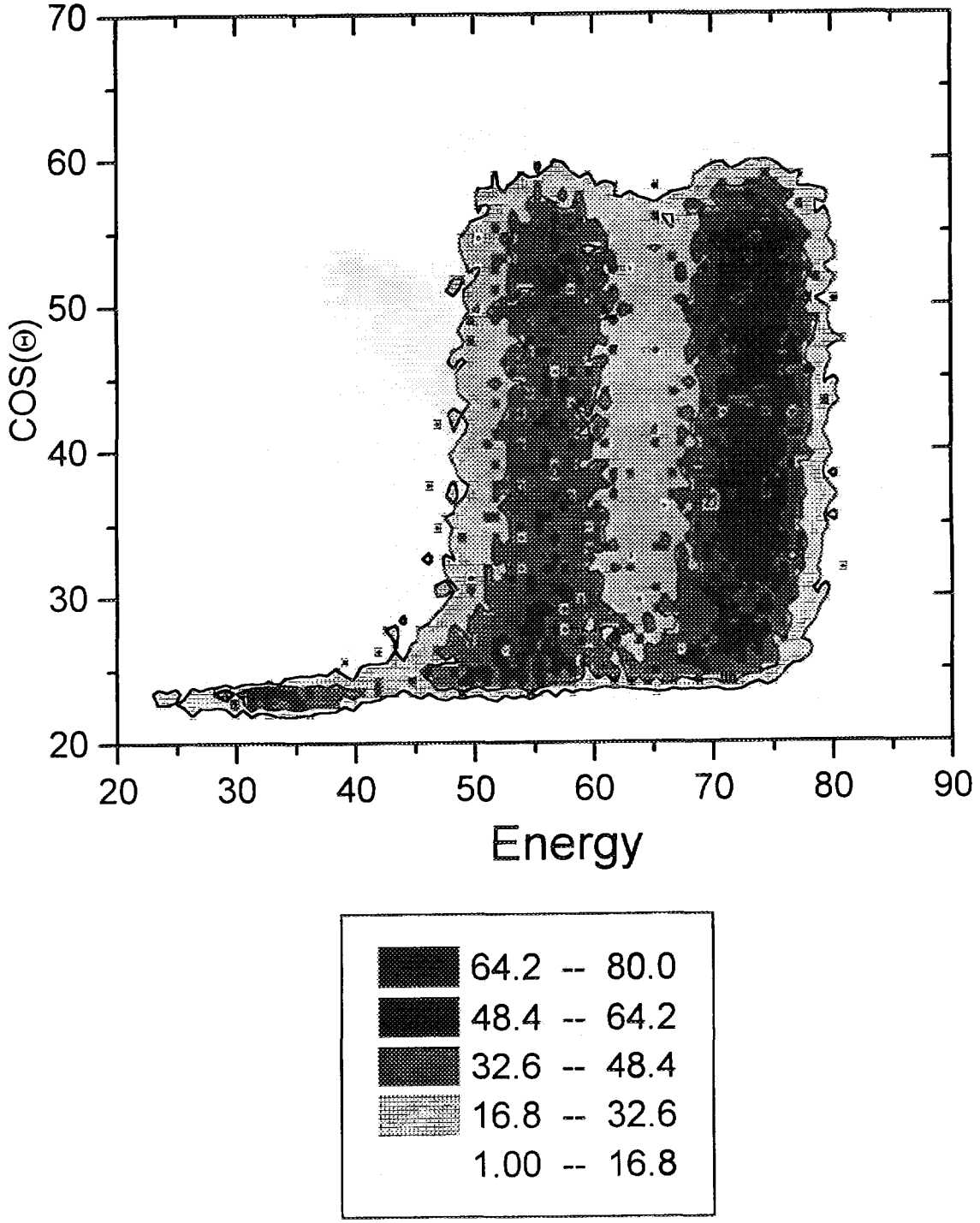

Fig.9. Cosine values derived from matrix of fig.8 as a function of fission fragments energy (arbitrary units).

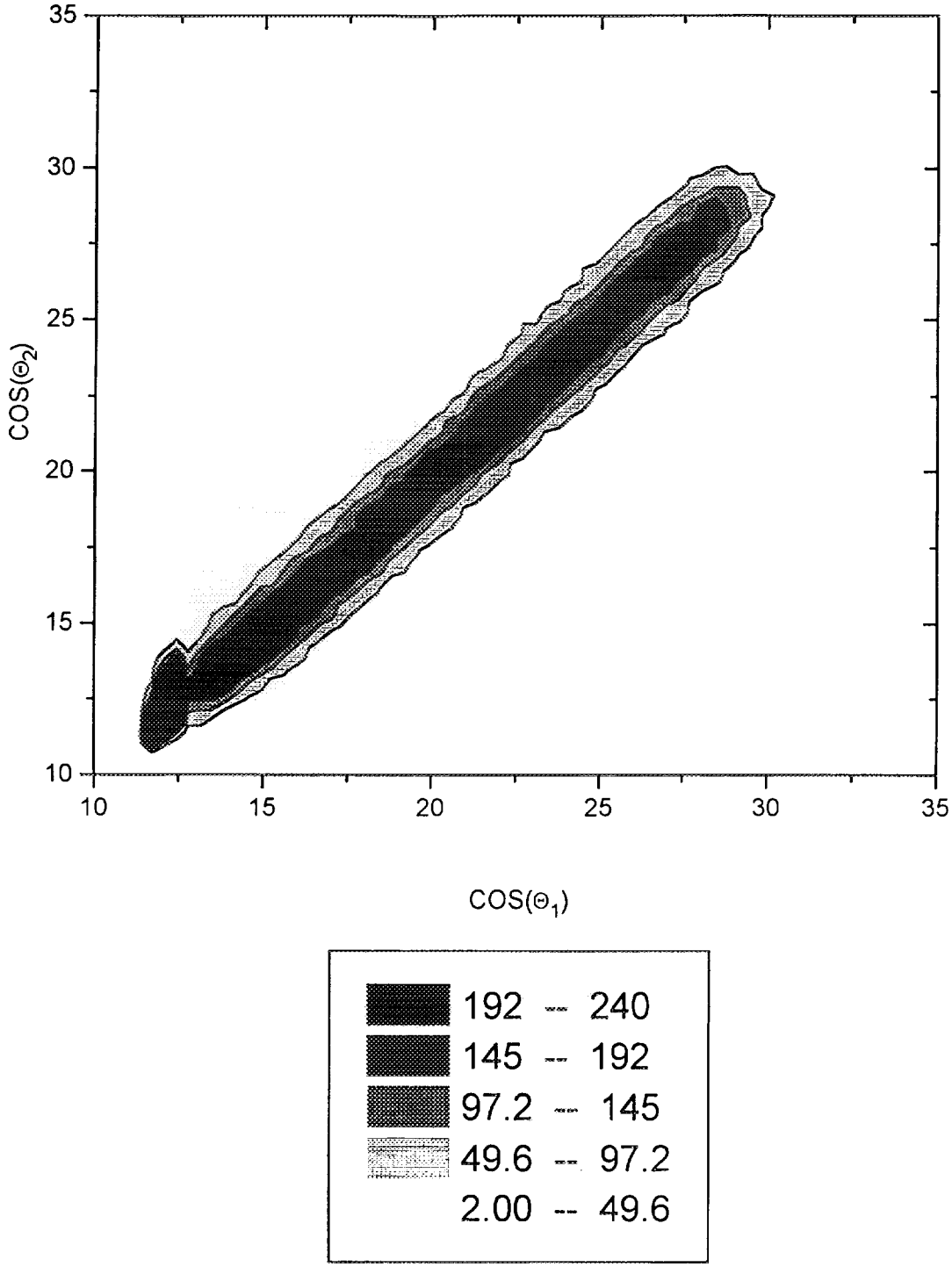

Fig.10. (cos_1 - cos_2) correlation matrix for all complementary fragments (^{252}Cf(sf)).

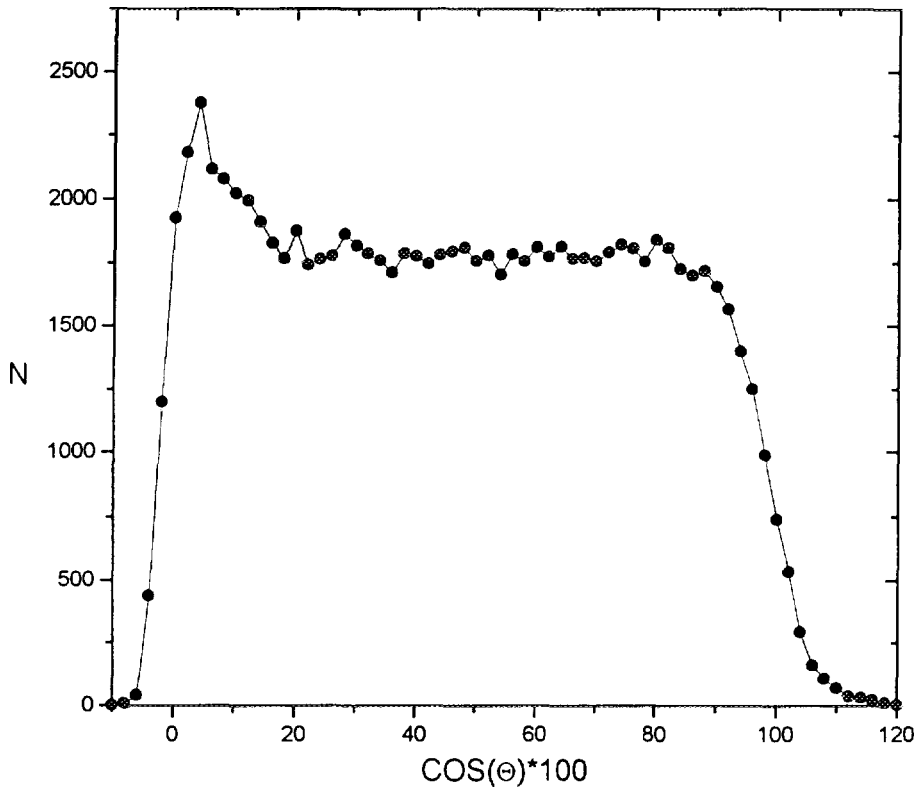

Fig.11. Angular distribution of
^{252}Cf spontaneous fission.

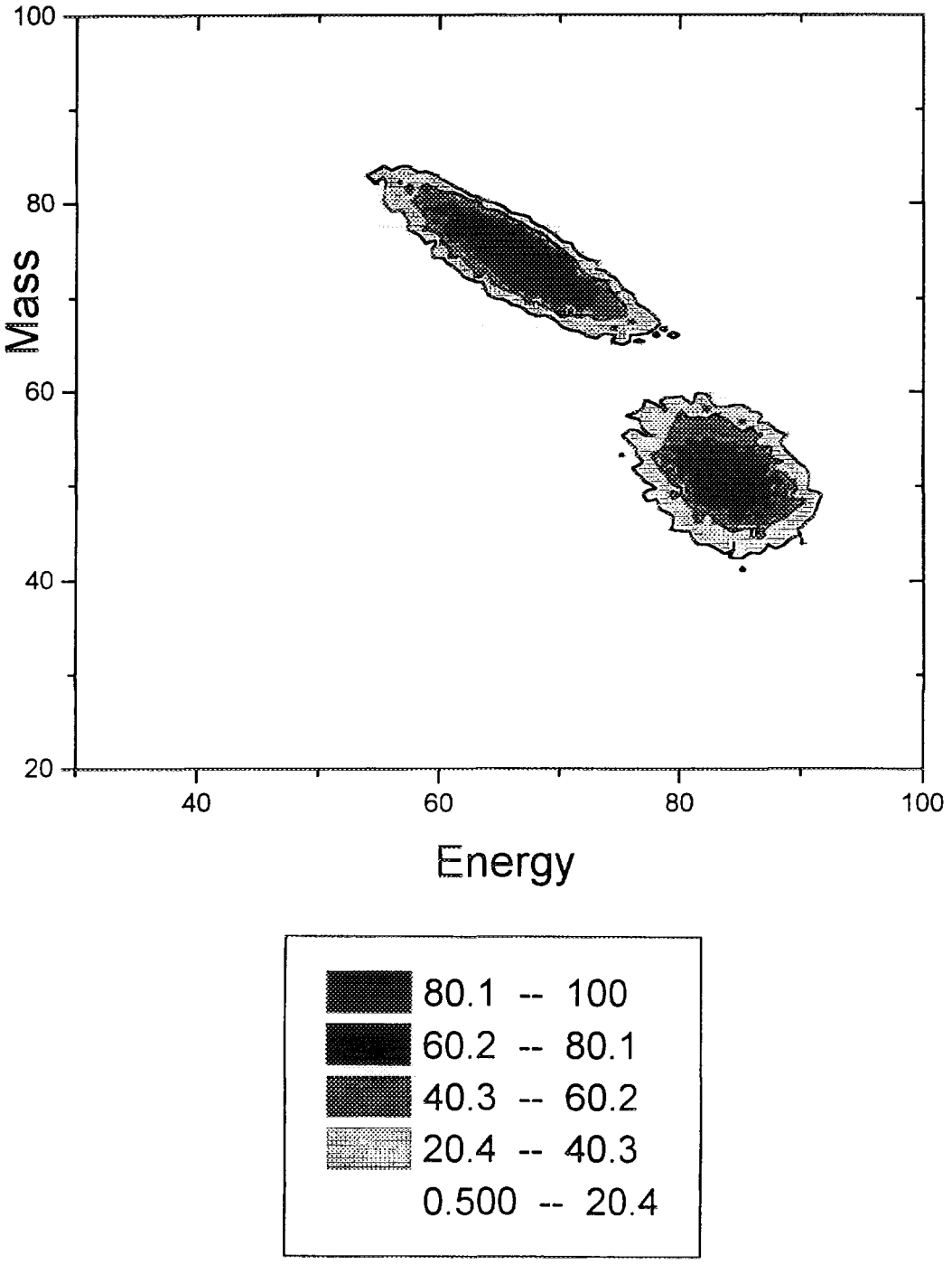

Fig.12. Two dimensional FF mass-energy matrix for ^{252}Cf(sf) (arbitrary units).

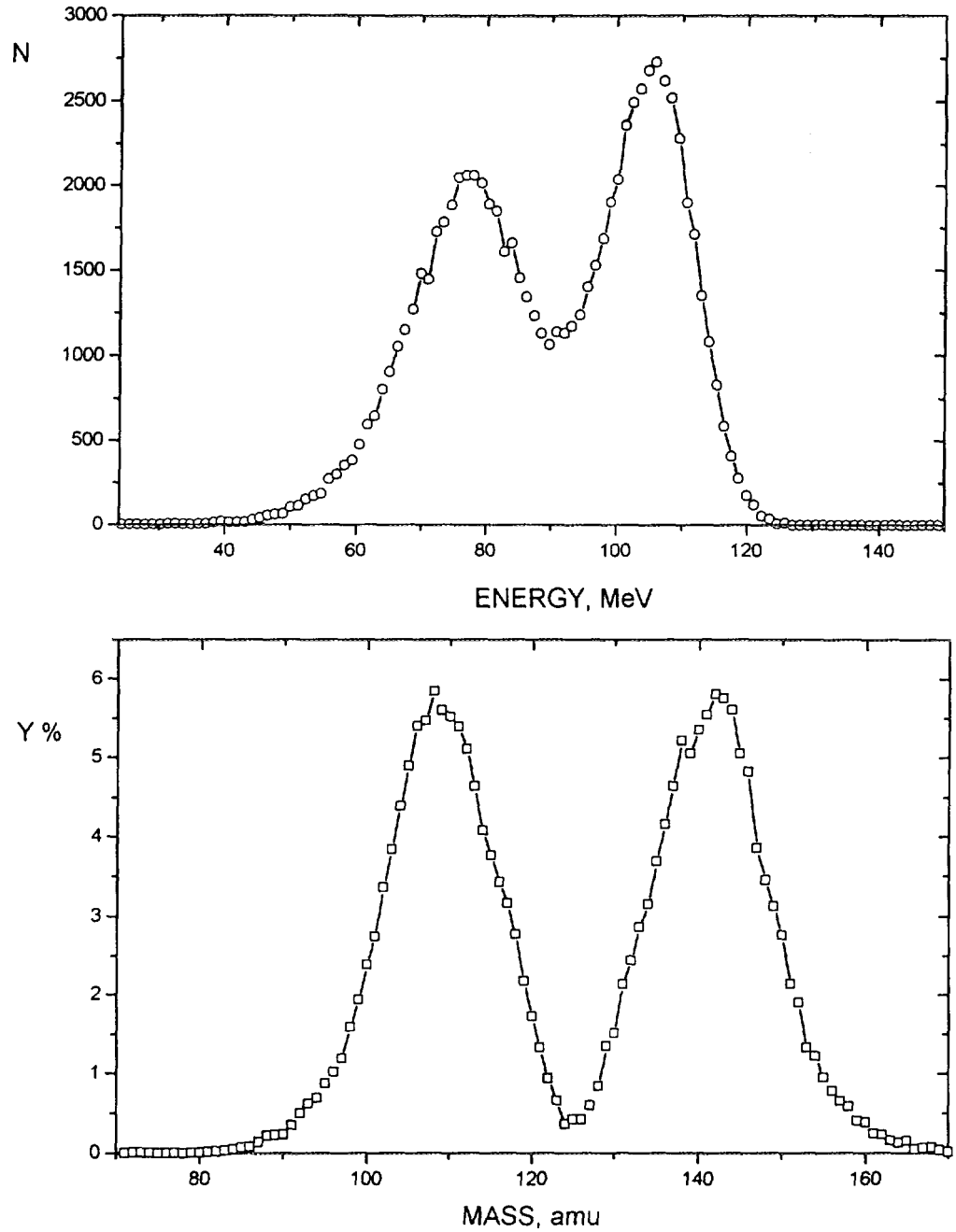

Fig.13. ^{252}Cf fission fragments energy and mass distributions (with grid, PHD, thickness corrections).

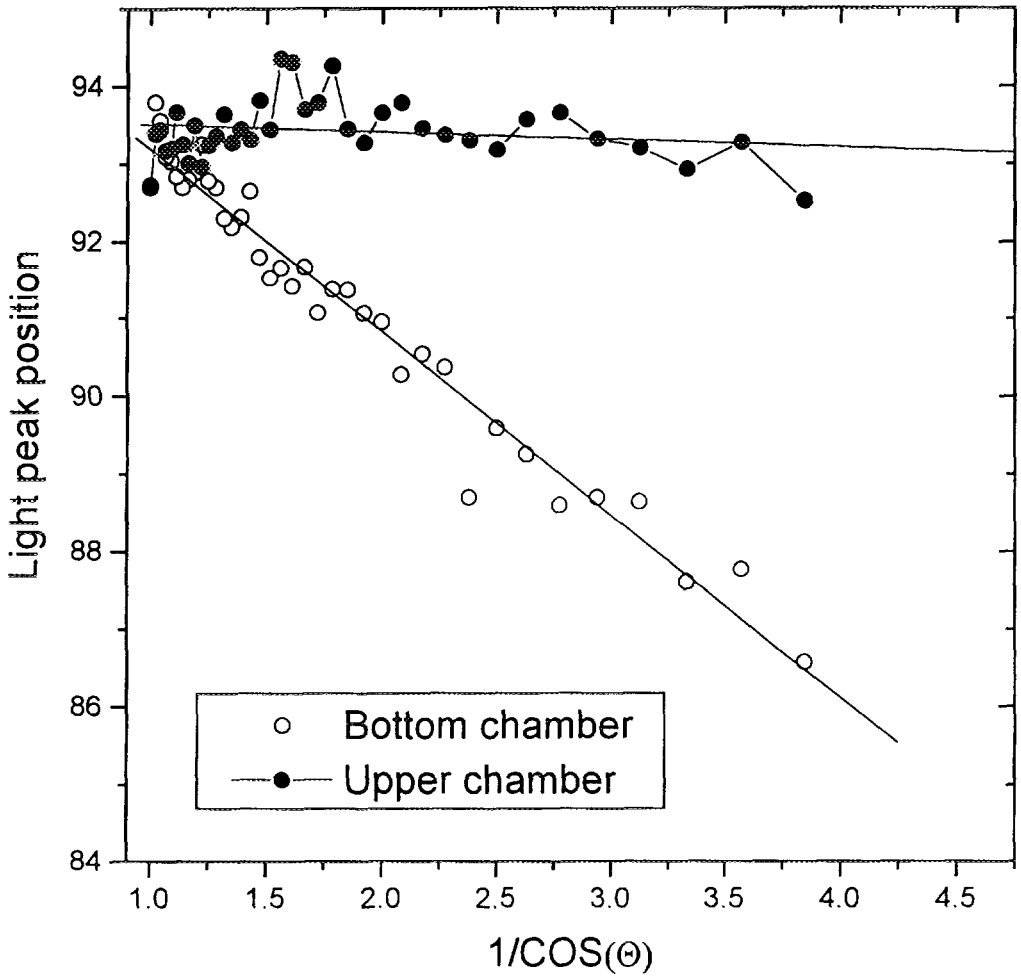

Fig.14. Fission fragments light peak position as a function of 1/cos value for two chamber parts.

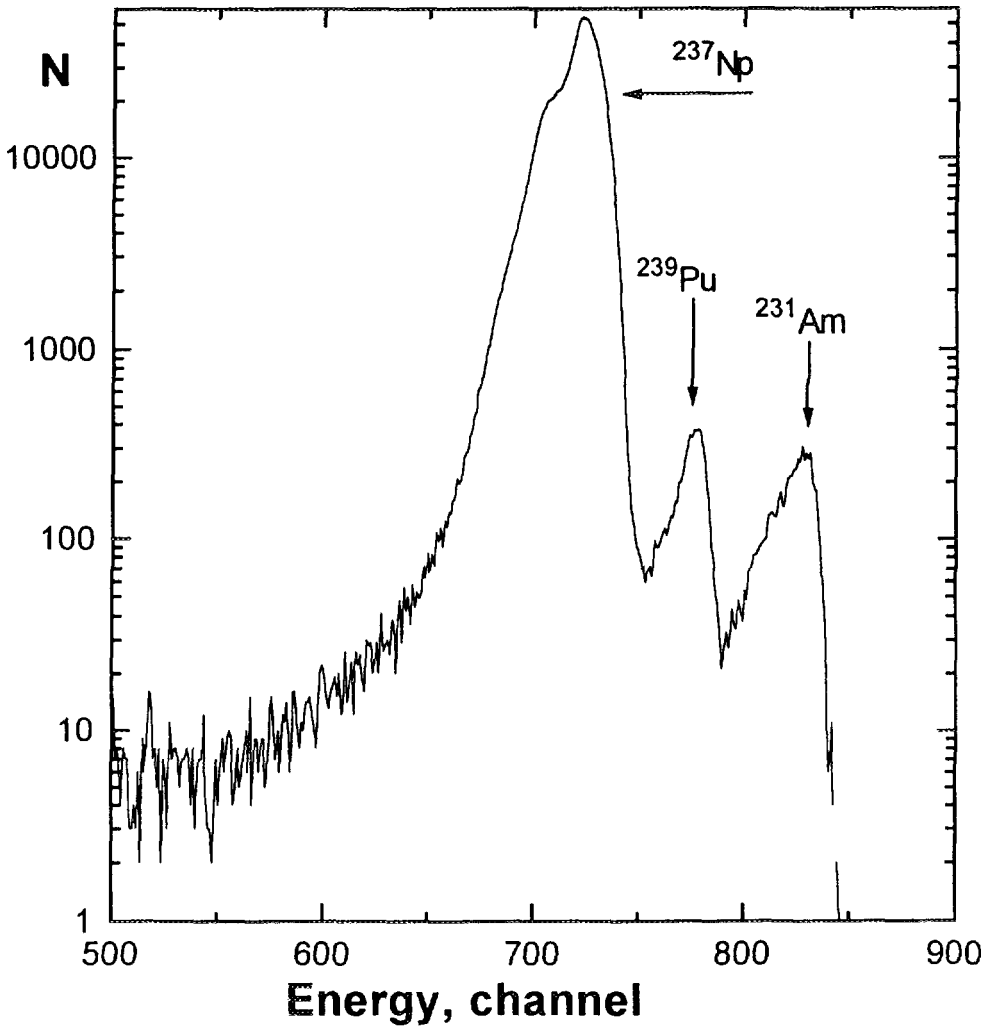

Fig.15. Energy spectrum of α-particles from neptunium target.

TABLE

Results of the target analysis.

Isotope	α-Particle energy, reference, keV	α-particle energy, experiment, keV	Number of nuclei, %
^{237}Np	4788	4788 ± 8	99.99+
^{239}Pu	5157	5152 ± 10	6.1 ± 0.1 E-3
^{241}Am	5486	5483 ± 10	1.06 ± 0.01 E-4

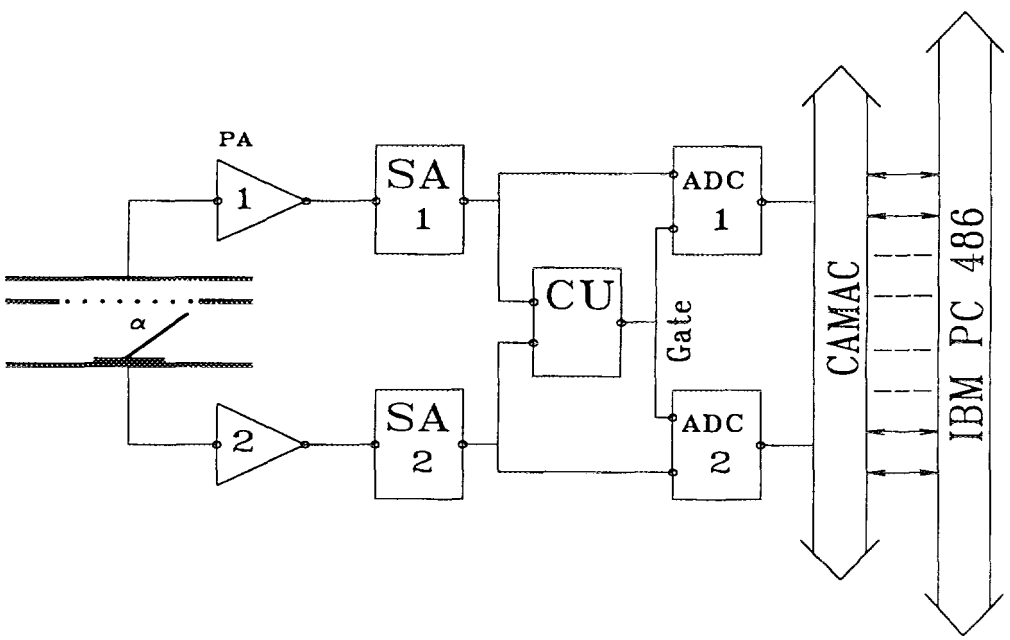

Fig.16. Scheme of the electronic setup.

3. 3 Measurements of periods, relative abundances and absolute yields of delayed neutrons from fast neutron induced fission of ^{237}Np.

V. Piksaikine
Institute of Physics and Power Engineering,
Obninsk, Russia

Abstract

The experimental method for measurements of the delayed neutron yields and period is presented. The preliminary results of the total yield, relative abundances and periods are shown comparing with the previously reported values. (Editor)

Measurements of periods , relative abundances and absolute yields of delayed neutrons from fast neutron induced fission of ^{237}Np

Presented by V.Piksaikine
Institute of Physics and Power Engineering,
Obninsk ,Russia

Workshop on the Evaluation of Actinide Nuclear Data and Measurements and Analysis of the Basic Nuclear Data for Minor Actinide, Mito, Japan, 27-31 May, 1996

1. Experimental method

An experimental set-up for measurements of the energy dependence of the total delayed neutron yields and periods from fast neutron induced fission was put into operation at the electrostatic accelerators of the IPPE. The experimental method employed in the measurements is based on periodic irradiation of the fissionable samples by neutrons generated from a suitable nuclear reaction at the accelerator target and measurement of the decay of delayed neutron activity. The general expression for such type measurement can be writen in the following form

$$\Sigma = \nu_d \cdot F \cdot \varepsilon(\chi_d) \cdot T[t_{i/c}; \{\alpha_i, \lambda_i\}]$$

where Σ - number of counts measured by the delayed neutron detector in a given time interval after irradiation of the sample, $\nu_d(E_n)$ - the energy dependence of the total delayed neutrons, $F(E_n)$ - number of fissions in the sample, $\varepsilon(\chi_d)$ - efficiency of the neutron detector which takes into account a delayed neutron spectrum effect on the detection, T - factor which takes into account the irradiation and counting times.

The developed method for measurement of the absolute delayed neutron yields includes two different types of experiment. The first one consists of the measurements of the delayed neutron relative yields and periods. In this type of experiment the measurements with different irradiation and delayed neutron counting time intervals are forseen to emphasize certain delayed neutron groups {αi, λi}. For the second type of experiment the experimental arrangement and measurement techniques were designed to use the irradiation time of the fissile material which is long compared to the longest delayed neutron period. In this case the above formula can be presented as

$$N_d = \sum_{t1}^{t2} N(t) = \langle \varepsilon \rangle \cdot F \cdot \nu_d \cdot \sum_i T_i \cdot \frac{a_i}{\lambda_i} \cdot (e^{-\lambda_i t_1} - e^{-\lambda_i t_2})$$

$$T_i = (1 - e^{-\lambda_i t_i})\left(\frac{n}{1 - e^{-\lambda_i T}} - e^{-\lambda_i T} \cdot \frac{1 - e^{-n\lambda_i T}}{(1 - e^{-\lambda_i T})^2}\right)$$

where λ_i and α_i - decay constant and relative yield of the i -th group of delayed neutrons, t_1 and t_2 - time of the beginning and the end of delayed neutron counting, n - number of cycles, T - duration of one cycle, which includes the irradiation and delayed neutron counting time, <ε> - neutron detector efficiency which takes into account the energy spectrum of delayed neutrons.

2. Neutron detector

The following specific features of the experiment on the delayed neutron yields and half-lives measurements have been considered in the course of the detector design. The detector should have minimum sensitivity to gamma rays since the Np-237sample to be investigated is highly gamma active. The neutron detector efficiency should not change considerably within 0 - 1.5 MeV energy range since the delayed neutron major contribution happens to be within this energy range. The neutron detector should have

small dead time since the delayed neutron counting rate varies by three orders of magnitude within 100 seconds after irradiation of the sample.

The BF-3 counter of SNM-11 type at the operational potential of 650 V in the proportional mode operation was chosen as the main detector counting unit. The manufactured detector is an assembly of 30 BF-3 counters distributed in polyethylene moderator along three concentric circles with diameters of 106, 160 and 220 mm. The outer diameter of moderator is 400 mm, its length is 300 mm. In the center of the detector there is a through hole with diameter of 36 mm to install the sample flight tube. The detector is shielded against the neutron background by borated polyethylene, boron carbide powder and cadmium sheets. The delayed neutron detector used in the present experiment is shown in Fig.1.

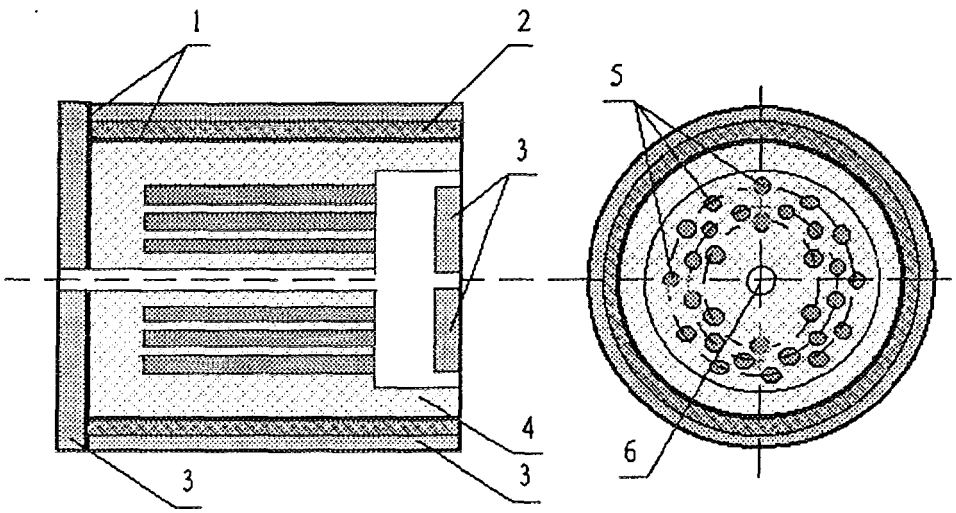

Fig.1. Delayed neutron detector.
1- cadmium sheet, 2- boron carbid powder, 3- boron plastic,
4- polythene, 5- $^{10}BF_3$ counters, 6- sample transporting hole.

The amplifiers and pulse discriminators for each BF-3 section have been manufactured. The output signals from these electronic channels are fed to a mixing module. The test of the neutron detector showed that the detector is insensitive to gamma rays of 2 grams Np-237 sample. The neutron detector dead time measured with Cf-252 spontaneous fission neutron source is 2.3± mcsec. The measurements was made to obtain the dead time of the mixing module. With this purpose the neutron detector was irradiated by the neutron flux from the $^{51}V(p,n)^{51}Cr$ at different value of the ion current. Total number of counts was registered from each of three electronics channels and total number of counts from the output of the mixing module.

The neutron detector has a smooth efficiency response function for the energy range which is typical for the delayed neutrons.

The above mentioned parameters of the detector meet the requirements in measuring the delayed neutron yields and half-lives.

3. Sample transfer system

The main requirements to be taken into account in desining a sample transfer system were to minimize the sample delivery time and ensure against the highly radioactive Np-237 sample against destruction.

The pneumatic transfer system has been constructed. It is capable to transport the sample for the time short enough to measure the delayed neutron yields with the shortest half-lives. Two electromagnetic valves are responsible for the sample transportation route. The stainless steel tube with diameter of 10 mm and wall thickness of 0.3 mm serves as a pneumatic flight guide. The final position of the sample in the neutron detector is fixed by the plug with adjustable central hole which provides the excessive pressure in front of the moving sample and smooths the contact between the sample and the plug.

The information on the sample location is obtained from two photodiodes and light sources installed on a flight tube at the sample irradiation position and the central point of the neutron detector.

The times of sample transportation from the irradiation position to the neutron detector during the test runs were from 300 msec to 500 msec depending on the weight of the samples under investigation.

4. Data acquisition and processing system

The electronic modules for the data acquisition and processing system were developed and constructed almost fully in the IPPE. A schematic diagram of general electronics arrangement is shown in Fig.2 .

The system makes it possible to measure the following parameters: pulse height distributions from two fission chambers located in front of and behind the sample at the irradiation position, time dependence of the neutron flux from the target, time dependence of the ion current on the target, and the time dependence of the delayed neutron activity from the irradiated sample.

The personal computer of the IBM type serves as a central processor controlling the irradiation time, the value of neutron flux at discrete time intervals, the number and width of the time channels for the delayed neutron counting.

The personal computer controls also the operation of the pneumatic transport system and the accelerator mode switches.

The experimental data are stored on the hard disc of the computer. Software for the data acquisition and processing system was written in the PASCAL language.

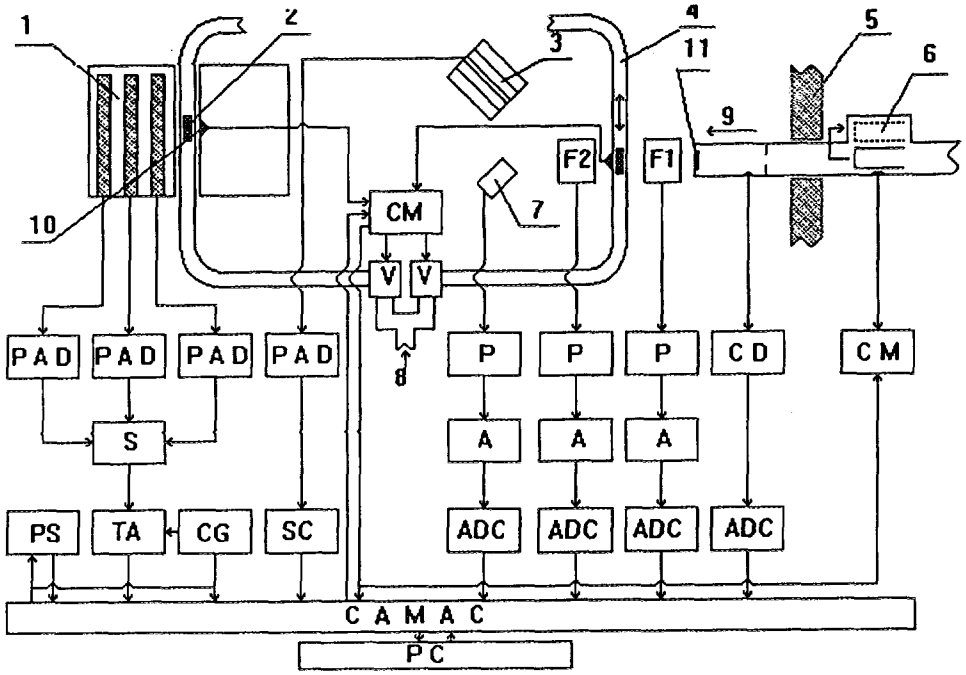

Fig.2. Schematic diagram of the general experimental arrangement and data acquisition and processing system.
P- preamplifier, A- amplifier, D- discriminator, TA- time analyser, SC- scaler, F1 and F2- fission chambers, V1 and V2- electromagnetic, valves, CD- charge digitizer, CM- control module, PS- preset scaler, CG- clock generator, S- summation module, ADC- analog digital converter, 1- neutron detector, 2- sample, 3- BF_3 neutron flux monitor, 4- pneumatic transfer system, 5- shielding, 6- Fradey cup, 7- ^3He spectrometer, 8- gas pressure, 9- ion beam, 10- sample position detector, 11- accelerator target.

5. Neutron detector efficiency.

The absolute efficiency of the 4π neutron detector was determined by two different methods. The first method was the activation method based on the (p,n) reaction and second one is based on the registration of the prompt neutrons from ^{252}Cf source coupled with a surface barrier detector. The Monte Carlo calculations were used to determine the relative efficiency.

5.1. Monte Carlo calculations of the energy dependence of the neutron detector efficiency

The application of the Monte Carlo method for the numerical modeling of radiation transport process in complex media is traditional at the present time. Succsesful imlementation of this method is connected with some advantages as compared with other methods. The main advantages are the following:

1. Monte Carlo method allows to fulfill the discription of a complex gemetric structure with minimum simlification.

2. Model of radiation interactions with materials can be improved to achieve the accuracy restricted only by the uncertainties in nuclear data.

3. Development of computer program for implementation of the Monte Carlo method is quite simple procedure which does not needs any knowledge of the numerical methods.

The choice of the Monte Carlo method to analyze of the processes occuring in the neutron detector is connected with the requirements for correct discription of geometric and physical models of radiation transport phenomena. To solve this problem the combination of the analog and non-analog modelling was used.

Monte Carlo method was used to solve the collision density eguation

$$\psi(x) = \int K(x' \rightarrow x) \cdot \psi(x')dx' + S(x), \qquad (1)$$

where $\psi(x)$ - collision density function,

$S(x)$ - neutron source,

$K(x' \rightarrow x)$ - function of transition from point x' to point x,

$x = \{x, y, z, \vec{\Omega}, E\}$ - point of the many dimentional phase space.

The objective of the calculations is to determine the functional value

$$I = \int \psi(x) \cdot \varphi(x)dx, \qquad (2)$$

where I - rate of the process under investigation,

$\varphi(x)$ - weight function of the neutron detector.

There is another approach to calculate the value I:

$$I = \int \psi^*(x) \cdot S(x)dx, \qquad (3)$$

where $\psi(x)$ - adjoint function related to the process determined by the $\varphi(x)$ function. $\psi^*(x)$ - is determined by the equation

$$\psi^*(x) = \int K^*(x' \rightarrow x) \cdot \psi^*(x')dx + \varphi(x), \qquad (4)$$

If there is a need to calculate the value I with different source function S(x) it is preferable to use the approach determined by the equation (4).

Numerical modelling of the neutron detector configuration was made on the basis of the MMKFK computer code [1]. This computer code was developed for wide range of implementations in reactor physics calculations and experiments, and it has passed many tests. In the present calculations of the energy dependence of the neutron detector efficiency three dimensions geometric module from the MMKFK library was used. Nuclear data group constants was taken from the ABBN-90 library [2]. The function ψ^* was calculated for every ring of BF_3 counters for the group energy intervals 0.01-0.0215, 0.0215-0.0465, 0.0465-0.1, 0.1-0.2, 0.2-0.4, 0.4-0.8, 0.8-1.4, 1.4-2.5, 2.5-4.0, 4.0-6.5, 6.5-10.5 MeV. If the function ψ^* is calculated the set of functionals (3) can be determined according the formula

$$I_S = \int \psi^*(E) \cdot S(E) dE,$$

$\psi^*(E)$ function was calculated for a set of the sources in the form of delta function $\delta(E_i\text{-}E)$ and is presented in the Table 1.

Table 1.

Energy interval, MeV	ψ^* Inner raw	ψ^* Middle raw	ψ^* Outer raw
0.01-0.0215	67.165+/-0.681	64.522+/-0.885	22.547+/-0.424
0.0215-0.0465	65.920+/-0.655	64.222+/-0.763	23.284+/-0.468
0.0465-0.1	64.245+/-0.679	65.712+/-0.666	25.656+/-0.520
0.1-0.2	62.000+/-0.629	65.252+/-0.745	26.802+/-0.497
0.2-0.4	58.510+/-0.613	67.670+/-0.798	29.468+/-0.470
0.4-0.8	51.715+/-0.589	65.366+/-0.744	31.940+/-0.523
0.8-1.4	43.756+/-0.500	59.726+/-0.657	33.125+/-0.505
1.4-2.5	35.115+/-0.420	51.167+/-0.604	31.550+/-0.471
2.5-4.0	29.438+/-0.409	44.366+/-0.522	29.070+/-0.399
4.0-6.5	20.954+/-0.269	33.677+/-0.334	24.453+/-0.409
6.5-10.5	13.942+/-0.270	23.407+/-0.357	17.691+/-0.240

The experimental values were used to test the Monte-Carlo results . For this purpose the relative efficiency of the neutron detector was integrated over the ^{252}Cf prompt neutron spectrum [3] for each ring of BF_3 counters. The measurements made separately for each ring showed a good agreement with the Monte-Carlo calculations for the count rate ratio of the inner-to-middle-to-outer rings of BF_3 counters. The count rate ratios 1.26 : 1.67 : 1 and 1.28 : 1.75 : 1 were obtained in the measurements and the Monte Carlo calculations, respectively. If we will take into account that the integration is fulfilled over the wide range of neutron energies it can be stated that the Monte Carlo calculations give the reliable results for the energy relative dependence of the neutron detector efficiency. Small deviation can be attributed to some anisotropy in the ^{252}Cf-surface barrier detector neutron source. This anisotropy is related to non 2π registation of the fission fragments by the surface barrier detector. The values of the calculated efficiency were corrected for the above deviations in the ring to ring ratio. The influence of the deviation on the final results of the experiment even without correction will be negligable because the energy range of the delayed neutron is ~ 0 - 1.5 MeV. The relative efficiency of the neutron detector is given in Fig.3.

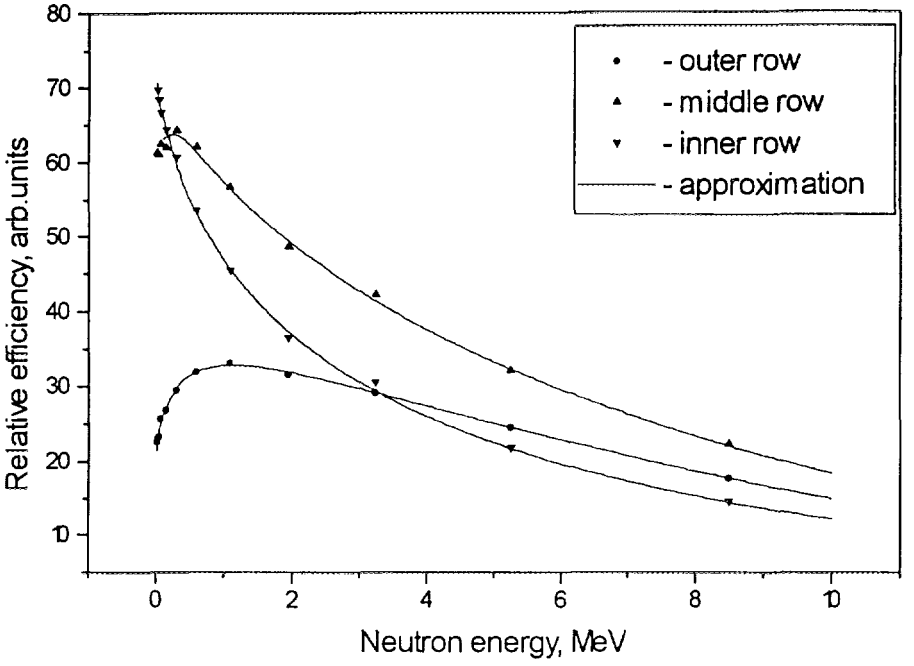

Fig.3. Relative efficiency of the delayed neutron detector calculated by Monte-Carlo method.

5.2. Activation method.

In the measurements of the neutron yield from the (p,n) reaction with 4π neutron detector every time the target is bombarded with the incident beam the ratio of neutrons detected to the total number of residual nuclei produced will give the efficiency of the neutron detector since one residual nucleus is produced for every neutron produced. This method is independent of current integration, target uniformity and target thickness measurements. The $^{51}V(p,n)^{51}Cr$ reaction has been chosen as it has nearly isotropic angular distribution in laboratory system and a suitable value of the decay half life of ^{51}Cr (27.702 days). The isotopic abundance of ^{51}V in elemental vanadium is 99.750 % with ^{50}V as the only other isotopic constituent. Decay of ^{51}Cr produces a 0.320 MeV gamma ray 9.83 % of the time.

The targets used in the present measurement were made from metallic vanadium by evaporation in vacuum on the copper backings of 0.3 mm thick and 11.6 mm in diameter. The vanadium targets were placed in the water cooled target holder perpendicular to the charged particle beam line (zero degrees) at the centre of the 4π neutron detector. A schematic diagram of experimental arrangement used in the measurements of delayed neutron detector efficiency by the activation method is presented in Fig.4.

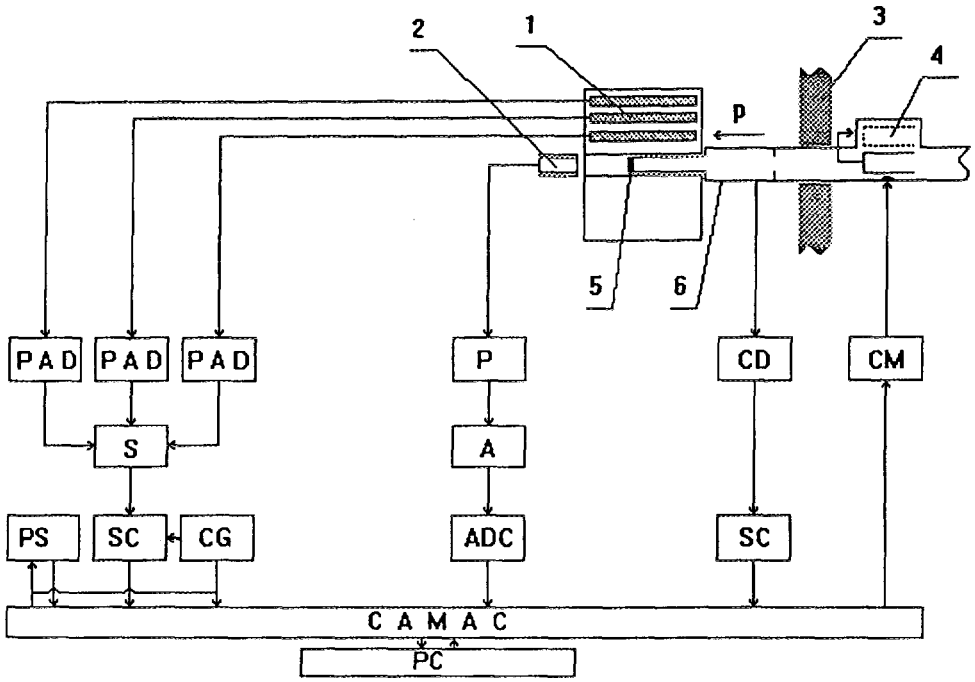

Fig.4. Schematic diagram of experimental arrangement for delayed neutron detector efficiency measurements. P- preamplifier, A- amplifier, D- discriminator, SC- scaler, CD- charge digitizer, CM- control module, PS- preset scaler, CG- clock generator, S- summation module, ADC- analog digital converter, 1- delayed neutron detector, 2- ^{3}He spectrometer, 3- shielding, 4- Faradey cup, 5- ^{51}V target, 6- target holder.

After irradiation an activity measurements for ^{51}Cr was made. This measurement involved counting 0.320 MeV gamma radiation with a Ge(Li) detector (see Fig.5.).

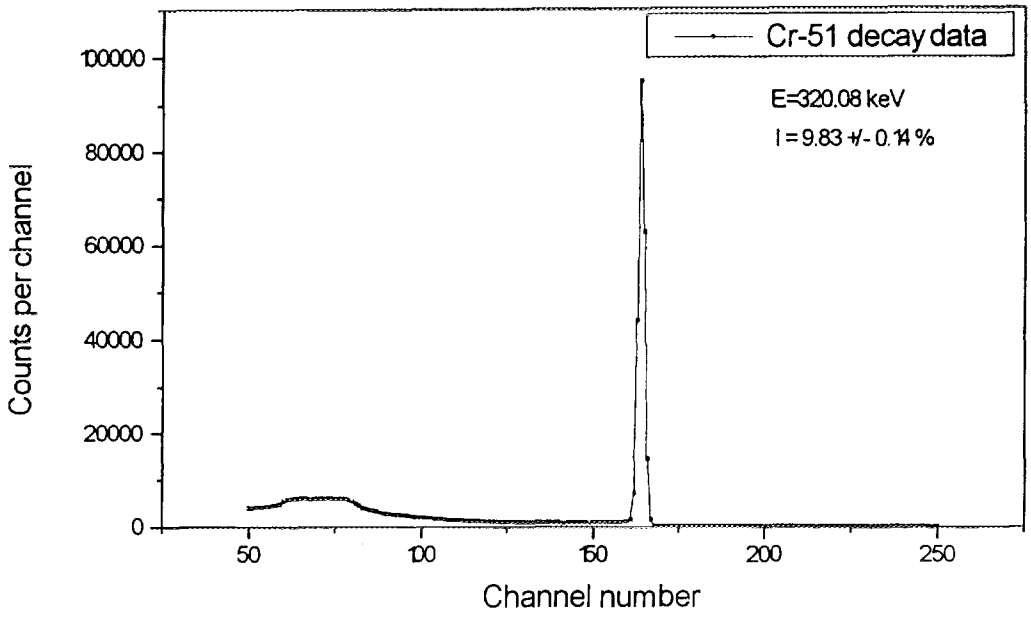

Fig.5. ^{51}Cr gamma-ray spectrum measured by Ge(Li) detector.
Irradiation time 3 hours.

Each irradiated target was counted in a well-defined geometric position close to the detector. Calibration of the Ge(Li) was ultimatly based upon two standard radioactive sources. One source was ^{152}Eu. The second was ^{133}Ba. Both of these standards were point source on thin backings. Neither standard gamma source yielded a gamma-ray line near 320 keV where the calibration was needed. Consequently, several computational steps were made in order to obtain the desired calibration.

5.2.1. Calibration of the Ge(Li) detector energy scale

The relationship between pulse height for a full-energy peak line and the gamma ray energy is nearly linear over a moderate range of energies if high-quality electronics components are used in the pulse analysis. Nonlinearities must be taken into account to realise the full accuracy potential of these detector systems. Nonlinear effects are especially impotant for low gamma ray energies or for calibration of very wide energy ranges.

Energy scale calibration was achived by utilizing two gamma ray sources: ^{133}Ba and ^{152}Eu. As a first step a calibration data base was obtained. These data consist of sets of multiplets (x_i, dx_i, E_i, dE_i), where x_i is the peak channel for gamma ray of energy E_i. The dx_i are the uncertainties in the peak channels while dE_i are the reported errors in the energies of the calibration lines. The calibration procedure was to represent the energy E as a function of x, E(x). The polynomial relation was choosen for this purpose

$$E(p,x) = \sum_{k=1}^{m} p_k x^{k-1}$$

5.2.2. Efficiency of the Ge(Li) detector.

Absolute efficiency of the Ge(Li) detector was obtained on the measurements performed using an absolutely-calibrated gamma-ray sources ^{133}Ba and ^{152}Eu. The relationship between efficiency ε and photon energy E was approximated by the formula with the purpose to obtain the value ε for the gamma-ray energy E = 320 keV

$$\ln(\varepsilon) = \sum_{j=1}^{m} p_j (\ln E)^{j-1}$$

5.2.3. Absolute efficiency of neutron detector

Absolute efficiency ε_n of 4π neutron detector was obtained on the basis of number events recorded by the neutron detector during irradiation time t and appropriate activity value of ^{51}Cr

$$\varepsilon_n = \frac{\Sigma_n}{t \cdot RR},$$

where RR = reaction rate related to activity of ^{51}Cr,
Σ_n = total number events recorded by the neutron detector,
t = irradiation time.

Reaction rates based on the measurements of ^{51}Cr activity have been calculated using the following expression:

$$RR = \frac{A}{b\varepsilon} \cdot \frac{\exp(\lambda\tau)\lambda}{f[1-\exp(-\lambda T')][1-\exp(-\lambda t)]} \cdot \frac{\delta_1}{\delta_2\delta_3\delta_4\delta_5},$$

where
A= peak area of the 320 keV gamma ray line of ^{51}Cr,
b= gamma-ray branching ratio,
ε = Ge(Li) detector efficiency in the vicinity of the 320 keV gamma ray energy,
τ = time from end of irradiation to start of count,
t = irradiation time,
T = live count time,
T' = real count time,
f = T/T' ,
λ = disintegration constant for ^{51}Cr isotope,
δ_1 = correction for finite source diameter,
δ_2 = correction for real coincidence summing,
δ_3 = correction for random summing,
δ_4 = correction for gamma-ray self-shielding,
δ_5 = correction for attenuation in external absorbers.

The neutron energy spectrum from the $^{51}V(p,n)$ neutron source was measured by the ^{3}He spectrometer installed behined the neutron detector(Fig.6)

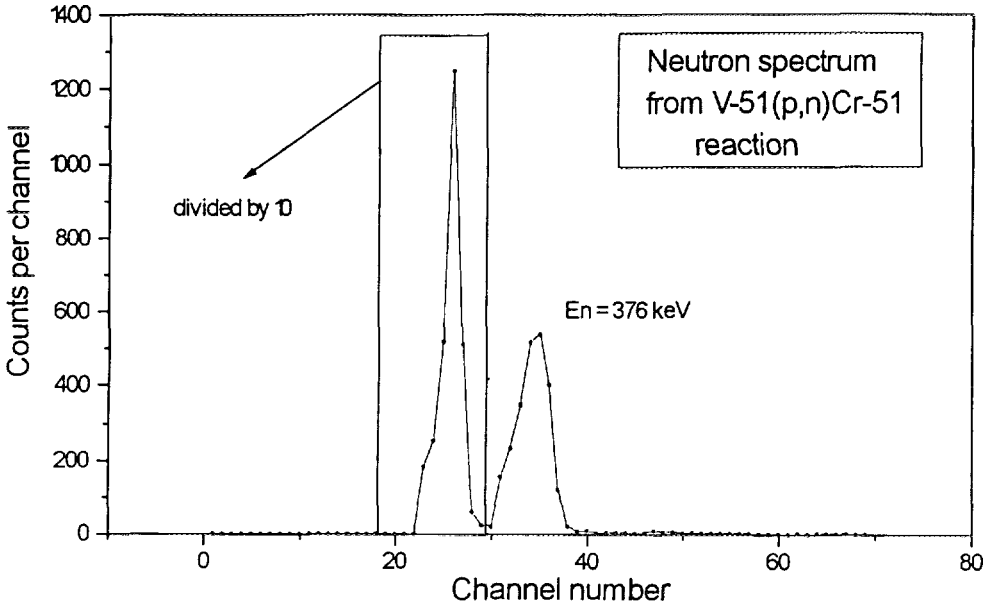

Fig.6. Neutron energy spectrum from $^{51}V(p,n)^{51}Cr$ reaction measured by ^{3}He spectrometer.

As a result the absolute value of 0.084 ± 0.004 for the neutron detector efficiency have been obtained in the vicinity of 0.376 MeV neutron energy.

5.3. Method based on ^{252}Cf neutron source.

The second method was based on the counting the prompt neutrons from spontaneous fission in ^{252}Cf source. The number of fission events was determined by a silicon surface barrier detector placed closely to ^{252}Cf source. Both the detector and the neutron source are placed in vacuum chamber located in the centre of 4π neutron detector. A fission pulse from the silicon surface barrier detector was used to initiate the process of counting the neutron detector output by the multiscaler module of the LP4840 multichanell analyser. Experimental data obtained for the outer row of BF_3 counters is shown in Fig.7. The value of background was obtained on the basis of the approximation of the experimental data by the expression ~ $a + b \cdot \exp(-ct)$.

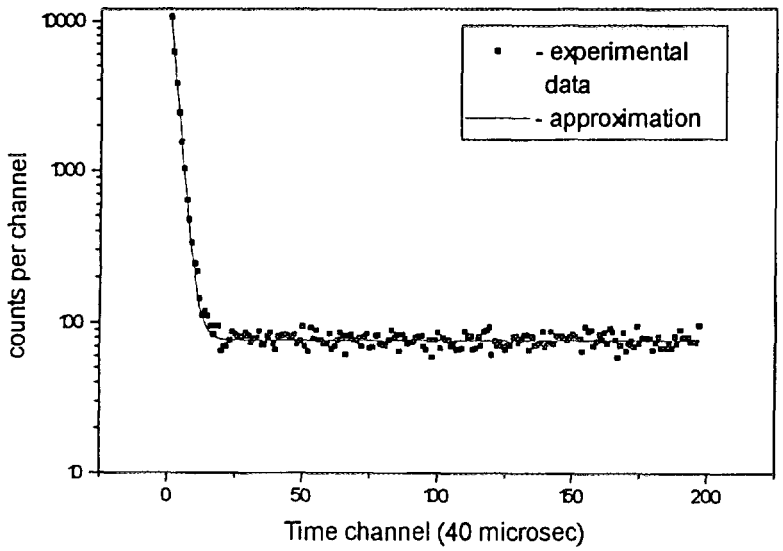

Fig.7. Time dependence of ^{252}Cf prompt neutrons registered by delayed neutron detector.

The value of the total number of the ^{252}Cf prompt neutrons obtained in such measurements was used to make normalization of the relative efficiency calculated by the Monte-Carlo techniques according the following formula

$$k = \frac{\int \varepsilon(E_n) \cdot N(E_n) dE_n}{\int \psi^*(E_n) \cdot N(E_n) dE_n},$$

$$\varepsilon(E_n) = k \cdot \psi^*(E_n),$$

where $\varepsilon(E_n)$ - absolute efficiency of the neutron detector,
$\psi^*(E_n)$ - relative efficiency of the neutron detector,
$N(E_n)$ - the ^{252}Cf prompt neutron spectrum [3],
k - normalization factor.

The value defined by the integral $\int \varepsilon(E_n) \cdot N(E_n) dE_n$ was measured in the multiscaler mode experiment for each row of the neutron detector.

The measurements of the efficiency of the neutron detector showed that count rate ratio between rings of BF_3 counts is very sensitive to the energy of the detected neutrons. Therefore it was proposed to use this effect for measurements of the average energy of delayed neutrons.

The resulting energy dependence of the neutron detector efficiency was obtained on the basis of polinomials fit to the normalized relative efficiency data

$$\varepsilon(E_n) = \sum_{m=1}^{m=k} A_m (\ln(E_n))^{m-1}$$

The results of the Monte Carlo calculations and its approximation data normalized by k normalization factor is shown in Fig.8.

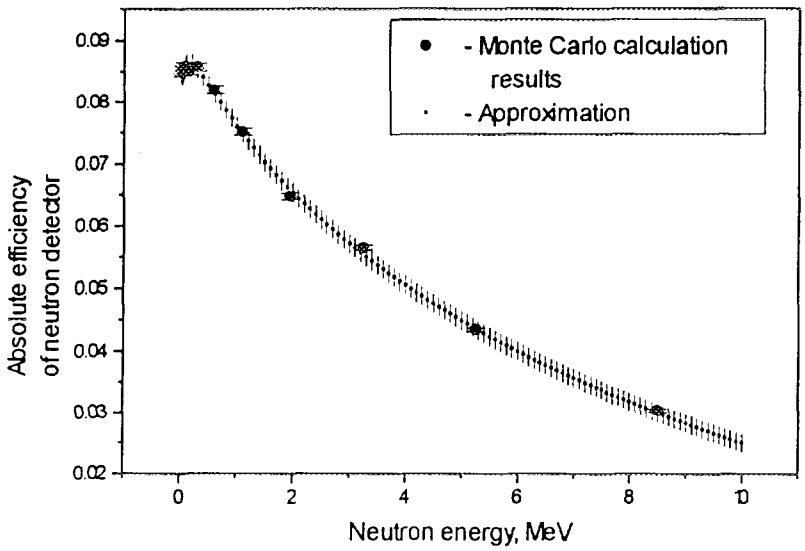

Fig.8. Absolute efficiency of delayed neutron detector.

The values of absolute efficiency obtained by both method are in agreement. But the values obtained by ^{252}Cf neutron source method have the better accuracy. Therefore these values was used in the final calculations of the total delayed neutron yield.

6. ^{237}Np sample.

The ^{237}Np samples were prepared from neptunium dioxed powder in the form of cylinders 0.56 cm in diameter and 0.35 cm in height. The sample fabrication process involved high preasure apparatus to increase the density of the neptunium samples up to 7 g/cm^3. Each sample was enclosed in stainless steel capsule with 0.3 mm thick walls. These capsules prevented the ^{237}Np from escaping during transportation of the samples between the irradiation and counting positions. The capsules utilized in the experiment passed the leak tests. Then the capsules with ^{237}Np were protected against shocks by enclosing them in thin titanium cans. Each can contains 4 capcules of the high density neptunium with total weight of up to 2 g. The total number of ^{237}Np atoms in the sample was $(5.1063 \pm 0.0025) \bullet 10^{21}$.

7. Fission rate measurements

The number of fission events occuring in the sample during irradiation is one of the parameters needed for the determination of the absolute total yields of delayed neutrons. Two methods are considered. The first one is based on the irradiation of the known number of atoms contained in the sample under investigation followed by nondestructive absolute gamma-ray assay of the fission product atoms contained in the sample. For obtaining the number of fissions in the Np-237 sample one needs to know the half-lives of the fission products, emission probabilities of the gamma rays and the fission yields of these fission products (Ru-103, I-131, Ba-140/La).

The second method is based on the experimental procedure in which the Np-237 sample is attached to two low-mass fission chambers and the entire assembly is placed at zero degrees near the accelerator target. The fission detectors of this assembly provides quantitative information on neutron fluence in the vicinity of the Np-237 sample where such irradiation is performed. The derived value of the neutron flux passed through the Np-237 sample is used to obtain the number of fissions in the Np-237 sample.

The second method was considered to be the more reliable. The established method has three distinct features: determination of the isotopic mass of the fissionable deposits, recording with precision a fraction of fission fragments originating within the deposit when exposed to a flux of neutrons, and, calculation procedure to obtain on this basis, the number of fissions in the Np-237 sample.

7.1. Fission chambers and isotopic mass of the fissionable deposits.

The fission ionization chambers are designed and constructed as low-mass, parallel-plate ionization counters. The backings of the fissionable deposits and the chamber electrodes are made of 0.2 mm thick aluminum and have a diameter of 20 mm. Thin deposits are made of neptunium dioxide. To reduce neutron absorption and scattering effects, the mass of each piece of the chamber has been kept to a minimum. Connections for electronic cables and gas tubing are made at the chamber manifold, more than 30 cm from the chamber. Conventional pulse processing electronics are used in the measurements. A 90% argon and 10% CO_2 gas mixture is used as the gaseous medium in the chamber.

A satisfactory separation between pulses from the ^{237}Np α-decay and majority of the fission fragments was achieved with a spacing of 0.5 cm between the deposit plate and the collector plates (0.2 mm thick Al). Testing of the chamber performance, made on the fast neutron flux at the cascade generator, showed that there is a good separation of the fission fragment peak and peak due to alpha particles, electronics noise and neutron-induced components. The peak-to-valley ratio of the pulse-height distribution is about 30. The ^{237}Np fission fragment spectrum is given in Fig.9.

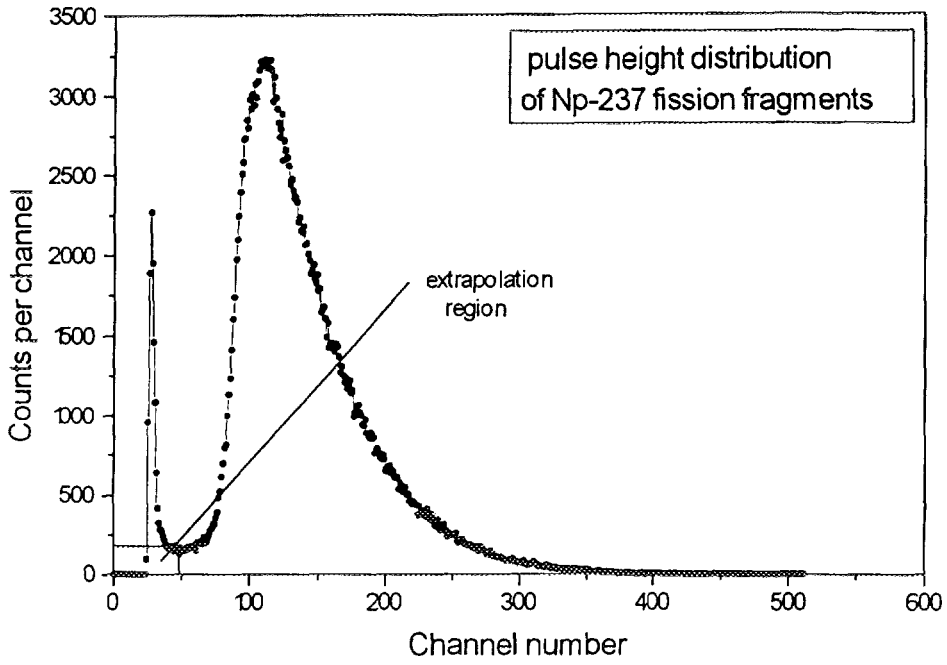

Fig.9. Pulse-height distribution for ^{237}Np fission.
The pulse-height distribution of valid fission pulses is assumed to be flat in the range from valey to zero channel.

The physical stability of the samples was assured by α-counting before and after the present experiment. Changes were less than 0.15% with counting statistics of 0.1%.

The isotopic mass assesment for the deposits is based on two methods: absolute alpha counting in the fission ionization chamber with the appropriate gas pressure value, and low-geometry alpha counting at various distances from a surface barrier detector. The α-spectrum obtained in 2π counting geometry is shown in Fig.10. Most of the the counts came from the ^{237}Np decay and 1.25 % came from the^{238}Pu and/or ^{241}Am decay.

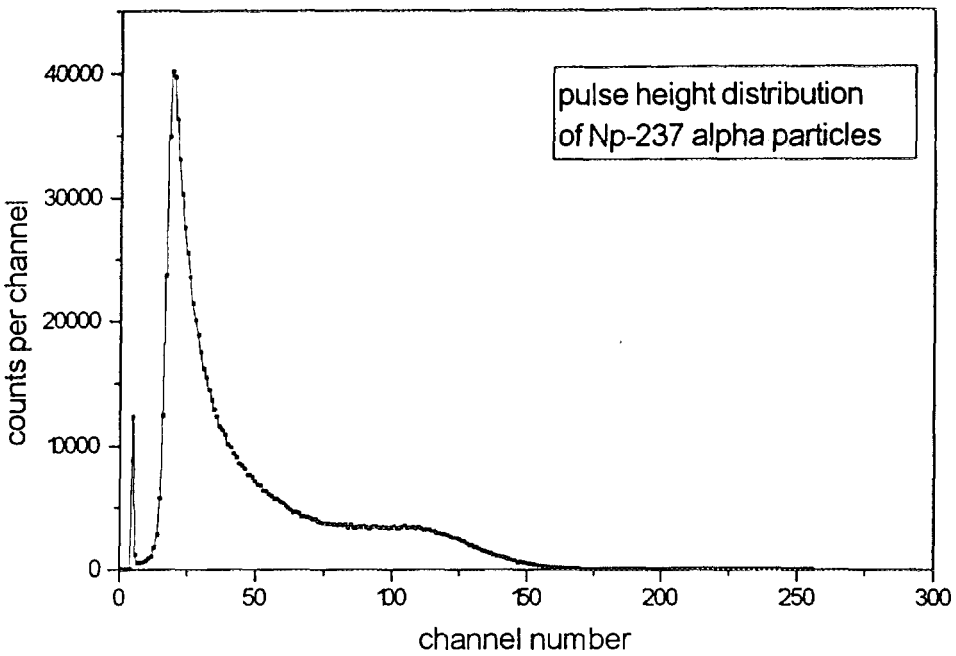

Fig.10. ^{237}Np alpha spectrum measured in 2π counting geometry.

The α-pulse height spectra also contain a low energy tail which ammounts to as much as 0.43 % for the deposit No.1 and 0.37 % for the deposit No.2. A value of (2.14 ± 0.01)10^5 y [5] was used for the half-life of ^{237}Np. A half-life of (87.74 ± 0.05) y was used for the α-decay of ^{238}Pu [6]. Analysis of α-spectra from both fission chambers yielded the number of ^{237}Np atoms $7.499 \cdot 10^{17}$ and $6.225 \cdot 10^{17}$ for the first and second fission chambers respectively. Corrections for random summing during alfa-particle counting were made. The value of this correction for the first chamber was 0.63 % and for the second one - 0.52 %.

The value of the fission chamber efficiency for the counting fission events depends mainly on the thickness of the fissionable deposits. Accuracy of this value is determined by the procedure used for the extrapolation of fission fragment pulse height distributions to zero pulse-height. In the present measurements the extrapolation to zero pulse-height was carried out with flat extrapolation assumption.

7.2. Neutron flux calculation

Knowledge of the neutron spectrum from the target which is limited to zero degrees is inadequate because the ^{237}Np samples and the neptunium deposits of fission chamber subtended substantial solid angles (as it is in typical poor-geometry irradiation environments). The neutron fluence must therefore be represented by an energy- and angle- dependent function, $\varphi(E_n,\theta)$.

For an accurate analysis of experimental ν_d data the precise value of the average effective neutron energy and its uncertainty as well as the energy and angle distribution of the incident neutrons are required. Without further corrections the measured ν_d value can be different from the true one due to a different energy and angle dependence of

some factors needed to introduce corrections in experimental data (e.g. attenuation factor). The influence of the neutron energy and angle distribution profile on the an experimental results depends on the shape of that distribution. In general such a distribution cannot be described by a single parameter, as e.g. in case of a Gaussian or a rectangular distribution.

The Monte Carlo method was chosen to calculate energy and angle distribution profiles for neutrons from T(p,n) source reaction, for incident proton energies from the threshold to 2 MeV, titanium-tritium targets and various irradiation geometries. The Monte Carlo neutron source results was used in further Monte Carlo calculations of the fission rate in the fission chambers and the ^{237}Np sample.

The kinetic neutron energy E_n in the laboratory system results from instantaneous projectile proton energy E_p and the angle of neutron emission, θ, according to the reaction kinematics. Protons hitting the target with an incident energy E_{po} are slowed down to energy $E_{po}-\Delta E_p$ within a titanium-tritium target. The energy loss ΔE_p is the first contribution to the neutron energy spread.

Angular straggling predominantly due to multiple small-angle scattering also occurs during the slowing down of the protons in the target.

A third contribution to the neutron energy spread results from the spread in neutron emission angles due to the finite size of the ^{237}Np samples, fission layer and beamspot. When using extended samples the variation of the distance beamsport to sample-volume element along the sample has to be considered additionally. Both the proton straggling and the finite solid angle subtended by the sample with respect to the neutron source contribute significantly to the width of the final neutron energy distributions according to the slope of the functional dependence neutron energy versus neutron emission angle.

The most correct way to calculate the final neutron energy distribution profiles for a variety of irradiation geometries and irradiation angles with the final purpose to obtain the fission rate in the sample under investigation is to introduce the Monte Carlo method. All contributions to the energy spread can be taken into account simultaneously as they physically occur. Therefore all existing correlations are then considered automatically. This procedure avoids the problems encountered in a different method to obtain the total energy spread in experiment from separatly estimated distribution widths for the various contributions to the final energy resolution, i.e. how to properly combine the corresponding distribution parameters. Adding the partial FWHMs in quadrature in oder to get the total FWHM would be correct if all distributions involved were Gaussian and correlations amongst these contributions could be neglected. The latter is certainly not fullfilled for the partial processes contributing to the total energy spread of the produced neutrons.

In the present analysis the Monte Carlo calculations for the T(p,n) neutron source were made on the basis of the approach developed by Kornilov and Kagalenko [7]. The azimuthal angle φ_i was taken as equidistributed one. In each history numbered by the index i the source coordinates and the coordinates of the point of interaction between the neutron and the sample are chosen by random sampling on the basis of equidistribution within the circular beam spot and within the ^{237}Np sample (or ^{237}Np deposit in fission chamber), respectively. The direction of the scattered proton and the neutron emission angle θ_i are fixed, as the direction of the emitted neutron is given by the coordinates of the source and sample element.

The neutron energy in the laboratory system $E_{ni}(E_{pi},\theta_i)$ and the yield anisotropy factor $f_i(E_{pi},\theta_i)$ are calculated for every history according to the reaction kinematics. The weight factor ω_i is given by the following expresion

$$\omega_i = \sigma(E_{pi}) \cdot c(E_{pi}) \cdot ((dE/dx)(E_{pi}))^{-1} \cdot f(E_{pi}, \theta_i) / d_i^2,$$

where $\frac{dE}{dx}(E_{pi})$ - the stopping power, $c(E_{pi})$ - the tritium concentration, $\sigma(E_{pi})$ - the source reaction cross section, d_i - distance between the point of the neutron origion in the target and the point of the neutron interaction within ^{237}Np sample or ^{237}Np deposit in the fission chambers.

Fission rate in the neuptunium sample during irradiation is the sum of incremental fission rate components, namely

$$R_f = \sum_{ijl} R_{fij}(E_l)$$

The incremental fission rates can be calculated using the following formula

$$R_{fij}(E_l) = \varphi_{fijl} . \sigma_f(E_l) \cdot n_f \cdot V_{fj} \cdot \eta_{fij}(E_l) \cdot l_{fij}^{-2} \cdot M_s,$$

where $\varphi_{fij}(E_l)$ - neutron/sr·sec, in the energy group E_l emitted from the target element i in the direction of the ^{237}Np sample element with volume V_{fj},

l_{fij} - distance from the neutron source target element i to the center of the sample element V_{fj},

n_f - number of atoms/cm^3 in the ^{237}Np sample,

$\sigma_f(E_l)$ - differential ^{237}Np fission reaction cross section in vicinity of neutron energy E_l,

$\eta_{fij}(E_l)$ - neutron absorption factor,

M_s - neutron multiple-scattering correction factor.

A neutron absorption factor for ^{237}Np sample is calculated by taking the sample, fission chamber and target holder construction materials into consideration. Calculation of the absorbtion factor $\eta_{fij}(E_l)$ is accomplished using the formula

$$\eta_{fij}(E_l) = \exp[(-\Sigma_f \cdot x_{ij} - \Sigma_b \cdot x_b) / \cos(\theta_{fij})] \ ,$$

where Σ_f - ^{237}Np sample macroscopic total cross section,

Σ_b - macroscopic total cross section for materials between the ^{237}Np sample and ion beam spot,

x_{ij} - sample thickness between point of neutron entrance and point of its interaction with sample material,

b - thickness of material between the sample and target beam spot.

The same calculational procedure was applied to fission chamber.

The developed approach was checked in an experiment which was conducted with the purpose to obtain the fission rates in the fission chamber for the different distances from the beam spot. The experimental results was compared with Monte Carlo calculation values. As can be seen in Fig.11 the calculated results can be considered as reliable.

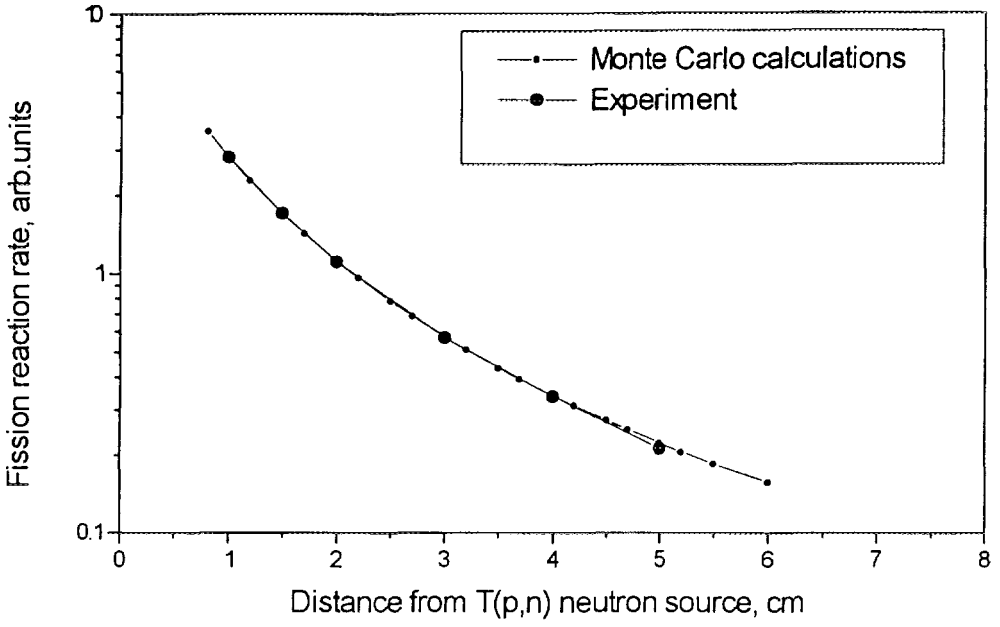

Fig.11. Fission reaction rates in the fission chamber at different distances from T(p,n) neutron source.

8. Accelerator equipment adjustment

In order to conduct the measurements of the total delayed neutron yields within the framework of the developed method, the work has been done on the appropriate preparation of accelerator systems. The main objective of this work was to design a device for switching on the ion beam to the accelerator target to start the irradiation of the Np-237 sample and switching off the ion beam from the target at the begining of the delayed neutron counting. Such a device has been constructed on the basis of the remotely controlled changes of the Faradey cup positions. The Faradey cup serves as a "beam stop" unit. The testing of the system shows that the time for switching off the ion beam is 150 msec. Control for accelerator mode operation is achived by the central processor of the data aquisition and processing system. Fig.12 presents the time dependence of the neutron flux incident on the sample after switching off the ion beam (t = 0 sec).

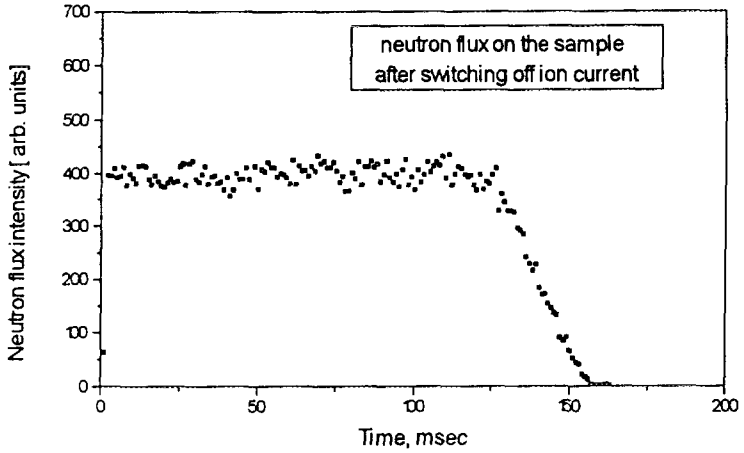

Fig.12 . Neutron flux intensity after end of irradiation.

9. Measurements of the total yield, relative abundancies and periods of delayed neutrons for fast netron induced fission of ^{237}Np

Measurements of the total yield, relative abandancies and periods of delayed neutrons have been made using the method developed on the basis of electrostatic accelerators of the IPPE. The set-up was installed at the cascade generator CG-2.5. Monoenergetic neutrons were generated by means of the $T(p,n)^3He$ reaction. The measurements included two independent types of experiments. The first type was conducted with the purpose to obtain the relaive abundacies and periods of delayed neutrons for ^{237}Np fission by 1.2 MeV neutrons. In the second type of experiment the total delayed neutron yield was measured.

9.1. Measurement of the total delayed neutron yields.

The total delayed neutron yield for fast neutron fission of ^{237}Np was measured using experimental arangement, which was discussed in details earlier and is shown in Fig.2. The neptunium sample was irradiated up to saturation during 300 sec. After irradiation the ion beam was cut off by the Faradey cup and the sample was delivered to the neutron detector for counting the decay of delayed neutron activities. Time interval for counting this activities was $\approx$ 700 sec. Time-channel widths of 0.01, 0.1, 1, 10 sec following in automatic sequence were used in the present measurement. After counting period the measurement procedure was repeated.

The fission rate in the neptunium sample was measured by two parallel-plate fission chambers positioned in the front of and behind the sample. The usually used geometry configuration is shown in Fig.13.

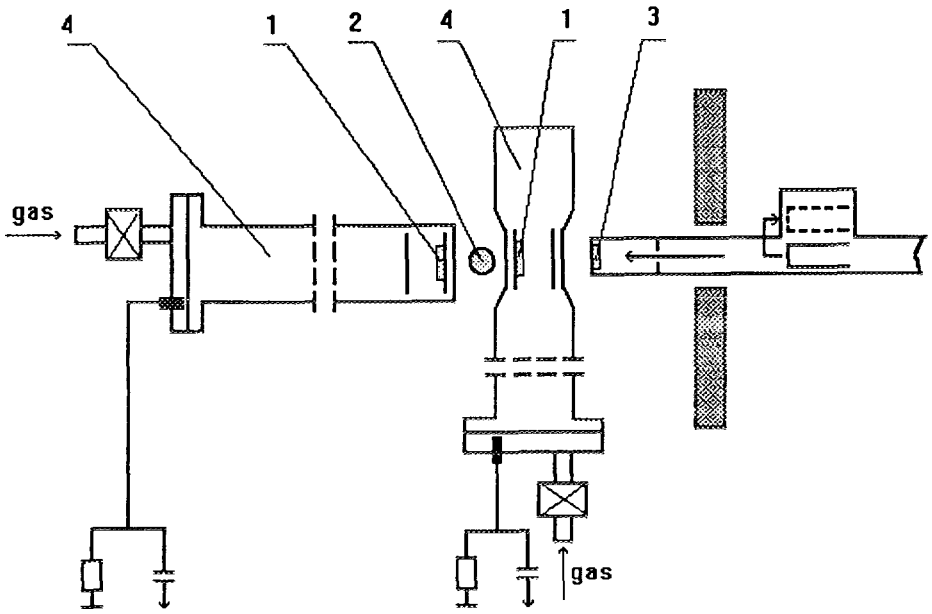

Fig.13. Geometry configuration used in measurements of the total delayed neutron yields.

9.2. Measurement of group periods and relative abundance values of delayed neutrons.

Measurement of group periods and relative abundace values of delayed neutrons was made on the basis of the same experimental configuration as it was in the case of the total delayed neutron experiment. To obtain the appropriate statistical accuracy needed for the fitting procedure the ^{237}Np sample was installed in the vicinity of the target. Only a relative neutron flux monitor was used since in this experiment there was no need for information on the fission rate in the neptunium sample. The decay delayed neutron data were recorded for each irradiation and then were accumulated in one curve for one measurement. An example of such data is shown in Fig. 14. The curve comprise of 69 irradiation data.

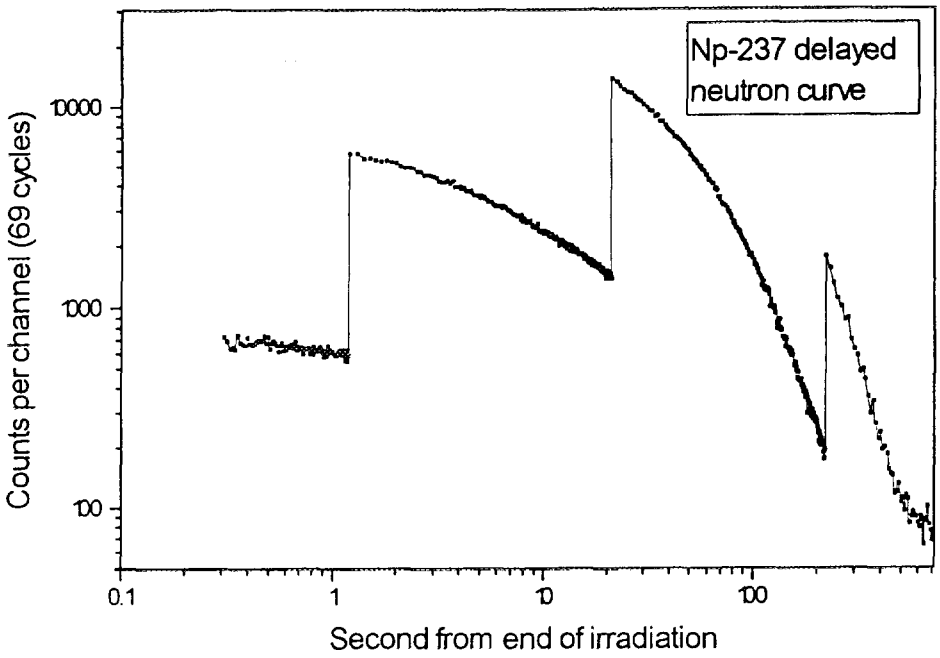

Fig.14. Delayed neutron intensity following of ^{237}Np irradiation by 1.154 MeV neutron.

9.3. Relative neutron flux monitor.

In both type of experiment it is essential to be able to relibly monitor neutron output from the source. Relative neutron-dose monitoring from irradiation to irradiation is required in oder to be able to normalize the results obtained from measurements where data for unknown processes and for standard are acquired from distinct exposures (i.e. space distribution of neutron flux from the target). Another reason why it is desirable to continuously monitor the neutron output from the source is that this monitoring provides a sensitive measure of the stability of the target and the constancy of the neutron spectrum. This aspect is espessialy important in the activation type of experiment in which there is a strict demand for the constancy of the neutron output during irradiation of the sample. Deterioration of the target is readily sensed during a measurement by changes in the neutron yield per unit of incident beam charge on the target.

A standard boron-triflouride detector in a typical "long-counter" type configuration was used. It provided a good efficiency, a high degree of stability, moderate sensetivity to changes in the neutron environment and insensitivity to radiation other than neutrons.

In the Figs.15 and 16 there are representative members of the set of recorded time dependence of neutron flux and ion charge during irradiation of the sample. Having such information one can readily make correction for dependence of neutron flux in time if this correction needed.

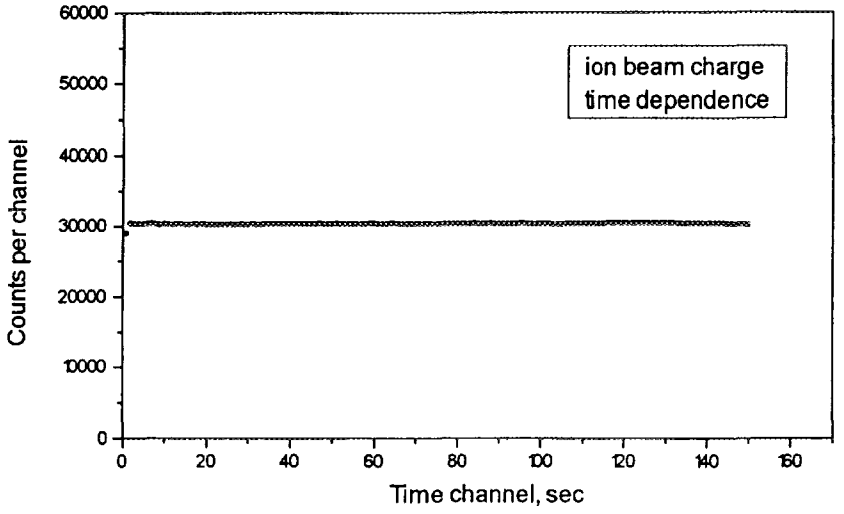

Fig.15. Time dependence of ion beam charge during irradiation.

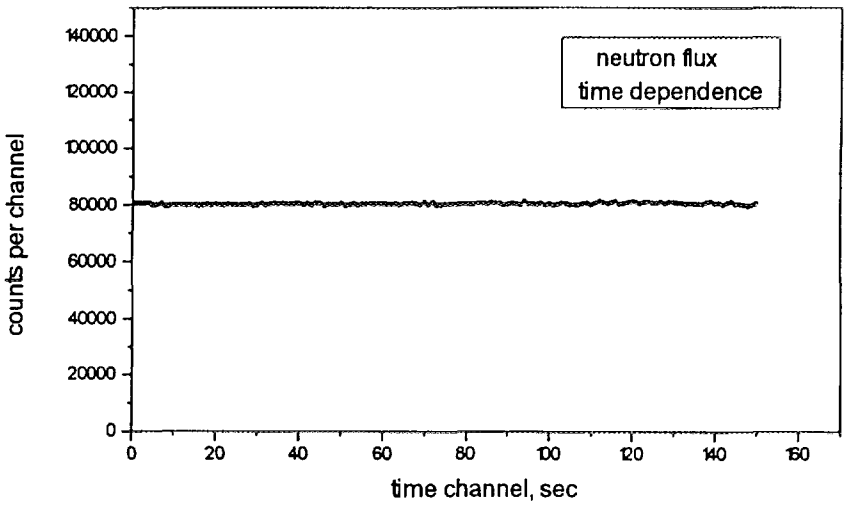

Fig.16. Time dependence of neutron flux during irradiation.

10. Preliminary experimental results

10.1. Group periods and relative abundance values

The total number of delayed neutrons $N(t_k)$ detected during a time channel t_k of duration Δt_k for the cyclic measurements can be given by

$$N(t_k) = \sum_i T_i \cdot \frac{a_i}{\lambda_i} \cdot e^{-\lambda_i t_k} (1 - e^{-\lambda_i \Delta t_k}) ,$$

where

$$T_i = (1 - e^{-\lambda_i t_i})\left(\frac{n}{1 - e^{-\lambda_i T}} - e^{-\lambda_i T} \cdot \frac{1 - e^{-n\lambda_i T}}{(1 - e^{-\lambda_i T})^2}\right),$$

λ_i and α_i - decay constant and relative yield of the i -th group of delayed neutrons, t_k - time channel, n - number of cycles, T - duration of one cycle, which includes the irradiation and delayed neutron counting time, t_i - irradiation time.

Group periods and relative abundance values for ^{235}U were obtained from a total of 55 irradiations. (A simultaneous solution of all periods and abundancies for the six group approximation were used) At the first step the analysis of delayed neutron decay data was made for the time $t \geq 3.5$ sec where the contributions from the two shortest periods can be neglected. In the analysis the least squares method were used with initial estimates for the group constants taken from [8]. As a result of analysis the periods and abundancies for the first and second groups were determined. Then these data were used(fixed) in analysis of delayed neutron decay curve for the time interval from $t \geq 0.3$ sec up to 720 sec (the whole time range used in the experiment). At this step the relative abundance and period were determined for groups 3 to 6. The final results are given in the Table 2 for the six group abundances, periods along with the values of Keepin [8] and Besant [9].

Table 2 . ^{235}U group relative abundances and periods

	Group number						
	1	2	3	4	5	6	reference
i							
a_i	0.040±0.004	0.233±0.006	0.181±0.007	0.422±0.008	0.101±0.005	0.024±0.001	Present
T_i	55.30±0.41	22.16±0.21	6.59±0.23	2.40±0.05	0.74±0.04	0.163±0.008	values
a_i	0.038±0.003	0.213±0.005	0.188±0.016	0.407±0.007	0.128±0.008	0.026±0.003	Ke [8]
T_i	54.51±0.94	21.84±0.54	6.23±0.26	2.30±0.07	0.519±0.035	0.178±0.016	Ke [8]
a_i	0.035±0.002	0.234±0.003	0.216±0.069	0.290±0.055	0.178±0.038	0.047±0.013	Be [9]
T_i	53.32±0.28	21.26±0.13	5.13±0.41	2.521±0.348	0.829±0.150	0.185±0.045	Be [9]

Group periods and relative abundancies for ^{237}Np were obtained on the basis of experimental data which were measured with different irradiation times. In the analysis of the delayed neutron time-dependence the data with irradiation time of 300 sec were used to obtain the group constants for the first and second group of delayed neutrons. These data were analysed with the iterative least squares program for the time interval 3.5 - 721 sec after end of irradiation. Group constants for the third to the sixth group have been obtained from the data measured in the experiment with irradiation time of 15 sec. The group constants obtained from the long time irradiation data were fixed in the analysis of short irradiation data. The analysed ^{237}Np data were obtained from the total of 265 irradiations. The final results on the relative abundances and periods of delayed neutrons for fission of ^{237}Np by 1.154 MeV neutrons are given in the Table 3.

Table 3. ^{237}Np group relative abundances and periods

	Group number						
i	1	2	3	4	5	6	ref.
a_i	0.032±0.003	0.257±0.077	0.205±0.008	0.395±0.009	0.095±0.005	0.0159±0.0008	Present
T_i	55.18±0.49	22.71±0.18	5.65±0.20	2.14±0.07	0.436±0.021	0.196±0.010	values
a_i	0.040±0.005	0.254±0.008	0.206±0.008	0.372±0.011	0.106±0.010	0.0221 a)	Be[10]
T_i	54.579±0.85	21.797±0.41	5.635±0.092	2.180±0.027	0.673±0.111	---	Be[10]
a_i	0.0400	0.2162	0.1558	0.3633	0.1659	0.0589	Br a)[11]
T_i	52.116	21.935	5.934	2.306	0.780	0.251	Br a)[11]
a_i	0.030±0.008	0.230±0.053	0.180±0.058	0.415±0.087	0.069±0.018	0.074±0.037	Ru a)[12]
T_i	55.452	21.865	5.251	2.113	0.672	0.277	Ru a)[12]
a_i	0.042±0.009	0.233±0.028	0.190±0.027	0.359±0.050	0.145±0.019	0.0314±0.014	Gu[13]
T_i	55.900	22.216	5.415	2.303	0.619	0.210	Gu[13]
a_i	0.035±0.003	0.230±0.023	0.066±0.031	0.144±0.061	0.400±0.050	0.124±0.029	Wa[14]
T_i	55.011	22.652	10.615	4.987	2.113	0.428	Wa[14]

a) - calculated values

10.2. Absolute delayed neutron yield

Absolute delayed neutron yield ν_d was obtained on the basis of the following formula

$$N_d = \sum_{t1}^{t2} N(t) = \langle \varepsilon \rangle \cdot F_S \cdot \nu_d \cdot \sum_i T_i \cdot \frac{a_i}{\lambda_i} \cdot (e^{-\lambda_i t_1} - e^{-\lambda_i t_2})$$

$$T_i = (1 - e^{-\lambda_i t_i})\left(\frac{n}{1 - e^{-\lambda_i T}} - e^{-\lambda_i T} \cdot \frac{1 - e^{-n\lambda_i T}}{(1 - e^{-\lambda_i T})^2}\right)$$

where N(t) - delayed neutron emission rate at time t after irradiation, λ_i and α_i - decay constant and relative yield of the i -th group of delayed neutrons, t_1 and t_2 - time of the beginning and the end of delayed neutron counting, n - number of cycles, T - duration of one cycle, which includes the irradiation and delayed neutron counting time, t_i - irradiation time, F - fission rate in the sample under investigation, $\langle \varepsilon \rangle$ - efficiency of neutron detector averaged over delayed neutron spectrum.

The delayed neutron production rate from a number of repetitive cycles can be considered as the production rate from a single cycle in the infinitely long sequence. In such case the fission rate F is the total number of counts in the sample divided by the time of one cycle irradiation t_i. The fission rate in the sample F_s can be represented by the following expression

$$F_S = \frac{N_S}{t_i} \int \phi(E_n, \theta, \varphi) \cdot \sigma(E_n) dE_n d\Omega_S ,$$

where N_s - number of atoms in the ^{237}Np sample,

Ω_s - solid angle subtended by the ^{237}Np sample,

$\phi(E_n, \theta, \varphi)$ - absolute neutron flux from the target.

The fission rate F_s was calculated by the Monte Carlo method on the basis of the approach discribed in the section . In this approach the relative neutron flux $\varphi = k \bullet \phi$ from the target was used. The absolute value of the neutron flux was obtained on the basis of the number of counts in the fission chamber N_c measured during irradiation period of the each cycle and appropriate Monte Carlo calculations

$$N_C = N_f \int k \cdot \varphi(E_n, \theta, \varphi) \cdot \sigma(E_n) dE_n d\Omega_f ,$$

where N_f - number of ^{237}Np atoms in the fission chamber deposit,

Ω_f - solid angle subtended by the fission chamber deposit.

The final expression for the fission rate in the sample can be written in the following form

$$F_S = \frac{N_C \cdot N_S \int \varphi(E_n, \theta, \varphi)\sigma(E_n) dE_n d\Omega_S}{N_f \cdot t_i \int \varphi(E_n, \theta, \varphi)\sigma(E_n) dE_n d\Omega_f}$$

The total yield of delayed neutrons for ^{237}Np was obtained for a total of 54 irradiations. The average energy of neutrons induced fissions in the sample is 1.154 MeV with standard deviation of 0.159 MeV. The irradiation time was 300 sec. A background for delayed neutron counting was determined by the analysis of delayed neutron curve using the iterative least squares procedure with fixed a_i , T_i which were obtained in a separate experiment. The value of background was 5.606 ± 0.114 counts per sec. The total counting time for one cycle was 721.2 sec. The total yield, based on the mean of data from both fission chambers was:

$$\nu_d = 0.01180 \pm 0.00072$$

Table 4. Total delayed neutron yield for ^{237}Np fission.

Neutron energy MeV	Total yield neutron/fission	Method	Reference
1.154	0.01180±0.00072	Experimental	Present value
Fast neutrons	0.0122 ± 0.0003	Experimental	Benedetti [10]
Fast neutrons	0.01142 ± 0.00160	Experimental	Gudkov [13]
Fast neutrons	0.01068 ± 0.00098	Experimental	Waldo [14]
Fast neutrons	0.0120 ± 0.0015	Calculation	Rudstam [12]
Fast neutrons	0.0128 ± 0.0013	Calculation	England [15]
Fast neutrons	0.0114±0.0012	Calculation	Brady [11]
Fast neutrons	0.0108	Evaluation	ENDF/B-5

References

1. V.Korobeinikov, MMKFK-2 computer code for reactor application.
2. Abagjan, et. al., ABBN-90 library of group constants.
3. W.Manhart, Proceedings of an Advisory Group Meeting

on Properties of Neutron Sources organized by the IAEA, Leningrad, USSR, 9-13 June, 1986, IAEA- TECDOC-410, p. 158.
4. R.C.Greenwood, R.G.Helmer, J.W.Rogers et al., Nucl. Tech., 25(2), 1975, p. 274.
5. W.L.Zijp, J.H.Baard, "Nuclear Data Guid for Reactor Neutron Metrology. Part I :Activation Reactions; Part II : Fission reactions", Report EUR 7164 EN (ECSC-EEC-EAEC, Brussels-Luxembourg, 1981).
6. A.Lorenz, First Coordinated Research Meeting on the Measurement of Transactinium Isotope Neuclear Data, report INDC(NDS)-96/N, IAEA, Vienna, 1978.
7. N.V.Kornilov, Proceedings of an Advisory Group Meeting on Properties of Neutron Sources organized by the IAEA, Leningrad, USSR, 9-13 June, 1986, IAEA- TECDOC-410, p. 230.
8. G.R.Keepin, T.F.Wimett and R.K.Zeigler, J. Nuclear Energy, 1956.
9. C.B.Besat, P.J.Challen, M.H.McTaggart et al., J. Br. Nucl. Energy Soc., 16, Apr., No. 2, p.161-176, 1977.
10. G.Benedetti, A.Cesana, V.Sanqiust, M.Terrani and G.Sandrelli, Nucl. Sci. Eng., 80, p. 379 , 1982.
11. M.C.Brady, T.R.England, Nucl. Sci. Eng., 103, p.129, 1989.
12. G.Rudstam, Nucl. Sci. Eng., 80, p.238, 1982.
13. A.N.Gudkov, V.M.Zhivun, A.V.Zvonarev et al., At. En., 66, p.100, 1989.
14. R.W.Waldo, R.A.Karam, Trans. Am. Nucl., 39, p.879, 1981.
15. T.R.England, W.B.Wilson, R.E.Schenter and F.M.Mann, Nucl. Sci. Eng., 85, p.139, 1983.

3. 4 Measurements of ^{237}Np secondary neutron spectra

Direction 3 (Group leader Kornilov N.V.)

Abstract

The activities carried out during the first year of the project are summarized. The main problems for Np spectra measurements arise from high intrinsic gamma-ray activity of the sample and admixture of the oxygen and iron nuclei. The inelastically scattered neutrons and the fission neutrons spectra for ^{237}Np were measured by time-of-flight spectrometer of the IPPE at incident neutron energies ≈1.5 MeV, and ≈0.5 MeV. A solid tritium target and a Li-metallic target were used as neutron sources. The neutron scattering on C sample (C(n,n) standard reaction) was measured to normalize the Np data. The experimental data should be simulated by Monte Carlo method to correct the experimental data for oxygen and iron admixture as well as for multiple scattering of the neutrons in the sample. Therefore the response function of the spectrometer, and the neutron energy distribution from the source were investigated in detail.

1. Experimental method

1.1 Pulsed neutron sources

The neutron spectra were measured by time-of-flight (TOF) technique with the EG-1 accelerator spectrometer of the IPPE (Ref.1,2). The parameters of the spectrometer are the following: pulse width is ≈2 ns, repetition rate is 2 MHz, flight path is ≈2 m, mean current on the target is 4-6 μA. The experimental layout is shown in Fig.1. The T(p,n) reaction in a solid tritium-titanium target was used as a neutron source at energy range 1-2.5 MeV. The target thickness was ≈0.4 mg/cm^2. Neutrons with the energy ≈0.5 MeV were produced with Li(p,n) reaction. The metallic Li-target was prepared inside the accelerator pipe 'in setu'. The target was evaporated on a steel polished backing 0.05 cm thick. The target thickness was ≈0.6 mg/cm^2. The water layer 0.1 cm thick cooled the target. In the main the experimental method was previously applied to carry out ^{235}U, ^{238}U secondary neutron spectra measurements [3].

1.2 Samples

Np sample was manufactured from NpO_2 powder packed in stainless steel container. The container is a cylinder with wall thickness 0.1 mm and bottom thickness 0.3 mm. The container weight is 19.9 g. The dimension of the powder volume is 45 mm in height and 47 mm in diameter.

The NpO_2 weight is 189.1 g. The carbon sample is 47 mm in outer diameter, 27 mm in inner diameter and 45 mm in height. The C-sample weight is 82.8 g. The samples were placed ≈10 cm away from the target.

1.3 Main detector

The neutron detector was a stilbene crystal with 70 mm in diameter and 50 mm thick. The scintillator was viewed by a photomultiplier tube (PMT) FEU-30. The detector face was covered with lead absorber 20 mm thick to reduce the gamma-ray background of the sample. In addition the pulse shape analysis was used to discriminate γ-rays. The count rate for the sample gamma-rays by the detector placed at ≈200 cm distance from the sample was ≈1.9 10^4 s^{-1} (no shielding) and it was ≈60 s^{-1} (20 mm Pb shielding). The detector was operated in fast-slow coincidence mode which allowed us to reduce the contribution of photomultiplier noise. The detector was shielded with a movable collimator.

1.4 Monitors

There were three monitors:

i) "long" counter to make relative measurements of the neutron yield;

ii) TOF monitors to check the neutron source parameters and the proton pulse width. The monitors consist of a plastic scintillator (25 mm in diameter and 5 mm thick) coupled with PMT FEU-143. One of them (3 in Fig.1) was placed 70 cm away from the target and the other one (10 in Fig.1) supplied with shielding was placed at ≈300 cm flight path to measure the neutron energy distribution of the target.

1.5 Spectra measurement

All spectra were measured at the angle 120-deg. Each measurement consisted of 10-12 runs with duration of about one hour. For each initial neutron energy at least two measurements were performed with the investigated sample. Some additional measurements were made of:

- neutron spectrum with the container,
- neutron spectrum with the C-sample,
- background spectrum (no sample).

The electronic set up is shown in Fig.2. For each run the following data arrays were collected: two-dimension distributions (TOF*pulse height (PH) - 512*128 channels) for main detector in coincidence with neutrons and gamma-rays (time channel width 1.005 ns); TOF spectrum for

monitor (10) - 512 channels (channel width 0.987 ns); TOF spectrum for monitor (3) - 2048 channels (channel width 0.22 ns). In addition the one-dimension spectra from ADC and TDC connected with main detector were collected as well. Two-dimension spectrum for Np-sample is shown in Fig.3.

2. Investigation of main detector properties

The main detector parameters were measured with the standard ^{252}Cf fission neutron spectrum (Ref.5), when the sample was replaced by the fast ionization chamber with ^{252}Cf source (Ref.9). Fission fragments count rate was 8.15 $10^4 s^{-1}$. The following parameters were measured in this experiment: detector efficiency, pulse height response, and time resolution as functions of neutron energies.

The detector efficiency was measured for two high voltage supplies i.e. 1.9 kV and 1.8 kV. In the first case the detector sensitivity to low energy neutrons was increased very much. However, high energy pulses were rejected due to the dynamic range limitation. This mode was applied to make inelastic neutron spectra measurements. In second case we have higher efficiency for high energy neutrons and this mode was used to measure the fission neutron spectra at ≈0.5 MeV. The detector efficiencies are shown in Fig. 4.

The time resolution depends on detector properties (scintillator, PMT, timing discriminator) and pulse height response for the separated neutron energy. The time resolution was described by the following expression:

$$\rho(t,t_0) = \sum_{i=1}^{i_{max}} a_i(E)\rho_i(t,t_0), \quad \sum_{i=1}^{i_{max}} a_i(E) = 1. \qquad (1)$$

where $\rho_i(t,t_0)$ is the time distribution for i-th pulse height channel; $a_i(E)$ is a pulse height response for neutron energy E; $\rho(t,t_0)$ is the time resolution for neutron energy E. We assumed that $\rho_i(t,t_0)$ and $\rho(t,t_0)$ are the Gauss functions. Hence the second central momentum σ of the $\rho(t,t_0)$ may be calculated with the formula:

$$\sigma^2(E) = \sum_{i=1}^{i_{max}} a_i(E)\sigma_i^2 \qquad (2)$$

Some responses of the detector are shown in Fig.5. The time resolution of the detector versus neutron energy is presented in Fig.6. The increase at E>4 MeV is accounted for by discrimination of high energy amplitudes.

3. Data processing

At the first stage of data processing the monitor time-of-flight spectra were applied to verify the quality of the accelerator performance in each run (time resolution, energy stability). The spectra of "good" runs were summed up. The time independent background was subtracted from overall spectra. The detector spectrum was measured as two-dimension array, therefore the zero-effect time interval was known for each PH channel. The contents of the channels in these time intervals were set to zero after the background was subtracted. After this procedure TOF distributions for each PH channels were summed up to calculate the total TOF spectra. This background subtraction resulted in the improvement of measurement accuracy in the low energy range of neutron spectrum. The resulting time spectrum was normalized to the counts of the "long" counter. The TOF spectra for the ^{237}Np run and the container run are shown in Fig.7,8 (time independent background was subtracted). Neutron energy increases with increasing of the TOF channel number.

The peak at ≈420 channel is due to sample γ-rays (fission and inelastic scattering). The smooth distribution at >310 channel is produced by fission neutrons. The following peculiarities of the ^{237}Np TOF experimental spectrum should be highlighted.

There are three peaks in the middle of TOF scale. The more intensive ones are connected with elastic scattering on Np (higher energies) and O nuclei. The peak at ≈230 channel (see also Fig.8) is due to the neutrons inelastically scattered by Fe nuclei. The sample nuclei ratio is 1:2:0.5 (Np:O:Fe) therefore, we can not use rather a simple procedure i.e. subtraction of the container spectrum from sample spectrum run to estimate the net spectrum. The correction for neutron scattering on the Fe nuclei (as well as O nuclei) should be calculated by Monte Carlo (MC) method. For this purpose the MC codes BRAND [6] which allows us to simulate all specific features of the experiment are used. To separate correctly peak-like contribution from admixture nuclei and the background neutrons due to scattering on target environment we investigated the neutron source properties in detail.

4. Neutron source spectrum

The energy-angular distribution of the neutrons escaped from the solid tritium target was calculated by Monte Carlo method according to the recommendation of Ref.7. The following factors were taken into account:

- space distribution and energy spread of incident protons,
- energy losses in target (target thickness and its distribution), energy and angle straggling,
- the variations of the neutron energy and reaction cross section with the angle of neutron escape.

A set of parameters and functions (proton energy losses, neutron energy versus angle) are needed for this calculation. Most of them were taken from well known systematics (see Ref.7) or were estimated by simple geometric measurements. The two parameters i.e. the average target thickness and the variation of the thickness were estimated from monitor data measured in the same experimental run. Experimental and MC calculated results presented in Fig.9 are in a quite agreement.

A monoenergetic neutron source has an admixture of background neutrons with energy $E<E_0$. These neutrons arise mainly due to scattering on the target environment and their contribution is rather small. However, being elastically scattered on sample nuclei (Np, O, Fe) they give the effect which is comparable with inelastic scattering. Therefore, an additional experiment with the main detector placed at various angles relative to the proton beam and for various incident proton energies was carried out. The targets on Cu and Mo backing were used in these measurements. The measured neutron spectrum from the Cu(Ti) target for 0^0 angle together with MC calculated spectrum are shown in Fig. 10. As one can see in Fig. 10 the experimental spectrum has a rather long low energy tail which can not be accounted for by neutrons scattered on target materials. There exists a particular problem for near peak region. The origin of these "tail" neutrons and the way of their accounting for in MC simulations are the task for further investigation.

4. Fission neutron spectra.

The inelastic scattered neutrons are interfered with fission neutrons. The fission cross section and number of prompt neutrons for ^{237}Np were measured at energy range of interest in many works. However, the fission neutron spectra were measured in two works only (≈5 and ≈7 MeV[8], 2.9 MeV, and 14.7 MeV[9]) and the results are rather scattered. Therefore to estimate the inelastic cross sections with high accuracy we need some additional measurements of fission neutron spectra. Besides, some basic problems for fission neutron emission still exist. As it was shown in works [10,11] the incorporation of the hypothesis about the neutrons being emitted during fragment acceleration improves the description of the experimental data in energy range from 0.01 MeV up to ≈30 MeV. Only one free parameter α (fragment kinetic energies at the moment of neutron emission) was used to fit the calculated curves to experimental data within experimental errors. Now we do not know the nature of this phenomenon (pre-acceleration emission or any correlation between fragment excitation and kinetic energies), however it seems that the fact that $\alpha<1$ should be used for data evaluation.

The TOF fission neutron spectra at ≈0.5 MeV neutron energy measured in the frame of the project is presented in Fig. 11. The Li-target was used in this experiment. The energy spread for incident neutrons was ≈50 keV. After the correction for sample size and admixture of O and Fe nuclei, the data will be analyzed by the method suggested in Ref.11. As an example, the results of the ^{238}U data analyses are shown in Fig. 12,13.

The fission spectrum will be evaluated with respect to carbon scattering in an absolute scale. This fact will give some additional information about the spectrum shape ($\nu\sigma$ data Ref. 3) The 0.5 MeV result together with the data measured in the 1-2 MeV energy range will serve as a basis for ^{237}Np fission neutron spectra analysis.

So one may conclude that the work planned for the first year of the project was carried out completely.

REFERENCES

1. N.V.Kornilov, A.B.Kagalenko et.al. Preprint FEI-2174, Obninsk,1991.

2. N.S.Birukov, V.N.Kanaki, V.I.Trikova, preprint FEI-2132, Obninsk, 1990.

3. N.V.Kornilov, A.B. Kagalenro., Nucl. Sci. and Engin. 120(1995)55,

4. W.Mannhart, Proc. Advisory Group Meeting on Properties of Neutron Sources, Leningrad, June 1986, Report IAEA-TECDOC-410, Ed. K.Okamoto, Vienna,1986, p.158.

5. V.Ya.Baryba, N.V.Kornilov, N.N.Semenova, VANT (Voprosi atomnoi Nauki i Techniki), 1977, 5(19), p45,

6. A.A.Androsenko, P.A.Androsenko et. al. VANT (Voprosi atomnoi Nauki i Techniki), ser Fizika i Tekh. Yadernykh Reaktorov, 1985, v.7, p.33.

7. N.V.Kornilov, see Ref.4, p.230.

8. Trufanov A.M., Lovchikova G.G., et al., Yader. Fyz., 55 (1992) 298,

9. Boikov G.S., Dmitriev V.D. et al., Phys. of Atomic Nucl., 57 (1994) 2047, Translated from Yad. Fyz. 57 (1994) 2126,

10. Kornilov N.V., Kagalenko A.B., Yad. Fyz., 57 (1994) 1240,

11. Kornilov N.V., Kagalenko A.B., Dubna 1994, ISINN-2, 116,

12. M.Baba, H.Wakabayashi, N.Ito et.al. Jour. of Nucl. Scien. and Tech.(1990), 27(7), p.601.

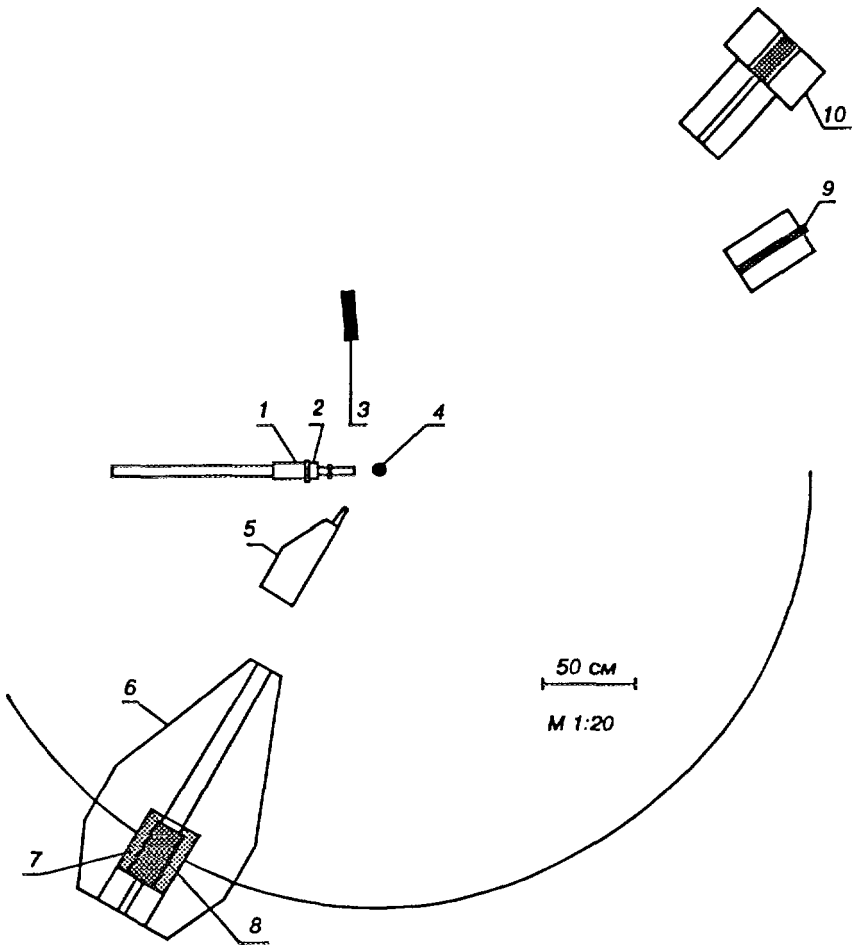

Fig. 1 Experimental layout of the IPPE spectrometer.
1 - pick-up electrode,
2 - neutron source,
3- TOF monitor for pulse width control,
4 - sample,
5 - shielding bar,
6 - shielding collimator of the main detector,
7 - lead shielding,
8 - main detector,
9 - long counter,
10 - TOF monitor for neutron target control.

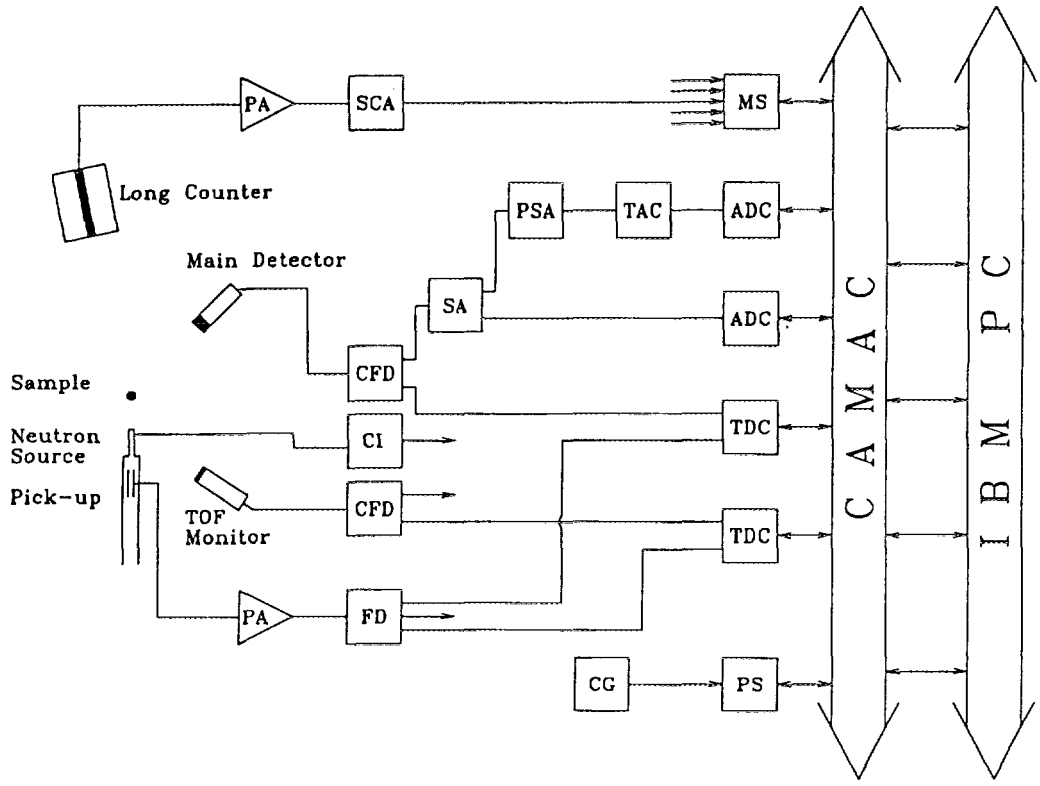

Fig.2 Electronic set up of the TOF spectrometer. CFD - constant fraction discriminator, SA - shape amplifier, PSA- pulse shape analyzer, TAC - time to amplitude converter, ADC - analog to digit converter, TDC - time to digit converter, CI - charge integrator, FD - leading edge discriminator, CG - clock generator, MS - multy channel scaler, PS - preset scaler.

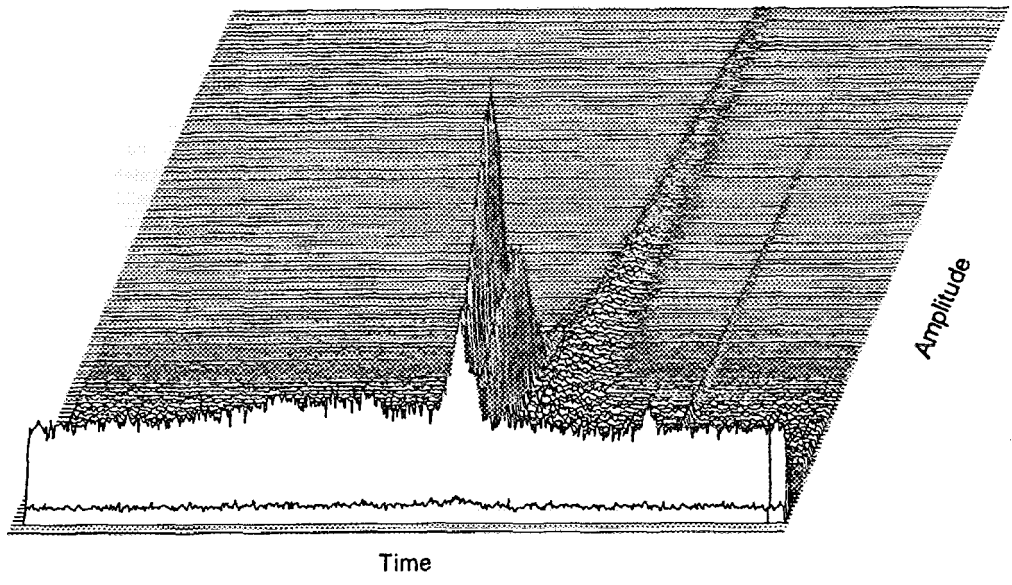

Fig.3 Two-dimension distribution for main detector (neutron coincidence).

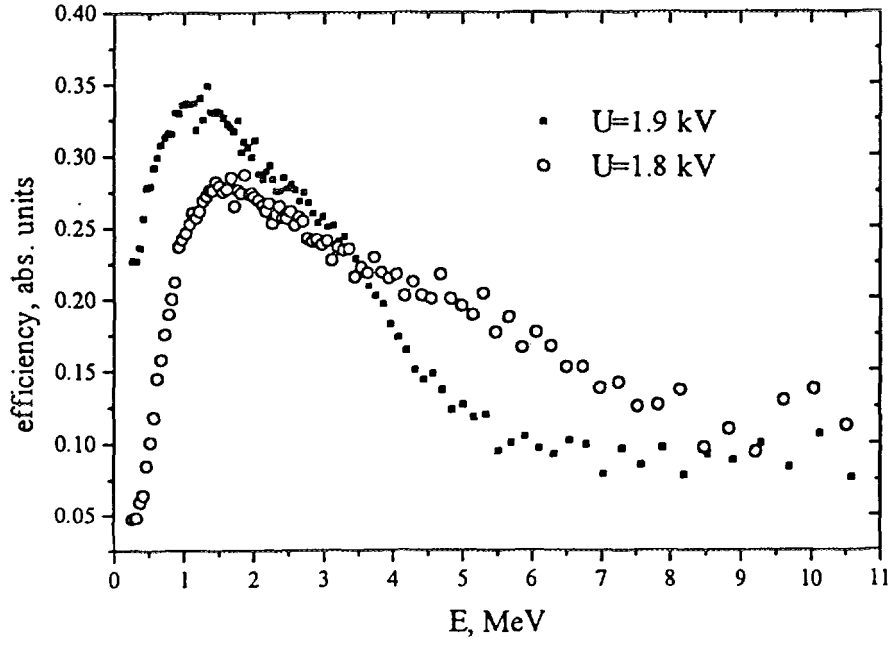

Fig.4 Main detector efficiencies as function of neutron energies for two high voltage supplies.

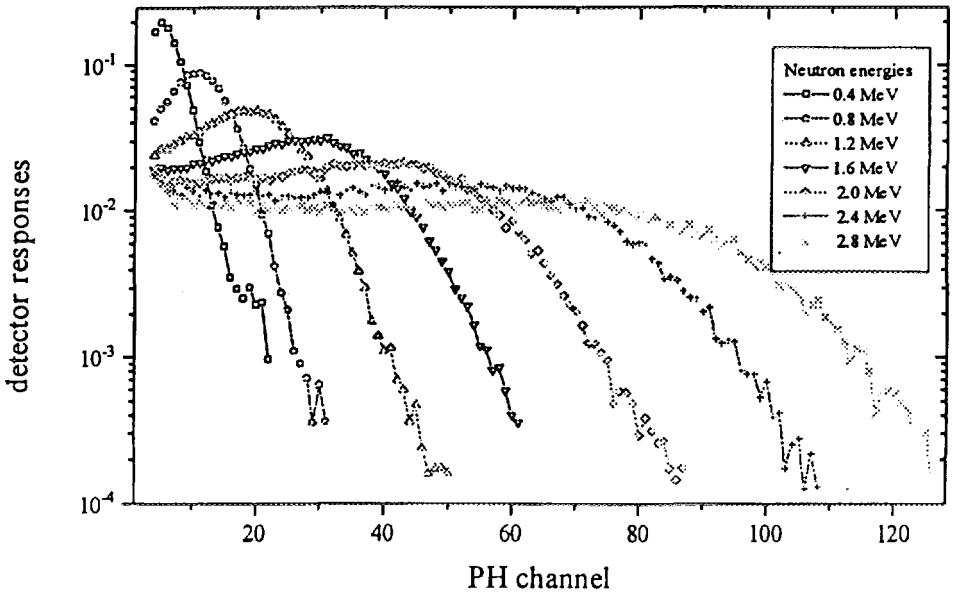

Fig.5 Detector responses versus PH channel for various neutron energies.

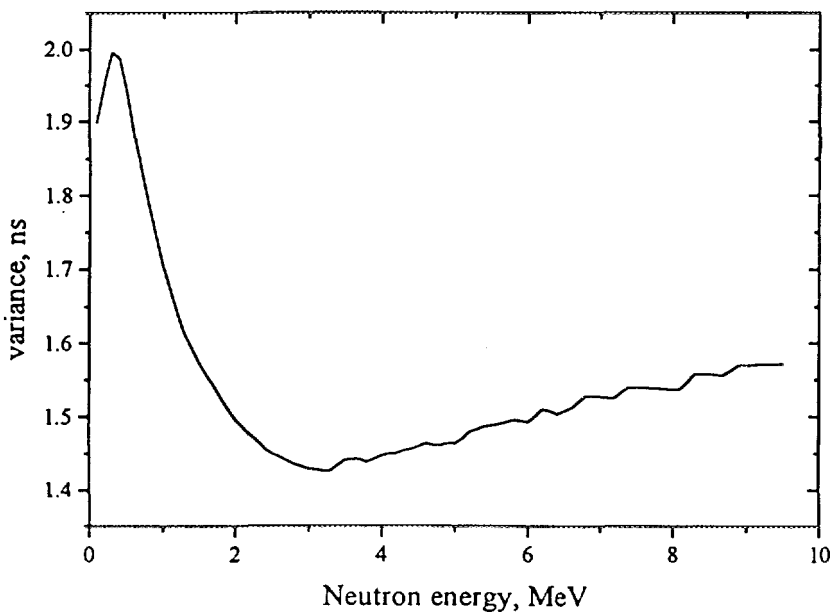

Fig.6 Time resolution of the detector as function of neutron energy.

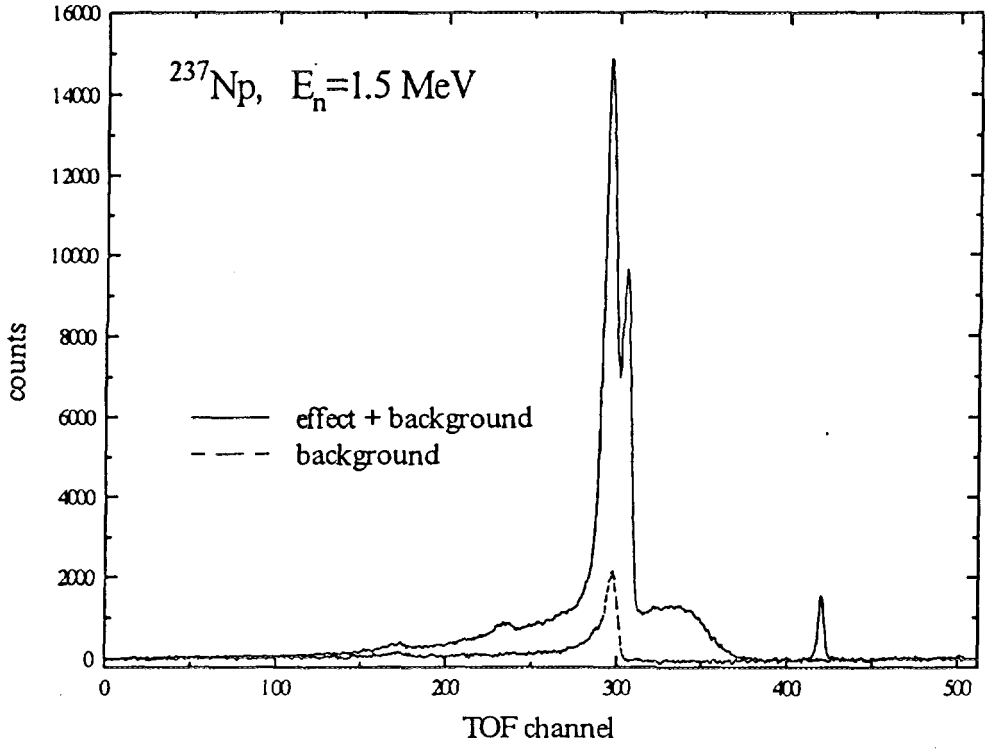

Fig.7 TOF spectra for Np sample run and no sample run after the subtraction of time independent background. The spectra are normalized for long counter number.

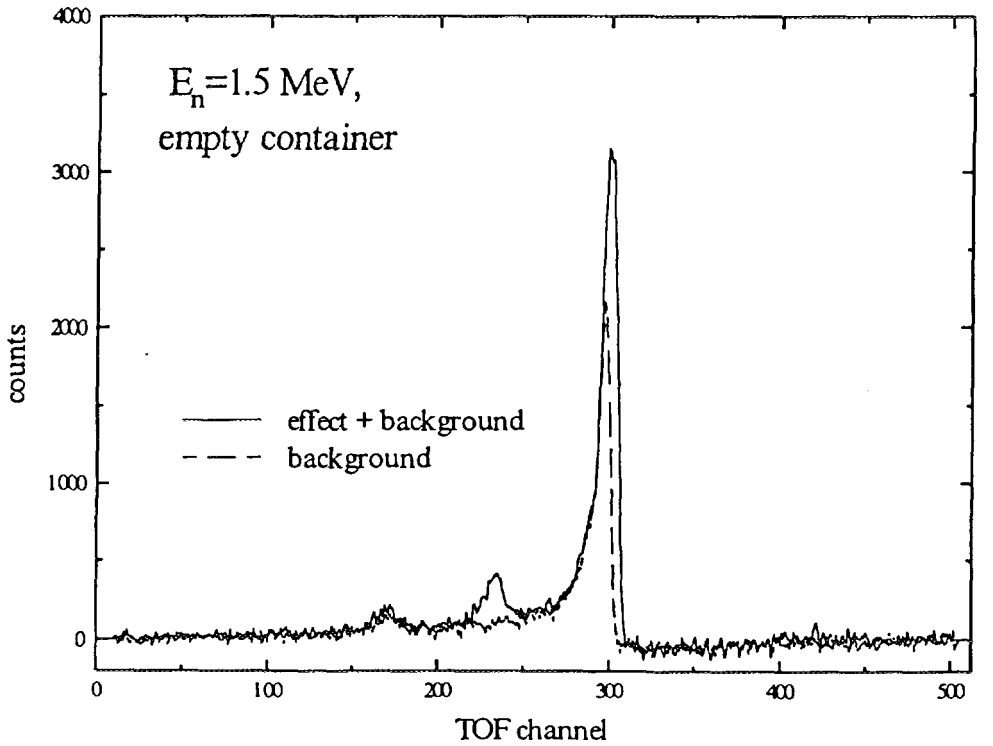

Fig.8 TOF spectra for container run and no sample run.

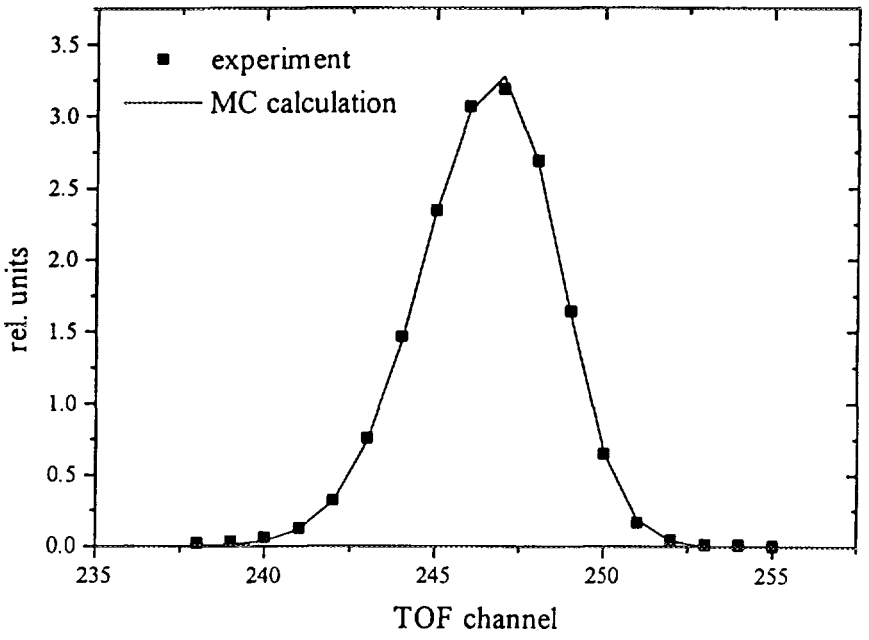

.Fig.9 TOF spectra for monitor detector at 45-deg.

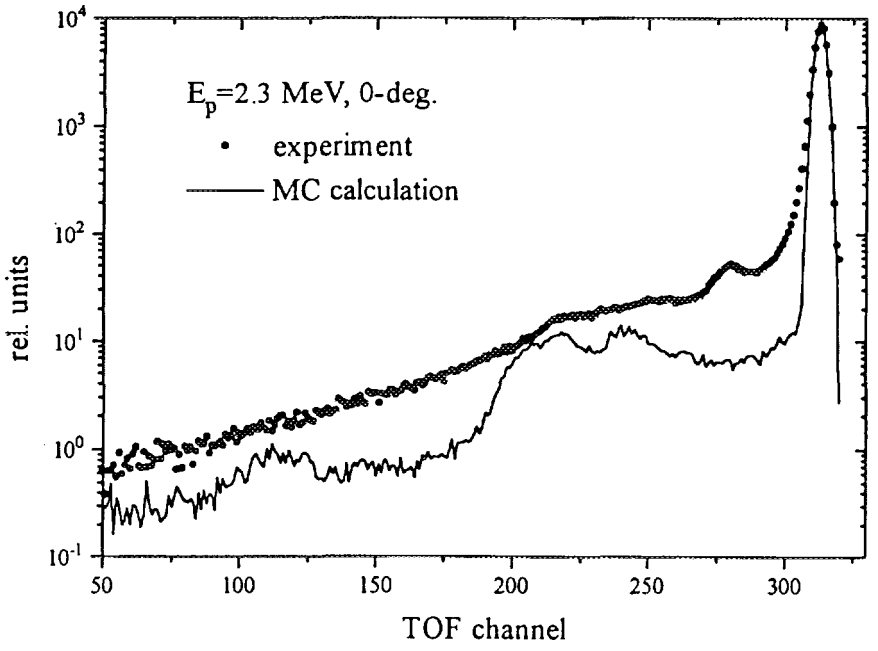

Fig.10 TOF spectra from the neutron source at 0^0 angle. Circles are the experimental data, line shows the MC result.

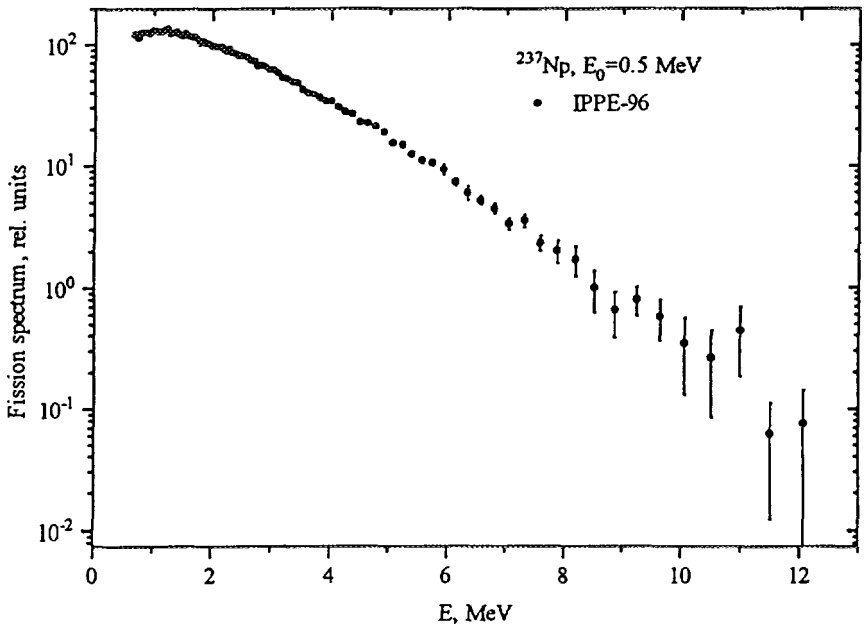

Fig. 11 Fission neutron spectrum for ^{237}Np at ≈0.5 MeV neutron energies. The spectrum is corrected for detector efficiency only.

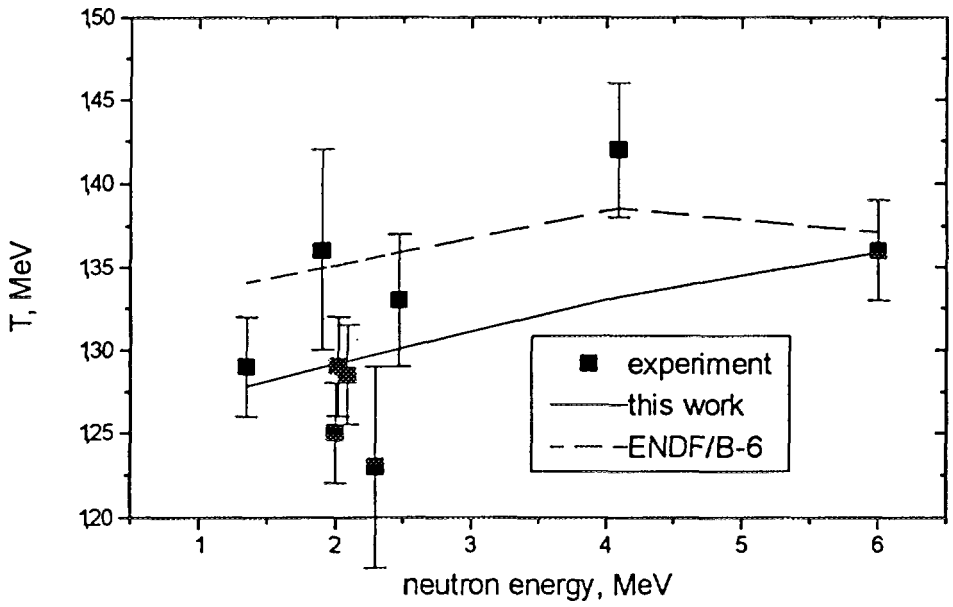

Fig.12 Experimental parameters T (squares) for ^{238}U versus neutron energies. Lines show the calculated values T=<E>/1.5.

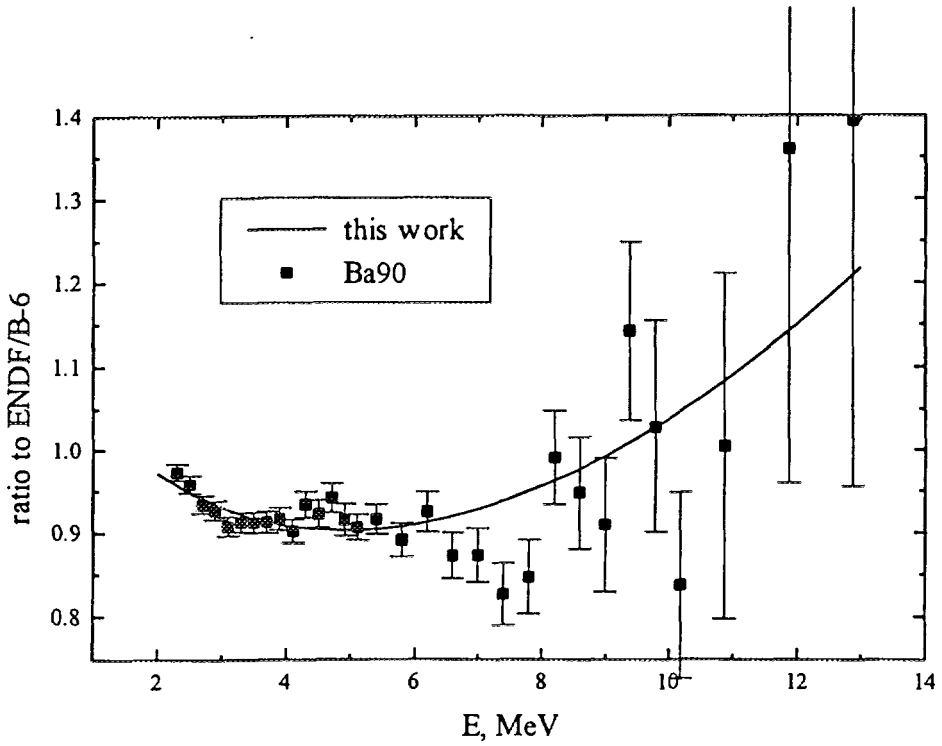

Fig.13 Ratio of experimental fission neutron spectrum [Ref. 12] and this work evaluation to the ENDF/B-VI data for ^{238}U at ~2 MeV neutron energy.

3. 5 Analysis of the evaluated data discrepancies for minor actinides and development of improved evaluation

A. Ignatyuk
Institute of Physics and Power Engineering,
Obninsk, Russia

Abstract

The work is directed on a compilation of experimental and evaluated data available for neutron induced reaction cross sections on ^{237}Np, ^{241}Am, ^{242m}Am and ^{243}Am isotopes, on the analysis of the old data and re-normalizations connected with changes of standards and on the comparison of experimental data with theoretical calculation. Main results of the analysis performed by now are presented in this report. (Editor)

ANALYSIS OF THE EVALUATED DATA DISCREPANCIES FOR MINOR ACTINIDES AND DEVELOPMENT OF IMPROVED EVALUATIONS
(group D-4, group leader A.Ignatyuk)

1. NEW CROSS SECTION EVALUATIONS FOR Np-237

The group activity was directed on a compilation of experimental and evaluated data available for neutron induced reaction cross sections on Np-237, Am-241, Am-242m and Am-243 isotopes, on the analysis of the old data and re-normalizations connected with changes of standards and on the comparison of experimental data with theoretical calculations. For Np-237 the analysis is completed and new recommended cross sections are prepared. Data for isotopes of Am are under consideration still. Main results of the analyses performed are presented in this report.

1.1. RESOLVED RESONANCE REGION

The analysis of the resonance parameters of resolved resonances for Np-237 was done up to 600 eV. The region of resolved resonances was restricted by 130-150 eV in previous evaluations. A statistical method of the resonance analyses was developed which allows to restore the average parameters of weak missed resonances. The average resonance spacing and the neutron strength functions obtained are shown in Fig. 1 and 2. The estimations of numbers of missed resonances are shown in Fig. 3 for two energy intervals: below 200 eV and below 600 eV.

Considerable attention was paid to the analysis of fission widths and elimination of contradictions in the description of intermediate structure of averaged fission cross sections for neutron energies above 100 eV. New experimental data on fission cross sections were included in the analysis. They were obtained by Dubna-Obninsk collaboration on the pulsed reactor of JINR in 1993 and by LANL physicists on their neutron spectrometer in 1994. The resulting set of resonance parameters reproduces well the observed intermediate structure of fission cross sections (Fig. 4). Corresponding group fission cross sections (75 groups) are 30-50% lower than JENDL-3.2 evaluations but approximately twice higher than ENDF/B-6. Corrected fission widths of the neutron resonances below 100 eV also result to fission cross sections lower than JENDL-3.2.

For the resolved resonance region the comparison of new evaluations of the total, fission and capture cross sections with previous ones is shown in Figs. 5, 6 and 7. The thermal cross sections and resonance integrals calculated with the selected set of resonance parameters reproduce accurately enough the experimental data available.

1.2. SCATTERING AND TOTAL CROSS SECTIONS FOR FAST NEUTRONS

There are no experimental data on the total and elastic scattering cross sections of Np-237 for the neutron energies above the resonance region. It means that the optical model parameters for Np-237 should be chosen on the basis of the data available for the neighboring nuclei. For U-238 the total neutron cross sections and elastic scattering angular distributions were analyzed by many groups and parameters of the deformed optical potential were defined with a high accuracy. The following parameters were obtained in the recent analyses:

Lagrange Ch. - 1982 (3 levels coupled):

$V_R = 46.20 - 0.3E_n$(MeV); $E_n < 20$ MeV; $r_R = 1.26$ (fm); $a_R = 0.63$ (fm)

W_s = 3.60 + 0.4 E_n (MeV); E_n < 10 MeV; r_s = 1.26 (fm); a_s = 0.52 (fm)

W_s = 3.60 + 4.0 (MeV); E_n > 10 MeV; W_v = 0.0

V_{sl} = 6.2 (MeV); r_{sl} = 1.12 (fm); a_{sl} = 0.47 (fm)

β_2 = 0.198; β_4 = 0.057

Young P. - 1995 (3 levels coupled):

V_R = 46.20 - 0.275E_n (MeV); E_n < 30 MeV; r_R = 1.26 (fm); a_R = 0.63 (fm)

W_s = 3.18 + 0.4 E_n (MeV); E_n < 8 MeV; r_s = 1.26 (fm); a_s = 0.52 (fm)

W_s = 6.38 - 0.046(E_n - 8.) (MeV); E_n > 10 MeV; W_v = 0.0 E_n < 8.0 MeV;

W_v = -1.4 + 0.175E_n (MeV); E_n > 8.0 MeV; r_v = 1.26 (fm); a_v = 0.63(fm)

V_{sl} = 6.2 (MeV); r_{sl} = 1.12 (fm); a_{sl} = 0.47 (fm)

β_2 = 0.198; β_4 = 0.057

Minsk - 1995 (6 levels coupled):

V_R = 45.685 - 0.260E_n (MeV); E_n < 20 MeV; r_R = 1.257 (fm); a_R = 0.653 -0.0068 E_n (fm)

W_s = 3.123 + 0.333 E_n (MeV); E_n < 10 MeV; r_s = 1.238 (fm); a_s = 0.447+0.0202E_n (fm)

W_s = 6.453 (MeV); E_n > 10 MeV; a_s = 0.75 (fm) for E_n>15 MeV; W_v = 0.0

V_{sl} = 6.062 (MeV); r_{sl} = 1.115 (fm); a_{sl} = 0.471 (fm)

β_2 = 0.214; β_4 = 0.055

The total cross sections calculated for these sets of parameters are shown in Fig. 8 together with experimental data available and the results of ENDF/B-VI and JENDL-3 evaluations. All sets of parameters give practically the same elastic cross sections for the neutron energy above .1 MeV but the absorption cross section is too low for the Minsk's potential for the energies below 8 MeV. On the other hand the absorption above 10 MeV is too low for the Lagrange's potential.

The following parameters were used by P.Young et al . (1995; 3 levels coupled) for ^{237}Np in calculations included in ENDF/B-VI evaluations:

V_R = 46.20 - 0.3E_n (MeV); E_n < 30 MeV; r_R = 1.26 (fm); a_R = 0.63 (fm)

W_s = 3.6 + 0.4 E_n (MeV); E_n < 8 MeV; r_s = 1.24 (fm); a_s = 0.52 (fm)

W_s = 6.38 - 0.046(E_n - 8.) (MeV); ;W_v = 0.0 E_n < 8.0 MeV;

W_v = -0.7 + 0.1E_n (MeV); E_n > 7.0 MeV; r_v = 1.26 (fm); a_v = 0.63 (fm)

V_{sl} = 6.2 (MeV); r_{sl} = 1.12 (fm); a_{sl} = 0.47 (fm)

β_2 = 0.214; β_4 = 0.074.

On the other hand the following parameters were recommended by P.Young et al. for Am-241 (1995; 5 levels coupled):

V_R = 46.23 - 0.3E_n (MeV); E_n < 30 MeV; r_R = 1.25 (fm); a_R = 0.60 (fm)

W_s = 3.314 + 0.45E_n (MeV); E_n < 8 MeV; r_s = 1.24 (fm); a_s = 0.55 (fm)

W_s = 6.914 - 0.046(E_n - 8.) (MeV); W_v = 0.0 E_n < 7.0 MeV;

W_v = -1.6 + 0.2E_n (MeV); E_n > 7.0 MeV; r_v = 1.26 (fm); a_v = 0.63 (fm)

V_{sl} = 6.2 (MeV); r_{sl} = 1.01 (fm); a_{sl} = 0.75 (fm)

β_2 = 0.210; β_4 = 0.0756

We think that the last set of parameters is preferable for the five coupled level scheme of Np-237. So we fitted the value of V_R to the neutron strength function given above and adopted the following set of parameters:

V_R = 46.10 - 0.3E_n (MeV); E_n < 30 MeV; r_R = 1.26 (fm); a_R = 0.63 (fm)

W_s = 3.2 + 0.4 E_n (MeV); E_n < 8 MeV; r_s = 1.24 (fm); a_s = 0.52 (fm)

W_s = 6.4 - 0.046(E_n - 8.) (MeV); E_n > 8 MeV;

W_v = 0.0 E_n < 8.0 MeV;

W_v = -1.4 + 0.175E_n (MeV); E_n > 8.0 MeV; r_v = 1.26 (fm); a_v = 0.63 (fm)

V_{sl} = 6.2 (MeV); r_{sl} = 1.12 (fm); a_{sl} = 0.47 (fm)

β_2 = 0.210; β_4 = 0.074

The total cross sections calculated for Np-237 and Am-241 with the both sets of parameters are given in Figs. 9 and 10 in comparison with ENDF/B-VI and JENDL-3 evaluations. The calculated absorption cross sections are given in Fig. 11. It is necessary to note that the neutron total and elastic scattering cross sections for Np-237 were obtained in JENDL-3 evaluation from calculations with the spherical optical model. The difference between these results and calculations with the deformed optical model (Fig. 12) amounts to 1 b for the elastic scattering cross sections for the neutron energies near 1 MeV and about .5 b for 10 MeV neutrons. The results obtained for the deformed optical model that were used in ENDF/B-VI and our new evaluations should be considered as more reliable.

The same conclusion is valid for the inelastic scattering cross sections. Statistical calculations with the deformed optical potential give more smooth behavior of excitation functions for the near threshold energies than similar calculations with the spherical optical potential. The deformed optical model describes also more correctly the direct reaction contributions to the inelastic scattering cross sections. The results of our calculations of the excitation functions of the lowest five levels and the total inelastic cross sections are presented in Figs. 13 -18.

We performed also the calculations of the total gamma-production cross sections and corresponding integral spectra of gamma-ray. The results are shown in Figs. 19, 20 and 21. Big difference between the calculated cross sections and ENDF/B-VI evaluations requires more accurate re-evaluations of all gamma-production cross sections.

1.3. FISSION CROSS SECTION EVALUATION

Experimental data from 17 works were used to evaluate the excitation function of the Np-237(n,f) reaction in the neutron energy range from 600 eV to 20 MeV.

The main criteria of the selection of microscopic data were:

1. Availability of the information needed to analyze the experiment.
2. Measurement technique.
3. Agreement of the microscopic data with the results of integral experiments.

Top priority was given to absolute measurements where no reference cross sections were used to determine the neutron flux and to time-of-flight experiments with simultaneous registration of the fission and acts of monitoring reaction.

In ten papers from seventeen ones the Np-237(n,f) cross sections were measured relatively to the fission of U-235. The use as the standard of the U-235 fission cross section from ENDF/B-VI instead of the old one (ENDF/B-V) results in decrease of Np-237(n,f) cross section by average 2 per cent in 0.1-2.0 MeV range and by 1.5 per cent in 2.0-3.0 MeV range.

We multiplied the ratio of Np-237 to U-235 fission cross sections measured by Behrens [3] in 0.11 - 18.89 MeV range by 1.051. This normalization factor was obtained from the values of the functional $<\sigma_{Np237(n,f)}>/ <\sigma_{u235(n,f)}>$ in 1-5 MeV energy range evaluated before. There is a lot of experimental data in good agreement for this interval. The ratio of the Np237 (n,f) evaluated averaged cross section on the spectrum of Cf-252 spontaneous fission, known from many works, to averaged microscopic data by Behrens [3] is equal to 1.055 which confirms our renormalization of Behrens data.

The analysis of experimental data on the ratio of Np-237 and U-235 fission cross sections indicates that relative energy trends of $\sigma_{Np237(n,f)}/\sigma_{u235(n,f)}$ measured by Terayama et al [10] in the energy range 4.19-6.99 MeV and by Goverdovskiy et al in 5.66-10.06 MeV energy range [8] coincides with the results of other authors. To make them agree in absolute values Terayama and Goverdovskiy results were multiplied by 0.96 and 1.079 correspondingly. Data on Np-237 fission cross section obtained by Terayama et al on $T(p,n)^3He$ neutron source for 0.70-2.99 energy range are in good agreement with the results of [11], [13], [15], [16]. So they were corrected only according to the new data on monitoring reaction U235(n,f) [17].

In the work by V.M.Kupriyanov et al [1] the Np-237(n,f) cross sections were measured against the fission cross sections of Pu-239. There are no recommended standard data for Pu-239 now. The data from two libraries were used to get absolute values: ENDF/B-VI [17] and JENDL-3.2 [33]. Below 1.6 MeV results of [1] disagree with the integral experiments no matter which data are used for Pu-239(n,f). The analyses of [1] data demonstrated that good agreement with the rest of the data may be obtained in 1.6-7.0 MeV region if Pu-239(n,f) monitoring data are taken from JENDL-3.2 [33].

Experimental data of Meadows et al [5] as well as that of Kupriyanov et al [1] on Np-237 fission cross section are systematically too low below 1 MeV in disagreement with the integral experiments available. Above this point Medows data agree well with the results of other authors so they were included in approximation process only above 1 MeV.

The approximating curve for the excitation function of Np-237(n,f) reaction in 0.1-20 MeV neutron energy range was obtained by statistical analysis of the experimental data by non-linear regression model using rational functions (Pade-approximation). The evaluated fission cross sections are given in Figs. 22 - 25 in comparison with experimental data discussed. Comparison of our evaluation with ENDF/B-VI and JENDL-3 is shown in Fig. 26.

The calculated group cross sections and their uncertainties are given in Table 1. In the calculation of the errors the data of all 30 experimental works analyzed were included [1-16], [19-33]. Covariance matrix of the group cross sections were obtained too.

The results of testing of the evaluated excitation function of the Np-237(n,f) reaction are given in Table 2 which demonstrates that for three neutron spectra our data and ENDF/B-V evaluation are in the best agreement with the integral experiments. However ENDF/B-V evaluation seems to be incorrect above 8.4 MeV were it's too high and disagrees with Behrens [3], Goverdovskiy [7], Lisovskiy [13], being oriented on

obsolete data by Pankratov et al [19]. Renormalization of Pankratov data to the new standard value at 14.7 MeV brings them to agreement with other experimental data.

1.4. CAPTURE CROSS SECTION EVALUATION

The analysis of experimental data available for the neutron radiative capture cross sections were performed for the neutron energies above .6 keV. It was shown that data by Stupegia et al (1967) and Trofimov (1983) should be dropped from the competitive estimation of the recommended cross sections because of the existence of geometry and background corrections that were not correctly included in the data processing.

The approximating curve for the capture cross sections on Np-237 above .6 MeV was obtained from the statistical analysis of experimental data in the same way as for the fission cross sections. The evaluated cross sections are given in Figs. 27 and 28 in comparison with experimental data discussed. Comparison with ENDF/B-VI and JENDL-3 evaluations is shown in Fig. 29.

2. VERIFICATION OF EVALUATED DATA ON FAST CRITICAL ASSEMBLY EXPERIMENTS

2.1 COMPARISON OF EVALUATED CROSS SECTIONS

The goal of this work is to verify the modern neptunium evaluated neutron cross sections by comparison of ^{237}Np reaction rates and reactivity coefficients measured in different fast critical assemblies. The absence of sufficient amount of neptunium leads to impossibility of providing of neptunium critical experiments. So the measurements of neptunium reaction rates and reactivity coefficients are the only possibility to verify the neptunium cross sections in the integral experiments.

There are three relatively independent modern evaluations of the ^{237}Np neutron cross sections stored in the evaluated nuclear data libraries ENDF/B-6, JEF-2.2 and JENDL-3.2. We have carried out the comparison of these data on the 28-group level. Evaluated neutron data were processed into the 28-group cross sections by the NJOY91.91 code. Group constants calculated from the mentioned data libraries were compared also with ^{237}Np group cross sections from ABBN-78 and ABBN-90 sets. ABBN-78 set contains the neptunium cross sections calculated on the basis of ENDF/B-4 data. ABBN-90 contains the neptunium cross sections calculated on the basis of ENDF/B-5 data with correction of (n,2n) cross section. Basis for this correction was measurement of the ^{236}Pu production cross section in the BN-350 reactor core.

In the Table 3 integral cross sections calculated from various libraries are compared. The cross sections at 0.0253 eV, resonance integrals (from 100 keV to 0.465 eV), average cross section on the integral fast reactor core spectrum (NEACRP fast model used), average cross section on ^{235}U fission spectrum and cross section of removing of fission neutrons under the fission threshold of ^{238}U are considered:

$$\sigma_{rem} = \frac{\int_0^{\infty} dE \chi_{235}(E)\sigma_f^{238}(E)\left\{\sigma_a^{Np237}(E) + \int_0^{E} dE' \sigma_s^{Np237}(E \to E')\left[1 - \frac{\sigma_f^{238}(E')}{\sigma_f^{238}(E)}\right]\right\}}{\int_0^{\infty} dE \chi_{235}(E)\sigma_f^{238}(E)}$$

The main difference appear in the fission resonance integral: according to JENDL-3.2 this integral is four times greater than calculated from ENDF/B-6 and JEF-2.2 data.

But fission cross sections averaged over the fast reactor spectrum or over fission spectrum differ only on 4÷5 percent. Noticeable difference exists in the number of the fission neutrons: the maximum estimation (JENDL-3.2) is 5 percent greater than minimum one (ABBN-90). In the same time fast neutron fission cross section estimated according to JENDL-3.2 is maximum: it is 7% greater than that calculated according to ABBN-90.

Some difference appears in the removal cross sections: minimum value (JENDL-3.2) is 16 percent lower than maximum value (ABBN-90). So differences in the evaluated neptunium neutron cross sections are great enough and it is the reason for its verification in the integral experiments.

2.2. FCA-9 ASSEMBLIES.

Actinide integral measurements were carried out on set of FCA assemblies to test the fission and capture cross sections of minor actinides (MA). The assemblies built for this purpose cover the systematic change of the neutron spectrum shape. The "softest" neutron spectrum was in FCA-9-1 assembly, the "hardest" was in FCA-9-7 assembly. The integral data measured are :

- the central fission rate ratio (FRR) of Np-237, Pu-238, Pu-239 ,Am-241, Am-243 and Cm-244 relative to the fission in U-235;
- the central sample worthies (CSW) of Np-237, Pu-238, Pu-239, Pu-240, Am-241 and Am-243.

All MA samples were about 20 grams in weight, the Pu-239 and U-235 ones were several times more. The exact description of the assemblies, experimental devices and obtained results of measurements were given in [1].

The results of measurements and evaluations are presented in Table 4 for CSW ratios of Pu - 239 / U - 235 and FRR of Pu - 239/U-235 (relative to the fission in U - 235)

The results of measurements and evaluation are presented in Table 5 for CSW ratios of Np-237/Pu-239 and FRR of Np-237/Pu-239

2.3. BFS ASSEMBLIES

The core of BFS-67 assembly was composed with 96% enriched metal plutonium, depleted uranium dioxide, sodium and stainless steel. This composition was similar to the SUPERPHENIX core.

About half of uranium dioxide in this composition was replaced with sodium for constructing of BFS-69 assembly core.

For both BFS assemblies the spectra were similar to the spectrum averaged over FCA assemblies. The integral data measured are:

(1) - FRR of Np-237 and Pu-239 relative to fission in U-235 ;

(2) - CSW of Np-237 ,Pu-239 and U-235.

All samples sizes were less than in FCA experiments. The Np and Pu samples were of three different size.

The starting point of neutron data testing is homogeneous calculation of FRR and first order perturbation theory using ABBN approach [2] . Evaluation of experiments means taking in account the heterogeneous structure of core cells, finite sizes of samples and group constant correction at calculation of CSW.

Heterogeneous structure of critical assembly's cell is taken into account by using the integral-transport approximation. Undisturbed group fluxes and adjoint fluxes are obtained from solutions of corresponding integral-transport equations in the cell approximation. Criticality is attained by modification of a neutron leakage. Perturbation of collision probabilities are taking in account too by calculation results using

perturbation theory (first type of correction). Consideration of a detailed energy structure of adjoint solution gives the additional contribution into the reactivity worth ratio (second type of correction).

Using samples of finite size, which are placed in the clearances between pellets of the facility results in the distortion of neutron flux on the sample position. The resonance self-shielding in the sample can be described by substitution of group factors of the self-shielding by the generalized factors, and by taking into account distortions of spectrum because of multiplication and slowing down of neutrons (third type of correction) [3].

Numerical calculations of all these effects are carried out using HEEPCM code [4]. The accuracy of calculations of the heterogeneous and bilinear effects was verified by means of comparison with calculation results obtained from the TULPE code, where another method is used [5]. In addition, a special program of measurements on series of BFS critical assemblies was fulfilled for investigation of calculation accuracy for such heterogeneous effects [3].

The results of measurements and evaluation are presented in Table 6 for CSW ratios of Pu-239/U-235. The table contains the results for three different types of Pu samples.

The results of measurements and evaluation are presented in Table 7 for CSW ratios of Np-237/U-235. The table contains the results for three different types of Np samples.

The results of measurements and evaluation are presented in Table 8 for FRR of Pu-239/U235 (F49/F25) and Np-237/Pu-239 (F37/ F49). The results were obtained with using two different measurements methods A and B.

2.4. COMPARISON OF CALCULATED AND EXPERIMENTAL DATA

Simple homogeneous spherical models of all considered experiments were constructed. Calculations were carried out in 28 group S_4-approximation by means of CRAB-1 code. The ABBN-90 group constant set was used, but neptunium-237 cross sections were variable. All calculation models were exactly critical. Criticality was achieved by adjustment of core radius. Experimental data were reduced to conditions of models (corrections on finite dimensions of samples and on heterogeneity were introduced). This reduced data are given in the Tables 9 and 10 in comparison with results of calculations performed by using different Np-237 neutron data. For reactivity worth ratios differences between calculation and experimental data are because percentage measure of differences are not adequate for the value with changed sign. For fission cross section ratios differences are given in the percent.

Better description of experimental fission ratio was achieved by using JENDL-3.2 data. Discrepancies between experiment and calculation are not systematic and can be fully explained by integral experiment uncertainty. The ABBN-90 set describes these data practically with the same accuracy (see Fig. 30 where discrepancies between experimental and calculated data are plotted dependent on value of reactivity worth ratio).

From consideration of reactivity worth ratios another picture is appeared. The ABBN-90 set leads to systematic deviations from experimental data. So old ENDF/B-5 evaluation is not appropriate. The more modern data JENDL-3.2 and other allows to describe reactivity worth ratios in the interval from -0.5 to +0.5 with about the same accuracy. Discrepancies between experimental and calculated data in this region can be explained by experimental uncertainties. But in the case of FCA-9-1 assembly (with the more soft neutron spectrum) JENDL-3.2 set leads to large negative ^{237}Np reactivity worth value. This discrepancy may be eliminated by correction of the capture cross section of ^{237}Np in keV-energy region.

REFERENCES :

1. V.M.Kuprijanov e.a. Atomnaja Energija, v.45, n.6, p.440, Dec.1978
2. R.Arlt,W.Meiling,G.Musiol e.a. Report ZFK-410, p.122,Jan.1980
R.Arlt,W.Meiling,G.Musiol e.a. Kernenergie,v.24,p.48,Feb.1981
3. J.W.Behrens, J.C.Browne, J.C.Malden,"Nuclear Science and Engineering", v.80, p.393 (1982).
4. I.D.Alkhazov,E.A.Ganza,L.V.Drapchinskij et al. Proceedings of the 3-d All-union Conf. on the Neutron RadiationMetrology at Reactors and Accelerators, v.2, p.201, Moscow, CNIIATOMINFORM, 1983
5. J.W.Meadows Nucl.Sci.Eng., v.85, p.271, Nov. 1983
6. K.R.Zasadny e.a. Trans.Amer.Nucl.Soc., v.47, p.425, Nov.1984
7. A.A.Goverdovskij e.a. Yadernye Konstanty, v.3(57), p.13, Sep.1984
8. A.A.Goverdovskij e.a. Preprint FEI-1552, 1984
9. R.Arlt,M.Josch,G.Musiol e.a. Isotopenpraxis,v.21, p.344, 1985
10. H.Terayama e.a. Progress Report NETU-47, 1986
H.Terayama e.a. Progress Report NEANDC(J)-122, Sep. 1986
11. V.A.Kalinin e.a. Yadernye Konstanty,,(4),3, 1987
12. J.W.Meadows Ann.Nucl.Energ., v.15, p.421, Aug.1988
13. P.W.Lisowski e.a. Neutron Induced Fission Cross Section Ratios for Th232, U235, U238, Np237 and Pu239. Proc. Int. Conference on Nuclear Data for Science and Technology, Mito, Japan, 1988, pp. 97-99
14. L.Desdin,S.Szegedi,J.Csikai Acta Physica Hungaria, v.65(2-3), p.271, 1989
15. P.W.Lisowski e.a. Neutron Induced Fission Cross Sections for Th232, U235, U236, Np237 and Pu239. Proc. of the Conference on Fifty Years with Nuclear Fission, NIST, Gaithersburg, MD, 1989, pp. 443-448.
16. A.D.Carlson et al. Measurement of the Fission Cross Section of Np237. Proc. Int. Conf. on Nuclear Data for Science and Technology, Gatlinburg, Tennessee, USA, May 9-13, 1994, Vol.1, pp. 40-42
17. ENDF/B-VI , Eval.L.Weston e.a. ORNL,LANL nov.1989, MAT=9237 ; Nuclear Data Standards for Nuclear Measurements, Report NEANDC-311 U, p.70-74, 1992
18. V.Pronyaev Physics Data No 13-8, Karlsruhe, 1995
19. V.M.Pankratov e.a. Atomnaja Energija, v.9, p.399, 1960
20. J.A.Grundl Nucl.Sci.Eng., v.30, p.39, Oct.1967
21. P.H.White,G.P.Warner Jour.Nucl.Energy, v.21, p.671, Aug.1967
22. J.A.Grundl Nucl.Sci.Eng., v.31, p.191, 1968
23. W.E.Stein, R.K.Smith, H.L.Smith. Proceedings Conf. Neutron Cross Sections and Technology, Washington, D.C., March 4-7, 1968, NBS Special Publication 299 , p.627 , U.S. National Bureau of Standards, 1968.
24. R.J.Jiacoletti, W.K.Brown, H.G.Olson. "Nuclear Science and Engineering", v.85, p.271-279 (1983).
25. Wu Jingxia e.a. J.China Nucl.Phys., v.6, p.369, Nov.1984
26. I.Garlea e.a. Rev.Roum.Phys., v.29, p.421, 1984
27. K.Kanda et al. Report JAERI-M-85-035, p.220, 1985.
28. J.W.Meadows,D.L.Smith,L.P.Geraldo Ann.Nucl.Energ., v.16, p.471,.1989
29. D.M.Gilliam e.a. Proc. 5-th ASTM-EURATOM Symposium on Reactor Dosimetry, Geesthacht, Germany, Sep.24-28, 1984, v.2, p.867, 1984
30. W.Mannhart Handbook on Nuclear Activation Data, IAEA Technical Report Series No.273, p.413, IAEA, Vienna, 1987
31. R.A.Anderl e.a. USDOE Report EGG-PHYS-5608, 1981
32. M.Nakazawa e.a. Report JAERI 1325, p.56, March 1992

33. Y.Kikuchi JENDL-3 Revision-2 - JENDL-3.2. Proc. of Int. Conf. on Nuclear Data for Science and Technology, Gatlinburg, Tennessee, May 9-13, 1994, vol.2, p.692
34. T. Mukaiyama et. all, Actinide Integral Measurements on FCA for Evaluating and Improving Their Cross Section Data, NEACRP - A- 684.
35. Abagyan L.R. et al. Group constants for reactor and shilding calculations (Russian). M., Energoatomizdat, 1981.
36. Dulin V.A. Sov. J. Atomic Energy, 1989, v.66, is. 2, p. 79.
37. Mikhailov G.M. et al. Voprosy Atomnoy Nauki I Tehniki. Ser. Nuclear Constants. 1989, is.4, p. 80.
38. Bednyakov S.M. et al. Voprosy Atomnoy Nauki I Tehniki. Ser. Nuclear Constants 1989, is. 3, p. 3-15.

Table 1. Group cross-sections and their unsertainties

Energy group [Mev] to [Mev]		Group number	Cross-section [mb]	Error [mb]	Error [%]
0.10	0.50	1	128.4051	3.0430	2.37
0.50	1.00	2	1110.1942	20.3269	1.83
1.00	1.50	3	1554.0171	31.8497	2.05
1.50	2.00	4	1660.8505	29.2081	1.76
2.00	2.50	5	1686.5603	31.0453	1.84
2.50	3.00	6	1673.4320	33.5468	2.00
3.00	3.50	7	1637.7837	35.3326	2.16
3.50	4.00	8	1588.5817	37.2016	2.34
4.00	4.50	9	1533.7239	38.9971	2.54
4.50	5.00	10	1486.8828	39.5065	2.66
5.00	5.50	11	1477.3051	40.0092	2.71
5.50	6.00	12	1553.3925	43.7358	2.82
6.00	6.50	13	1742.5873	50.2650	2.88
6.50	7.00	14	1977.7614	57.0616	2.89
7.00	7.50	15	2148.1658	58.6502	2.73
7.50	8.00	16	2222.4963	56.1083	2.52
8.00	8.50	17	2232.7900	51.9368	2.33
8.50	9.00	18	2212.8984	49.0289	2.22
9.00	9.50	19	2181.9744	48.8127	2.24
9.50	10.00	20	2149.0144	50.4632	2.35
10.00	10.50	21	2118.1917	52.6140	2.48
10.50	11.00	22	2091.8398	54.7099	2.62
11.00	11.50	23	2071.9329	57.0738	2.75
11.50	12.00	24	2060.7778	59.9983	2.91
12.00	12.50	25	2061.0898	62.5186	3.03
12.50	13.00	26	2075.1733	62.6041	3.02
13.00	13.25	27	2094.5366	60.7533	2.90
13.25	13.50	28	2111.3787	58.0558	2.75
13.50	13.75	29	2130.1106	54.2955	2.55
13.75	14.00	30	2149.5510	49.3420	2.30
14.00	14.25	31	2168.4104	43.4213	2.00
14.25	14.50	32	2185.4871	37.6970	1.72
14.50	14.75	33	2199.8435	34.5194	1.57
14.75	15.00	34	2210.9114	36.0120	1.63
15.00	15.25	35	2218.5020	41.5773	1.87
15.25	15.50	36	2222.7449	48.7689	2.19
15.50	15.75	37	2223.9878	55.6407	2.50
15.75	16.00	38	2222.6924	61.2642	2.76
16.00	16.25	39	2219.3525	65.4291	2.95
16.25	16.50	40	2214.4373	68.3372	3.09
16.50	16.75	41	2208.3604	70.3905	3.19
16.75	17.00	42	2201.4690	72.0481	3.27
17.00	17.25	43	2194.0430	73.7308	3.36
17.25	17.50	44	2186.3013	75.7626	3.47
17.50	18.00	45	2174.4541	79.7965	3.67
18.00	19.00	46	2151.2634	91.8426	4.27
19.00	20.00	47	2122.8970	113.0189	5.32

Таблица 2. Integral experimental data for the Np237(n,f) reaction

U-235 THERMAL FISSION NEUTRON SPECTRUM - ENDF/B-6 EVALUATION

Library	MAT	<SIG>, mbarn	C/E	90%-Responce range, MeV
ENDF/B-VI	9346	1329.1	0.9780	0.690 - 5.700
ENDF/B-V	9337	1355.1	0.9971	0.690 - 5.600
JENDL-3D	9331	1342.5	0.9879	0.690 - 5.600
JENDL-3.2	9346	1343.1	0.9883	0.690 - 5.600
FEI-eval.	9346	1354.7	0.9968	0.690 - 5.600
EXPERIMENT	[29]	1359.0+-28.5		

CF-252 SPONTANEOUS FISSION NEUTRON SPECTRUM - PTB EVALUATION

Library	MAT	<SIG>, mbarn	C/E	90%-Responce range, MeV
ENDF/B-VI	9346	1333.6	0.9835	0.720 - 6.100
ENDF/B-V	9337	1359.6	1.0027	0.690 - 6.100
JENDL-3D	9331	1346.4	0.9929	0.690 - 6.100
JENDL-3.2	9346	1346.9	0.9933	0.690 - 6.100
FEI-eval.	9346	1358.5	1.0018	0.690 - 6.000
EXPERIMENT	[30]	1356.0+-22.0		

CFRMF = COUPLED FAST REACTIVITY MEASUREMENT FACILITY (IDAHO)

Library	MAT	<SIG>, mbarn	C/E	90%-Responce range, MeV
ENDF/B-VI	9346	563.32	1.0280	0.450 - 4.600
ENDF/B-V	9337	585.70	1.0688	0.425 - 4.500
JENDL-3D	9331	572.12	1.0440	0.450 - 4.500
JENDL-3.2	9346	577.55	1.0539	0.425 - 4.500
FEI-eval.	9346	585.46	1.0684	0.425 - 4.500
EXPERIMENT	[31]	548.0+-18.1		

SIGMA-SIGMA = COUPLED THERMAL/FAST URANIUM + BORON CARBIDE

Library	MAT	<SIG>, mbarn	C/E	90%-Responce range, MeV
ENDF/B-VI	9346	590.93	0.9306	0.450 - 4.300
ENDF/B-V	9337	613.55	0.9677	0.425 - 4.200
JENDL-3D	9331	600.30	0.9468	0.450 - 4.200
JENDL-3.2	9346	605.30	0.9547	0.425 - 4.200
FEI-eval.	9346	613.39	0.9674	0.450 - 4.200
EXPERIMENT	[32]	634.0+-22.2		

Table 3. Cross section of ^{237}Np averaged on the different spectra

a) E=0.0253eV.

set	total	capture	fission	elastic	inel	NU	MU
ABBN90	186.63	169.101	.017	17.51	.000	2.700	.0028
ABBN78	186.60	169.100	.020	17.48	.000	2.700	.0028
JENDL-3.2	193.51	165.987	.023	27.50	.000	2.541	.0028
ENDF/B-6	195.78	181.020	.018	14.74	.000	2.636	.0028
JEF-2.2	195.78	181.020	.018	14.74	.000	2.537	.0028

b) Resonance integral

set	total	capture	fission	elastic	inel	NU	MU
ABBN90	929.76	771.804	.322	157.05	.589	2.701	.0070
ABBN78	931.65	770.393	.315	160.35	.591	2.701	.0065
JENDL-3.2	970.99	798.286	.892	171.49	.317	2.541	.0120
ENDF/B-6	951.92	794.968	.218	156.45	.281	2.637	.0118
JEF-2.2	952.24	794.946	.210	156.80	.252	2.535	.0075

c) Fast reactor (NEACRP test)

set	total	capture	fission	elastic	inel	NU	MU
ABBN90	11.49	1.693	.320	8.66	.812	2.927	.1302
ABBN78	11.49	1.692	.320	8.66	.810	2.926	.1228
JENDL-3.2	11.93	1.826	.321	8.99	.793	2.764	.1926
ENDF/B-6	11.65	1.729	.308	8.79	.826	2.874	.1515
JEF-2.2	11.79	1.728	.305	9.06	.692	2.780	.1289

d) ^{235}U fission spectrum

set	total	capture	fission	elastic	inel	NU	MU
ABBN90	7.80	.171	1.330	4.62	1.676	3.051	.4738
ABBN78	7.80	.171	1.330	4.62	1.673	3.051	.4792
JENDL-3.2	7.83	.179	1.319	5.01	1.325	2.890	.5543
ENDF/B-6	7.57	.194	1.307	4.34	1.729	2.998	.5504
JEF-2.2	7.59	.195	1.288	4.58	1.524	2.908	.4768

e) Removal cross section

SET	CAPTURE	ELASTIC	INELASTIC	FISSION	SUMMA
ABBN90	.0415	.0124	1.6749	1.6538	3.3827
ABBN78	.0411	.0117	1.6633	1.6528	3.3690
JENDL-3.2	.0428	.0126	1.1278	1.6453	2.8285
ENDF/B-6	.0469	.0084	1.2382	1.6373	2.9308
JEF-2.2	.0494	.0119	1.1968	1.6030	2.8611

Table 4

Assemb. FCA	EXP. virgin	Correction of 1 and 2 types	Correction of 3 type for Pu	Correction of 3 type for U	EXP. evaluated
CSW ratio Pu-239 / U-235					
9-1	1.476	-.023	-.146	+.109	+1.416
9-2	1.617	-.010	-.127	+.124	+1.604
9-3	1.713	-.009	-.008	+.016	+1.712
9-4	1.708	-.006	-.079	+.089	+1.712
9-5	1.750	0	-.075	+.081	+1.756
9.7	1.745	-.002	-.065	+.060	+1.738
FRR Pu-239 / U - 235					
9-1	.957	-.021	-.003	0	+.933
9-2	1.030	+.004	-.002	0	+1.032
9-3	1.11	+.004	-.002	0	+1.112
9-4	1.17	+.003	-.002	0	+1.171
9-5	1.23	+.002	-.003	0	+1.229
9-7	1.21	0	-.001	0	+1.209

Table 5

Assemb. FCA	EXP. virgin	Correction of 1 and 2 types	Correction of 3 type for Pu	Correction of 3 type for U	EXP. evaluated
CSW ratio Np-237 / Pu - 239					
9-1	-.865	+.179	-.220	-.073	-.979
9-1	-.242	+.072	-.042	-.013	-.225
9-3	-.014	+.021	-.014	+.005	-.002
9-4	+.054	+.006	-.005	+.006	+.061
9-5	+.158	+.002	-.004	+.010	+.166
9-7	+.117	+.001	-.003	+.007	+.122
FRR Np-237 / Pu-239					
9-1	.209	.012	.002	.001	.224
9-2	.320	.012	.001	0	.333
9-3	.384	.007	.002	0	.393
9-4	.344	.003	.002	0	.349
9-5	.398	.002	.002	0	.402
9-7	.353	0	.002	0	.355

Table 6

Assembly	Type of sample	EXP VIRGIN	ZERO SIZE of samples	correction of 1 and 2 types	EXP evaluated
67-1	Pu - A	1.350 ± .020	1.327 ± .021		
	Pu - B	1.406 ± .008	1.365 ± .009		
	Pu - C	1.404 ± .005	1.352 ± .007		
	averaged value		1.353 ± .019	+.011	1.364 ± .019
69-1	Pu - A	1.591 ± .018	1.560 ± .020		
	Pu - B	1.607 ± .007	1.552 ± .008		
	Pu - C	1.592 ± .004	1.528 ± .006		
	averaged value		1.541 ± .019	-.002	1.539 ± .019

Notes:
Pu - A size : Nl = 0.0044 (barn $^{-1}$)
Pu - B size : Nl = 0.0076 (barn $^{-1}$)
Pu - C size : Nl = 0.0091 (barn $^{-1}$)

Table 7

Assembly		VIRGIN EXP	ZERO SIZE of samples	correction of 1 and 2 types	evaluated experiment
67-1	Np - A	-.240 ± .011	-.250 ± .011		
	Np - B	-.228 ± .006	-.240 ± .008		
	Np - C	-.228 ± .005	-.245 ± .007		
	averaged value		-.245 ± .010	+.023	-.222 ± .011
69-1	Np - A	-.120 ± .010	-.128 ± .010		
	Np - B	-.119 ± .006	-.130 ± .007		
	Np - C	-.114± .003	-.131 ± .004		
	averaged value		-.130 ± .005	+.021	-.109 ± .006

Notes:
Np - A size : Nl = 0.00220 (barn $^{-1}$)
Np - B size : Nl = 0.00285 (barn $^{-1}$)
Np - C size : Nl = 0.00455 (barn $^{-1}$)

Table 8

Assembly	FRR	EXP	EXP	Correction of 1 type	EXP
		VIRGIN	ZERO size of chambers		evaluated
67 - 1	F49 / F25A	1.003 ± .010	1.005 ± .010	+.010	1.015 ± .012
	F37 / F49A F37 / F49B	.235 ± .006 .232 ± .005	.236 ± .006 .234 ± .005		
	averaged value		.235 ± .005	+.003	.238 ± .006
69 - 1	F49 / F25A	1.068 ± .010	1.070 ± .010	+.007	1.077 ± .010
	F37 / F49A F37 / F49B	.298 ± .005 .288 ± .007	.300 ± .005 .290 ± 007		
	averaged value		.297 ± .006	+.002	.299 ± .007

Notes: A - thermal column calibration method
B - absolute fission rates technic

Table 9. Comparison of experimental and calculated CSW data (ρ_{237} / ρ_{235}).

Assembly	Experiment	(Calculation - Experiment)*100			
		ABBN-90	ENDF/B-VI	JEF-2	JENDL-3.2
FCA-9-1	- 1.390	- 3.6	- 1.5	- 5.0	- 15.0
FCA-9-2	- 0.361	5.7	- 1.0	- 5.5	- 9.8
FCA-9-3	-0 .003	12.9	3.6	- 1.2	- 2.6
FCA-9-4	0.104	15.0	5.9	1.4	3.8
FCA-9-5	0.291	14.2	5.1	0.3	3.2
FCA-9-6	0.433	17.7	9.0	3.6	6.9
FCA-9-7	0.204	14.1	7.5	4.0	6.7
FCA-10-1	- 0.002	6.9	0.8	- 2.1	- 2.1
BFS-67-1	- 0.222	8.8	5.0	3.3	1.9
BFS-69-1	- 0.109	8.8	4.0	2.0	1.0

Table 10. Comparison of experimental and calculated FRR data (f_{237} / f_{235}).

Assembly	Experiment	(calculation / experiment - 1) × 100			
		ABBN-90	ENDF/B-VI	JEF-2	JENDL-3.2
FCA-9-1	0.209	1.0	- 1.9	-2.9	1.0
FCA-9-2	0.344	- 1.2	- 3.8	- 4.7	- 1.5
FCA-9-3	0.437	- 2.1	- 4.6	- 5.5	- 2.5
FCA-9-4	0.409	4.2	0.7	0.0	2.9
FCA-9-5	0.494	2.4	- 0.9	-1.4	1.2
FCA-9-6	0.599	- 0.2	- 3.0	- 3.8	- 1.3
FCA-9-7	0.429	5.4	1.6	0.9	3.7
FCA-10-1	0.357	- 2.2	- 5.3	- 5.9	- 3.1
BFS-67-1	0.242	2.5	- 0.4	-1.2	2.5
BFS-69-1	0.322	0.6	- 2.2	-3.5	0.5

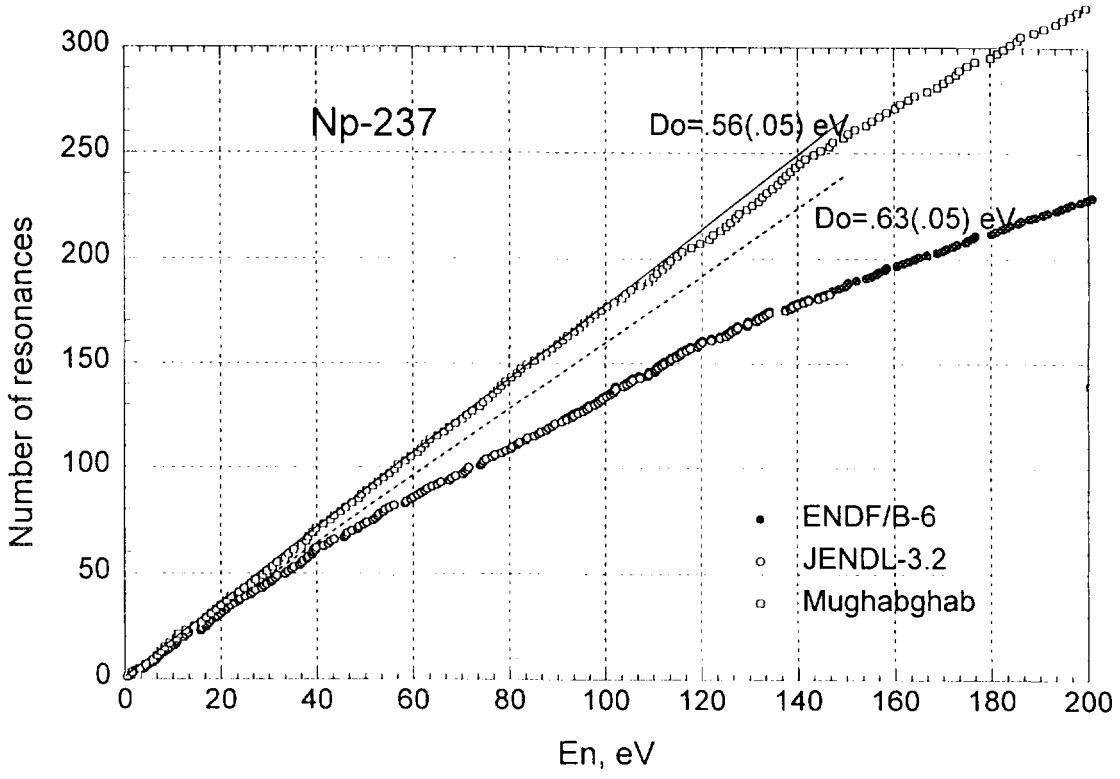
Np-237
Do=.56(.05) eV
Do=.63(.05) eV
ENDF/B-6
JENDL-3.2
Mughabghab
Number of resonances
En, eV
0
50
100
150
200
250
300
0
20
40
60
80
100
120
140
160
180
200

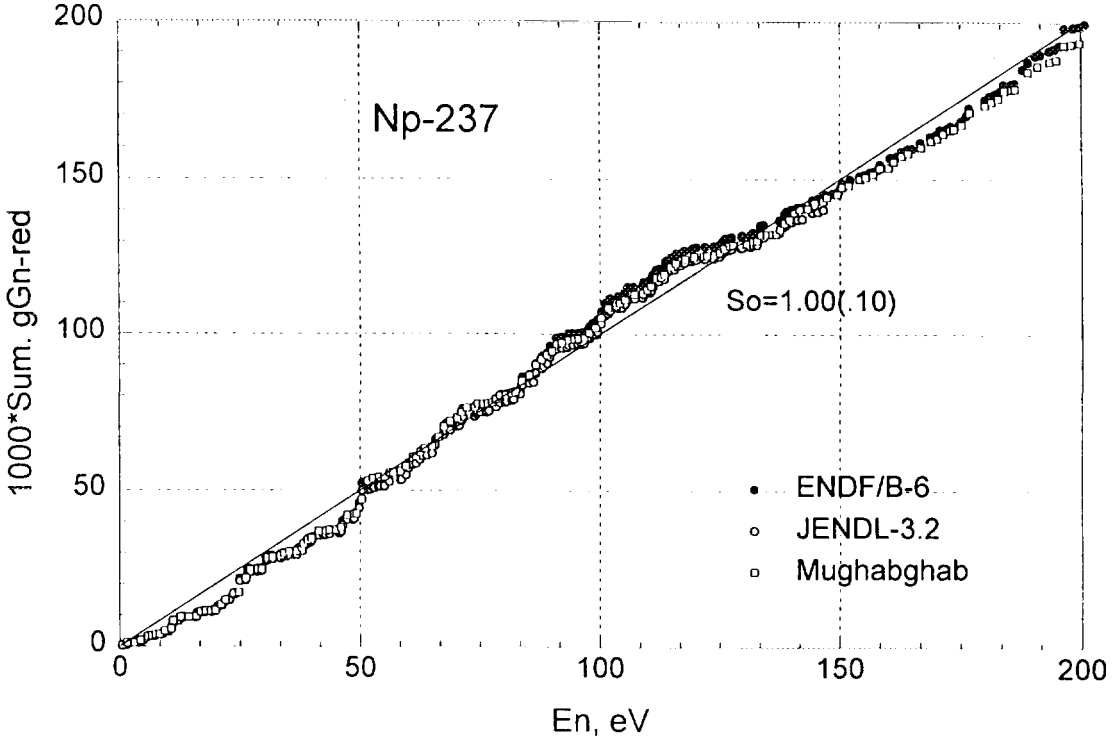
Np-237
So=1.00(.10)
ENDF/B-6
JENDL-3.2
Mughabghab
1000*Sum. gGn-red
En, eV
0
50
100
150
200
0
50
100
150
200

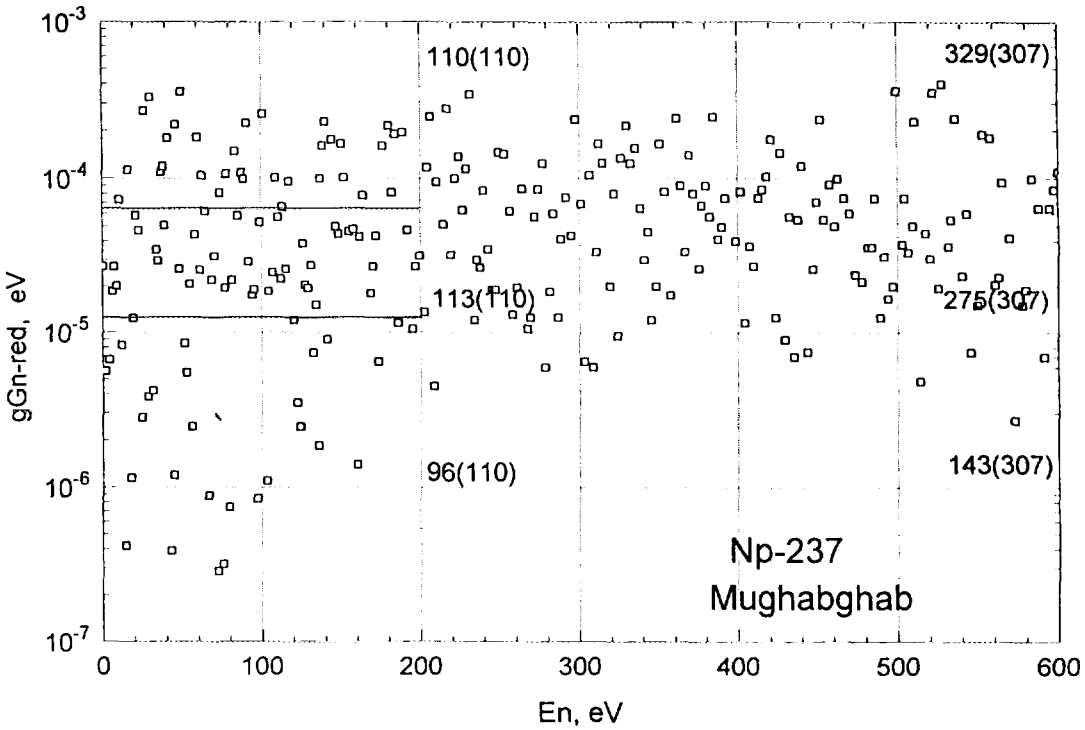
gGn-red, eV
En, eV
110(110)
329(307)
113(110)
275(307)
96(110)
143(307)
Np-237
Mughabghab

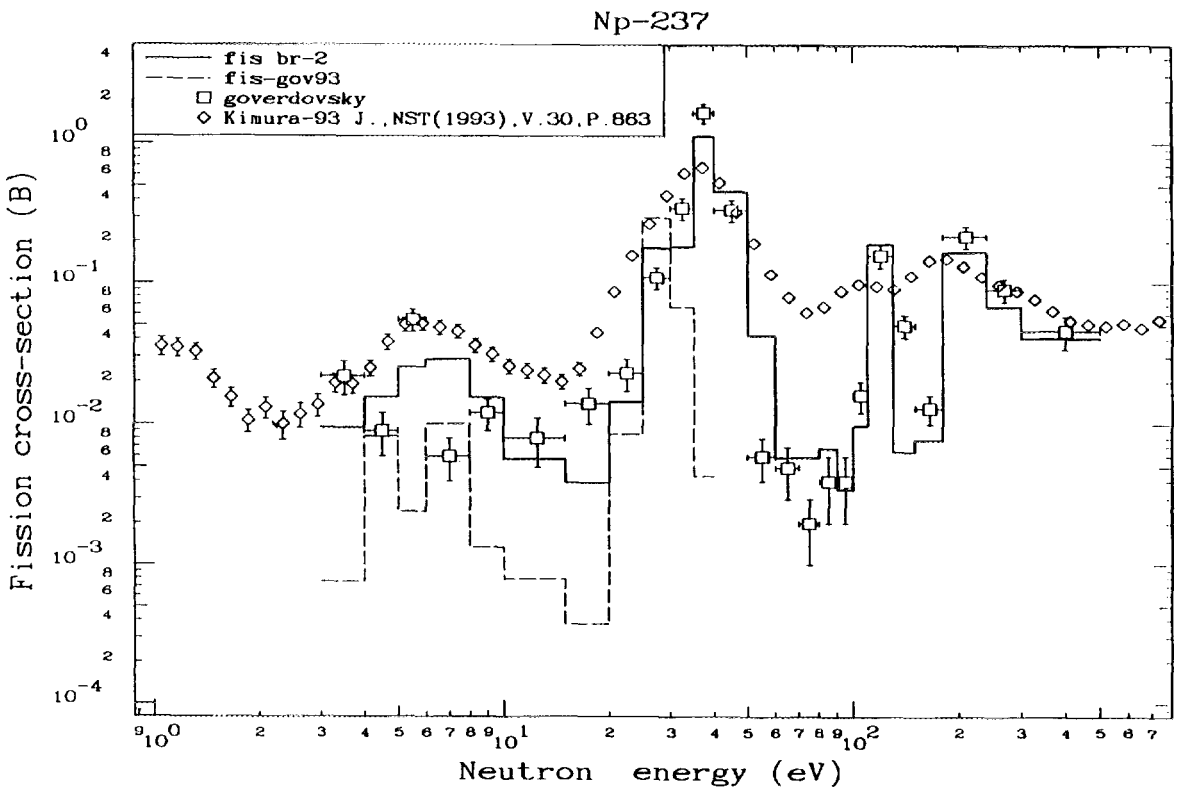
Np-237
fis br-2
fis-gov93
goverdovsky
Kimura-93 J.,NST(1993),V.30,P.863
Fission cross-section (B)
Neutron energy (eV)

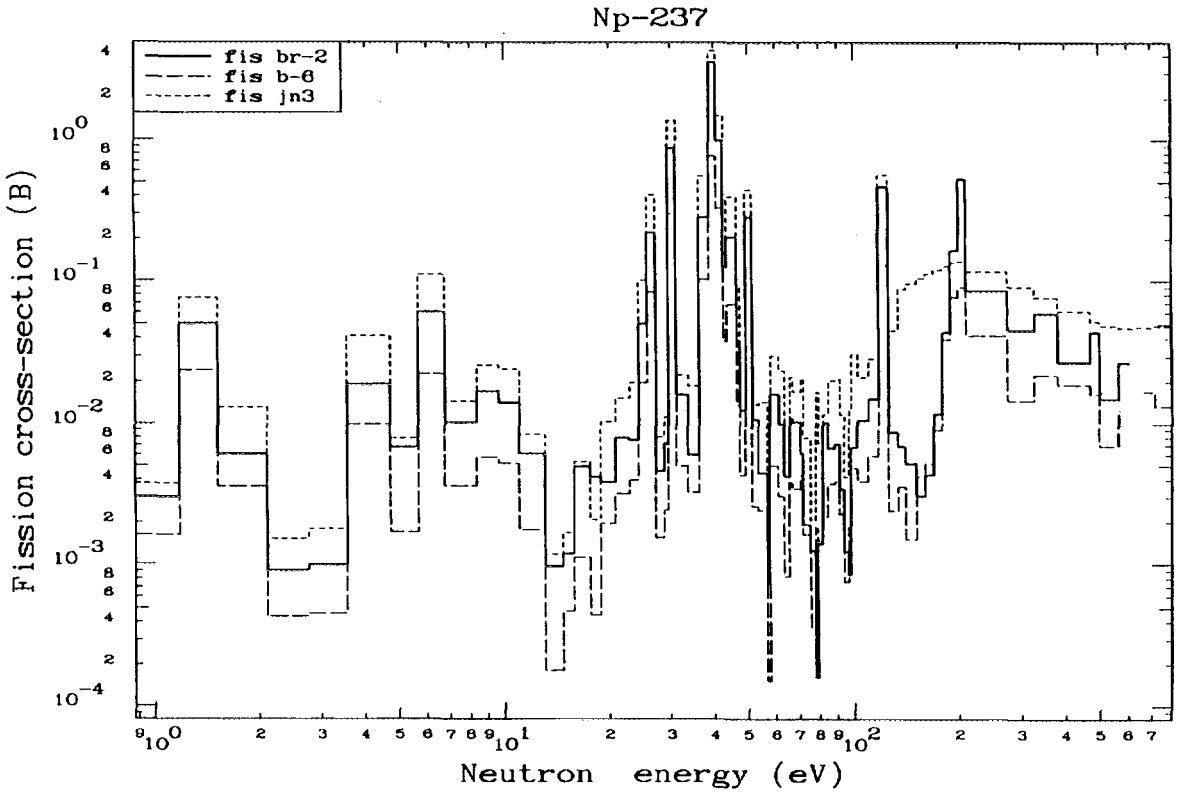
Np-237
fis br-2
fis b-6
fis jn3
Fission cross-section (B)
Neutron energy (eV)

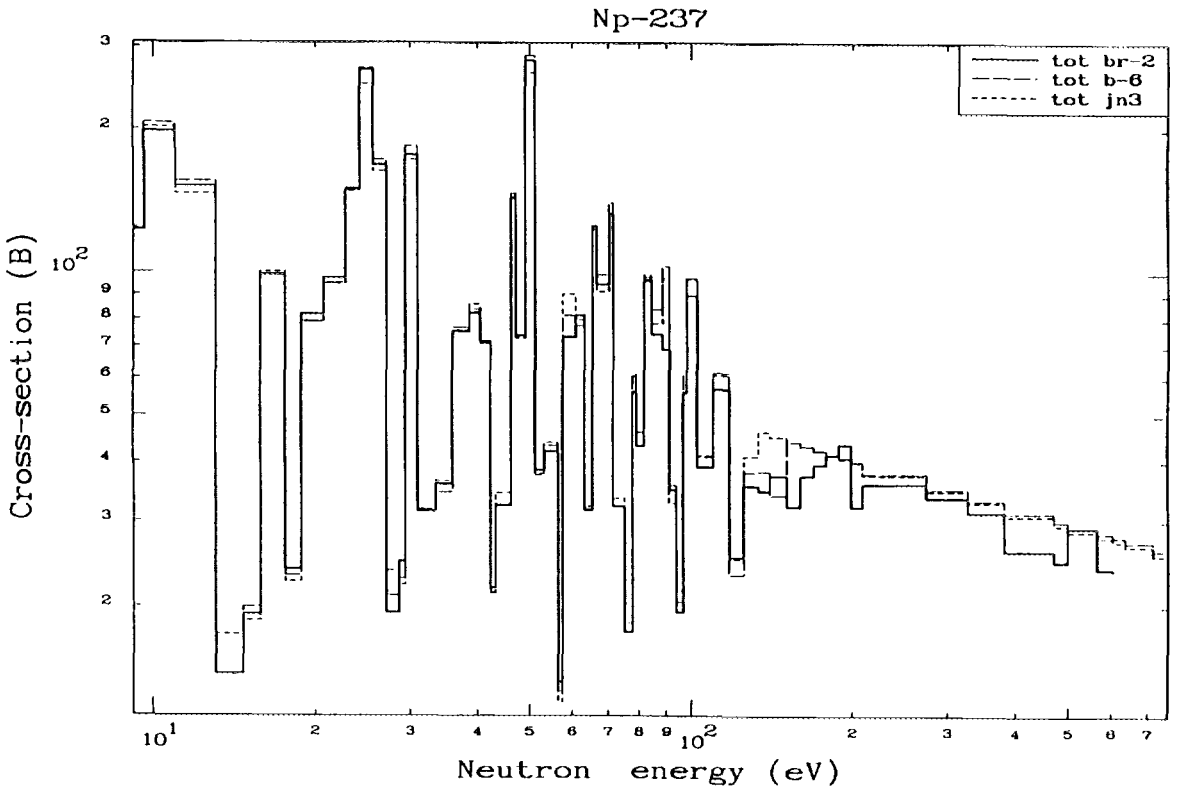
Np-237
tot br-2
tot b-6
tot jn3
Cross-section (B)
Neutron energy (eV)

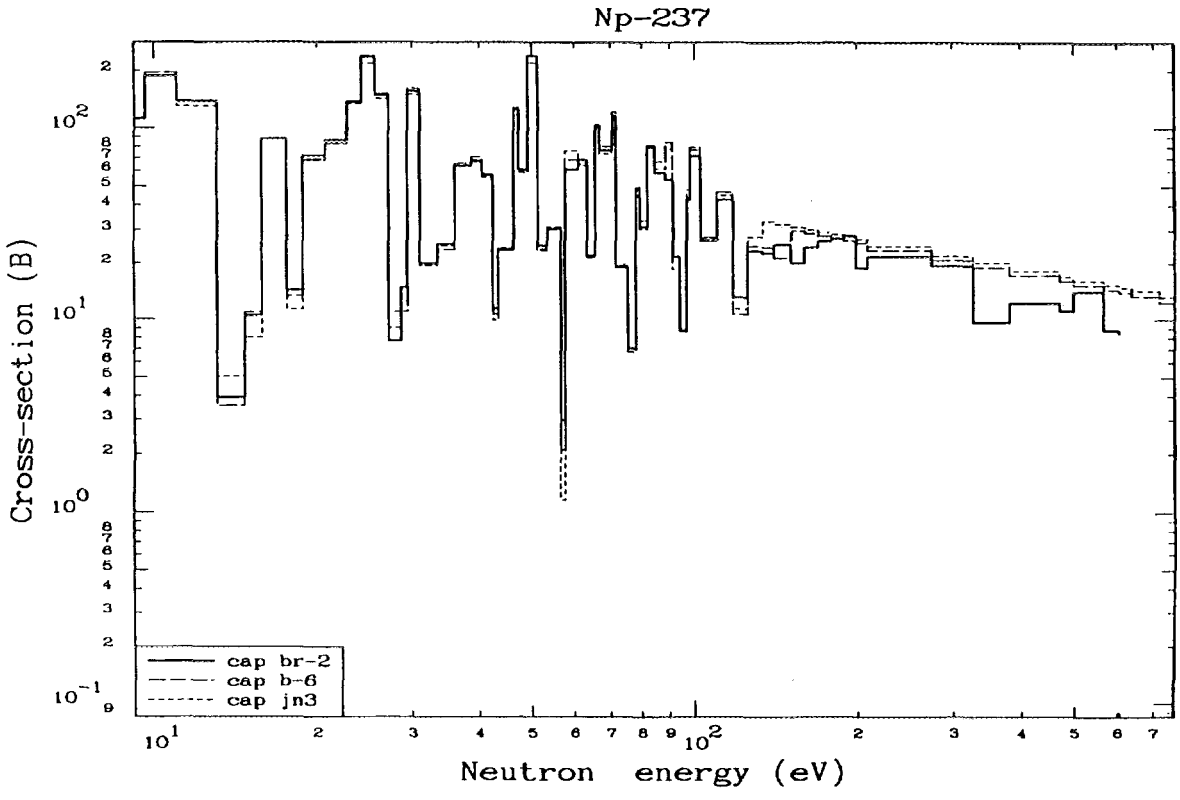
Np-237
Cross-section (B)
Neutron energy (eV)
cap br-2
cap b-6
cap jn3

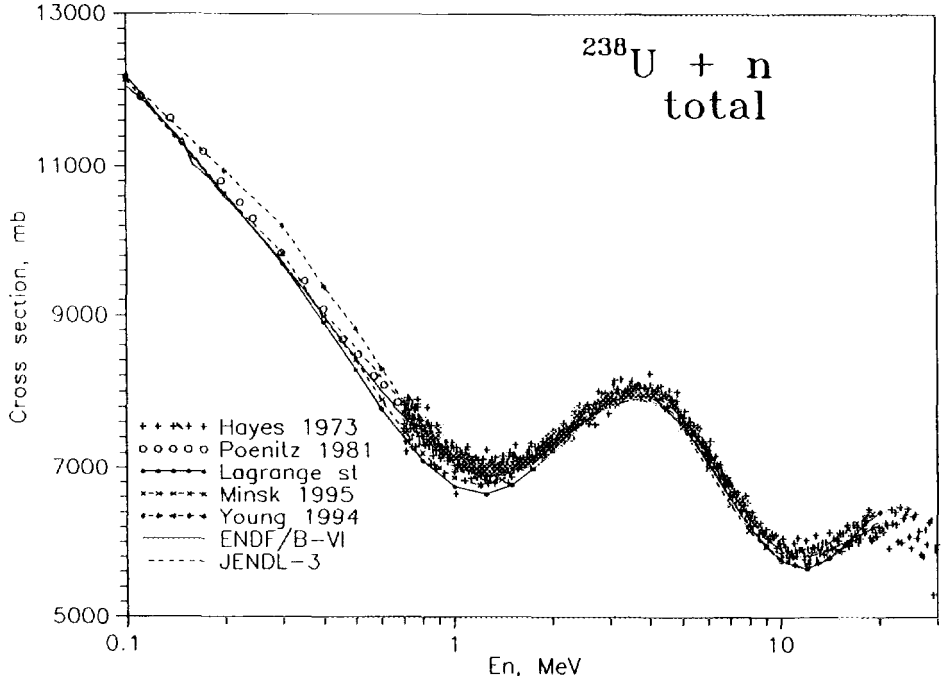
238U + n
total
Cross section, mb
En, MeV
Hayes 1973
Poenitz 1981
Lagrange st
Minsk 1995
Young 1994
ENDF/B-VI
JENDL-3

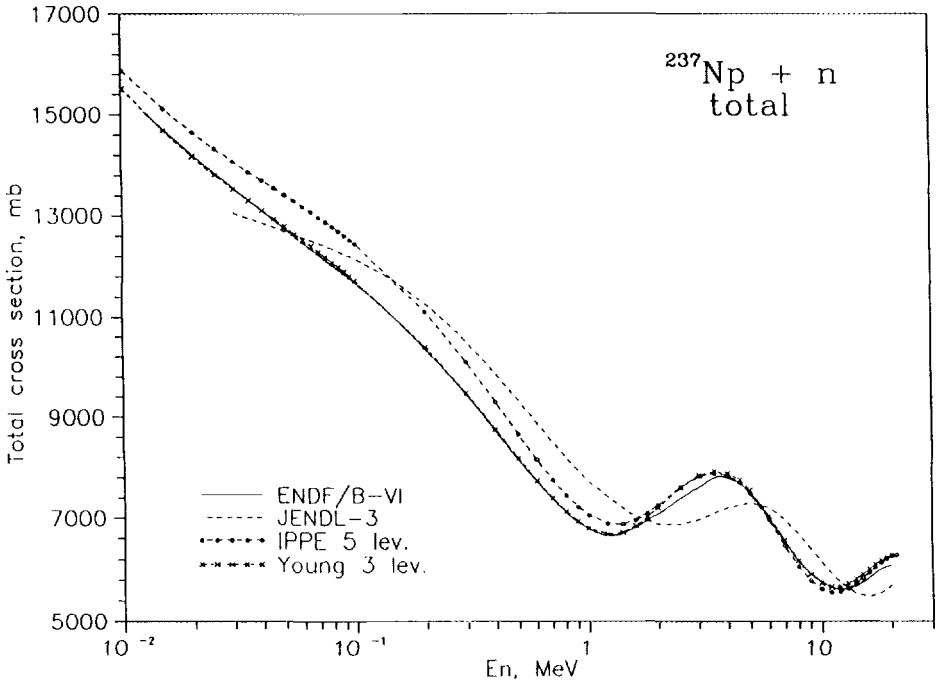
^{237}Np + n
total
Total cross section, mb
17000
15000
13000
11000
9000
7000
5000
ENDF/B-VI
JENDL-3
IPPE 5 lev.
Young 3 lev.
10 -2
10 -1
1
10
En, MeV

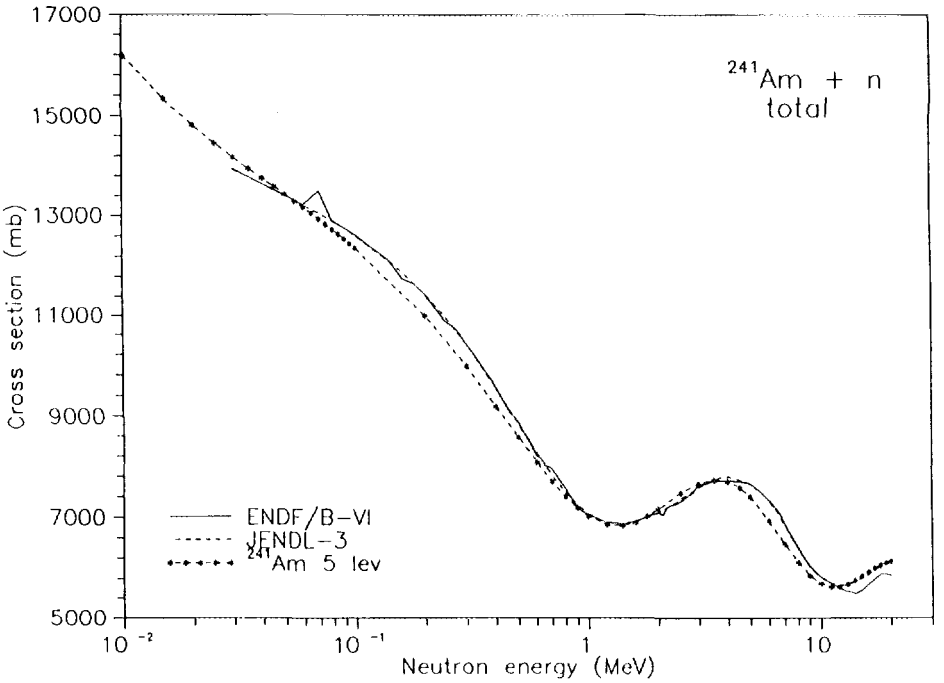
^{241}Am + n
total
Cross section (mb)
17000
15000
13000
11000
9000
7000
5000
ENDF/B-VI
JENDL-3
^{241}Am 5 lev
10 -2
10 -1
1
10
Neutron energy (MeV)

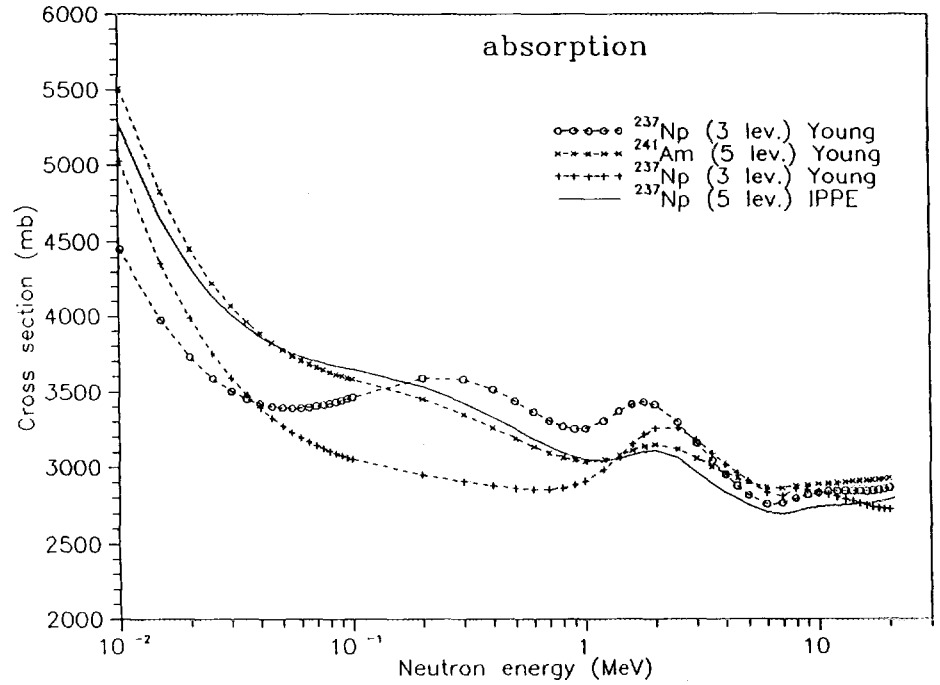
absorption
^{237}Np (3 lev.) Young
^{241}Am (5 lev.) Young
^{237}Np (3 lev.) Young
^{237}Np (5 lev.) IPPE
Cross section (mb)
Neutron energy (MeV)
6000
5500
5000
4500
4000
3500
3000
2500
2000
10^{-2}
10^{-1}
1
10

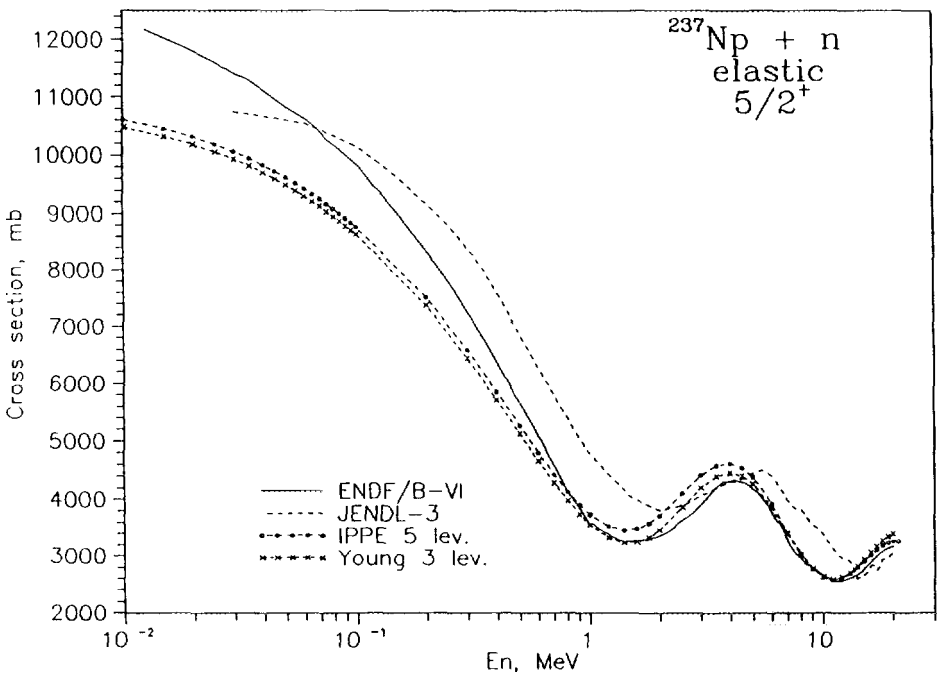
^{237}Np + n
elastic
5/2^{+}
ENDF/B-VI
JENDL-3
IPPE 5 lev.
Young 3 lev.
Cross section, mb
En, MeV
12000
11000
10000
9000
8000
7000
6000
5000
4000
3000
2000
10^{-2}
10^{-1}
1
10

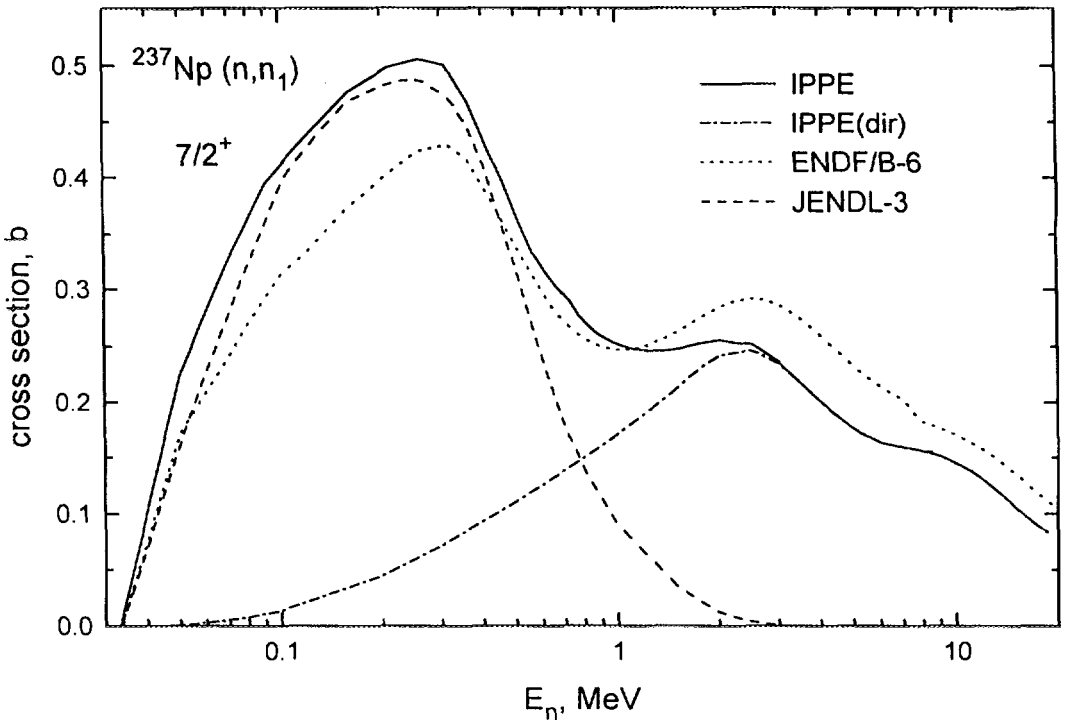
^{237}Np (n,n$_1$)
7/2$^+$
IPPE
IPPE(dir)
ENDF/B-6
JENDL-3
cross section, b
0.0
0.1
0.2
0.3
0.4
0.5
0.1
1
10
E$_n$, MeV

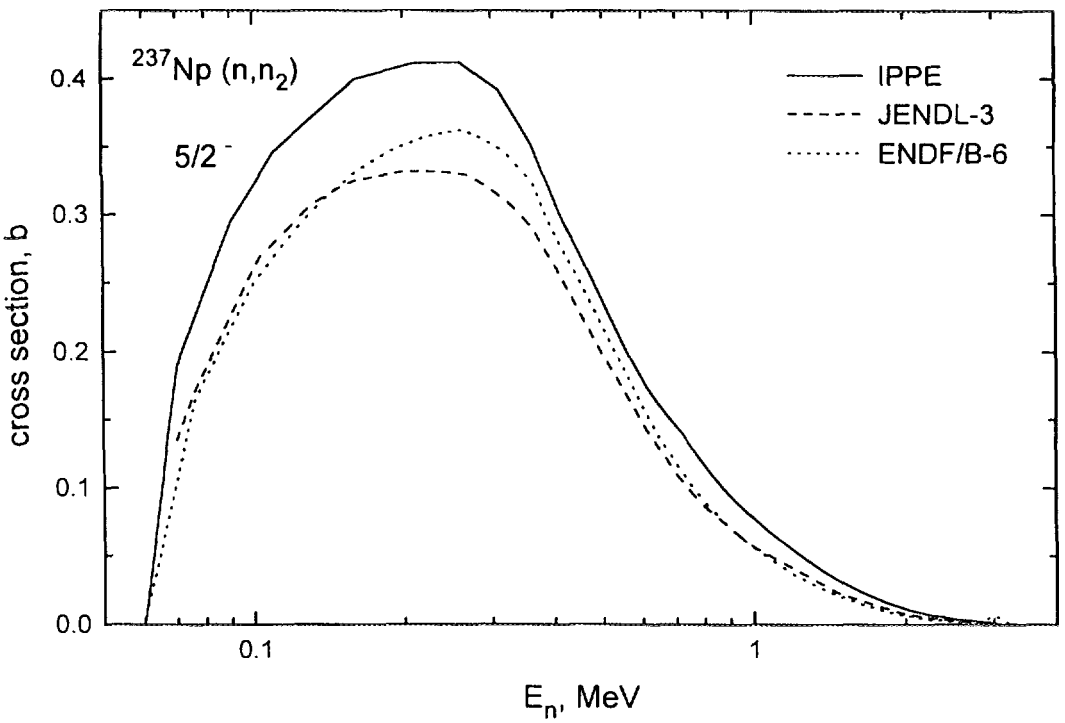
^{237}Np (n,n$_2$)
5/2$^-$
IPPE
JENDL-3
ENDF/B-6
cross section, b
0.0
0.1
0.2
0.3
0.4
0.1
1
E$_n$, MeV

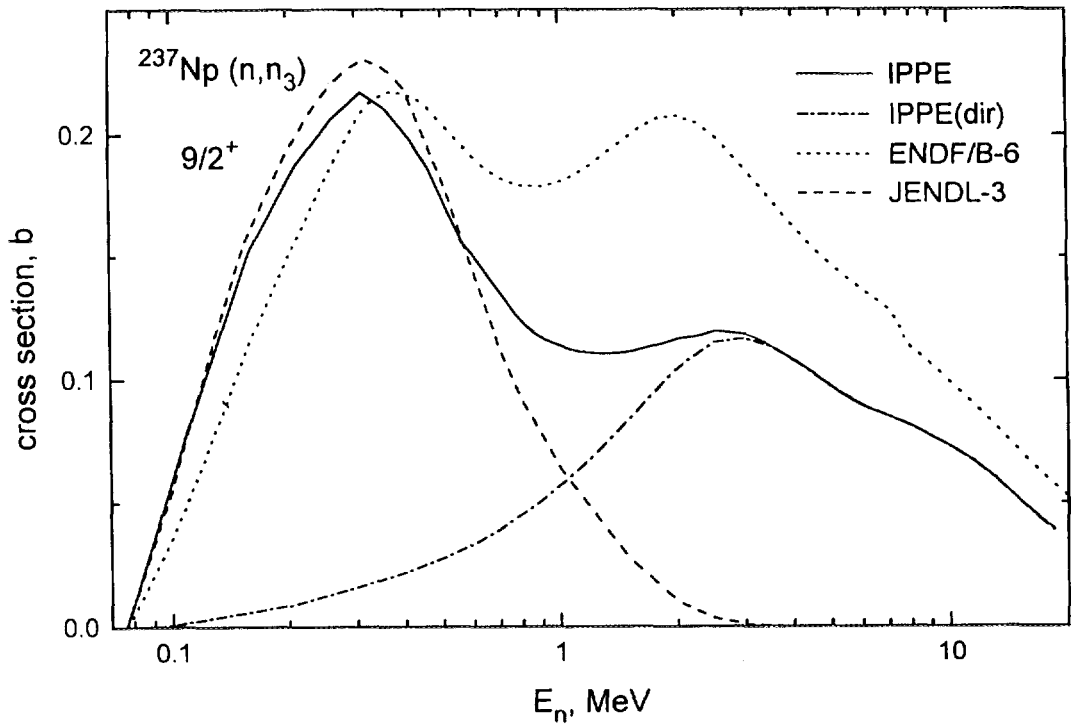
^{237}Np (n,n$_3$)
9/2$^+$
IPPE
IPPE(dir)
ENDF/B-6
JENDL-3
cross section, b
0.0
0.1
0.2
0.1
1
10
E$_n$, MeV

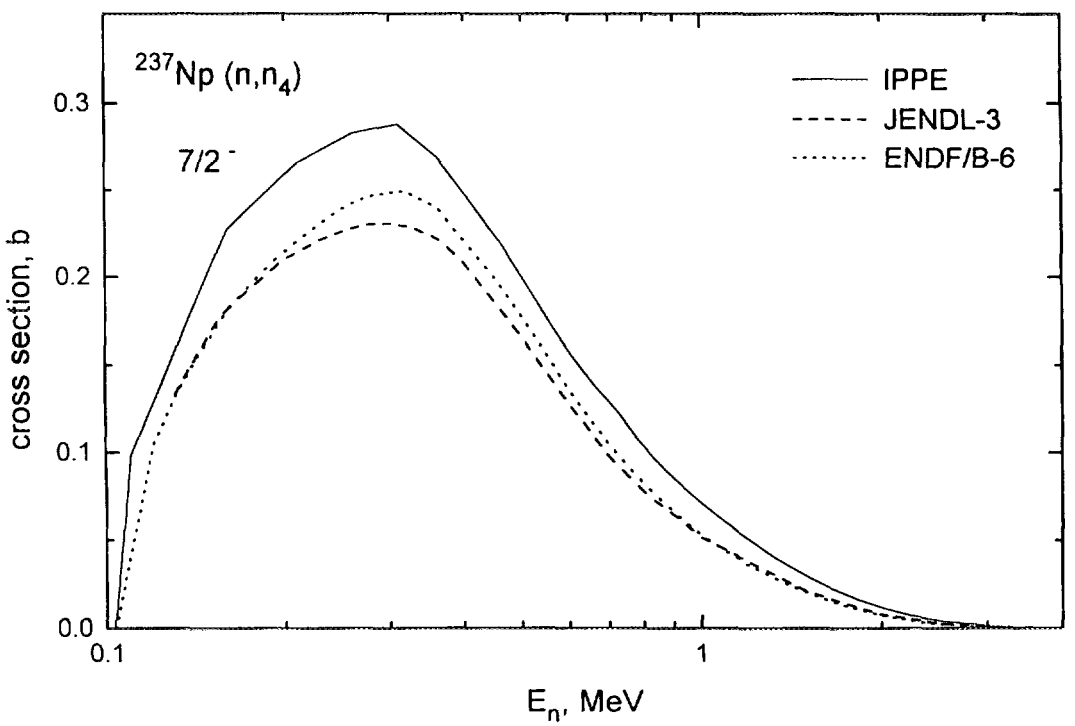
^{237}Np (n,n$_4$)
7/2$^-$
IPPE
JENDL-3
ENDF/B-6
cross section, b
0.0
0.1
0.2
0.3
0.1
1
E$_n$, MeV

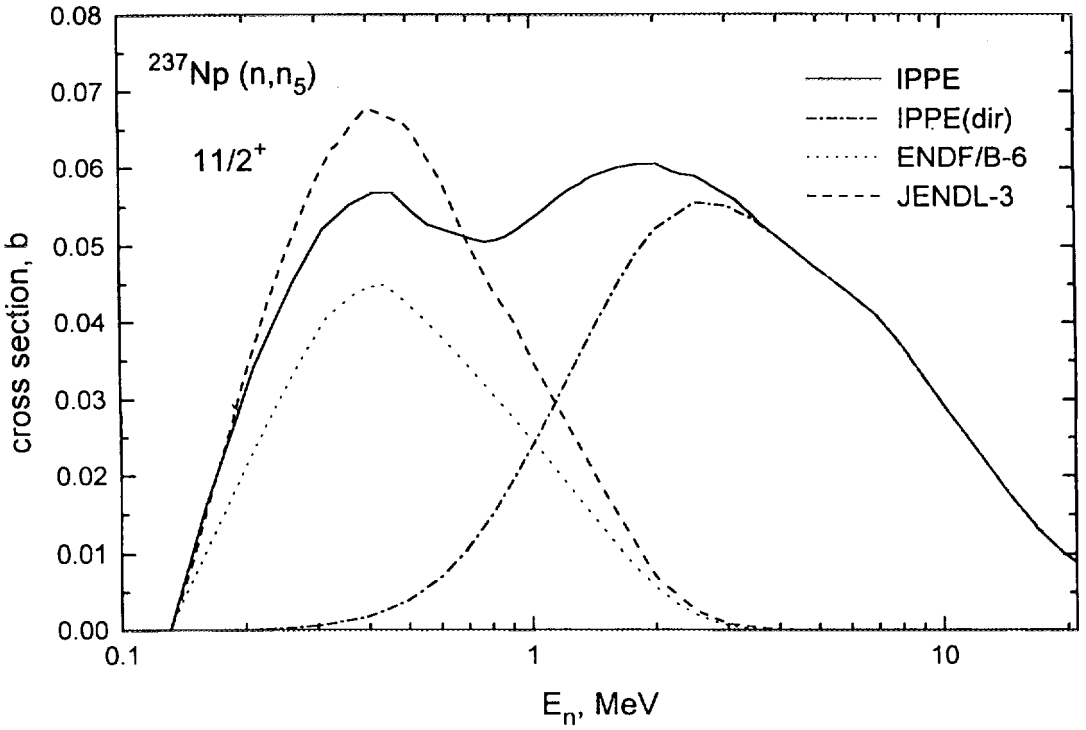
^{237}Np (n,n$_5$)
11/2$^+$
IPPE
IPPE(dir)
ENDF/B-6
JENDL-3
cross section, b
E$_n$, MeV

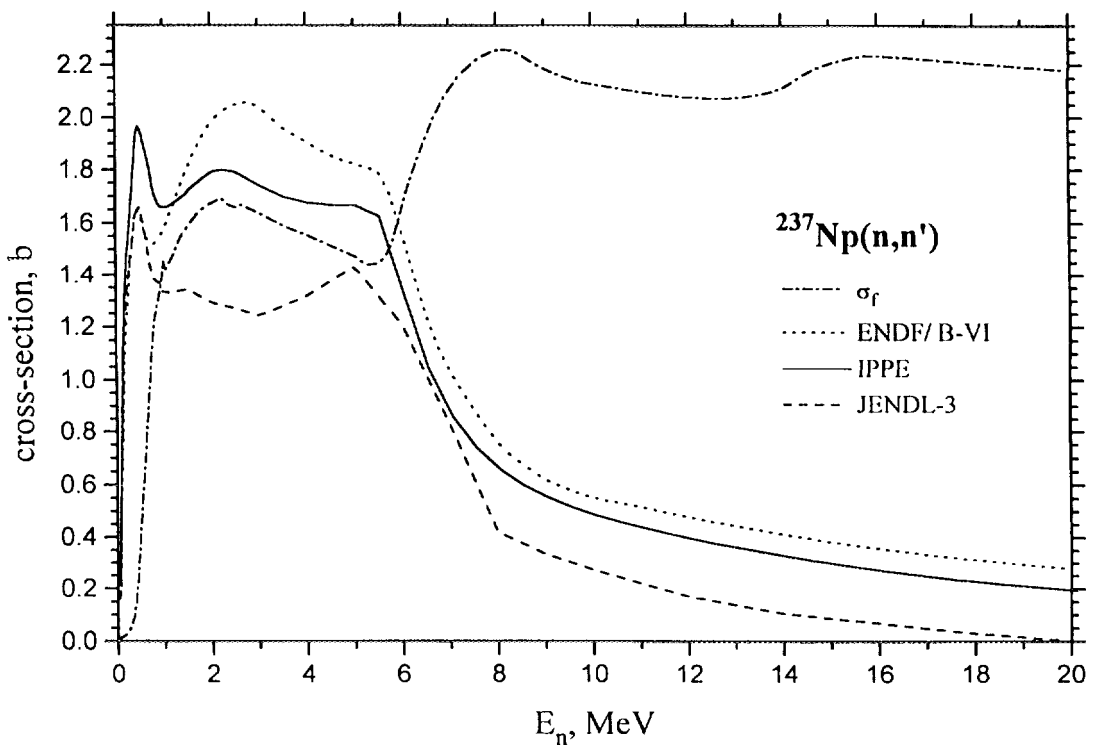
^{237}Np(n,n')
σ_f
ENDF/B-VI
IPPE
JENDL-3
cross-section, b
E$_n$, MeV

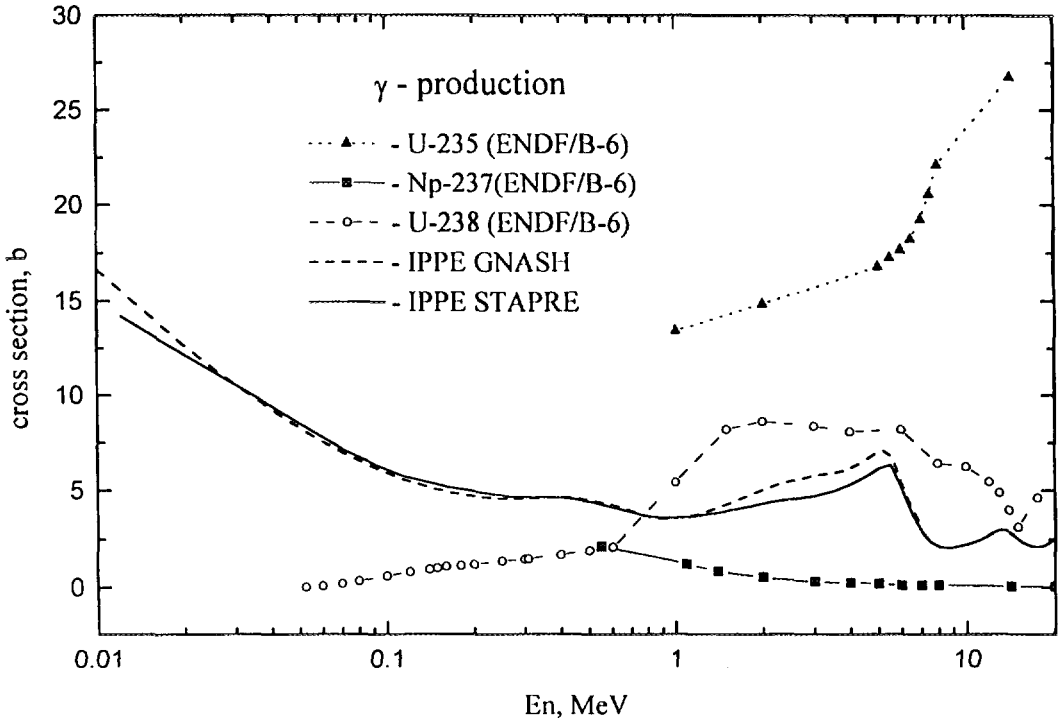
γ - production
- U-235 (ENDF/B-6)
- Np-237(ENDF/B-6)
- U-238 (ENDF/B-6)
- IPPE GNASH
- IPPE STAPRE
cross section, b
En, MeV

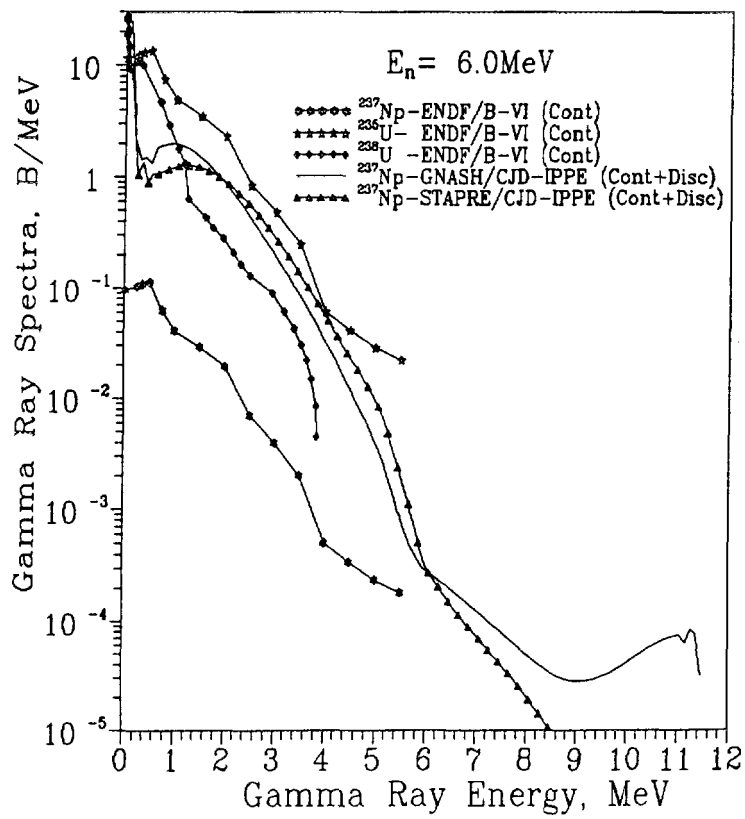
E_n= 6.0MeV
^{237}Np-ENDF/B-VI (Cont)
^{235}U- ENDF/B-VI (Cont)
^{238}U -ENDF/B-VI (Cont)
^{237}Np-GNASH/CJD-IPPE (Cont+Disc)
^{237}Np-STAPRE/CJD-IPPE (Cont+Disc)
Gamma Ray Spectra, B/MeV
Gamma Ray Energy, MeV

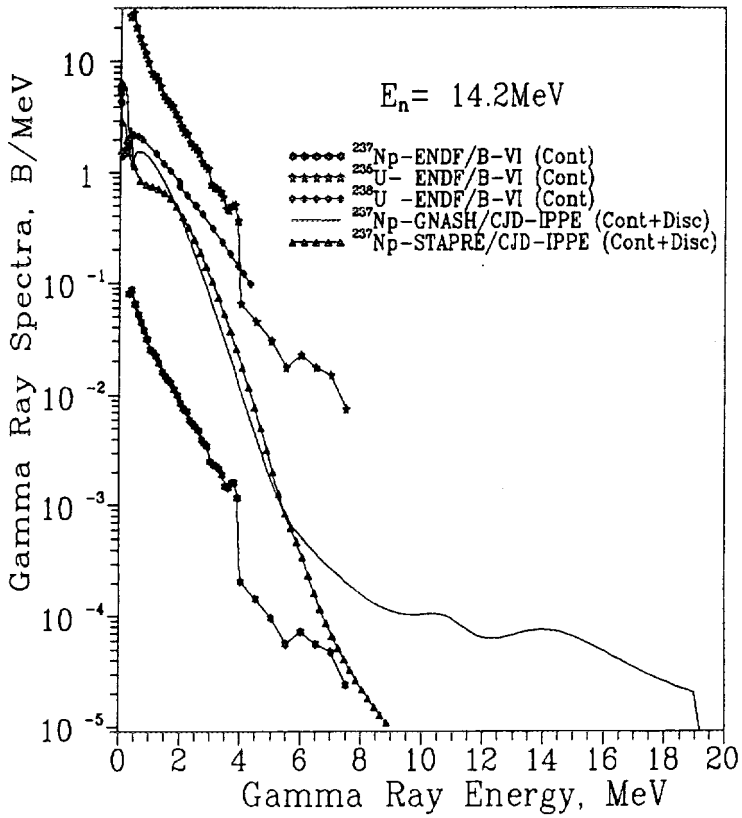
E_n= 14.2MeV
^{237}Np-ENDF/B-VI (Cont)
^{235}U- ENDF/B-VI (Cont)
^{238}U -ENDF/B-VI (Cont)
^{237}Np-GNASH/CJD-IPPE (Cont+Disc)
^{237}Np-STAPRE/CJD-IPPE (Cont+Disc)
Gamma Ray Spectra, B/MeV
Gamma Ray Energy, MeV

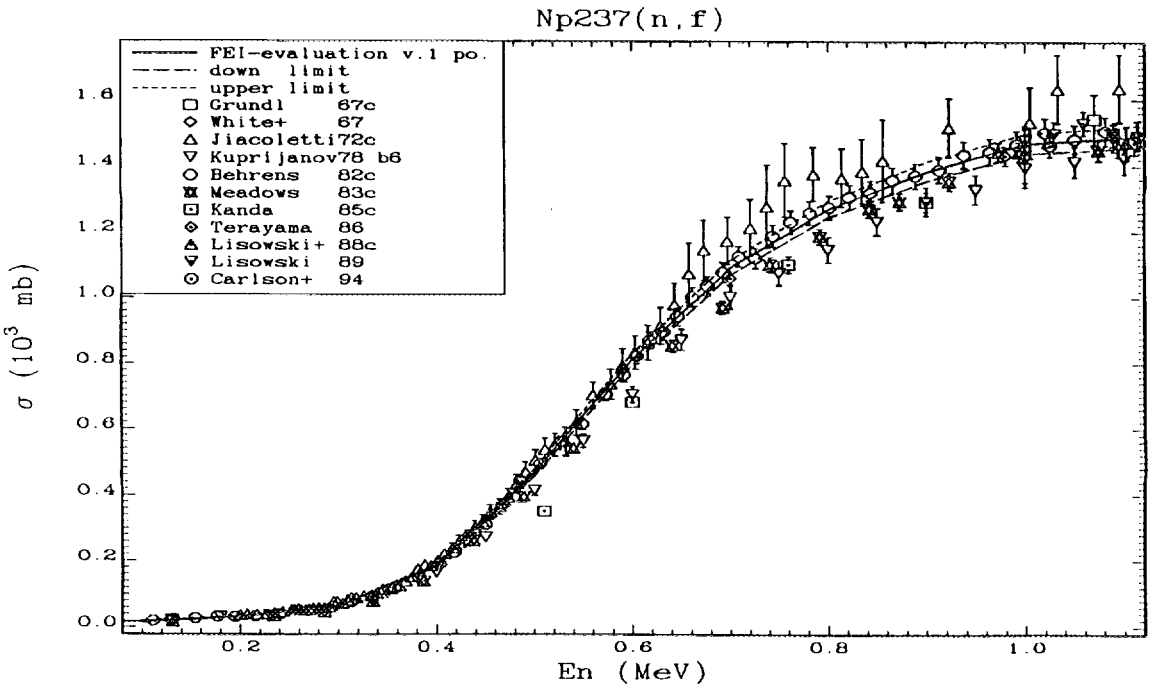
Np237(n,f)
FEI-evaluation v.1 po.
down limit
upper limit
Grundl 67c
White+ 67
Jiacoletti72c
Kuprijanov78 b6
Behrens 82c
Meadows 83c
Kanda 85c
Terayama 86
Lisowski+ 88c
Lisowski 89
Carlson+ 94
σ (10^3 mb)
En (MeV)

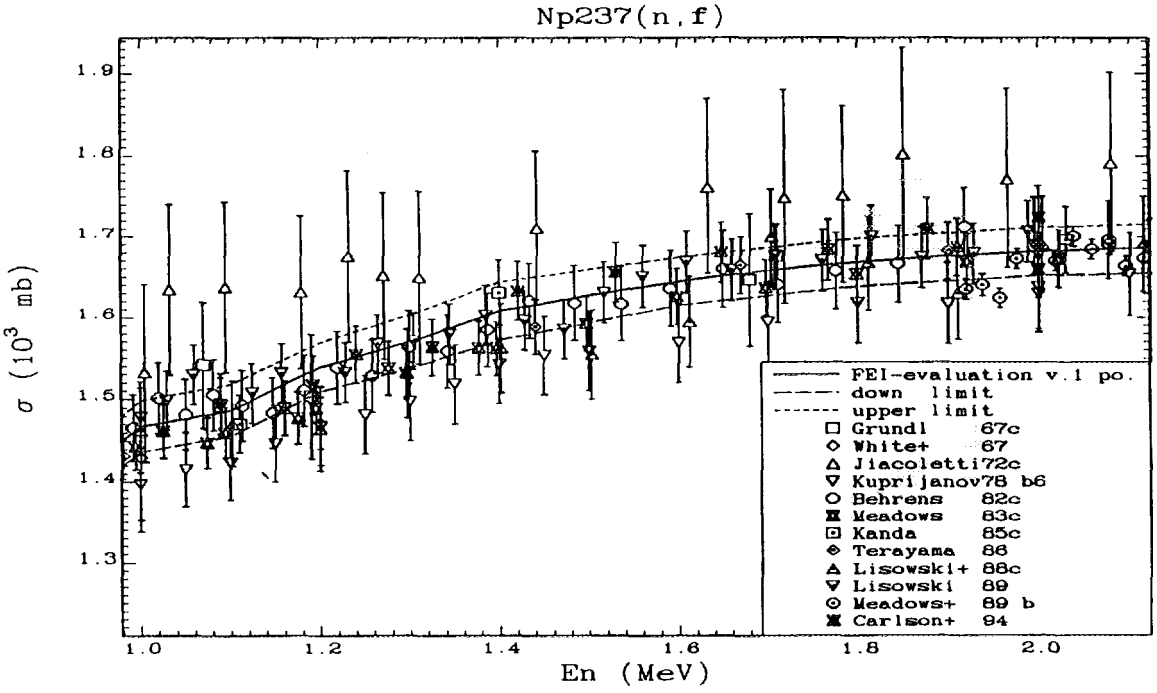
Np237(n,f)
σ (10³ mb)
En (MeV)
FEI-evaluation v.1 po.
down limit
upper limit
Grundl 67c
White+ 67
Jiacoletti72c
Kuprijanov78 b6
Behrens 82c
Meadows 83c
Kanda 85c
Terayama 86
Lisowski+ 88c
Lisowski 89
Meadows+ 89 b
Carlson+ 94

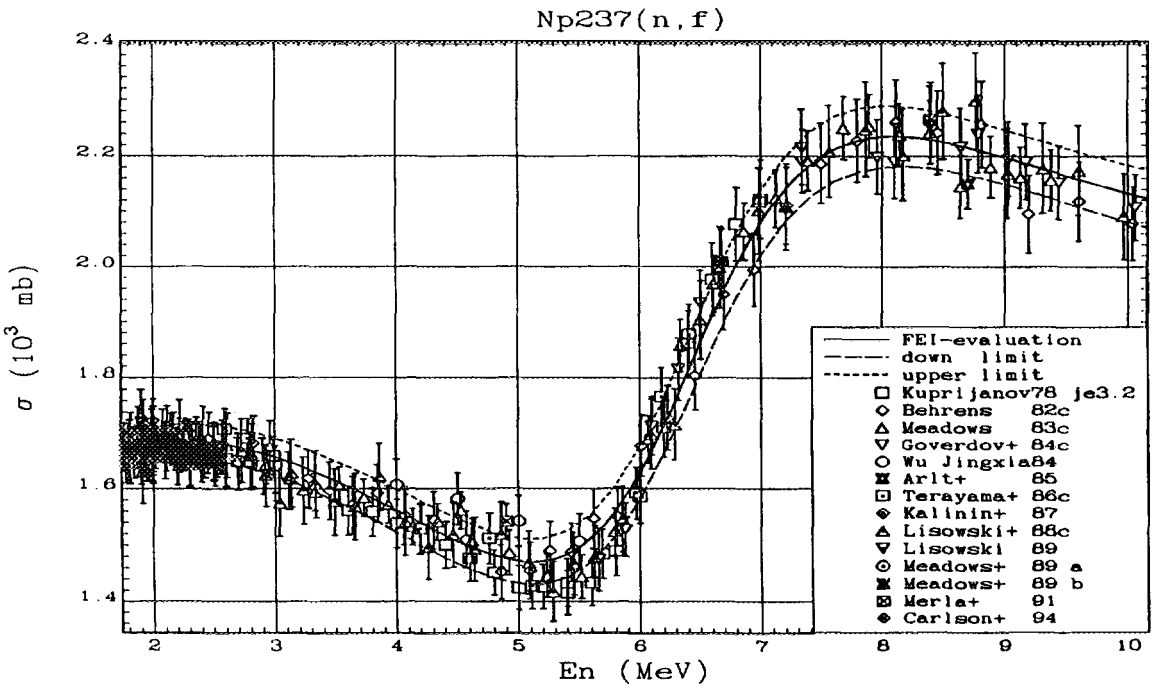
Np237(n,f)
σ (10³ mb)
En (MeV)
FEI-evaluation
down limit
upper limit
Kuprijanov78 je3.2
Behrens 82c
Meadows 83c
Goverdov+ 84c
Wu Jingxia84
Arlt+ 85
Terayama+ 86c
Kalinin+ 87
Lisowski+ 88c
Lisowski 89
Meadows+ 89 a
Meadows+ 89 b
Merla+ 91
Carlson+ 94

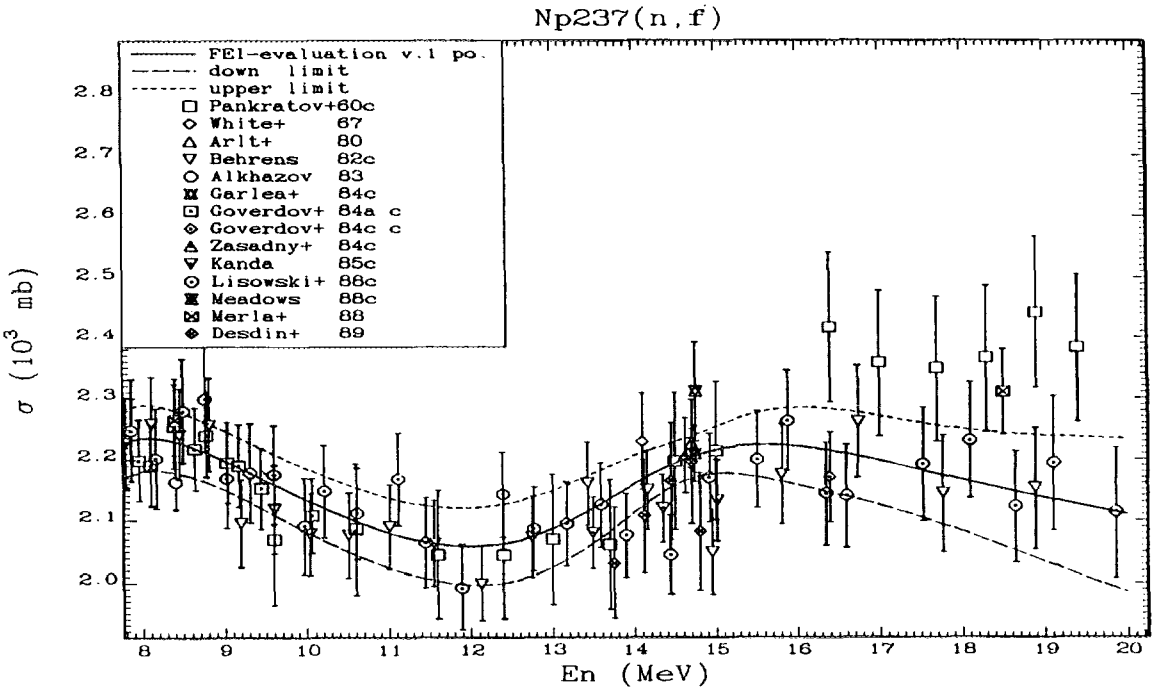
Np237(n,f)
FEI-evaluation v.1 po.
down limit
upper limit
Pankratov+60c
White+ 67
Arlt+ 80
Behrens 82c
Alkhazov 83
Garlea+ 84c
Goverdov+ 84a c
Goverdov+ 84c c
Zasadny+ 84c
Kanda 85c
Lisowski+ 86c
Meadows 88c
Merla+ 88
Desdin+ 89
σ (10³ mb)
En (MeV)

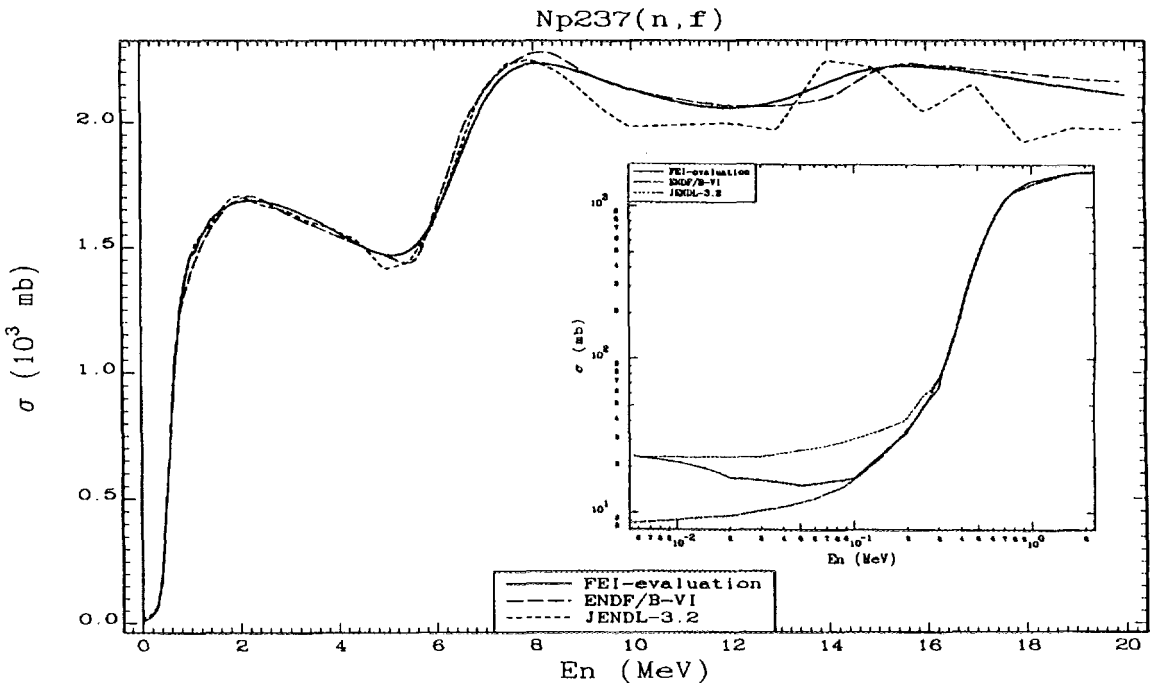
Np237(n,f)
FEI-evaluation
ENDF/B-VI
JENDL-3.2
σ (10³ mb)
En (MeV)

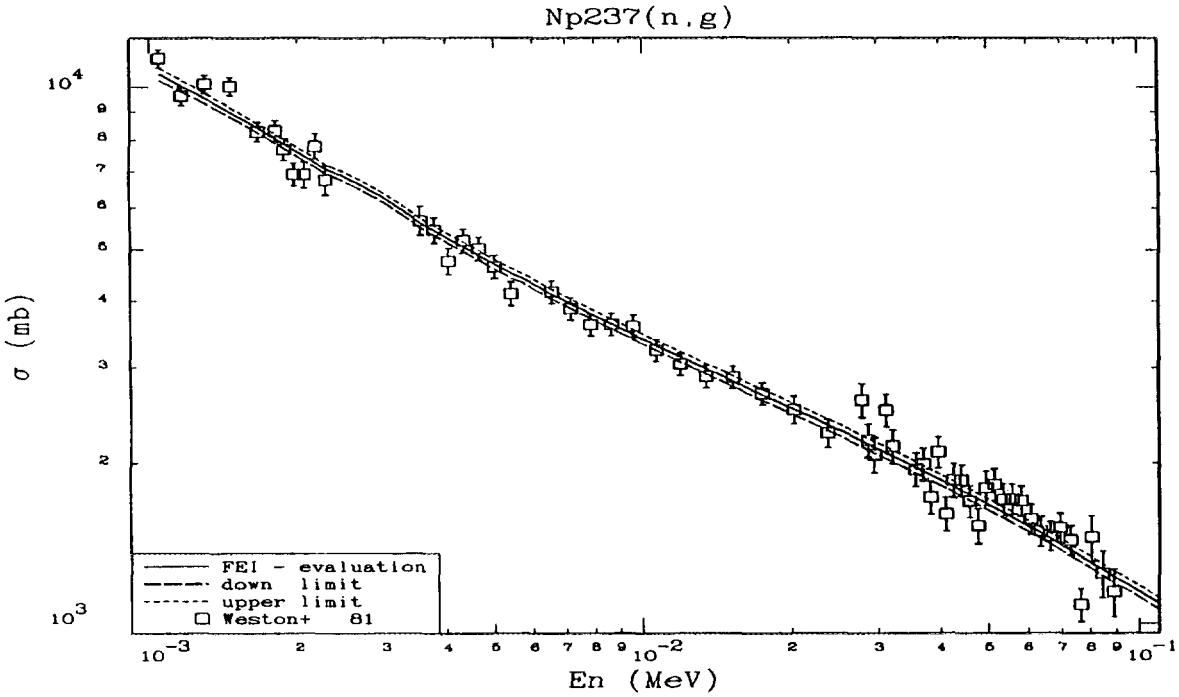
Np237(n,g)
σ (mb)
En (MeV)
FEI - evaluation
down limit
upper limit
Weston+ 81

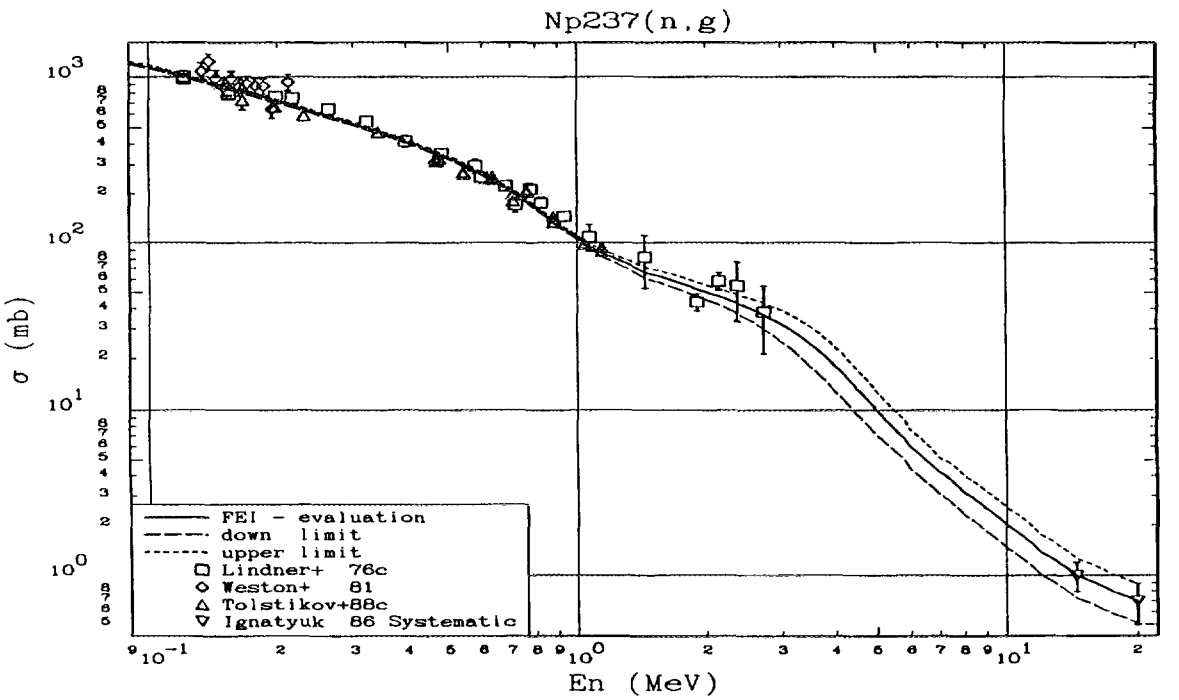
Np237(n,g)
σ (mb)
En (MeV)
FEI - evaluation
down limit
upper limit
Lindner+ 76c
Weston+ 81
Tolstikov+88c
Ignatyuk 86 Systematic

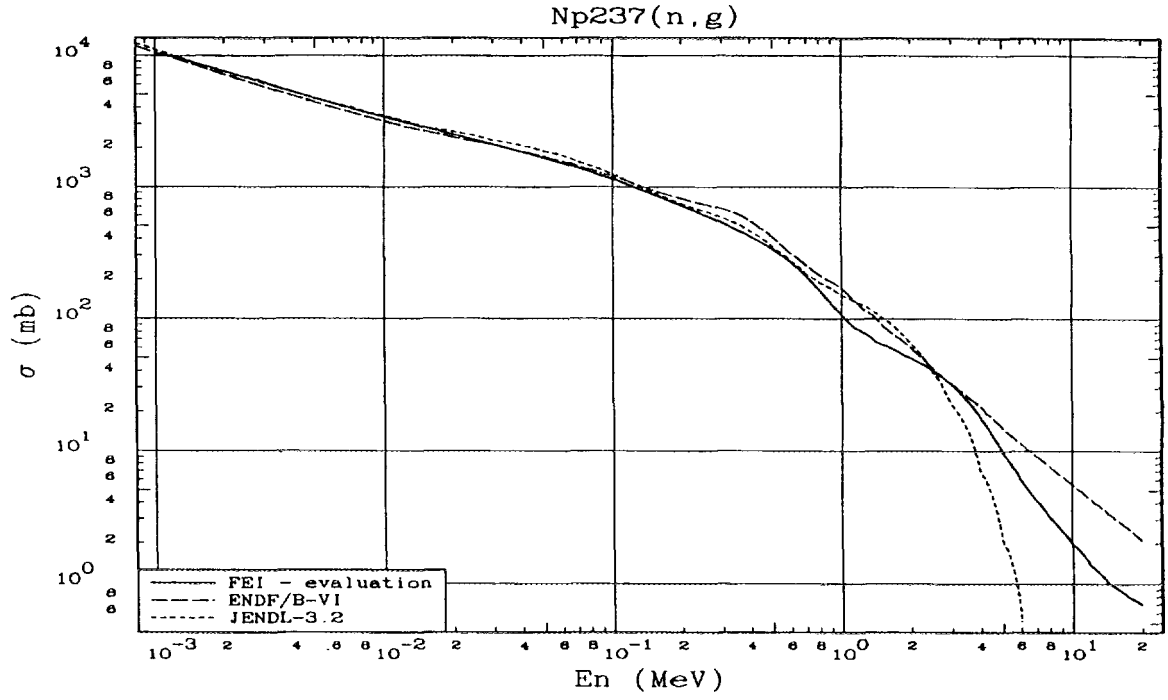

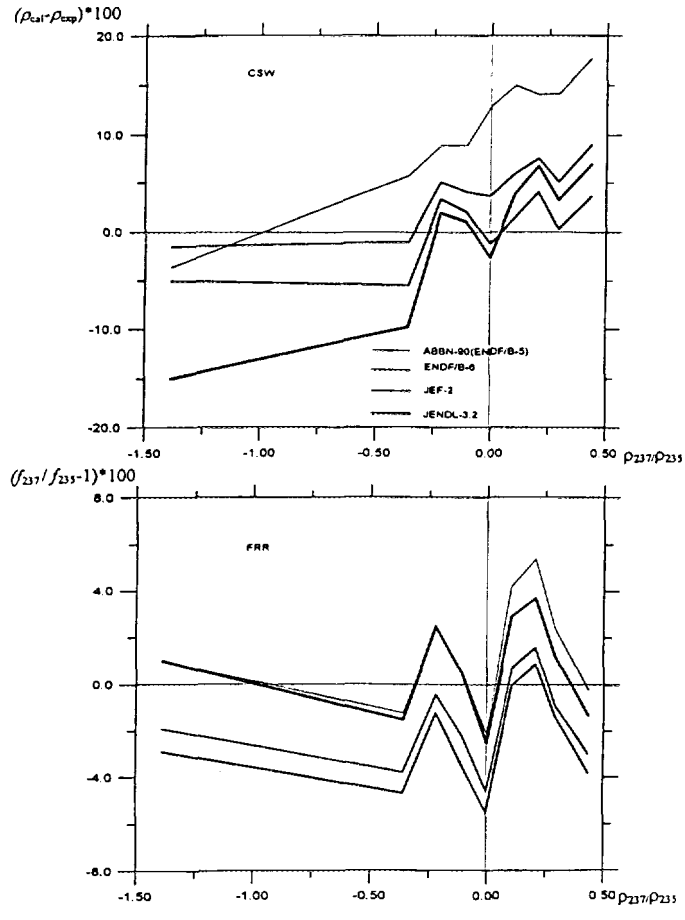

Fig. 30. Comparizon of the integral experimental and calculated data

Appendix Summary of ISTC Workshop on Nuclear Data for Minor Actinide

27-31 May 1996, JAERI, Tokai-mura, Ibaraki-ken, Japan

Improvement of minor actinide data is very important for transmutation projects using actinide burner reactors. The data needed are for ^{237,238}Np, ^{238,242}Pu, ^{241,242g,242m,243}Am and ^{242,243,244,245,246}Cm. The corresponding data for most important cross sections should be obtained on the basis of ISTC projects: "Measurements of the fission neutron spectra for minor actinides" (St.Petersburg, N 183-p), "Measurements and analysis of basic nuclear data for minor actinides"(Obninsk, N304-p), "Evaluation of actinide nuclear data" (Minsk, N b-03). The results obtained during the first year of projects were discussed on the Workshop. Some results of JAERI activity on improvement of nuclear data for minor actinides were considered too.

The following results should be noted:

i) The measurements of the fission neutron spectra for spontaneous fission of Cm-244 and -246 are performed in KRI;

ii) The preliminary results of precise measurements of the fission cross sections of Cm-244, -245, -246, -247 and Am-242m by neutrons with energies from 0.15 to 7 MeV were obtained in IPPE;

iii) The experimental equipment for measurements of the secondary neutron spectra, fission product yields and delayed neutron yields for the Np-237 target were developed and tested in IPPE. The first measurements of corresponding data were performed.

iv) The improved evaluations of most important neutron cross sections for Np-237 were obtained in IPPE;

v) New evaluations of neutron cross sections for Cm-243, -245 , -246 and Am-241 were performed in RPCPI. The complete files of evaluated data in ENDF-VI format were prepared;

All participants have agreed that the activity on projects is developing in accordance with original schedules and the final results of projects will improve essentially the basic neutron data for minor actinides that are important for future progress in technology of nuclear waste transmutation.

Possibilities of further measurements and evaluations for JENDL Actinide File have been discussed. Priorities for data requests should be set up by considering the present status of experimental and evaluated data.

国際単位系 (SI) と換算表

表1　SI基本単位および補助単位

量	名称	記号
長さ	メートル	m
質量	キログラム	kg
時間	秒	s
電流	アンペア	A
熱力学温度	ケルビン	K
物質量	モル	mol
光度	カンデラ	cd
平面角	ラジアン	rad
立体角	ステラジアン	sr

表2　SIと併用される単位

名称	記号
分，時，日	min，h，d
度，分，秒	°，′，″
リットル	l，L
トン	t
電子ボルト	eV
原子質量単位	u

1 eV = 1.60218 × 10^{-19} J

1 u = 1.66054 × 10^{-27} kg

表3　固有の名称をもつSI組立単位

量	名称	記号	他のSI単位による表現
周波数	ヘルツ	Hz	s^{-1}
力	ニュートン	N	$m \cdot kg/s^2$
圧力，応力	パスカル	Pa	N/m^2
エネルギー，仕事，熱量	ジュール	J	N·m
工率，放射束	ワット	W	J/s
電気量，電荷	クーロン	C	A·s
電位，電圧，起電力	ボルト	V	W/A
静電容量	ファラド	F	C/V
電気抵抗	オーム	Ω	V/A
コンダクタンス	ジーメンス	S	A/V
磁束	ウェーバ	Wb	V·s
磁束密度	テスラ	T	Wb/m^2
インダクタンス	ヘンリー	H	Wb/A
セルシウス温度	セルシウス度	℃	
光束	ルーメン	lm	cd·sr
照度	ルクス	lx	lm/m^2
放射能	ベクレル	Bq	s^{-1}
吸収線量	グレイ	Gy	J/kg
線量当量	シーベルト	Sv	J/kg

表4　SIと共に暫定的に維持される単位

名称	記号
オングストローム	Å
バーン	b
バール	bar
ガル	Gal
キュリー	Ci
レントゲン	R
ラド	rad
レム	rem

1 Å = 0.1 nm = 10^{-10} m

1 b = 100 fm^2 = 10^{-28} m^2

1 bar = 0.1 MPa = 10^5 Pa

1 Gal = 1 cm/s^2 = 10^{-2} m/s^2

1 Ci = 3.7 × 10^{10} Bq

1 R = 2.58 × 10^{-4} C/kg

1 rad = 1 cGy = 10^{-2} Gy

1 rem = 1 cSv = 10^{-2} Sv

表5　SI接頭語

倍数	接頭語	記号
10^{18}	エクサ	E
10^{15}	ペタ	P
10^{12}	テラ	T
10^{9}	ギガ	G
10^{6}	メガ	M
10^{3}	キロ	k
10^{2}	ヘクト	h
10^{1}	デカ	da
10^{-1}	デシ	d
10^{-2}	センチ	c
10^{-3}	ミリ	m
10^{-6}	マイクロ	μ
10^{-9}	ナノ	n
10^{-12}	ピコ	p
10^{-15}	フェムト	f
10^{-18}	アト	a

（注）

1. 表1－5は「国際単位系」第5版，国際度量衡局 1985年刊行による。ただし，1 eVおよび1 uの値はCODATAの1986年推奨値によった。
2. 表4には海里，ノット，アール，ヘクタールも含まれているが日常の単位なのでここでは省略した。
3. barは，JISでは流体の圧力を表わす場合に限り表2のカテゴリーに分類されている。
4. EC閣僚理事会指令ではbar，barnおよび「血圧の単位」mmHgを表2のカテゴリーに入れている。

換算表

力	N(=10^5 dyn)	kgf	lbf
	1	0.101972	0.224809
	9.80665	1	2.20462
	4.44822	0.453592	1

粘度　1 Pa·s(N·s/m^2) = 10 P(ポアズ)(g/(cm·s))

動粘度　1 m^2/s = 10^4 St(ストークス)(cm^2/s)

圧力	MPa(=10 bar)	kgf/cm^2	atm	mmHg(Torr)	lbf/in^2(psi)
	1	10.1972	9.86923	7.50062 × 10^3	145.038
	0.0980665	1	0.967841	735.559	14.2233
	0.101325	1.03323	1	760	14.6959
	1.33322 × 10^{-4}	1.35951 × 10^{-3}	1.31579 × 10^{-3}	1	1.93368 × 10^{-2}
	6.89476 × 10^{-3}	7.03070 × 10^{-2}	6.80460 × 10^{-2}	51.7149	1

エネルギー・仕事・熱量	J(=10^7 erg)	kgf·m	kW·h	cal(計量法)	Btu	ft·lbf	eV
	1	0.101972	2.77778 × 10^{-7}	0.238889	9.47813 × 10^{-4}	0.737562	6.24150 × 10^{18}
	9.80665	1	2.72407 × 10^{-6}	2.34270	9.29487 × 10^{-3}	7.23301	6.12082 × 10^{19}
	3.6 × 10^6	3.67098 × 10^5	1	8.59999 × 10^5	3412.13	2.65522 × 10^6	2.24694 × 10^{25}
	4.18605	0.426858	1.16279 × 10^{-6}	1	3.96759 × 10^{-3}	3.08747	2.61272 × 10^{19}
	1055.06	107.586	2.93072 × 10^{-4}	252.042	1	778.172	6.58515 × 10^{21}
	1.35582	0.138255	3.76616 × 10^{-7}	0.323890	1.28506 × 10^{-3}	1	8.46233 × 10^{18}
	1.60218 × 10^{-19}	1.63377 × 10^{-20}	4.45050 × 10^{-26}	3.82743 × 10^{-20}	1.51857 × 10^{-22}	1.18171 × 10^{-19}	1

1 cal = 4.18605 J (計量法)
= 4.184 J (熱化学)
= 4.1855 J (15 °C)
= 4.1868 J (国際蒸気表)

仕事率　1 PS (仏馬力)
= 75 kgf·m/s
= 735.499 W

放射能	Bq	Ci
	1	2.70270 × 10^{-11}
	3.7 × 10^{10}	1

吸収線量	Gy	rad
	1	100
	0.01	1

照射線量	C/kg	R
	1	3876
	2.58 × 10^{-4}	1

線量当量	Sv	rem
	1	100
	0.01	1

(86年12月26日現在)

SELECTED PAPERS OF ISTC WORKSHOP ON NUCLEAR DATA OF MINOR ACTINIDES May27~31, 1996, JAERI, Tokai, Japan